SETTLEMENT OF FOUNDATIONS ON JOINTED ROCK

(A SURVEY OF DEFORMABILITY DUE TO JOINTS, PREDICTED BY THE FINITE ELEMENT METHOD)

by

Oldrich Hungr

Thesis submitted to the School of Graduate Studies of the University of Ottawa in partial fulfillment of the requirements for the degree of Master of Applied Science (Civil Engineering.

August 1974

CONTENTS

LIST OF FIGURES AND TABLES

*Numerals in parantheses refer to corresponding items in the list of references.

LIST OF PLATES

LIST OF SYMBOLS

A	area
B	width of footing
C	joint contact ratio (11)
b	joint depth
E	modulus of deformation
E_{eff}	effective modulus of deformation (6)
E_f	foundation modulus, field modulus of deformation
E_n	modulus of deformation perpendicular to joints
E_s	modulus of deformation parallel to joints
f	friction coefficient
G	modulus of rigidity
G_{ns}, G_{sn}	moduli of rigidity in transverse anisotropy
i	angle of inclination of asperities (39)
j_c	real area of contact (11)
j_t	joint thickness (11)
k_n, k_{nn}	normal unit joint stiffness coefficient (19)
k_s, k_{ss}	shear unit joint stiffness coefficient (19)
k_{ns}, k_{sn}	offdiagonal unit joint stiffness coefficients (19)
m_v	volume decrease coefficient
N	normal force
p, q	contact pressure
RQD	rock quality designation (10)
S	joint spacing
T	shear force
u	pore-pressure
W	load

x	horizontal coordinate
z	vertical coordinate
α	dip angle
Δh	normal displacement, dilatancy, aperture thickness
δ	shear displacement, settlement
δ_y	displacement at yield point
$\delta_{0.5p}$	displacement at one half the peak stress
$\delta_p, \delta_s, \delta_{max}$	displacement at the peak stress
ϕ	angle of internal friction
ν	Poisson's ratio
$\nu_{ns}\nu_{sn}$	Poisson's ratios for transverse anisotropy
σ_n	normal stress
σ_a	apparent normal stress (11)
σ_t	true normal stress on contact area (11)
σ_v	vertical stress
σ_h	horizontal stress
τ	shear stress
τ_y	yield shear stress
$\tau_{0.5p}$	shear stress at one half the peak load
τ_p, τ_{max}	ultimate shear strength, shear stress at peak load
τ_{res}	residual shear strength

ABSTRACT

An approach to estimating the deformability of rock masses under the foundations of structures was surveyed, involving the use of a Finite Element computing technique and laboratory measurements of joint deformability. The purpose of this survey was to initiate a practical method of attack and, through solving a limited number of problems, to assess its feasibility and the difficulties arising from its use.

An overview of literature is given, which deals with the settlement tolerances of structures, main methods of approach to the characterization of deformation of rock masses, and the theory of, and ways of measuring the deformability of rock joints.

It was concluded from the literature survey, that two distinct methods of approach are being used to estimate settlement of footings on rock. One of these is the "continous"approach in which the rock mass is considered to be a continuous medium with unique elastic parameters determined by large scale "in situ" deformability testing (plate-load test most widely used). The other method may be called the "discontinuous" approach, in which the blocks of intact rock and the discontinuities comprising a rock mass are considered as separate structural elements. Of the two, the "continous" approach is more often used.

It was found that research is lacking in the area of interpretation of plate-load tests and, particularly, in deformability testing of rock discontinuities.

A direct shear testing machine capable of testing samples up to six inches in crossection was designed and built.

Samples of natural and saw-cut rock joints from three types of rock were collected and tested to obtain the normal and shear stiffness coefficients. The results were averaged using a simple regression analysis. A method was demonstrated, by which the normal stiffness parameters for joints can be used to correlate with the results of a plate-load testing program.

Using a manual technique of field sampling, it was only possible to obtain samples that were unweathered and unfilled.

It was found that, for the particular type of joints tested, the shear stiffness coefficient depends on the magnitude of both the normal and the shear stress. Therefore, using a single value of the unit shear stiffness coefficient, k_s, in computations may be injustified.

The off-diagonal stiffness coefficient, k_{ns}, was determined as being of the same order of magnitude as the shear stiffness coefficient.

Finite element models of rock subgrades under a strip footing were created, containing a single joint and a joint set, horizontal and inclined. Comparisons between the finite element settlement solutions and simplified analytical solutions are presented.

It is concluded that the simplified solutions often contain a considerable error. In the case of a rock mass containing a single joint set, a theoretical explanation of this error is suggested.

Finally several recommendations for further research are made.

AKNOWLEDGEMENTS

The work reported herein was financed by the National Research Council of Canada under grant No. C 1211.

The author's sincere thanks are extended to the following persons, who expressed interest in his work and provided valuable help, advice or stimulation:

Messrs F. Capellar, M. Gyenge, G. Herget, N.A. Toews, and Y.S. Yu of the Mines Branch of the E.M.R., Professors N.J. Gardner and P. Gélinas of the Faculty of Science & Engineering, University of Ottawa, Messrs F.C. Argue, C. Lavigne, R. Moore and C. Trim, technicians of the Department of Civil Engineering, University of Ottawa, and Prof. B. Ladanyi of Ecole Polytechnique, Montreal.

P. Paine, an undergraduate of the Department of Civil Engineering assisted dilligently in conducting the tests.

The author's problems and uncertainities were made easier through the understanding and stimulating guidance of his supervisor, Dr. D.F. Coates.

Finally, I am obliged to my wife, Klema, for sacrificing a great amount of her time to type the text.

PREFACE

The allowable bearing capacity of rock is limited mainly by the considerations of deformability due to jointing. Its values, as allowed by different building codes, vary within a wide range (for example NBCC-70-0 to 20 ksf, New York Building Code-16 to 120 ksf, Chicago Building Code-0 to 200 ksf), and experts sometimes suggest that much higher values than those given by the building codes can be used! Consequently, it is obvious that any contribution to the methods of predicting rock deformability would be of positive practical importance.

The purpose of the present research program, documented by this Thesis, is to survey several aspects of the question of deformability of a rock mass considered as a discontinous medium. The word "survey" is used above, because the scope of the Thesis is too wide to allow concentration on any one detail in a great depth, and at the same time too narrow to permit a thorough treatment of every aspect of this exceedingly complex problem. The aim of this work was to try out some relatively new techniques of rock testing and numerical modelling and to assess, mainly qualitatively, their potencies, limitations and difficulties in use.

Specific conclusions were drawn where possible, but these should by no means be considered definite or final, nor should they be taken as the most important product of this work. Rather, it is hoped by the author that his experiences and findings, reported on the following pages, might serve as a springboard to a future researcher, who will select a more narrowly defined subject and carry his work to conclusive, practical results. Even the design of the direct shear testing machine, described in Part II is, in the author's opinion, subject to improvements.

The Thesis is divided into three Parts, dealing respectively with the survey of the existing literature, testing of rock discontinuities for deformability, and finite element modelling simulation of certain configurations of rock masses. The objectives of each Part are stated in its opening paragraph and its mutual interrelationships with the others should become clear in the course of reading the text.

PART I

Literature Survey

Objectives: The purpose of this first part of the Thesis is to roughly outline the present status of the problem of settlement of rock foundations, as well as the related problem of deformability of rock joints, as reflected by the published literature. The outline is divided into two Chapters.

Chapter 1 deals with the general problem of the determination of settlement of foundations on rock. It begins by presenting some data on settlement tolerances for structures, proceeds by describing the two basic approaches to the problem, e.g. the "continuous" and "discontinuous" approach and concludes by mentioning briefly the main tool of each of the above schools, e.g. the plate-load test "in situ" and the Finite Element Method.

Chapter 2 is devoted to one of the chief topics of the "discontinuous" approach, namely it surveys the available data and ideas connected with the deformability of planar rock discontinuities (joints). Perhaps as a result of the prevalent use of limit equilibrium methods of analysis in Rock Mechanics, the literature of rock discontinuities deals mainly with strength of joints. Therefore the information on deformability behaviour collected in Chapter 2 is derived, with few exceptions, as a byproduct of strength research and, consequently, useful quantitative conclusions are scant. Instead, emphasis is placed on the general qualitative understanding of deformational behaviour of different types of joints both in shear and compression.

Also, an overview is presented of the currently used testing methods for joints as well as the quantitative parameters defined by some workers to describe deformational and strength behaviour of rock discontinuities.

CHAPTER I

Deformation of Rock Masses under Foundations of Structures

Section 1.1 Settlement Criteria

Most of the structures founded on rock, perhaps with the exception of those cases where slope stability or large horizontal forces are involved, are safe with respect to bearing failure(10). Consequently, the main problem facing the designer of foundations on rock is the one of settlement. Then again, the total settlement of such structures is generally insignificant, and therefore the designer is chiefly concerned with differential settlements and interaction of the structure and its foundation. The two relevant criteria to be considered are the safety against structural failure and the required performance of the structure. The criterion of safety is encountered in rigid continuous structures such as arch and buttress dams, continuous bridges and tall frame buildings. The criterion of performance must also be met in smaller buildings of frame or rigid bearing wall design and in some special purpose structures such as nuclear reactors or industrial halls.

Several authors have attempted to present specific settlement criteria for buildings. Thus for example Skempton and MacDonald(45) define the allowable angular distortion coefficient δ/l as the ratio of the differential settlement between two columns divided by the length of the span. On the basis of a statistical treatment of a large number of performance observations,

they establish the limiting values of the coefficient, the exceeding of which may result in structural damage. For the traditional type of beam and column frame structure they suggest 1/300 as the limiting value of the angular distortion coefficient, byond which cracking of the panel walls may occur. Distortions of the skeleton frame itself could, according to the authors, occur at δ/l larger than 1/150. More rigid frames, however, may show much greater sensitivity to differential movement. For example buckling of diagonal braces in steel frames has been observed at an angular distortion equal to 1/600.

It was pointed out (Ripley's discussion, (46)) that the statistical observations do not include data on sensitivity of equipment contained in the buildings and other data pertaining to use. Thus the above criteria can be taken only as rough guidance, while the design should take into consideration the specific conditions of each case.

J.Feld (16) also gives a summary of general criteria and notes that the time-rate of settlement constitutes another important factor for structural damage considerations, as the structure may need time to adjust itself to new support conditions by plastic flow. This remark may not be particularly relevant to foundations on rock because in rock usually a large part of the deformations occurs instantaneously.

No similar studies are available for bridges as obviously bridge designs are much more varied. Settlement criteria must therefore be determined entirely on the basis of structural analysis of each particular case.

As an example of a special purpose structure one may cite the project, described by Ward and Burland (51), of housing for a nuclear reactor. This structure occupies a site of several acres and across this large area the allowable maximum differential settlement is specified as only a fraction of an inch.

Arch dams are especially sensitive to differential settlements. Yielding of the foundation rock may change entirely the stress distribution in both the abutments and the crown and may create occurrence of intolerable tensional stresses. All theories of structural design for arch dams make use of foundation stiffness parameters. An experimental study on small scale physical models has been carried out in Portugal (44), which yielded the following general results:

1. The influence of the E_f/E_c factor, in which E_f is the deformation modulus of the foundation and E_c that of the concrete, on the state of stresses in the dam is little important when the factor is greater than ½, important when it is between 1/8 and ¼ and very important when it is less than 1/8. Consequently, the stress state only becomes significantly effected by foundation yielding when the deformation modulus of the rock is about one quarter of that of concrete. When the factor E_f/E_c is 1/16, a variation in the magnitude of the foundation modulus of 20% would be tolerated by a conventional design. But it is known that standard in situ testing procedures may involve uncertainities greater than 20%, so that in the case of low quality rocks such variance must be taken into account.

2. Local variations of E_f along the length of the foundation may reach a factor of 3.0 but they have only a local influence upon the state of stresses.

3. The author considers the influence of time on deformation of rock foundations usually quite small and irrelevant.

In conclusion of this Section it can be seen that the settlement problem of rock foundations is a real one. For example, we may imagine a frame structure spanning 30 ft with one column being supported by solid rock with negligible settlement, whereas the other rests on a fault zone. Using the limiting value of the coefficient of angular deformation of 1/300 we find that a settlement of only 1.2 inches might produce structural damage. On the other hand, rock is not a readily yielding material, and in most cases the settlement criteria would not be exceeded by a very large margin. Consequently no large precision is generally required for settlement predictions in rock.

Section 1.2 Statement of the Problem of Determination of Settlement of Foundations on Rock.

Rock is essentially an elastic material, capable of storing and transfering mechanical energy. Consequently, settlement problems on such material have to be solved by using an elastic theory which may or may not be augmented by considerations of nonlinear elastic or time dependent behaviour.

The first purpose of this Section is to list those particular characteristics inherent to rock masses, which complicate settlement predictions. Secondly, the chief methods of obtaining such predictions will be outlined in general terms.

The majority of solutions of stress-strain problems available from the theory of elasticity is derived under the assumptions of perfect elasticity, continuity, homogeneity and isotropy. Rock in the mass, however, does not fulfill these assumptions and consequently the following general properties have to be recognized (32).

Nonlinearity and Rheidity of the rock substance are often observed in compression, or other testing. Nonlinearity is characterized by curved stress-strain diagrams, indicating a dependence of the tangent modulus of deformation upon the level of stress. Some rock types, expecially basic igneous rocks, exhibit nearly linear behaviour almost up to the failure stress. In other cases, nonlinear behaviour needs to be taken into an account in calculations by some method, for example such as that described in Fig. 1.1, page 17. Many types of rock undergo a time dependent (rheidic) deformation under a sustained stress.

Such behaviour is more difficult to account for in computation but in many instances it can be neglected with sufficient accuracy in foundation problems (44). Under the limited scope of this work, rock substance will be assumed as being a linearly elastic medium in which strains are directly proportional to stresses and independent of time.

Heterogeneity is due to the variations in composition and structure. Typically, more or less well defined quasihomogeneous zones may be recognized, such as single layers, weathered zones, dykes or instrusions. Such zones are described by their deformation parameters, which can often be regarded as constant throughout the zone.

Discontinuity may be of primary origin, such as bedding planes, voids and cavaties, or it may be caused by previous failure by fracture or shear. The latter type of discontinuities includes joints and faults. Crystal structure of rock substance may appear in the form of cleavage, schistosity or foliation. The effects of discontinuity upon the stress-strain behaviour of rock are:

1. Redistribution of stresses, where these cannot be transfered the discontinuity and
2. Increased deformability due to closure, opening or slip along planar discontinuities.

Internal Stresses occur in rock masses as a result of gravity and tectonic forces. Their effects may be simply superimposed on the effects of the applied loads, as long as the assumption of linear elasticity can be made on the entire area of the problem

The principle of superposition cannot be applied, however, where plastic behaviour exists such as rock yielding or opening or slippage along discontinuities. In the later case the deformed state of the rock mass under the action of the internal stresses must be taken as a starting point for the analysis of the imposed loading configuration.

Anisotropy occurs frequently in rocks as a result of an ordered crystal structure of the substance or as a result of the structure of the mass, for example thin layering, schistosity and foliation.

With respect to the above characteristics of a rock mass it is evident that deformability problems in such media are difficult to solve. Questions fall in three categories:

1. Determination of the mechanical properties of the materials.
2. Exploration of the geometrical configuration of the rock structure.
3. Prediction of the deformations under the influence of the expected loading.

The answers to the questions which fall into the fist two categories are used in the third category, and it is therefore logical to begin the discussion from there.

There are two basic methods of dealing with the question of rock deformations (26). The first, sometimes called the traditional method, considers rock to be a continuous medium. The advantage of this approach is that use can be made of the numerous analytical solutions obtained from the theory of elasticity of a continuous body.

Solutions exist, which include the effects of certain kinds of anisotropy and heterogeneity. Some of these will be discussed in the last part of this Thesis.

It is necessary for this approach to be realistic, to define the "overall" elastic parameters for the rock mass, that would include the properties of both the rock substance and the structural discontinuities. Thus in fact we seek to replace the discontinuous medium by a statically equivalent continuum. How successful would such replacement be depends upon whether it will be possible to ascertain correctly the magnitude of the overall elastic parameters. The most established way to measure these parameters is by in situ deformability tests. Of these the most widely used, the plate load test, will be discussed briefly in Section 1.3. Other methods include flatjack testing, radical jacking in borehole or adit and hydraulic chamber tests.

The second approach consists of treating the rock mass directly as a discontinuum. The means of doing this consist of the special theory of mechanics of discontinua developed by Trollope (48), Hayashi (22) and others, small scale physical modelling (for example Krsmanovic and Milic (23)), and finally numerical modelling based on the Finite Element Method (Goodman et al (19), Zienkiewicz et al (58)). Of these three methods, the last one will be utilized and discussed in the final part of this work.

The theory of the discontinuous approach has made much progress in recent years. With a sufficient amount of expenditure and effort it may be possible to account theoretically for almost any configuration of loading and rock structure. Difficulty, however, remains with obtaining the data for such analyses.

It is necessary to know the detailed geometrical configuration of the rock structure. For this purpose a "joint survey program" (12) has to be conducted in which the rock mass is explored by a number of boreholes, adits, or, where available, outcrops. The amount of work can be reduced by applying structural geological knowledge. In the words of N.Duncan (12) "The engineer's aim is to express, or have expressed for him, in a quantitative way, the present and future sub-surface conditons on the site, within the context of what is geologically feasible." Specialized literature exists (for example Price (41)), that can provide the engineer with quite a deep insight into the occurence and character of rock discontinuities.

The last and perhaps most formidable problem facing the designer who uses the discontinuous approach is the determination of the mechanical properties of all structural elements of the rock mass, e.g. the rock substance and the discontinuities. This is usually done by laboratory testing. For the rock substance alone the testing procedures have been well developed and standardized. Tests on discontinuities, on the other hand, have been conducted only recently, and in this field there are many uncertainties. One Chapter of the first part of this Thesis as well as the whole of the second part will discuss the deformation behaviour of discontinuities.

Section 1.3 Plate Load Testing in Situ.

The purpose of plate load testing is to subject the rock mass to compression on a scale so large, that the local effects of the discontinuous and heterogeneous features would become negligible. The interpretation of these tests with the assumption of continuity yields overall elastic parameters of the mass. In an inverse procedure, such parameters can then be used to predict settlements of the proposed structure.

The test load is applied onto the foundation surface through a loading plate, circular or square in shape. Plate sizes of up to three feet in diameter have been used. It is difficult, without previous knowledge of the deformation moduli of the foundation rock, to take the stiffness of the plate into account in the interpretation formulas. For this reason investigators attempt to utilize plates that are either very rigid or very flexible. (10) Rigid plates have only been used in smaller scale testing and have proven unsatisfactory due to plastic yielding of the rock material under the edges of the plate, which makes interpretation difficult (10). Flexible plates, on the other hand, have been used extensively, their flexibility being provided by wood, rubber or hydraulic cushions (49). The load on the plate can be obtained by a dead weight (for example, a large tank filled with water, (51)), or hydraulic jacks. With the latter method, obtaining a suitable reaction becomes quite a difficult problem. The most common solution is conducting the plate load test in an exploratory adit, where the force is created by jacking against the opposite wall. If it is more desirable to conduct the test

on the surface, rock anchors may be used to provide the required reaction (55).

Instrumentation of a plate load test may include measurements of both surface and subsurface deflections. In the case of an anchor test the anchor drill hole may be instrumented by extensometers, in which case the point of anchoring serves as the reference datum (55). Alternatively, the surface displacements may be measured by levelling from a distant reference point (51). In the tunnel jacking test the diametral deformation of the tunnel may be measured by a wire extensometer equipped with an electrical or mechanical gauge. It is also recommended that a hole be drilled into the wall behind the plate and again instrumented with extensometers so that the deflection may be measured at several depths (50).

Loading is applied in several cycles, the maximum load in each cycle being held until further creep deformation becomes small. By cycling the load, it is possible to distinguish the elastic, viscous and permanent deformation (7). Long-term tests have been conducted, in which the load had been held for as long as one year. But the creep deformation over such a long period does not appear to be significant (51). Due to the lack of more refined procedures, the majority of investigators use the simple Boussinesq theory for interpretation of the test results, integrating for the particular shape of the loaded surface and assumed rigidity of the plate. It is known, however, that the inherent assumptions of the Boussinesq's solutions are never fulfilled in a natural rock mass. If the tests are performed on the surface, the modulus of elasticity is often found to increase with the depth due to surface weathering and stress relief cracking (13).

In the case of a tunnel jacking test, a cracked zone disturbed by blasting or stress relief is always found around the perimeter of the tunnel. In addition to these "systematic" heterogeneous attributes of the rock masses, there exists an unlimited range of random features such as layers, joints, faults, altered zones or intrusions which invalidate the above assumptions.

The most common situation is the variation of the deformation modulus with depth such as in layered media. Several investigators have attempted to improve their interpretation by accounting for the heterogeneity of the ground in dealing with deformations, while invariably making the assumption that the Boussinesq's stress distribution is valid. The problem is thus reduced to one of scale (43). A plate load test is not a scale model of the prototype foundation even if the differences in shape and design details were disregarded. This is because it naturally is not possible to reduce the structural fabric of the tested ground to a corresponding scale. Waldorf et al (49) suggested a scaling technique by which one breaks down the measured settlements of the plate into fractions proportional to thickness and assumed average stress in horizontal layers. (A similar approach was shown in a paper on settlement in layered soils by Fischer (17). Deere et al (10) advise computing variation of the elastic properties with depth on the basis of subsurface deformations measured by borehole extensometers installed under the plate, using Boussinesq's formulas for subsurface settlements. Probably the most correct approach was demonstrated by Benson et al (1), who utilized a finite element program to fit a function of deformation modulus to the measured values of subsurface settlement by trial and error.

An important improvement in the plate load test interpretation is the use of solutions for transverse anisotropy (55, 21) or solutions which aknowledge the nonlinear deformation behaviour of the rock (13). Further discussion of some details relevant to the interpretation of the plate load tests will be presented in Part III.

In respect to the large amount of effort and expense involved in conducting a plate load test, it is evident that, even for large projects, the number of tests that can be economically carried out is severely limited. On many sites, however, the ground properties are extremely varied, and it is therefore necessary to correlate the results with the findings of suitable subsurface exploration programs. The exploration techniques used for such purpose include core logging, visual inspection of the rock features in shafts or with the use of borehole cameras, and sonic logging. With the exception of the Modified Core Recovery (RQD) and the sonic velocity ratio(10) no index has as yet been accepted as a standard. Good results have been reported (51, 3) by authors, who used verbal classification systems of rock discontinuities devised for the purposes of their particular projects. This leads one to a conclusion that it would be highly desirable if a universal, detailed system of classification of joints and joint systems could be developed and calibrated by general use. Besides spacing and attitude, this system would have to include, and measure quantitatively, such vital properties of joints as thickness and degree of weathering.

In conclusion one finds, in the voluminous literature on plate-load testing, that the testing technique itself is well developed and more or less standard. On the other hand, research is lacking

in the field of interpretation, especially where dealing with heterogeneous and discontinuous attributes of the rock mass. Also lacking is a reliable and inclusive system of classification of rock discontinuities.

Section 1.4 Finite Element Modelling Techniques.

The Finite Element Method is a numerical scheme, well adapted to automatic computation, which has recently found extensive use in the field of applied mechanics. It utilizes the Rayleigh-Ritz principle to define displacement functions on a number of finite subspaces (elements) into which the original domain of the problem is divided (56). The functions are usually defined in the form of polynomials, their order being dependent upon the number of connecting points (nodes) in each element and the number of degrees of freedom. The plane strain computer programs used for geotechnical problems generally utilize linear displacement functions (6). The size and number of the elements is arbitrary, their shape being usually triangular or quadrilateral.

The fact, that each displacement function is defined only on its particular subspace, makes the method exceptionally suitable to problems involving complex boundary conditions and heterogeneity. The method can include the effects of anisotropy, by using more general stress-strain relationships, and nonlinearity, utilizing an iterative procedure illustrated in Fig. 2.1.

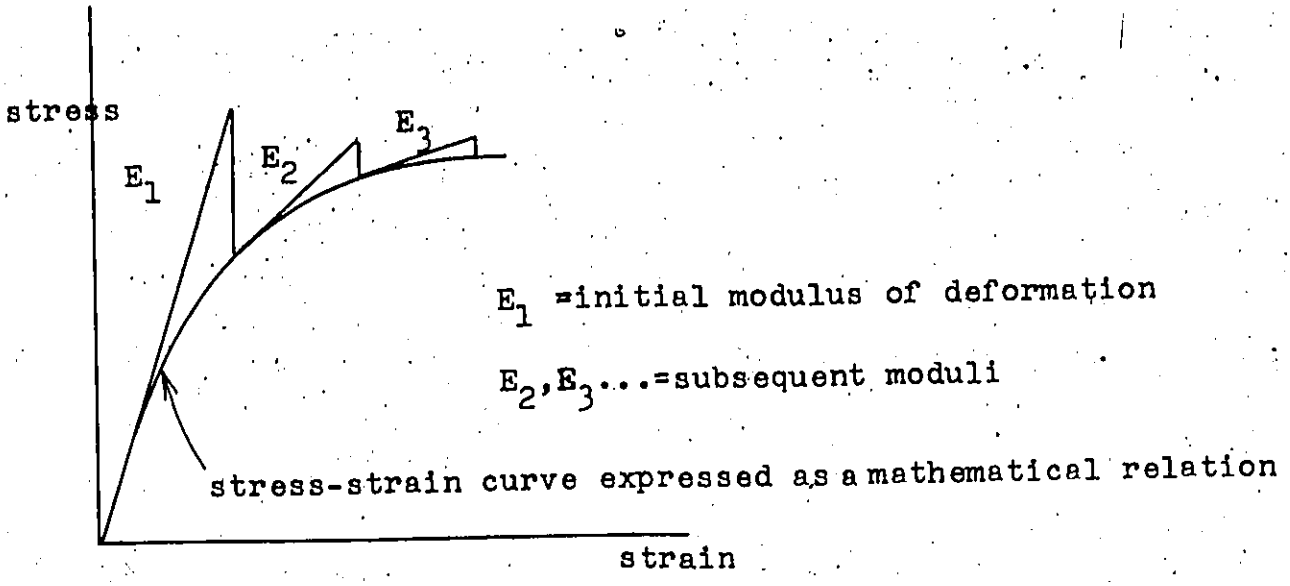

Fig. 1.1
Approximation of a nonlinear stress-strain curve by an iterative procedure. (Tangent modulus of deformation calculated on the basis of strain obtained in the previous step.)

The iterative procedure can also be used to account for the "no tension" behaviour (57). Residual stresses may be included in the solution as a boundary condition or directly as a body force inside each element (6).

Of special interest to rock mechanics has been the development of a one-dimensional element simulating the behaviour of planar discontinuities such as faults or joints (19). The stiffness equation for the element is derived in the same way as that of an ordinary quadrilateral element, the only exceptions being that it is considered of zero width, and the usual stress-strain relationships for continuum are replaced by joint stiffness equations (19):

$$\delta_n = \frac{\sigma_n}{k_{nn}} \qquad \text{Eqn. 1.1}$$

$$\delta_s = \frac{\tau_s}{k_{ss}} \qquad \text{Eqn. 1.2}$$

where: δ_n is the normal displacement across the joint

δ_s is the tangential displacement across the joint

σ_n is the normal stress acting on the joint

τ_s is the shear stress acting on the joint

k_{nn} and k_{ss} are the normal and shear unit joint stiffness coefficients defined as stresses required to cause an unit displacement across the joint.

A more rigorous consideration of the stress-deformation relationships in a rock joint brings to one's attention the fact, that the normal displacement also depends on the normal stress, through the phenomenon of dilatancy to be discussed in the following Chapter. The complete stress-displacement equation for a joint element then takes the following matrix form:

$$\begin{Bmatrix} \sigma_n \\ \tau_s \end{Bmatrix} = \begin{bmatrix} k_{nn} & k_{ns} \\ k_{sn} & k_{ss} \end{bmatrix} \times \begin{Bmatrix} \delta_n \\ \delta_s \end{Bmatrix} \qquad \text{Eqn. 1.3}$$

To the author's knowledge, there has been only one published report on using this more rigorous approach, the chief difficulty being that of obtaining suitable data.

The one-dimensional element can be used in conjunction with all types of linear displacement continuum elements.

Nonlinear attributes of joints can be accounted for by a similar iterative procedure as mentioned above (19): If the normal stress in any joint element becomes tensile in the first approximation, both k_{nn} and k_{ss} are set to zero and the calculation is repeated.

Similarly, if the shear stress on the joint exceeds the shear strength given by the Coulomb's strength envelope, k_{ss} is set to a residual value as indicated in Fig. 2.2.

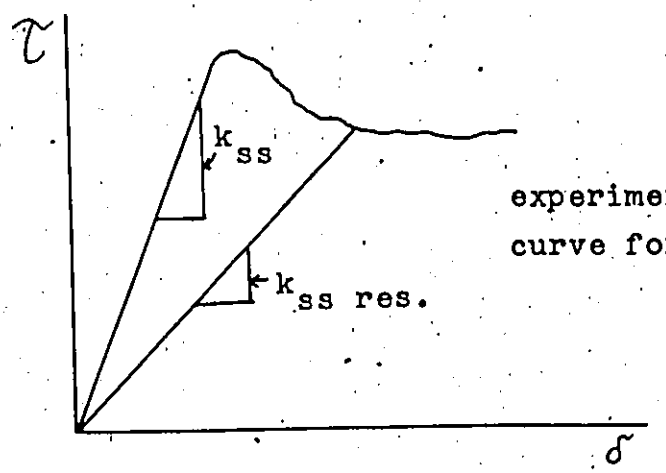

experimental stress-displacement curve for the joint

Fig. 1.2
Idealization of the sliding behaviour of joints in a Finite Element Solution (19).

Another nonlinear phenomenon, the joint closure, may be taken into an account by increasing the magnitude of the coefficient k_{nn} by a certain amount whenever the normal displacement across the joint element exceeds a specified value (thickness of aperture). Thus, the parameters required for each joint are k_{nn}, k_{ss}, k_{ss} residual, c (cohesion), ϕ (angle of friction), and Δh (aperture thickness). The iterative procedure is continued until a stable solution is found.

The use of the Finite Element Method extended by the joint elements may prove to be the most powerful means yet of approaching stress-deformation problems in rock masses while aknowledging their discontinuous nature. The main obstacle to such use however remains in the difficulty of obtaining suitable data concerning the behaviour of joints, such as the above mentioned stiffness parameters.

CHAPTER II

Deformability and Strength of Joints.

Section 2.1 Classification.

Joints, in geological terminology, are cracks in rock, distinct from bedding planes, which occur in spacing of at least several inches; and along which there has been no relative tangential movement in the geological history (2). This definition is a result of geological classification of discontinuities by origin. In rock mechanics such classification becomes less relevant (20) and the term joint will therefore be used in this work to describe all discontinuities in which two dimensions prevail over the thickness. Consequently, under the term joint we may imagine fractures, partings, bedding planes and thin faults.

Practical qualitative engineering parameters which can be applied to field classification of joints and joint systems, based on their external features were suggested by D.U. Deere (9):

- attitude: Strike and dip
- spacing:
  - < 2" very close
  - 2" - 1' close
  - 1' - 3' moderately close
  - 3' -10' wide
  - > 10' very wide
- tightness: tight (core can be fitted together exactly)
  open
- irregularity:
  - plane slick
  - curved smooth
  - irregular rough
- filling material distinguished by thickness, type and hardness

- alteration : fresh

altered by discoloration

severely altered

Another method of classification is based on the internal properties of joints, rather than external features. R.E. Goodman (20) divides joints into four types according to their shear deformation behaviour. This is depicted by the typical $\tau - \delta$ diagrams for each joint type in Fig. 2.1 (20).

Type 1 includes healed joints and incipient fractures.

Fig. 2.1
Different types of shear behaviour of joints (20).

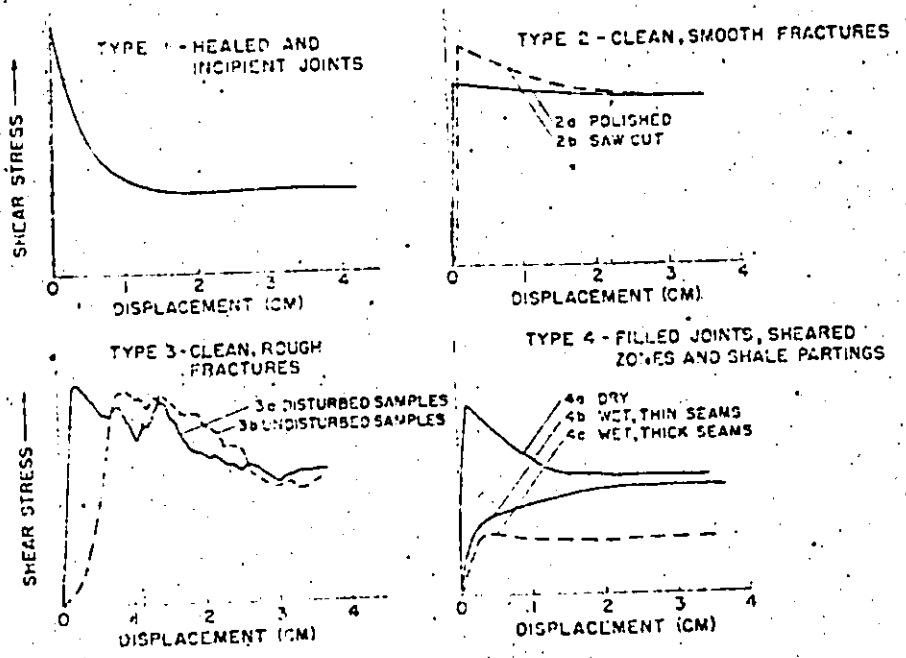

It is characterized by a sharp drop in strength as soon as the high initial peak is exceeded. Intact rock would also behave in a similar way. Smooth and polished discontinuities are represented as types 2a and 2b respectively in Fig. 2.1. Samples of this type do not exhibit a very large difference between the peak and residual strengths. Actually, for many smooth fractures the residual strenth is higher due to the development of ploughing (39). Type 4 represents rough, clean fractures which show secondary peaks due to repeated interlocking of the asperities after the initial failure. Considerable amount of yielding may be required for such behaviour to appear. With very small displacement the shape of the curve for these samples may fall between those of Type 1 and 2. Under Type 4 are described filled joints, sheared zones and shale partings which are sensitive to moisture content.

Classification using relative magnitudes of the numerical stiffness parameters, devised by Goodman, Taylor and Brekke (12) will be described in Section 2.5.

The qualitative classification of joints provides:

1. A tool for field surveys, which helps to define limits to generalization of test results, and

2. A means for grouping and consequently better understaning of test results.

In every case such classification must be supplemented by quantitative information in the form of numerical parameters, which will be discussed in Section 2.5.

Section 2.2 Testing Methods.

Shear tests on rock discontinuities may be carried out in the laboratory and in situ. Three basic arrangements of laboratory tests are shown schematically in Fig. 2.2. Fig. 2.2a represents a triaxial test on a rock core, drilled at a sharp angle across a joint, or an originally intact core purposely fractured or sawn. This test is usually applied to investigation of the strength properties rather than deformability and it is often conducted in the form of "multistage triaxial" (Heuze and Goodman, (23)). The confining pressure is set to a predetermined value and the vertical pressure is gradually increased to cause an incipient failure.

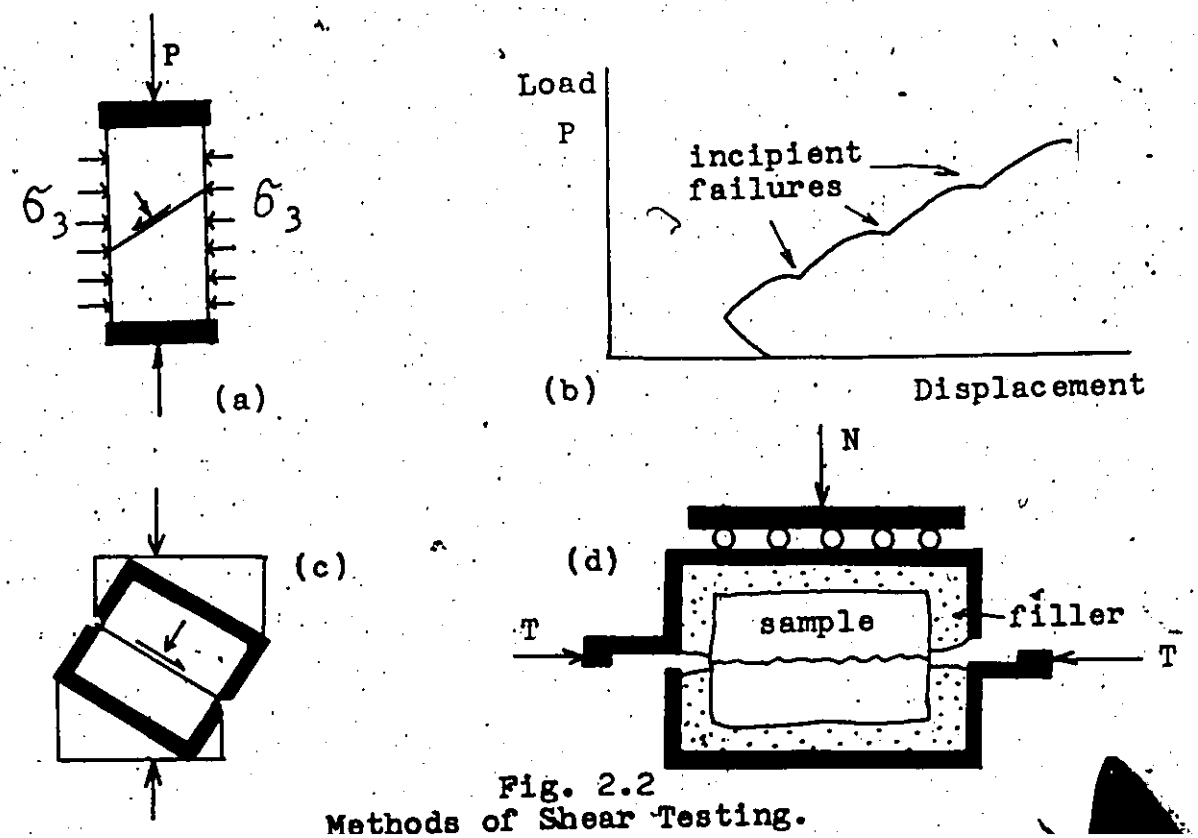

Fig. 2.2
Methods of Shear Testing.

Then the confining pressure is raised by a step and the process repeated, every time producing a singular Mohr's circle. The resulting load-deformation curve is shown in Fig. 2.2b. While this test is very efficient for obtaining failure envelopes of clean, tight joints, its usability for deformability testing is limited because:

a) Normal and tangential deformations are difficult to measure.

b) It is difficult to keep the normal force independent of the tangential force and

c) Large displacements cause tilting of the sample which invalidates the results.

Goodman (20) advises on the basis of a finite element analysis, that in wider joints of higher compressibility than the surrounding rock there exists in a triaxial test a very uneven distribution of stresses and the stress concentrations are different in the upper and lower walls of the joint.

The test arrangement in Fig. 2.2c eliminates disadvantages a) and c) of the triaxial test but retains the interdependency of the normal and tangential stress which again makes it impossible to measure the separate influence of the two on deformations.

The most convenient arrangement for deformability testing is the direct shear test depicted by Fig.2.2d. The test requires separate sources of load in the vertical and tangential direction. A specimen, which may either be a core or a block, is encased in concrete or epoxy with a suitable filler. One of the casings is usually fixed, whereas the tangential mobility of the other is provided by a slip bearing.

The shearing plane is usually horizontal but may also be vertical, the normal force being applied horizontally. The tangential force acts either parallel to the shearing plane or has a slight inclination. The source of the tangential load should be flexibly attached to allow free normal displacement (Fig. 2.3). Both tangential and normal displacements are measured. The normal displacements are sometimes measured in all four corners of the casing, to register any unusual tilting.

Table 2.4 presents parameters of some testing machines in use throughout the world. Of these, one of the most sophisticated is the testing machine of the Institute of Soil and Rock Mechanics of the Frederican University in Karlsruhe, Germany, described by N. Rangers, Fig. 2.3 (43).

In the following paragraphs some of the more important aspects of shear testing equipment will be discussed, together with problems that have to be overcome.

Lateral confinement is either provided for (plane strain test) or not provided for (plane stress test). The reason for excluding lateral confinement is, that certain irregularities of the tested surface may act as a pivot around which horizontal rotation of the upper half of the specimen may tend to occur. Such rotation introduces lateral stresses of unknown magnitude and distribution. It is the author's opinion, that such stresses must also occur in the field, where the lateral confinement does exist. Most machines apply the plane strain concept. Possibly the best solution to this problem is the arrangement by Rengers (43), who confines his specimens, but provides an "almost no deformation" load cell in the lateral direction to measure the lateral force (Fig. 2.3).

Fig.2.3

Shear testing machine of the Institute of Soil and Rock Mechanics of the Frederican University in Karlsruhe, Germany (43)

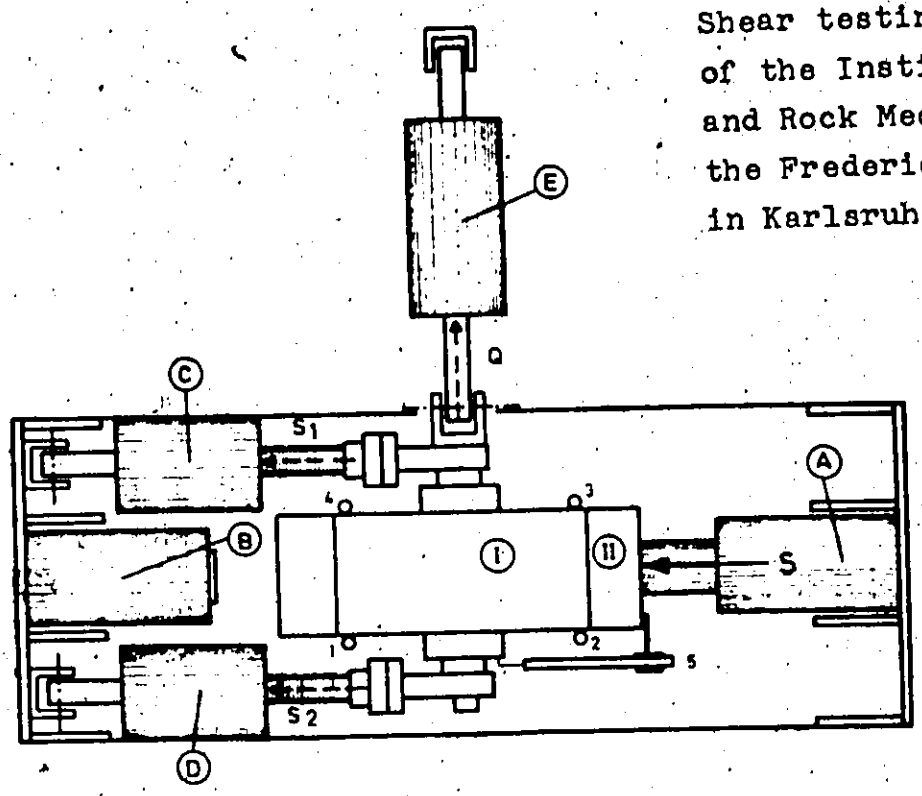

(a) Top view

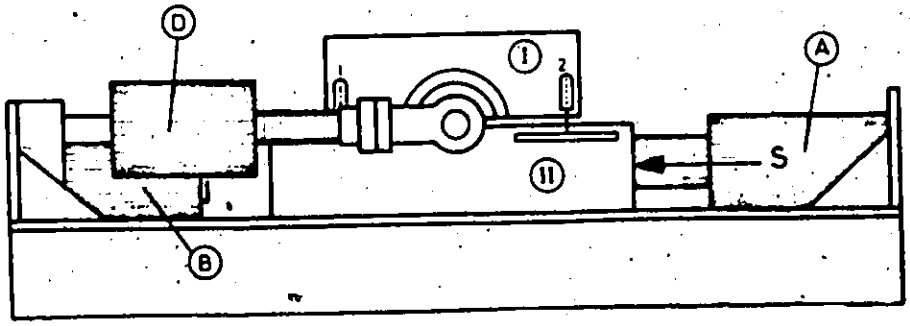

(b) Side view

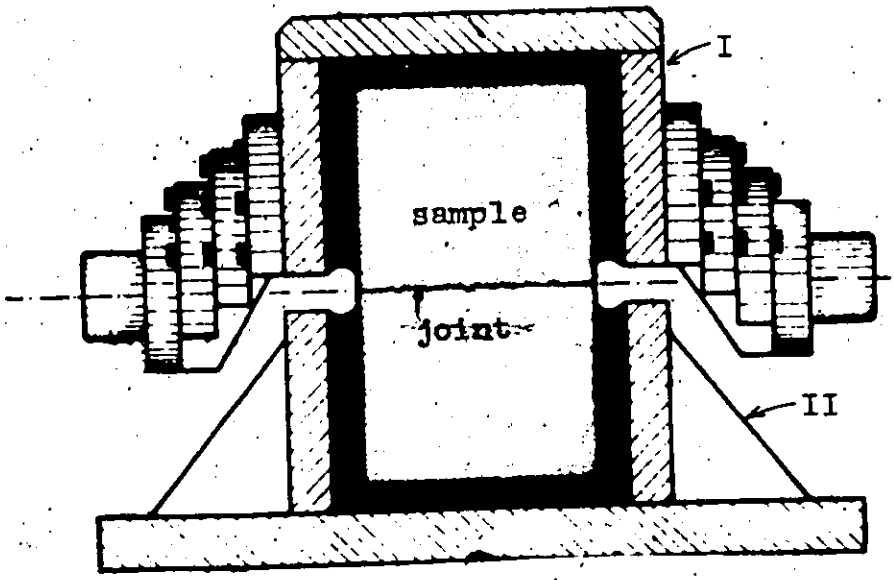

(c) crossection

Legend:

I, II - shear boxes

A, B - 50t hydraulic jacks

C, D, E - load cells

1, 2, 3, 4 = normal displacement gauges

5 - shear displ. gauge

Ref.	Schematic arangement	Sample Area	Shear Load	Normal Load	Max. Shear Stress	Max. Normal Stress	Slip bearing	Gauges	Special Features
Evdokimov, Sapegin, USSR (15)	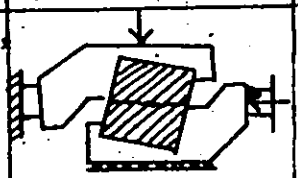	100 cm diam. core (1240 sq.in)	hydraulic jack 600 ton (metiric)	hydraulic jack 500 ton (metric)	75 kp/cm^2 (1070 psi)	65 kp/cm^2 (920 psi)	roller	mechanic. ±0.01 mm and ±0.002 mm	probably the largest in the world. samples encased in reinf. concrete
Krsmanovic, Jugoslavia (30)	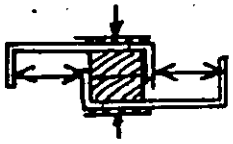	1600 cm^2 (248 sq.in)	four hydr. jacks tot.100t (metric)	two hydr. jacks tot.50t. (metric)	80 kp/cm^2	40 kp/cm^2	roller	-	plane stress machine both casings movable
Hoek, Britain (24)	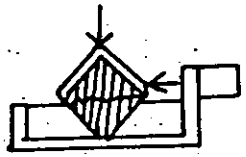	25 sq. in	hydraulic jack 5 ton	hydr. jack 5 ton	400 psi	400 psi	flex. yoke (steel rope)	-	primarily a field tool manufactured commercially
Rengers, Germany (43)	see Fig.2.3 page 26	600 cm^2 (93 sq.in)	hydraulic jack 100ton (metric)	four air bellows 50 ton (metric)	166 kp/cm^2 (2360 psi)	83 kp/cm^2 1180psi	teflon	LVDT's 4 vertic. 1 horiz.	lower sample longer to keep the area constant
Coulson, U.S.A. (8)	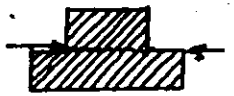	54 sq.in	worm gear 20 tons	hydraulic jack 75 ton	740 psi	270 psi	roller	LVDT's 4 vertic. 1 horiz.	---
Kenty U.S.A. (27)	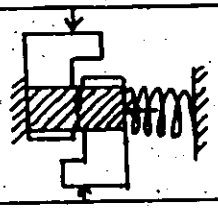	28 sq.in	compression testing machine 10 tons	coil spring 5 ton	720 psi	350 psi	ball bearing	-	suggested to the ASTM for standard. boxes made of alluminium

Table 2.4 Examples of direct shear testing machines.

Distribution of the normal stress. Because the tangential pressure is applied by the casing to the upper and front surfaces of the sample whereas the resistance is developed along the joint plane itself, there is also a possibility of overturning moments acting in the vertical plane. Theoretically, such moments should be eliminated by aligning the direction of the tangential force into the center of the loaded area, but experience shows that this sometimes does not help(20). The probable reason is, that the whole system of sample, infilling and casing is not sufficiently rigid and misalignment occurs by deformation of this system. The distribution of the normal and shearing stresses along the discontinuity will then be nonuniform. To prevent this as far as possible, it is necessary to

1. Align the applied forces precisely into the center of the tested surface
2. Choose specimens without anomalous features or surface irregularity and
3. Provide as rigid and complete confinement of the sample as possible.

Size of the specimens. The influence of the size of the specimens is inverse to that in uniaxial compression tests. The larger the plane tested, the higher the probability of occurrence of more significant surface irregularities. This phenomenon was noted by Evdokimov and Sapegin (15), who conducted laboratory tests on small samples (10 x 10cm) and large samples (cores 100cm diameter). They found increasing values of shear resistance in proportion to the size of the test. The magnitude of such proportionality will

obviously depend on the particular characteristics of each rock, so that correcting factors for small scale testing are not readily available. It is possible that this effect may be diminished by taking a larger number of samples from each joint. Also one should correct for any large scale curvature of the joint plane.

Normal force. In most designs of testing machines the normal force is kept constant during the test . Usually this is accomplished by using weight hangers or by regulating the oil pressure in the vertical jack during the progress of sliding. In a novel approach, the machine by Rengers (43) utilizes compressed air. Pressure is applied by four circular bellows made of Hart Rubber, such as are being used for the suspension of railroad cars and trucks. Each of the bellows develops a pressure of 10 this pressure remains constant allowing free vertical desplacement of several centimeters, or tilting. Some investigators (Lochner, (.35)) do not attempt to keep the normal pressure constant but rether measure its variation during the test. Such an approach has some advantage for testing for strength and will be discussed further in Section 2.3 in connection with dilatancy effects.

Field Tests in Situ.

The purpose for conducting shear tests in situ is to test large surfaces, in order to eliminate the effects of scale. There are, however, other factors which make this kind of test more difficult to interpret. Very large test blocks inevitably contain discontinuities or weaknesses other than the joint being tested and these, being deprived of the natural confinement, may lead to disruption of the block and uneven distribution of the stresses.

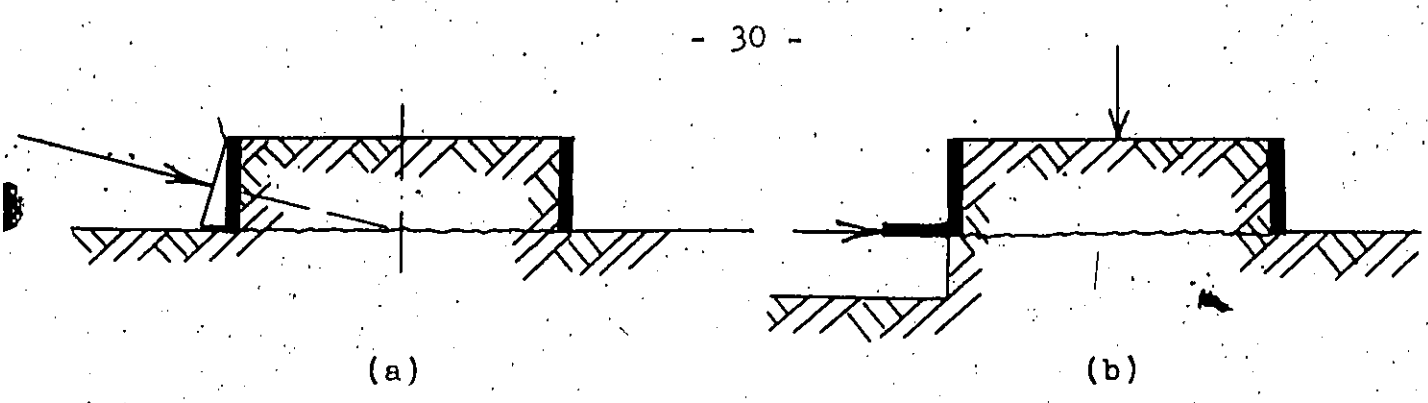

Fig. 2.5
Direct shear tests in situ (13).

The arrangement in Fig. 2.5a is the one most commonly used. The test block is encased in a frame of reinforced concrete or structural steel. Loads are applied by hydraulic jacks, but sometimes the normal load is provided by self-weight. One of the largest field tests ever conducted was carried out in the foundation excavation of the Bratsk Hydroelectric Project, USSR, where a block 7 x 7m of diabase rock was sheared off along a series of discontinuities. The procedures and results of this test as described by Evdokimov and Sapegin (15) illustrate the complex instrumentation and difficult interpretation procedure required to obtain conclusive results from such a test. The technique is very expensive due to the labor required and can usually only be conducted in connection with large and important projects.

Section 2.3 Behaviour in Shear and Sliding

Paragraph 2.3.1 Smooth Surfaces

The linear shear strength envelope is generally considered valid for smooth rock surfaces. For polished specimens the cohesion is zero, but there is a small cohesion intercept for saw-cut surfaces.

The residual strength of smooth planes is usually of the same order, or larger than the initial one. No general friction theory for rock has as yet been accepted. The "cold welding" theory (4) is not considered universaly valid. One of the arguments against the theory is the fact, that most minerals (except some, for example quartz) do not exhibit any significant difference between static and kinetic friction (25). In metals, on the other hand, such effect is observed and is usually explained by the above theory.

Fig. 2.6a shows a variation of the friction coefficient with displacement, obtained from triaxial tests on granite containing a planar, ground discontinuity (5). As the graph shows, the shearing resistance would increase throughout a fair amount of displacement.

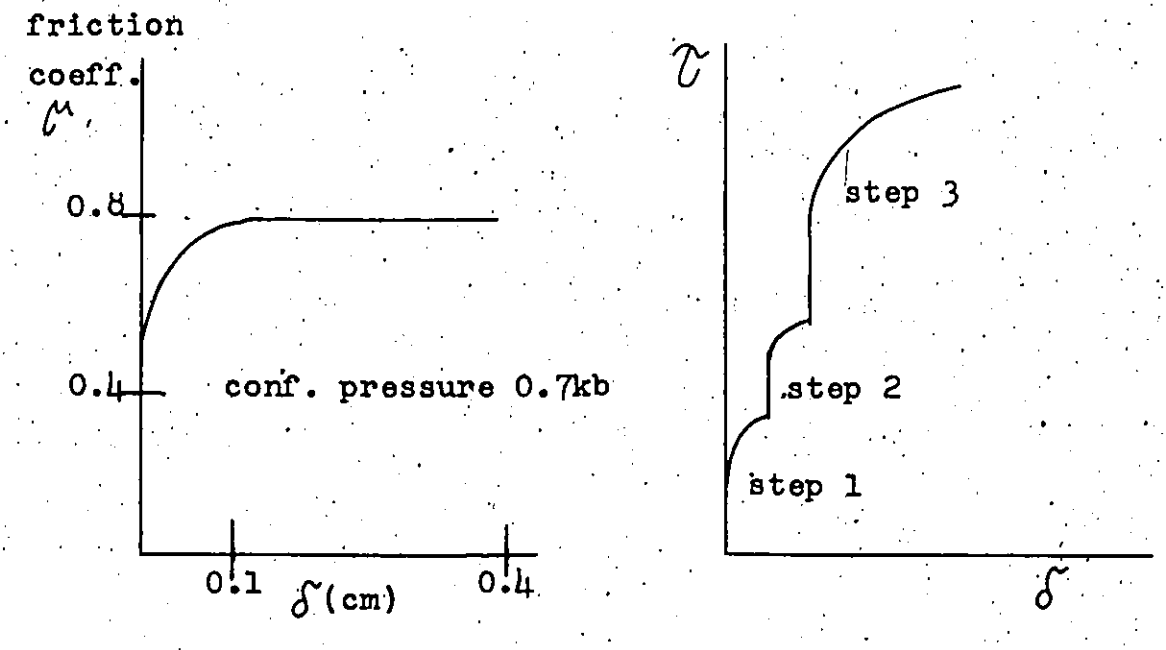

Fig. 2.6

Stress-displacement curves for smooth rock surfaces (5) and (39)

Similar behavior was observed on polished samples of limestone by Patton (39), Fig. 2.6b. Drawing from these results we could describe the characteristic shear behaviour of polished surfaces as follows: Very small or no displacement occurs until the initial shearing strength is reached. After the first movement, the shearing force must be continually increased to effect further movement, but after some displacement a constant residual value of friction is obtained.

Scratching and gouging is usually observed on the sheared surfaces after the test, and it is thought that this phenomena explains the increase of shearing resistance with displacement (39). Therefore, if a failure theory is sought for polished surfaces, it will probably have to contain some shearing and ploughing terms, such as developed by Bowden and Tabor (4) for metals.

Stick-slip oscillations are observed on some types of rocks (quartz) and are generally explained by a mechanical theory utilizing the difference between static and kinetic friction and the elastic flexibility of the loading system.

Almost all natural rock surfaces are more or less irregular, either by origin or due to weathering. Therefore polished surfaces will not commonly be encountered with the exception of slickensides on fault walls. Smooth, unpolished surfaces differ from polished ones by having a residual strength of the same order or lower, than the peak one . Gouging of the surface is again observed and is probably due to brittle failure of asperities (5). It is probable that friction of saw-cut surfaces differs from that for irregular surfaces only quantitatively, and it will not, therefore, be given separate discussion here.

Paragraph 2.3.2 Effects of water.

Horn and Deere (25) have shown by their experimants on friction of minerals that moisture has different influence on different types of rocks. Whereas the friction of softer minerals such as micas and talc is decreased by the addition of moisture, the friction of the harder ones is increased. The explanations of this behaviour are complex and not too well developed. An important fact is that the antilubricating effect of water on hard minerals diminishes with roughness of the samples and finally becomes nebligible at certain "critical roughness" (25). As these harder minerals usually form the contacts of clean, unfilled joints, we can conclude that for such joints the effect of moisture will be small, unless they are polished. On the other hand in joints filled with soft and altered minerals, moisture can play a significant role, especially where high sensitivity is encountered, In such cases the change in shear deformation behaviour would be similar to that shown in Fig. 2.7. Practices of soil mechanics apply to testing of these joints, e.g. it is important that the moisture content existing in the field be retained in the sample. For this reason, samples are often packed in parafin wax immediately after their excavation.

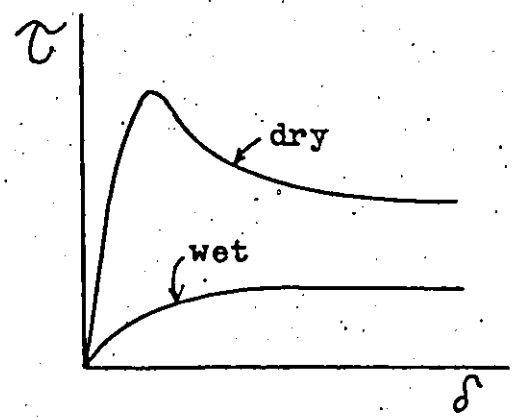

Fig. 2.7
Stress-displacement curves for filled joints

Besides the influence of moisture on friction of minerals, water also changes the mechanical conditions in a joint by creating pore pressures. This phenomenon was studied on granite samples by Byerlee (5), who concluded that the theory of effective pressures was in agreement with the behaviour observed. The Coulomb's Law for clean joints under the groundwater level can be stated:

$$\tau = c + (\sigma_n - u) \tan \phi \qquad \text{Eqn. 2.1}$$

where u represents the pore pressure,
c is the cohesion, and
τ and σ_n are the shear and normal stresses respectively

The important conclusion from this paragraph is that, unless we deal with filled joints or polished surfaces, the deformation behaviour will not be affected by the presence of water, except for the change in normal stress caused by pore pressure. This can be accounted for by using effective stresses.

Paragraph 2.3.3 Irregular Joints.

A simple explanation of the mechanism involved in shearing of irregular rock surfaces was given by Patton (39 & 40) and Goldstein et al (18). Both conducted experiments on plaster of Paris specimens, cast with geometrically simple irregularities or teeth. Fig. 2.8 shows the results of Patton (40) in shearing such specimens under two different values of constant normal force N. The mode of failure is seen to be dependent on the magnitude of the normal stress. When the normal force, N, is low

(case 1), the deformation increases elastically to some value, at which sharp increase in displacement occurs and the top specimen begins sliding up along the inclined surfaces of the teeth. The movement continues with constant shearing force until a point is reached, when the strength of the teeth is exceeded and they fail by shear or bending failure. The resistance to sliding then decreases to a residual value - $\tau_{1\ res}$. At high N (case 2), on the other hand, the shearing stress at the base of the tooth attains a critical value sooner than sliding up becomes possible and the teeth fail in shear immediately after reaching the peak strength of the material. Thus, except for the curvature of the $\tau - \delta$ curve for case 1 , the pre-peak stiffness of the joint (being defined as the slope of the $\tau - \delta$ curve) is basically constant, notwithstanding the ultimate mode of failure.

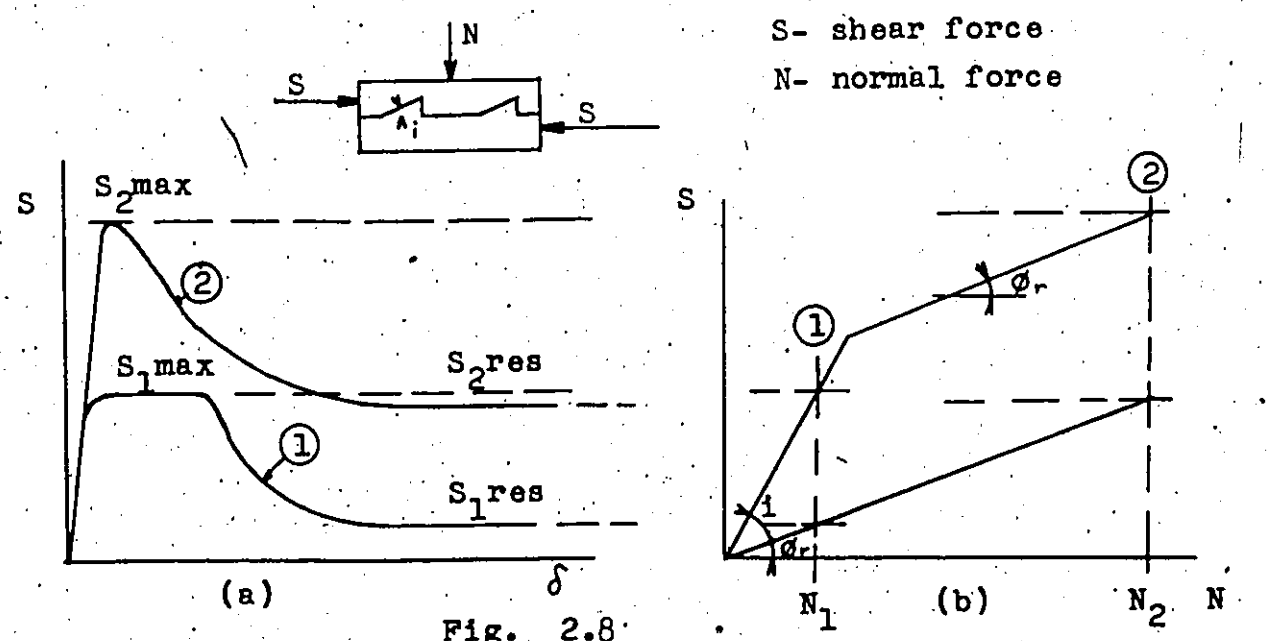

Fig. 2.8
Shearing behaviour of artificial joints (40).

With the assumption of ideally interlocking teeth, the only reason why there is any pre-failure movement at all must be due to elastic or plastic deformation of the areas of contact, (fig. 2.9),

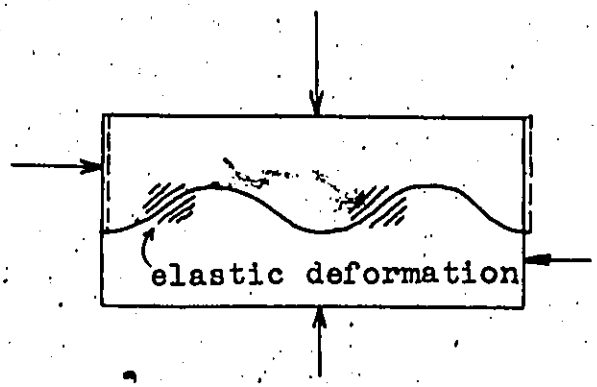

Fig. 2.9
Pre-sliding deformation of closed joints (53).

Withers (53) computed such deformation approximately for the case of sinusoidal teeth, using the Theory of Elasticity. He does not give any quantitative predictions of the pre-failure stiffness, but he shows by an energy analysis that the bearing of these deformations upon the magnitude of the peak stress is negligible.

The after-failure shape of the $\tau - \delta$ curve, on the other hand, is affected by the normal stress. Fig. 2.10 after Patton (39) shows the shear resistance envelopes at different magnitudes of post-failure displacement. It can be seen, that while almost no resistance is lost with movement of 0.05 inches and less at low normal loads, a large drop of resistance occurs at large normal loads where the shearing failure prevails.

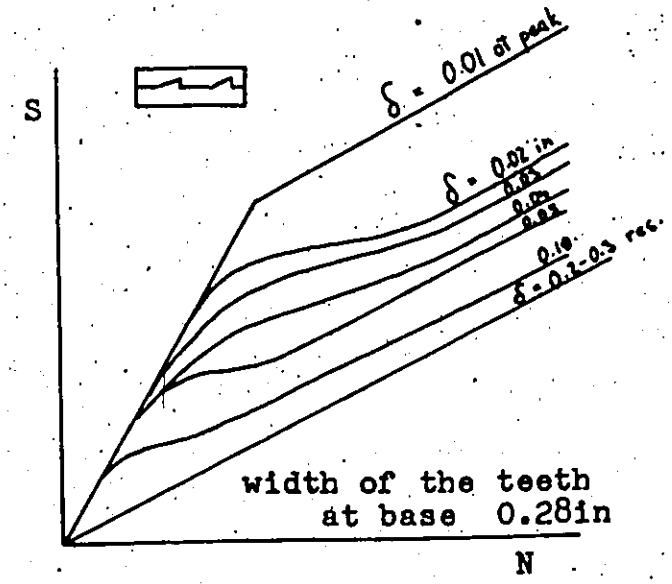

Fig. 2.10
Post-failure shear strength

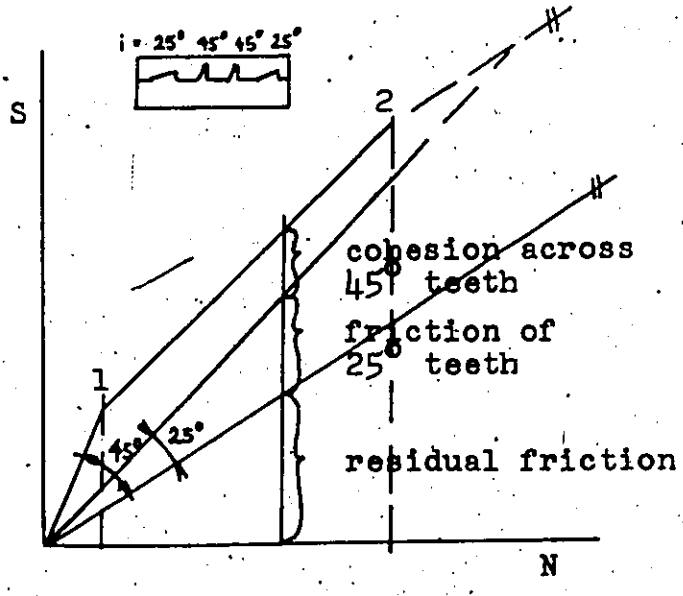

Fig. 2.11
Effects or asperities with different

Figure 2.1 shows another result by Patton (39). This is the result of experiments on samples, which contained teeth of two different inclinations, namely 25° and 45°. The modes of failure change at different magnitudes of the normal load for the two kinds of teeth. In the range between points 1 and 2 the resistance is derived from three components, as shown in Fig. 2.1 . It is interesting, that the cohesion across the 45° teeth in this case is only about one half of that measured on specimens with 45° teeth only. Patton explains this by an experimental error , but it could also be explained as a result of nonsimultaneous development of the peak strength on the two kinds of teeth. In other words, by the time the 25° teeth start sliding, the deformation may already have caused partial failure of the 45° teeth and a consequent decrease in their strength. Such results might be useful for explaining the fact that the pre-peak portions of the τ - δ curves for real rocks are often curved as in Fig. 2.12 and not straight as in Fig. 2.8a. The same consideration was used by Ladanyi and Archambault (33) to derive a theoretical curved strength envelope for rock joints with a shape similar to that often found from natural samples.

Figure 2.11 shows a typical set of shear stress-displacement curves and failure envelopes obtained by Krsmanovic et al (31) from tests on clean, irregular limestone joints. The failure envelopes are curved, which could be partially explained by Patton's results if one assumed a large variety of different inclinations. The stress-displacement graphs also exhibit considerable curvature. One important feature of these graphs is the fact that the parameter τ_{max} / δ_s, where τ_{max} is the peak strength and δ_s is the corresponding displacement, remains approximately constant and independent of the normal force. Therefore we may conclude, that

the stiffness parameter k_s may be independent of the magnitude of the normal force, as long as it is crudely approximated by τ_{max}/δ_s. If we took into account the different curvatures of the pre-peak portions of the $\tau-\delta$ curves, the stiffness would not be entirely independent of σ_n.

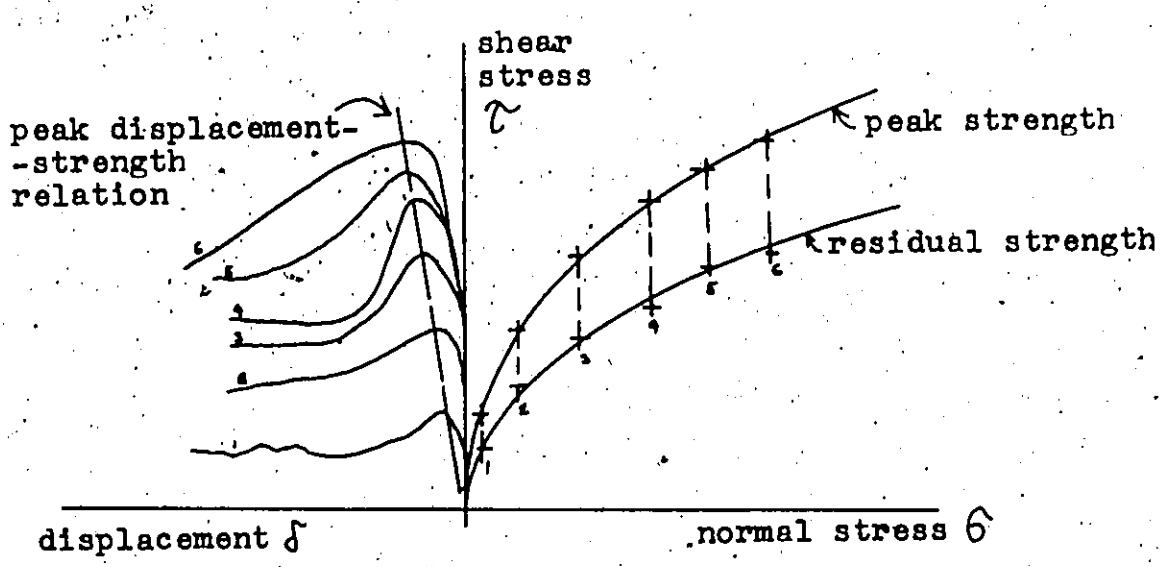

Fig. 2.12
$\tau-\delta$ curves for natural joints (31).

Byerlee (5) also found a strength-displacement relation for rough fractured samples of granite similar to that shown in Fig. 2.12. The frictional resistance was largest at a displacement of 1 mm and then fell steadily. He noted by microscopic studies, that at δ = 1 mm some irregularities were sheared off but others were intact. At $\delta > 1$ mm most irregularities were sheared off and the surface was covered by angular particles. This suggests brittle failure of asperities. A notable fact is that some asperities fail completely before the peak strength of the sample is reached. This snows that different types of asperities have different

deformational behaviour and it could explain the curvature of the pre-peak portion of the τ-δ graphs. Byerlee also concluded, that maximum frictional resistance occurs at closest contact of asperities. Therefore the tangential stiffness of the joint k_s will be greatly decreased if the joint is not completely interlocked. Consequently k_s will be dependent on the distribution and magnitude of the joint aperture.

Paragraph 2.3.4 Dilatancy and "Sliding Up".

Dilatancy is an effect, often observed before shearing failure in rocks, by which the volume of the material subjected to shearing strain increases. It was explained by Mencl (37) by the following two causes:

1. Tangential stress caused by the shearing force changes the state of stress in the body,
2. At high shear strain a change of the internal structure of the material occurs.

Dense and strong rocks generally exhibit an increase in volume (dilatancy), whereas porous and weak materials, like joint fillings, contract (contractancy). The volume change only occurs in the failure zone. An example of dilatancy for claystone samples is shown in Fig. 2.13, (37).

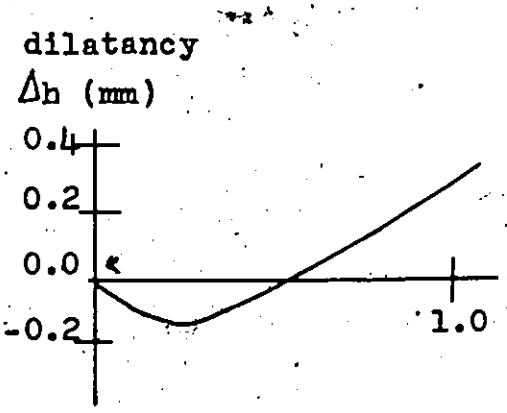

Fig. 2.13
Normal movements during shear of a claystone sample (37).

The shearing zone contracts slightly at first, but then it increases in volume.

Generally, shearing zones in fractures of dilatant material (hard rock) are relatively thin, so that the amount of dilatancy is rarely significant. On the other hand, contractancy of soft filling materials especially in wide joints may be fairly large.

Another phenomenon causing normal movements during shear along discontinuities is sliding up (or down) along the inclinations of asperities. This behaviour is often also included under the term dilatancy. It is observed right at the peak stress at low normal loads, but considerably after the peak stress at high normal loads (20). This is consistent with Patton's observations, which show sliding up at failure for low normal stress. According to this theory, the amount of sliding up should equal to

$\Delta h = \delta \times \tan i$, corresponding to the direction of the movement up or down the inclinations (which is given by the difference between disturbed and undisturbed samples.).

Fig. 2.14 shows plots of τ versus σ_n obtained by Locher (35) on sandstone. The machine used in these tests was not equipped for keeping the normal load constant, so that any amount of dilatancy causes an increase in normal stress. The change of the normal stress during the test is recorded by curves 1 and 2 for the two directions of movement.

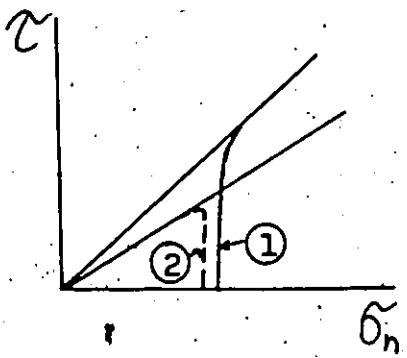

Fig. 2.14
Stress paths for dilatant (1) and contractant (2) movement along joints (35).

It can be seen, that the "sliding up" effect begins at the moment of failure. The figure also demonstrates the difference in shearing strength for the two directions of movement.

Sliding up movement usually does not follow exactly the curved surfaces of the asperities. Rengers (43 & 42) surveyed joint surfaces by stereomicroscope and devised a method by which he geometrically predicted amounts or sliding up, assuming that the surface or the irregularities will be followed exactly. Then he conducted shearing tests on the samples which had been surveyed. The results of both predictions and tests are shown in Fig. 2.15.

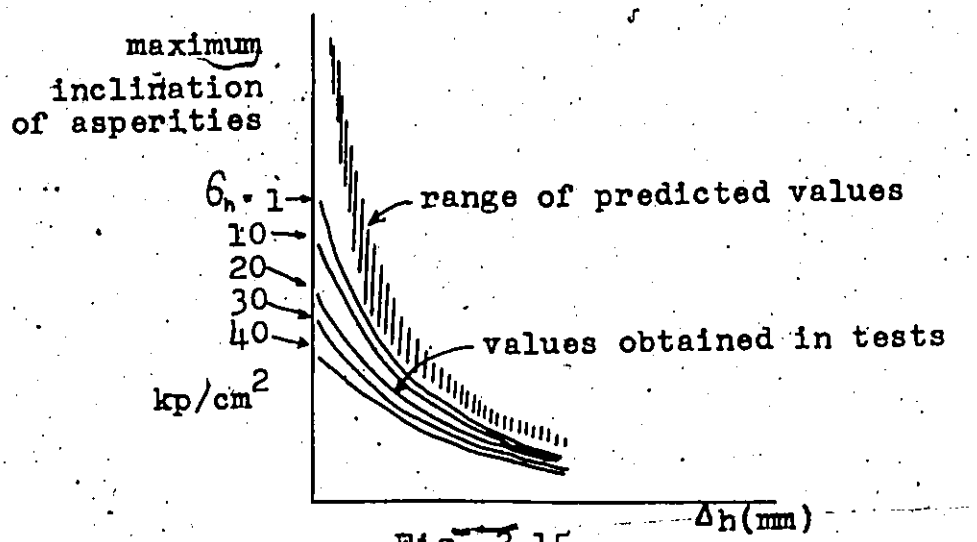

Fig. 2.15
Dependence of dilatancy on normal stress (43).

The actual amount of sliding up is always lower than the amount predicted, and more so with increasing normal stress. This is explained by Rengers by the fact, that some asperities are sheared through rather than slid over. In correspondence with Patton's theory, their number increases with the value or the normal stress.

The effects of the normal movement caused by shear upon the shearing process itself is described by Withers (53), who restates

Coulomb's Law as:

$$\tau = (\sigma_i + k\Delta h) \tan (\phi + i) \qquad \text{Eqn. 2.2}$$

where σ_i is the initial normal stress and
k is the elastic constant of the confining mass.

The coefficient k could be enumerated by E/l where E is the in situ deformability modulus of the mass and l is the effective length of free deformation. Near the surface, l is equal to infinity and k is consequently zero. In confinement l will be dependent on the total structure of the mass, for example joint spacing. In a regularly jointed mass where all joints are subjected to the same shear, l would equal to the spacing. As most of the dilatant effects occur near or at the peak strength, the pre-peak stiffness of the joints will not be affected.

Paragraph 2.3.5 Filled Joints.

A typical set of stress-deformation diagrams shown in Fig. 2.16 for a 6 cm wide joint in limestone, filled with clay was obtained by Krsmanovic et al(31). The deformation and strength behaviour of such joints is similar to that of the filling material alone. With the thickness of the filling decreasing, or the amplitude of the joint irregularities increasing, however, the shearing behaviour will change and will become more similar to

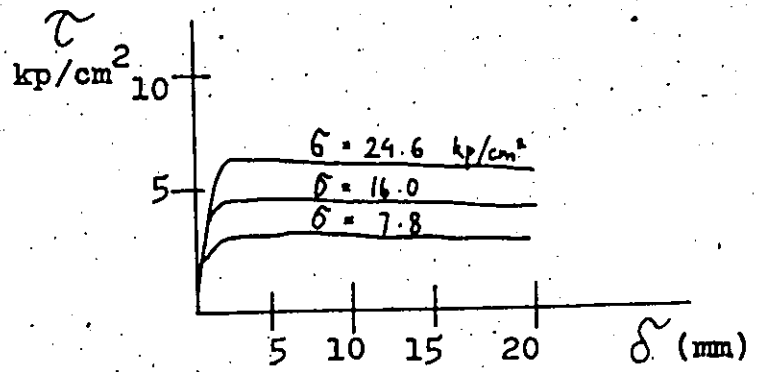

Fig. 2.16
Stress-displacement curves for filled joints (31).

that for clean, irregular joints. This was shown by Goodman (20) who conducted experiments on artificial samples made of plaster of Paris, with geometrically irregular joints, filled with crushed mica. He defined percentage of joint filling as the ratio of thickness of the filling (measured perpendicularly to the mean plane of the joint) to the amplitude of the irregularities times 100. The variation of the shearing stiffness and strength of the joint with the percentage filling is shown in Fig. 2.17, and compared with the properties of the filling material itself.

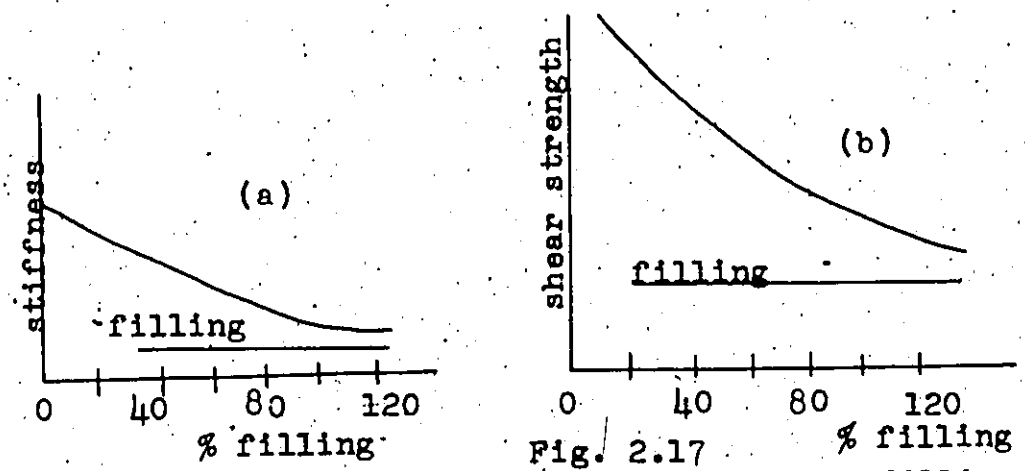

Fig. 2.17 Shear stiffness and strength versus percentage filling for artificial joints (20).

Both stiffness and strength are appreciably higher than those of the filling material alone, for percentages up to well above 100%. This indicates the influence of stress concentrations in the filling material, caused by the irregularities. The dependence of the normal deformations on percentage of joint filling is shown by the idealized curve in Fig. 2.18. The effects of sliding up and contractancy cancel each other at 80% filling.

As is the case with clays in any other engineering situation,

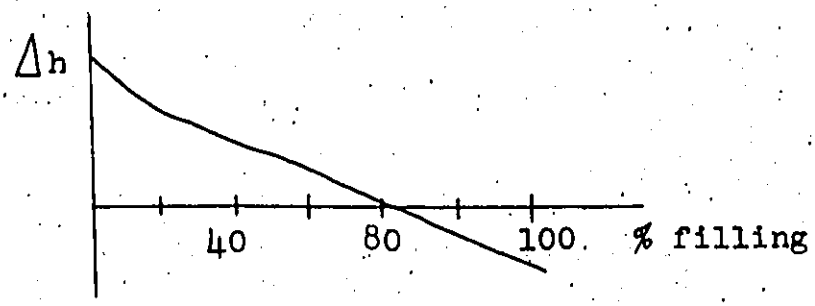

Fig. 2.18
Normal deformation versus percentage joint filling for artificial joints (20).

care must be taken of sensitivity. Shrinkage or squeezing out of the soft infilling material will only cause normal displacements, but swelling may decrease the shearing resistance of the joint radically. The decrease is due partly to the loss of the shearing strength of the filling material itself and partly to the diminishing of the effective stress on the rock asperities. The concept of effective stresses could be applied, if the pressures involved were known.

Section 2.4 Joint Closure and the Concept of Contact Stresses.

Walls of a natural joint are never in contact over their entire surface. Duncan and Hancock (11) developed a method for measuring the actual contact area. A sheet of pressure sensitive paper is inserted between the two halves of a sample, which is then subjected to compression. Load is increased in steps and the sensitive paper is removed or replaced by a fresh sheet after each step. The contact area appears on the sensitive paper as a pattern, called an impressograph. The area can then be measured by a planimeter or by a special apparatus measuring the intensity of light

passing through the impressograph. On the basis of a large number of such experiments Duncan (12) arrived at the following conclusions:

a) The real contact area is often only a fraction of the apparent total area across the joint,

b) The contact area increases as a function of the applied load,

c) Induced tensile fracture of asperities may occur at high loads,

d) The stresses on the contacts often attain values considerably in excess of the uniaxial compressive strength of the rock material.

With the help of these results, the process of joint closure is described by Duncan on three diagrams shown in Fig. 2.19. In diagram (a), at low load, the tips of the asperities are in the state of triaxial stress. The pressures on the small contact area are very high, and exceed the penetration strength of the material (usually given as three times the uniaxial strength). The asperity deforms plastically as shown in diagram (b). The contact area is increased and the state of stresses changes

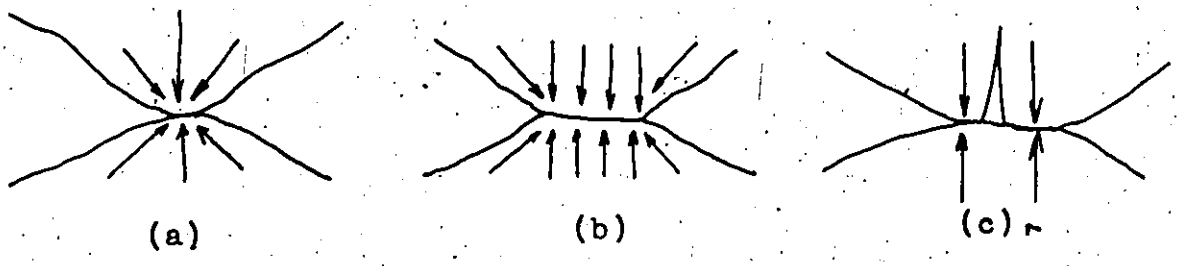

Fig. 2.19
Three stages in the process of joint closure (12).

gradually from triaxial to uniaxial. Vertical closure of the joint is observed. When the contact surface is flattened out sufficiently, almost a true uniaxial stress condition exists and induced tensional fractures form, if the uniaxial strength is exceeded.

The above process may be described quantitatively with the help of the following parameters (Duncan and Hancock (11)).

- average stress $\sigma_t = \frac{W}{j_t}$ is the stress induced on the whole apparent area of the sample j_t by the load W.
- joint contact factor $C = j_c/j_t$, where j_c is the real area of contact, determined from impressographs.
- thickness of the joint j_t, defined as the closure, which must occur for the joint surfaces to be perfectly in contact (C = 1.0). It is the maximum aperture depth along the joint. Its measurement is accomplished by a precise feeler gauge, a cast of thixotropic material in wider joints or seimic velocity across the sample.

The last method must be evaluated by correlation, but is advantageous, because measurement can be conducted during loading of the sample.

Using the above parameters, the contact stress on the surface asperities is:

$$\sigma_a = \frac{W}{j_c} = \frac{\sigma_t}{C} \qquad \text{Eqn. 2.3}$$

The actual relationship between σ_t and C, recorded by Duncan(12)is shown in Fig. 2.20. The curve is nonlinear, because P decreases with increasing contact area as described above. The ultimate failure of the sample occurs approximately at

$C = \frac{\sigma_t}{U_c}$ where U_c is the uniaxial strength of the material.

Reversing this relationship:

σ_t at failure = U_c x C Eqn. 2.4

Because C is always smaller than 1.0, we can see, that a sample in uniaxial compression, containing a horizontal discontinuity, will fail at lower stress than a continuous sample.

Deformation of the joint is described by the coefficient of volume decrease:

$$m_v = \frac{\text{change in unit volume}}{\text{change in pressure}}$$ Eqn 2.5

It is also given by an expression:

$$m_v = \frac{dJ_t}{J_t} \times \frac{1}{d\sigma_t}$$ Eqn 2.6

So that $dJ_t = m_v J_t d\sigma_t$ (J_t is the original thickness of the joint and dJ_t is the change in thickness).
Such relationship is plotted in Fig. 2.21, obtained also by Duncan (12).

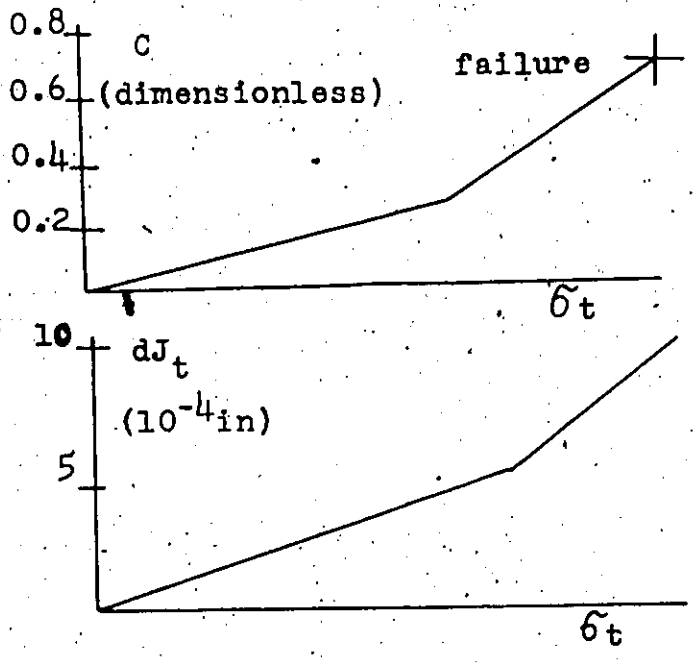

Fig. 2.20
Joint contact factor versus total normal stress (12).

Fig. 2.21
Change in joint thickness versus total normal stress (12).

It may be seen, that that the relation to the applied stress of the joint thickness is similar to that of the contact factor. Figure 2.21 actually represents a stress-deformation curve for a clean joint.

Section 2.5 Deformation Parameters for Joints, Summary.

At the end of this Chapter it is necessary to review the parameters which serve for a quantitative numerical description of the stress-strain behaviour of joints.

Goodman, Taylor, and Brekke (19) define three basic parameters describing pre-failure deformability of joints:
"k_s", the unit shearing stiffness along the joint has already been introduced in Sections 1.4 and 2.3. It has dimensions of force/length^3 and represents the slope of the pre-peak portion of the τ - δ curve. In a rough approximation it can be evaluated as τ_{max}/δ_{max} where τ_{max} is the peak shear strength and δ_{max} the corresponding displacement (Fig. 2.22).. Another, probably more realistic method is to evaluate k_s as the tangent of the secant angle at the yield point, the later being defined as the point where the τ - δ curve becomes nonlinear.

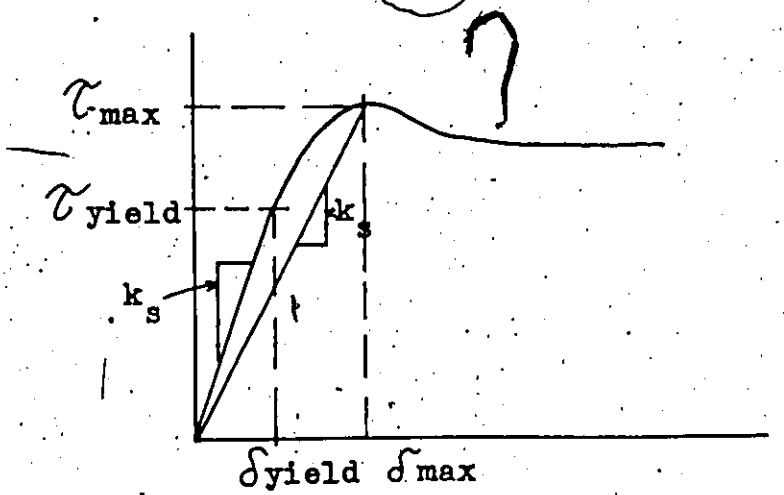

Fig. 2.22
Two methods of evaluating k_s.

Goodman (20) collected a large number of results from laboratory and in situ direct shear tests on different types of joints. The values of k_s range between 0.05 x 10^4 and 12 x 10^4 psi/in

(140 and 3200 kp/cm^3). The differences between k_s computed from the peak strength and that obtained from the yield point reach as high as a factor of 10, although often they are much smaller.

"k_n", the unit normal stiffness across the joint, has the same dimensions as k_s and represents the relationship of normal stress to normal displacement. The relationship is usually nonlinear as shown in Fig. 2.21[1]. Numerical values of this coefficient are virtually impossible to find in the existing literature as indeed are any accounts of normal compression tests on rock joints, with the exception of the work carried out by N. Duncan (12 &11).

"S", the shearing strength of the joint, is given by a shear strength envelope. The envelope is generally curved, but a Mohr-Coulomb strength envelope or some more complex function can be fitted to the data.

A classification of joints on the basis of the magnitude of the three parameters has been suggested (19). The parameters could be rated as high, moderate or low although the authors do do not define precise numerical limits to such descriptions.

Another parameter, mentioned by Ref.19, is k_{ns} (force/length^3) representing the tangential stress required to cause a unit displacement in the normal direction. This would describe dilatancy or contractancy of the joint and would be related to both k_s and σ_n. Similarly, k_{sn} would express the tangential movement (due to sliding down the inclinations of the asperities), which could accompany the application of the normal stress. Although most of the workers who conducted direct shear tests measured normal

---

[1] The slope of the curve is given by $m_v \, \sigma_t$, but m_v is not a constant.

deformations, the published information from which the magnitude of k_{ns} could be derived is scant. To the author's knowledge no experiments have ever been carried out to find the value of k_{sn}.

Literature related to the topic of shearing behaviour of rock discontinuities is extensive. As a result of the prevalent use of limit equilibrium methods in rock mechanics problems, practically all of this literature is preoccupied mainly with shear strength. Any published information on deformability of joints thus appears only as a byproduct of the investigators' effort. With increased use of both physical and numerical modelling techniques, however, it seems that specialized research on deformability of discontinuities is needed.

On the theoretical side such research may follow the lines pioneered by Ladanyi and Archambault (33). Specifically, the fact that, during shear, different asperities are undergoing different modes of failure simultaneously, if investigated further, could perhaps bring one to conclusions on:

1. Whether, and to what extent, should the stress-deformation curves be linear, and
2. What kind of relation is there between the unit shear stiffness coefficient and the magnitude of the normal stress?

Such conclusions would throw light on experimental results and might possibly pave the way to development of methods of estimating shear deformability parameters from the geometry of joint surfaces.

On the experimental side, advances could be made in all aspects of joint deformability measurements, but especially in:

1. Developing suitable classification systems for joints and correlating them with experimental results,
2. Proving relations among the different parameters and variables involved such as k_s and σ_n, k_s and τ_{max}, k_s and k_{ns}, etc.
3. Obtaining basic numerical values, especially for parameters k_n, k_{sn} and k_{ns} for different types of joints.

The following part of this Thesis will be concerned with some of these questions.

PART II

Laboratory Measurement of Deformability and Strength of Planar Discontinuities in Rock.

Objectives: Testing of discontinuities as important elements of the structural system represented by a rock mass is becoming quite widespread tool of rock mechanics at least in connection with large projects (cf. Section 2.2). The purpose of this part of the present research program was to make an attempt at developing a method of sampling and testing rock joints with a particular emphasis on determining the behaviour and quantitative parameters relating to deformability rather than strength. The following two chapters describe the sampling procedure, sample preparation, testing machine and, finally, the results of a testing program involving joints in three types of rock. In Chapter 5 the results are discussed both from quantitative and qualitative point of view with the aim of:

1. Presenting deformational parameters for the particular types of discontinuities tested, and estimating the significance of these parameters in respect to the deformability of the rock mass, and
2. Qualitative description of the observed behaviour in its different aspects and relationships.

For convenience in presentation, the bulk of the numerical and other data has been moved to Appendix A.

CHAPTER III

Sampling

Section 3.1 Description of the Samples.

Specimens for the present testing program were extracted from the two most abundant rock formations in the Ottawa area, namely the Ottawa Limestone and the Nepean Sandstone.

Limestone, constituting a great part of the Ottawa Formation, occurs in the vicinity of the Capital in thicknesses of at least 150 ft (52) and frequently it outcrops or lies immediately below the surface deposits. The samples were obtained at a quarry of Francon Co. Ltd. on the eastern outskirts of the City, where the horizontally lying strata are exposed to a height of about 100 ft. The rock is dark gray in color, fine grained to crystallic, medium hard (hardness approximately 3 to 4) containing fossils. The thickness of beds at this location varies from a few inches to about five feet with no particular trend. Bedding planes are planar and horizontal, rather diversified in roughness and degree of weathering. Most of these planes are tightly closed, although occasionally some are found containing clay infilling in thickness of up to 3/4 of an inch. In addition to bedding planes, the rock contains a large number of horizontal cracks which may be the result of the strong tendency of the rock to split parallel to the bedding. Shaley partings, often curved and of variable thickness are also common. Vertical joints are not quite systematic and rarely continuous across more than one or two beds.

The Nepean Sandstone Formation spreads, directly under the surface, across the western vicinity of the City of Ottawa, reaching a thickness of up to 500 ft (52). The samples were taken from a highway cut adjacent to the property of the Mines Branch on Moodie Drive. The rock is composed of fine to medium-fine rounded particles of quartz, cemented very lightly with siliceous material. The outcrop is approximately 30 ft high and reveals planar, horizontal jointing spaced 4-6 inches and more. Master vertical joints are spaced about 12 ft. Other vertical joints are discontinuous and irregular in spacing and strike. Few of the joints are weathered and most, with the exception of the vertical master joints, are tightly closed. No filled joints were noticed at the site.

The third and smallest group of samples originates from a deep mine at Wawa on the northern shore of Lake Superior. The rock is siderite, light green, very fine grained and waxy in appearance, medium hard. The specimens were cut from a 10 inch core of solid rock and fractured by triaxial testing. Although siderite typically develops conchoidal fracture, the cracks tested were planar and smooth, with the exception of step-like ridges fractions of an inch in height. The orientation of the fractures was about 60^{o} to the axis of the core (Shear cracks).

Altogether ten samples each were tested of limestone and sandstone, and six of siderite. In each group two specimens were divided artificially by a fairly smooth saw cut, the rest were natural joints. Table A.1, Appendix A, contains description of each sample using the classification of joints slightly modified from that suggested by Deere (9) which was mentioned in Part I.

The recorded factors are:

Tightness:
- bonded or incipient
- tight (hair crack)
- closed
- open or filled.

Surface features:

Primary curvature: (irregularities with wavelength greater than 6")
- planar
- slightly curved (amplitude $< \frac{1}{2}$ inch across the width of the sample, e.g. 6")
- curved (amplitude $> \frac{1}{2}$ inch across the width of the sample).

Secondary curvature: (irregularities with wavelength smaller than 6")
- given average approximate amplitude/wavelength (example 0.5/2 means 0.5" amplitude and 2" wavelength).

Surface roughness:
- smooth
- rough — angular / rounded

(roughness can be seen by naked eye).

Alteration:
- fresh
- discoloured
- weathered in depth

Contact (observed after test):
- well distributed
- concentrated in one or two large spots
- isolated in several small spots.

Contact area was not measured, but it could be estimated from the extent of crushed zones which are visible on the photographs of sample surfaces after testing (Plates 7 to 11).

As will be explained in the next Section, the sampling procedure resulted in a rather selective choice of joints to be tested. Most of the samples were taken from fresh, closed, unfilled horizontal fractures. This is an unfortunate fact, but it had to be accepted under the limitations of the present testing program. Only samples No. 1 and No. 6 can be identified as containing major bedding planes. No open, filled or heavily weathered joints had been sampled although such samples would have been highly desirable.

Section 3.2 Sampling Technique.

The process of obtaining the samples consisted of the following steps:

a) Extracting blocks, divided by joints, from the outcrop and transporting them into the laboratory.

b) Cutting samples of appropriate size (6" x 6" x 5" max) out of the blocks.

c) Casting the samples in concrete

d) Cementing the casts in the steel boxes of the direct shear machine.

Blocks were separated from the outcrop manually, with the help of hammers, chisels and crowbars. With such technique one cannot, in most cases, remove blocks without opening the joint they contain, unless the later is well bonded. Clean, unfilled and nonweathered joints can easily be reassembled, as long as no more serious disturbance of the joint surface is allowed such as shearing off or crushing the asperities. For this reason the blocks were handled

with care during their transport to the laboratory. Heavily weathered, compound or filled joints, on the other hand, are irreparably disturbed when opened, as the filling gouge falls out. Reassembling of such samples is impossible.

Another disadvantage of the manual technique is that one can only obtain blocks in such parts of the outcrop where there is abundance of vertical fractures or, in other words, where the rock mass is sufficiently broken. In these areas, however, the major joints are not likely to be preserved. On the whole it is hardly possible, by using the manual technique, to obtain samples from other than clean, closed joints. To sample thick weathered or filled joints one would have to use more sophisticated methods of rock separation such as hand diamond sawing, large diameter core drilling or wire saws (20).

In the laboratory the samples were cut in suitable size out of the blocks using a 36" diameter diamond saw. Cutting was done on both halves of the block assembled and clamped together. The finished sample was bound tightly with wire (Plate 6). The shape of the cross section of the specimens was not kept exactly rectangular in order to save on the amount of cutting.

Diamond saw cutting presents another problem when sampling filled joints because the cutting fluid would inevitably enter the joint causing leaching out or swelling the gouge.

The finished samples were cast in cement mortar in a three-part plywood mold shown in section in Fig. 3.1b which can also be seen on Plate 6 . The mortar was prepared of medium sand and alumina cement ("Cement Fondu") mixed in a ratio of 3 : 1. The 24 hour crushing strength of the mortar was measured as 5 500 psi.

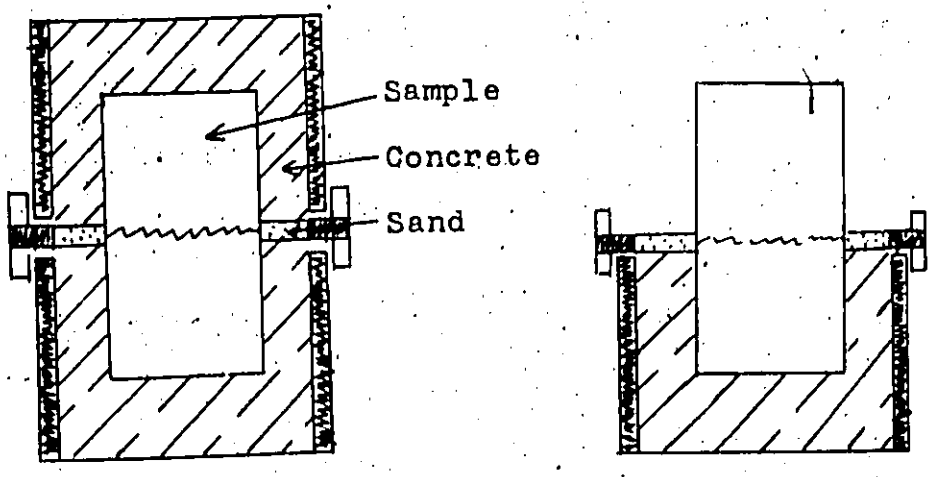

(a) (b)

Fig. 3.1
Casting Procedure.

The casting procedure was as follows: The bottom half of the mold was filled three quarters full of low-slump mortar. The sample, assembled and bound with wire, was set into the mortar so that the average plane of the joint would be above and parallel with the edge of the form. Then, the middle part of the mold was put in place and filled with sand (Fig. 3.1b). Finally the top part of the mold was placed and filled with mortar (Fig. 3.1a). The size of the cast was ½ inch smaller than the inside of the shear boxes.

On the day of the testing the samples were placed in the steel boxes of the direct shear testing machine and the gaps between the cement cast and the box were filled with molten sulphur capping compound (2-hour crushing strength measured as 2 500 psi). The reason for choosing this method of double casting was to utilize the short hardening time of the sulphur compound in conjunction with the superior strength and workability of the cement mortar. The casts could in this way be prepared in advance, and be cemented in the boxes only a couple of hours before commencing the test.

CHAPTER IV

Equipment and Testing Procedure.

Section 4.1 Direct Shear Testing Apparatus.

The following paragraphs will describe the direct shear machine which has been designed and built in the soil mechanics laboratory and the machine shop of the University of Ottawa.

The design philosophy was derived from the considerations listed in Section 2.2 of the Literature Survey. The basic arrangement as well as the size of the machine is very similar to the design by Kenty (27) as described in Table 2.4. (Page27).

The maximum size of the samples was chosen to be 6" x 6" blocks or 6" diameter cores. This is approximately the largest size which would allow the use of the relatively simple concepts of load application and restraints as described later in this Section, and to keep the cost of the equipment below a reasonable limit.

Similar criteria apply to the maximum loading capacity of the machine. Considering the parts available and the overall proportions of the apparatus, the maximum normal working load was chosen to be 6 tons. This will produce a normal stress of 330 psi on the 6" x 6" block or 420psi on the 6" core. Higher stresses can, of course, be achieved if smaller samples are used. The chain of structural elements which transfers the tangential load from its source into the shear boxes is designed for a working load of 10 tons. Thus, the ratio of the maximum tangential to the maximum

normal force is 2 : 1, which should be sufficient to bring to failure most of the possible types of joints, including those that are bonded.

Provisions were made in the design to restrain the shear boxes from tilting in the plane of the applied forces and to prevent them from shifting laterally. Refer to a schematic diagram (Fig. 4.1) of a natural joint plane in the field, containing a rock element which could potentially become a sample for direct shear testing. The movement of the small element, due to the large scale of the whole structure, will obviously occur irrotationally and in a pre-determined direction. In a shear box, on the other hand, the sample may tend to rotate around an axis perpendicular to the plane of the applied forces as shown in side view in Fig. 4.2a, or shift in an oblique direction as shown in top view in Fig. 4.2b.

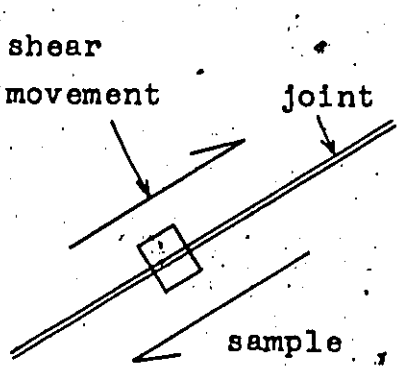

Fig. 4.1
Sample in a rock mass.

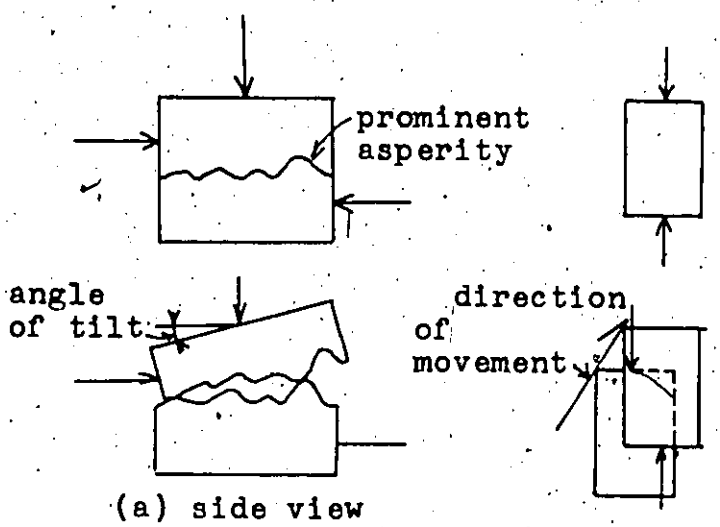

Fig. 4.2
Movements of a sample in direct shear test

Such behaviour is caused by the local irregular nature of the joint asperities. If the sample is not restrained from moving laterally or tilting, some asperities, which would otherwise have been sheared through, will be simply ridden over. Then, as the mode of failure of the asperities directly influences both the strength and deformation properties of the tested surface (40), the measured parameters may be unrealistic. It has to be noted, that in the case of strength, the error will always remain on the safe side, e.g. the strength measured will be lower than that existing in the field. In the case of deformability, the error will be indeterminate.

In order to avoid the need for two loading jacks the design utilizes the TINIUS-OLSEN SUPER-L compression testing machine as a source of the tangential load. The shearing plane is therefore vertical, the normal load being applied horizontally. Such arrangement has been used elsewhere with apparent success (27 & 35). The normal force is applied by a rubber pneumatic bellows similar to that used by Rengers (43) as mentioned earlier.

The general side and top views of the apparatus are shown in Fig. 4.3 and 4.4. The tangential load T from the testing machine is transmitted through the rigid shoes B into the boxes C which contain the rock sample cast in cement mortar, with the joint plane aligned on the gap between the boxes. The normal load N is created by the air bellows D, supported by the frame E of four U profiles and two tiebars. Normal movement of the boxes is facilitated by a Teflon slip bearing F. Two hardened steel pins G, bearing through spherical seats onto the brackets H and I, provide restraint to lateral movement.

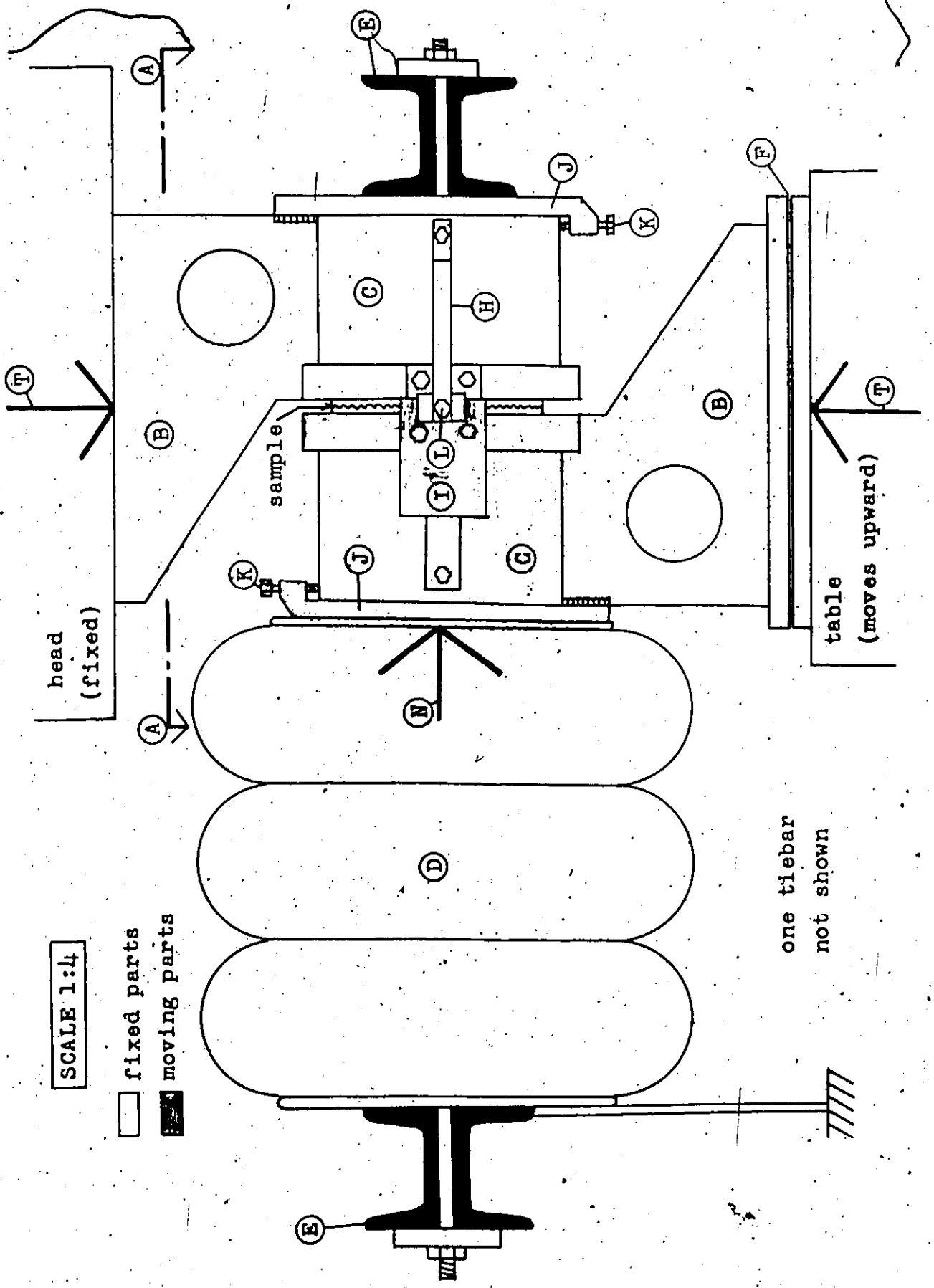

Fig. 4.3 Side view of the direct shear testing machine

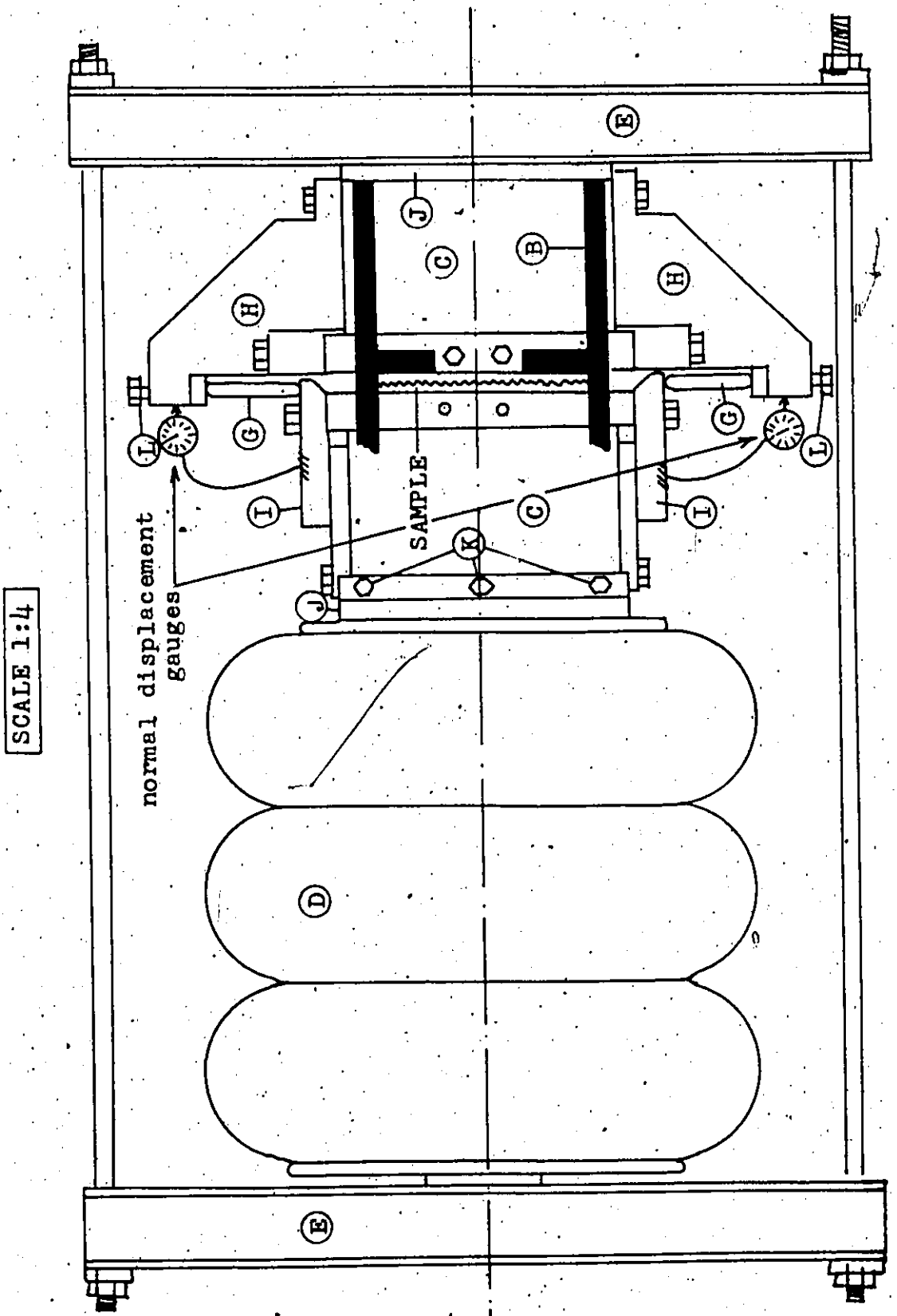

Fig.4.4 Top view of the direct shear testing machine (section A-A)

In the following paragraphs each part of the apparatus will be discussed in more detail. For a better understanding of the design, the reader is referred to the photographs, Plates 1 to 4.

The shoes B are made of two parallel steel plates ½" thick, connected by a stiffener plate of the same material. They are sufficiently wide in contact with the table and head of the universal testing machine to provide restraint against tilting of the boxes in the plane of the forces T and N, and to absorb any moments which could originate in this plane by misalignment of the applied forces.

The slip bearing F consists of two 12" x 9" x ½" plates, one of which has one side polished and the other one lined with Teflon sheet. The friction coefficient of the bearing has been measured as 7% when dry and less than 5% when lubricated with machine oil. Accordingly the movement along the bearing may be expected to introduce errors in the order of 5% in the magnitude of the normal force. Other types of bearings, such as rollers or hydraulic cushions, were considered but rejected.

The back-plates J are welded at their ends to the shoes and so form units with them. The boxes, on the other hand, are separate and are held in place by the pressing bolts K and by other bolts projecting from the shoe stiffeners. The bolts K are designed to withstand overturning moments which might tend to rotate the boxes.

The boxes are cut from a standard 7" x7"x3/8" hollow structural section, reinforced by steel strips which are welded at the sides. The shape of the boxes is square, and the bolts projecting from the

stiffeners use the same arrangement of holes as needed for the lateral restraint brackets, so that the boxes can be attached to the shoes by any of their four sides. This makes it possible to test a sample in all four directions, without having to remove it from the boxes and recast it.

The air bellows are manufactured by the Firestone Tire Co. for use in pneumatic suspension of trucks. They are capable of creating a force of 12 000 lb with a pressure of 120 psi. The air pressure is supplied from the central compressed air system in the laboratory and regulated by a precise pressure relief valve.

The lateral restraint provided by the spherically seated hardened steel pins is only effective for the first quarter of an inch of the shearing displacement. After that, as shown in Fig. 4.5, the tilt of the pins becomes so large, that the lateral component of the movement they allow becomes larger than 0.01".

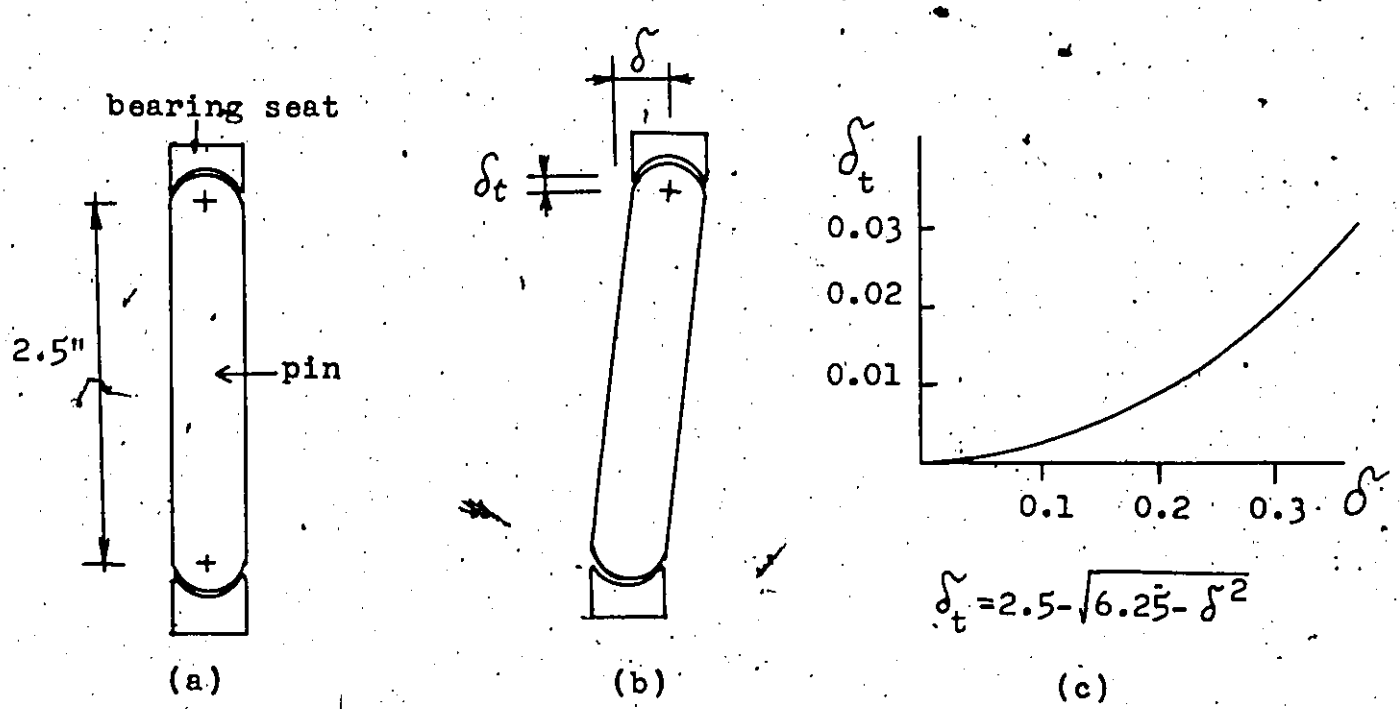

Fig. 4.5
Effectiveness of the lateral restraint.
a) Pin in the original position, b) Pin after movement,
c) Relationship between shear displacement and the lateral movement.

It is considered, however, that after such a displacement the peak strength of the joint is exceeded, most of the prominent asperities of the sample are sheared off and the rock does not exhibit much of a preferred direction of shearing any more. Such behaviour has actually been observed during the present experimental program. The bolts attaching the brackets to the boxes are placed in oval holes, so that the gap between the boxes can be varied between 3/8" and 7/8" depending on the unevenness of the tested joint, while keeping the proper alignment of the pins. The pins are instrumented by strain gauges, so that the magnitude of the lateral force can be estimated.

The structural chain of the pins and brackets is designed for the maximum working load of 3 tons. The ratio between the applied tangential load and the resulting lateral force is indeterminate and no record of its measurement can be found in the literature. Rengers (43) designed his machine for the same ratio 2: 1 as is used here, and he does not report any problems.

The tangential displacement is measured by one linear potentiometer connected to a Moseley XY recorder. The recorder is adjusted so that 0.1" of displacement appears as 5.6" on the plot but it was only found practical to measure displacements larger than 0.001". The reason for this limited precision is not in the instrumentation itself but it lies in the overall precision of the test. An allowance was made for the deformation of the system of the box, sample and cast, as will be described below, but this could only be done on the basis of an estimate and the margin of possible variations could well reach close to 0.001". Consequently, attempting to measure with higher precision would probably be irrelevant. The normal displacement is measured at two points by

mechanical gauges with a sensitivity of 0.001", placed as shown in Fig. 4.4.

The procedure for running a single test is as follows:

1. Set the pressure in the bellows to a predetermined value, which will be kept constant automatically during the test by the pressure relief valve.
2. Increase the shearing load by the controls of the universal testing machine in steps of 500 or 1000 lb, taking readings after each load on the two normal displacement gauges, and the strain readings on the pins.

The shear load-displacement diagram is drawn automatically by the XY recorder.

Section 4.2 Testing Program.

The testing program consisted of two parts e.g. the joint closure tests determining the stiffness of the joints under normal loading only and the direct shear tests aimed at observing the behaviour of the joints under combined normal and shear load. Twenty six samples of three types of rock were tested (Section 2.1).

After placing each sample into the direct shear apparatus, the closure test was conducted first. Before commencing the test, the sample was stressed to approximately 150 psi of normal pressure, in order to allow the two halves to "set" together without excessive crushing of the asperities. After this, the normal pressure was relieved to slightly above zero (just so that the aperture would not reopen) and the two normal displacement gauges were zeroed.

Then the pressure in the bellows was slowly increased in steps of 10 psi of air pressure and readings on the gauges were taken after each step. This was carried to the maximum air pressure of 90 psi. (This corresponds to the actual normal pressure of about 350 psi across the joint, depending on the size of the sample). Finally, the normal pressure was relieved back close to zero and the rebound reading was taken. With the closure test thus completed, the sample was then subjected to the direct shear test.

In order to obtain more results, each sample was tested in shear at four different values of normal stress, corresponding to 20, 40, 60 and 80 psi of air pressure in the bellows. Thus each sample was loaded in four cycles, starting with the lowest normal pressure and finishing with the highest. In the first three cycles, shear loading was increased only to such a point, where the load-displacement curve started indicating signs of yielding. On reaching this point the tangential load was immediately removed, the pressure in the bellows raised and a new cycle was started. In this way data were obtained only for the pre-failure portion of the stress-strain curve in the first three cycles. In the last cycle (80 psi) loading was continued past the peak and as far as the range of the recorder would allow (this was about 0.2"). The reason for removal of the tangential load on reaching the maximum strength was not to disturb the shearing plane excessively in a single cycle. No attempt was made to return the sample into its original position after the completion of a cycle. The assumption behind such procedure is that the pre-peak displacement is so small that few of the prominent asperities are overriden , and consequently, the surface damage suffered by the sample after this displacement has a negligible effect on the shearing properties

in the following cycles, under a higher normal stress. The validity of this assumption will be discussed further with the presentation of the results. After completion of the four cycles, the normal load was completely removed, the sample was returned into its original position and then brought to an ultimate failure at 20, 30 and 60 psi bellows pressure without recording the displacement. These failure loads were then designated as residual for the first three cycles. Curves thus obtained would look typically as shown in Fig. 4.6.

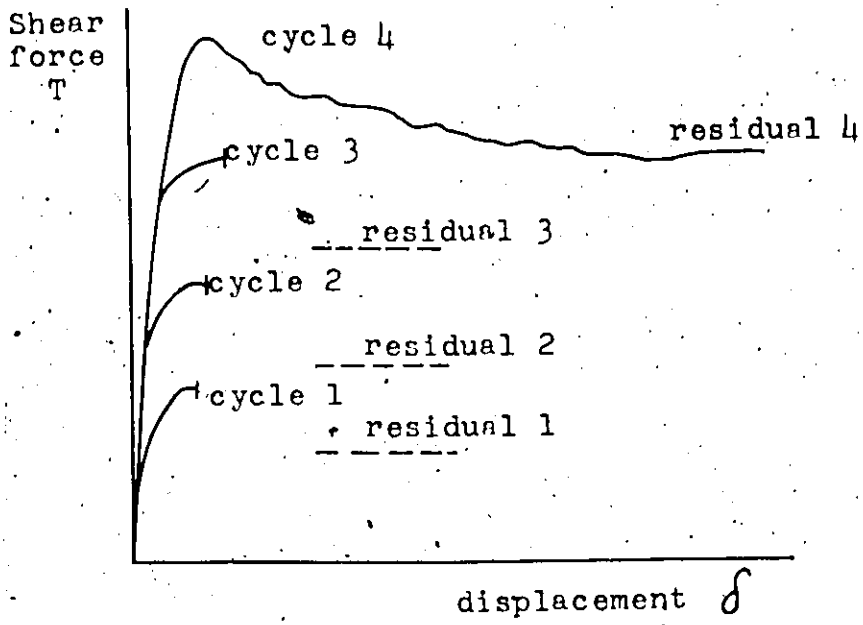

Fig. 4.6
Plot resulting from a direct shear test.

The high degree of approximation in this aspect of the procedure is obvious. Thus for example the residual strength at a load of 2000 lb was measured on a surface damaged by undergoing a long displacement under 8000 lb. Also the displacement needed to attain the residual strength was not measured. But the procedure was accepted, because observation of the post failure behaviour was not the main purpose of this work.

The influence of the rate of loading was also considered. Sample No. 9, which was a limestone saw-cut was tested with a loading rate of approximately 70 psi/min and re-tested with a rate of 1500 psi/min. The resulting stress-displacement curves were almost equal as they would be if the loading rate was constant. This is an indication that, within a practical range, the loading rate has little influence on the results. The actual loading rate used in the tests was roughly 100 psi/min.

CHAPTER V

Results and Conclusions.

Section 5.1 Computer Simulation of a Direct Shear Test.

In order to shed more light on the influence of the design of the direct shear machine upon the state of stresses on the tested surfaces, a simple analysis was carried out using a plane strain finite element computer program.

The basic arrangement and input parameters of the problem are shown in Fig. 5.1. The sample and its concrete cast are simulated by rectangular elements having the properties of rock, and the tested joint is created by onedimensional joint elements with typical stiffness parameters. The influence of the steel casing of the shear box is simulated by assumed boundary conditions. The normal stress is applied uniformly on the top of the upper half of the sample.

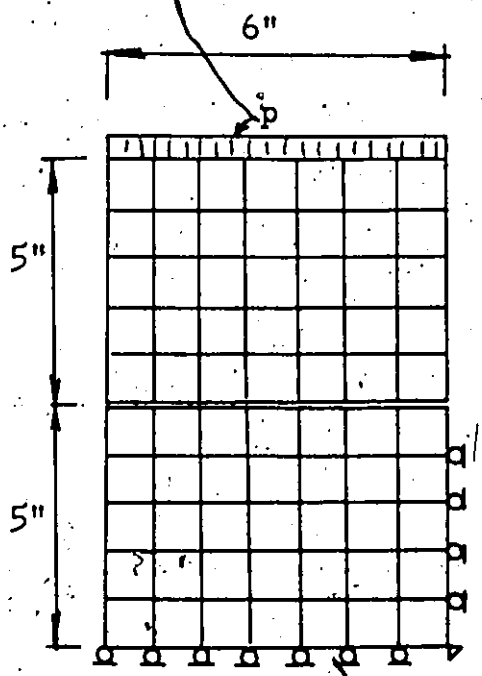

Fig. 5.1

Normal pressure p = 100psi
E = 500 000 psi
μ = 0.2
k_s = 2 000 lb/in^3
k_n = 6 000 lb/in^3
c = 0.0 psi
ϕ = 45°
maximum amount of joint closure = 0.01"
tensional strength = 300 psi
tension limit across the joint = 0.0

Four different modes of application of the shearing load and the resulting distributions of the normal and shearing stresses on the joint plane are shown in Fig. 5.2a, b, c, and d.

In case (a) it is assumed that the tangential load is transferred from the casing uniformly onto the side of the upper half of the sample. The resulting normal stress distribution is close to that, which would be predicted by considering the reactions on the upper half of the sample as on a rigid body. The shear stress is proportional to the normal stress. As could be expected, both of the stresses are highly nonuniform and partial opening of the joint is produced by tension.

Case (b) simulates the application of an inclined load. Again, the resulting stress distributions correspond almost exactly to those that would be predicted by the rigid body consideration and are uniform. Naturally the normal stress is dependent on the magnitude of the shear load.

In case (c) a couple is acting on the side of the sample, balanced in such a way, that the moment about the average plane of the joint is zero. This would, with a great amount of simplification, represent the design illustrated in Fig. 5.2e, which is the most commonly used design of the direct shear testing machines. The couple results from the action of the lever through which the tangential load is applied.

In case (d) a uniform, irrotational displacement of the left side of the upper half of the sample is input. This is the case which corresponds to the design of our testing machine as described in Section 4.1.

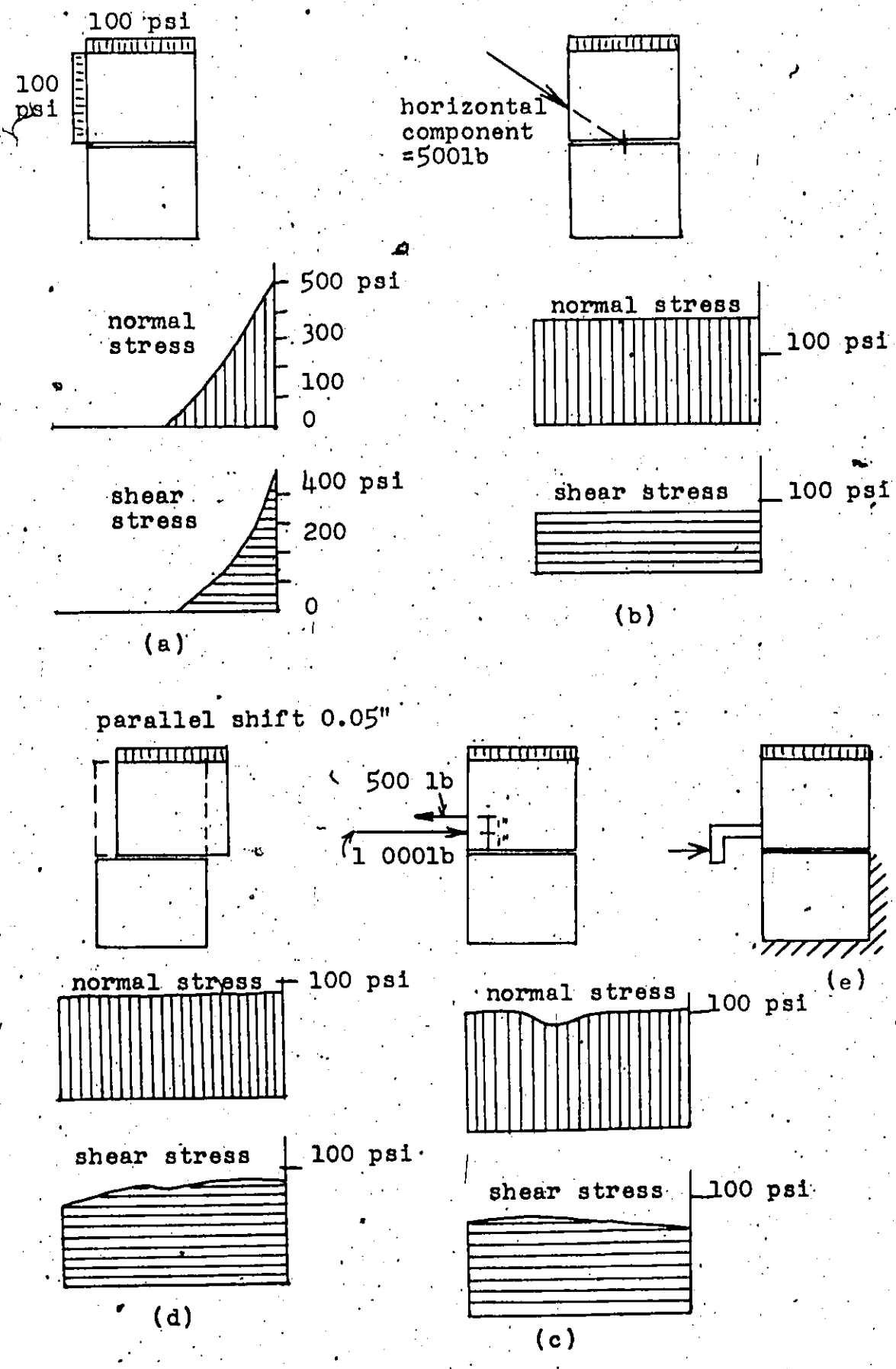

Fig. 5.2 Stress distributions in models of direct shear tests

The resulting normal stress is uniform, whereas the shear stess increases with length along the joint by about 60%, due to the compressibility of the material. In the actual situation this variation may be smaller, because of the added stiffness contributed by the sides of the casing.

Section 5.2 Results of the Joint Closure Tests.

The results of the closure tests are summarized by the stress displacement plots, obtained from the data recorded by the normal pressure gauges, as shown in Appendix A.

The method of conducting these tests was described in Section 4.2, Page 67. At each value of the air pressure applied in the bellows, two readings were obtained from the mechanical gauges recording the normal deformation across the joint. These were then averaged to obtain the resulting amount of joint closure Δh. Similarly as in the case of the shear tests (see page 77) a check was made on the deformation of the whole system of boxes and casts by stressing a sample of solid concrete by the maximum load. The deformation of the system, however, proved to be negligible so that no correction needed to be applied.

In most cases the readings on the two gauges were quite different, indicating rotation of the free box around a vertical axis. This rotation may be due simply to the nonuniform stiffness along the tested joints but there is also reason to suspect that it may be caused by a certain amount of misalignment in the normal loading system, resulting in an uneven distribution of stress along

the joint in a horizontal direction. Further experience in using the machine would be necessary in order to clear this point.

The resulting relationship between normal stress and joint closure was roughly linear as shown in two sample plots in Fig. 5.3. Such a result may be expected due to the relatively low stresses which were applied (12)

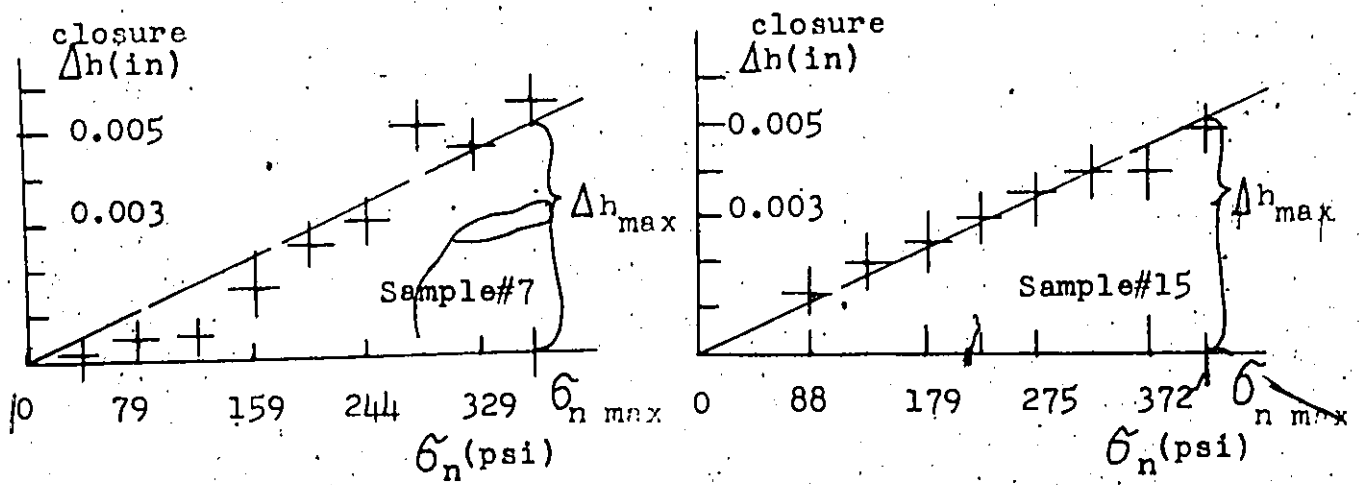

Fig. 5.3
Two samples of the measured relationship between normal stress and joint closure. a) Limestone sample, b) Sandstone sample.

The normal unit stiffness coefficient, k_n (page 47), was computed by the formula:

$$k_n = \frac{\sigma_{n\ max}}{\Delta h_{max}} \quad (lb/in^3) \qquad \text{Eqn. 5.1}$$

in which σ_n is the maximum normal stress applied and Δh is the corresponding closure, inferred from graphs similar to those shown in Fig. 5.3 by fitting a straight line approximately to the measured data. The resulting values of the coefficient for thirteen of the samples are shown in Table 5.4. The test was not conducted with any of the siderite samples, as these contained only perfectly clean, fitting fractures which would obviously have a very high stiffness.

No correlation between field description of the joints (Table A.1, App.A) and the value of k_n could be found, because all the tested joints with the exception of No.5 fall into a single class in respect to opening, and consequently exhibit stiffness of the same order. Sample No.5, which was a bonded, very thin joint, has the highest stiffness value.

Table 5.4 Results of the closure tests.

Sample No.	σ_n^{**} max. psi	Δh^{**} max. in	k_n 10^4 lb/in^3	Sample No.	σ_n^{**} max. psi	Δh^{**} max. in	k_n 10^4 lb/in^3
1	277	0.007	4.0	11	364	0.005	7.3
2	*			12	393	0.007	5.6
3	322	0.006	5.4	13	364	0.004	9.1
4	*			14	342	0.004	8.6
5	340	0.002	17.0	15	372	0.004	9.3
6	346	0.004	8.7	17	*		
7	329	0.005	6.6	18	293	0.005	5.9
8	not performed			20	293	0.006	4.9

* Result invalidated by excessive rotation

** For definition see page 75

The mean value of the coefficient k_n was obtained by simple averaging and is equal to 8.35×10^4 psi/in for the limestone samples and 7.25×10^4 psi/in for sandstone. The range of the measured values is 4.0×10^4 and 17.0×10^4 for the former and 4.9×10^4 and 9.3×10^4 for the latter type of rock.

Section 5.3 Interpretation of the Load-Displacement Plots.

A typical shear load-displacement curve that could be obtained from the direct shear tests is shown in Fig. 5.5. A correction must be made because this curve contains the displacement due to the deformation of the whole system of the boxes and the cast in addition to that which occurs along the joint itself. To find the magnitude of the correction, a block if concrete was prepared, which did not contain a rock sample and without a discontinuity. The block was cemented in the shear boxes and subjected to load in the usual way. The resulting load-deformation relation appeared as a straight line inclined at a small angle (1^0 9') to the load axis (Fig.5.5). It is reasonable to assume, that this line represents the inherent deformability of the system. In interpretation of the load-deformation grephs the line was used to subtract the system deformation from the measured values of the displacement. No correction was made for the changed area of the sample because the range of the measured displacements was very small.

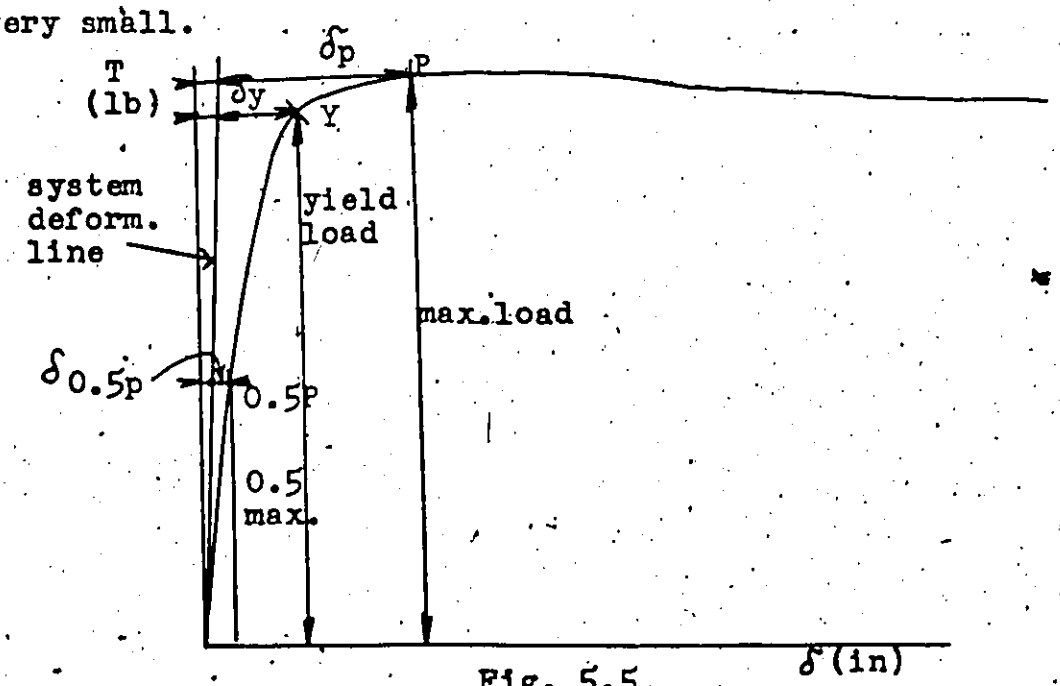

Fig. 5.5
Interpretation of a shear load-deformation curve. (The angle between the vertical axis and the system deformation line is exaggerated here.)

As can be seen in Fig. 5.5, the pre-peak portion of the load-displacement curve is nonlinear. To record the actual shape of the curve, three characteristic points were used. First is the peak point, P, defined as the point in which the curve attains zero or very flat, constant slope for the first time. The stress and displacement at this point are designated by τ_p and δ_p respectively. The second characteristic point, 0.5P, is the point corresponding to 50% of the peak load. This point was defined arbitrarily to account for the stiffness of the joint in the first half of the loading range. The third point, Y, called the yield point, is the point of the maximum curvature of the plot. This point is an upper limit of load, up to which the curve could still be approximated by a straight line with some degree of validity. In some cases Y merges with P.

The stiffness coefficient k_s (page 48) is determined at all three points using the relation:

$$k_s = \frac{\tau}{\delta} = \frac{\text{load}}{A_x \delta} \qquad (\text{lb/in}^3) \qquad \text{Eqn. 5.2}$$

where: τ is the shear stress, δ the corresponding displacement and A the sample area.

In cases, where the displacement was so small as to be unmeasurable, an arbitrary value of 0.001 inches was assigned in order to avoid infinite stiffness values.

The coefficients obtained from the points 0.5P and Y are designated as $k_{s0.5P}$ and k_{sy} respectively and they are considered as limits of values that could reasonably be assigned to the particular joint with the given normal stress. The stiffness at peak is recorded under the symbol τ_p / δ_p, and it would, in

many cases, be quite unrealistic to interpret the value of k_s from this, due to the large amount of yielding which preceded.

The values of normal displacement, Δh, were also recorded at each of the above points. The "off-diagonal" stiffness coefficient k_{ns} (page 49) was then computed as:

$$k_{ns} \frac{\tau}{\Delta h} \quad (lb/in^3) \qquad \text{Eqn. 5.3}$$

The resulting three values of the coefficient were designated as k_{nsp} for point P, k_{nsy} for point Y and $k_{nsO.5P}$ for point 0.5P. In addition to the above data, the applied normal stress, σ_n, and the residual stress, τ_{res}, were recorded for each loading cycle.

Section 5.4 Discussion of the Results of the Direct Shear Tests.

The results of the direct shear tests are represented by the shear force-displacement plots, included in Appendix A. Fig. 5.6 presents typical plots for six specimens. The tests were conducted in the manner described in Section 4.4.

General shear stress-displacement behaviour of the tested samples may be described as follows:

At low stress, the discontinuity deforms more or less linearly but a gradual yielding begins at a certain percentage of the maximum strength. This point of nonlinearity may lie quite high, as for example for samples 14 and 15 (Fig. 5.6), or the curve sometimes may not exhibit any initial linear portion at all, such as that of sample 5. The extent of linear behaviour may also be dependent on the magnitude of the normal stress as can be seen in the case sample 25.

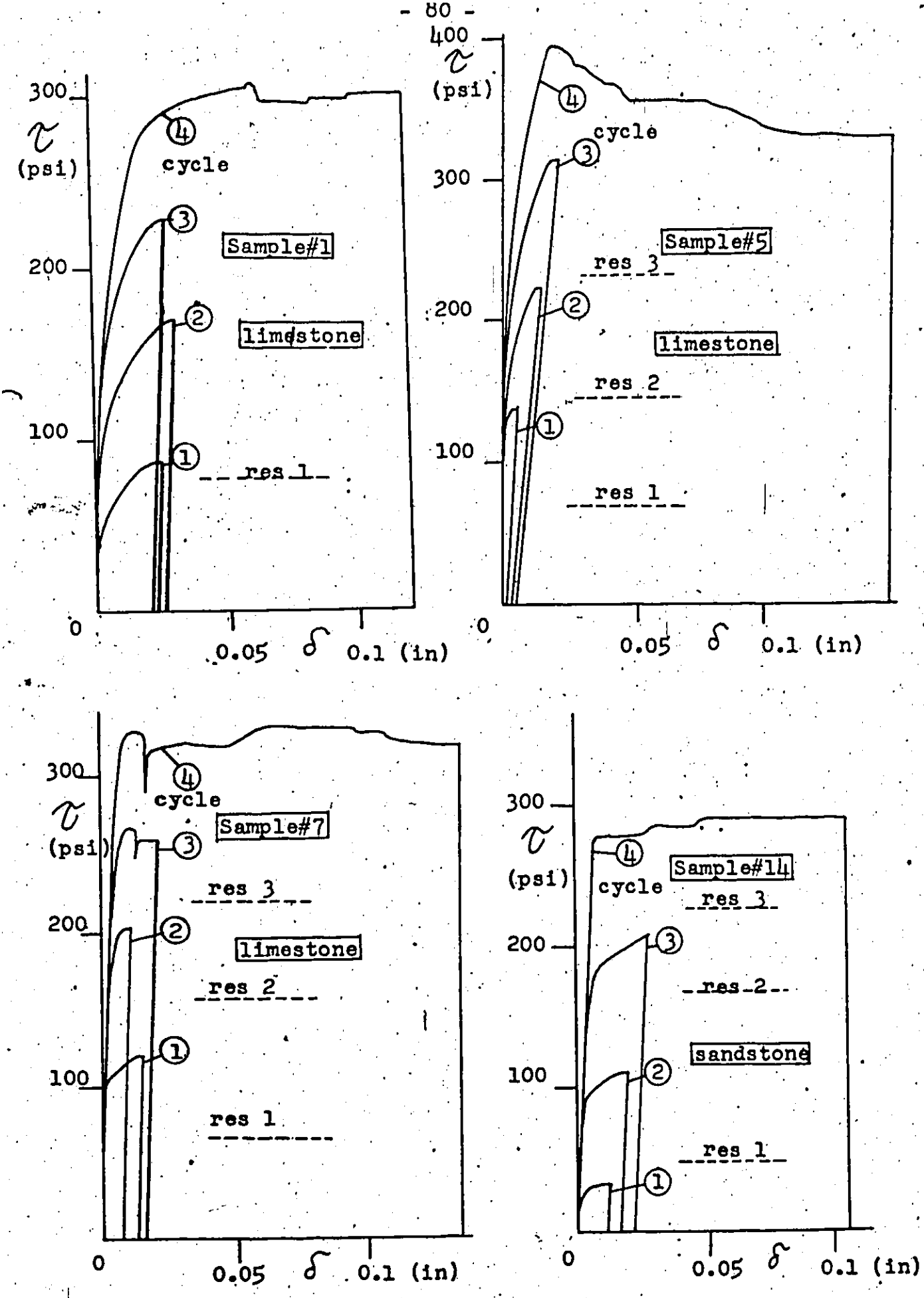

Fig. 5.6 $\tau - \delta$ diagrams resulting from direct shear tests
(continued on the following page)

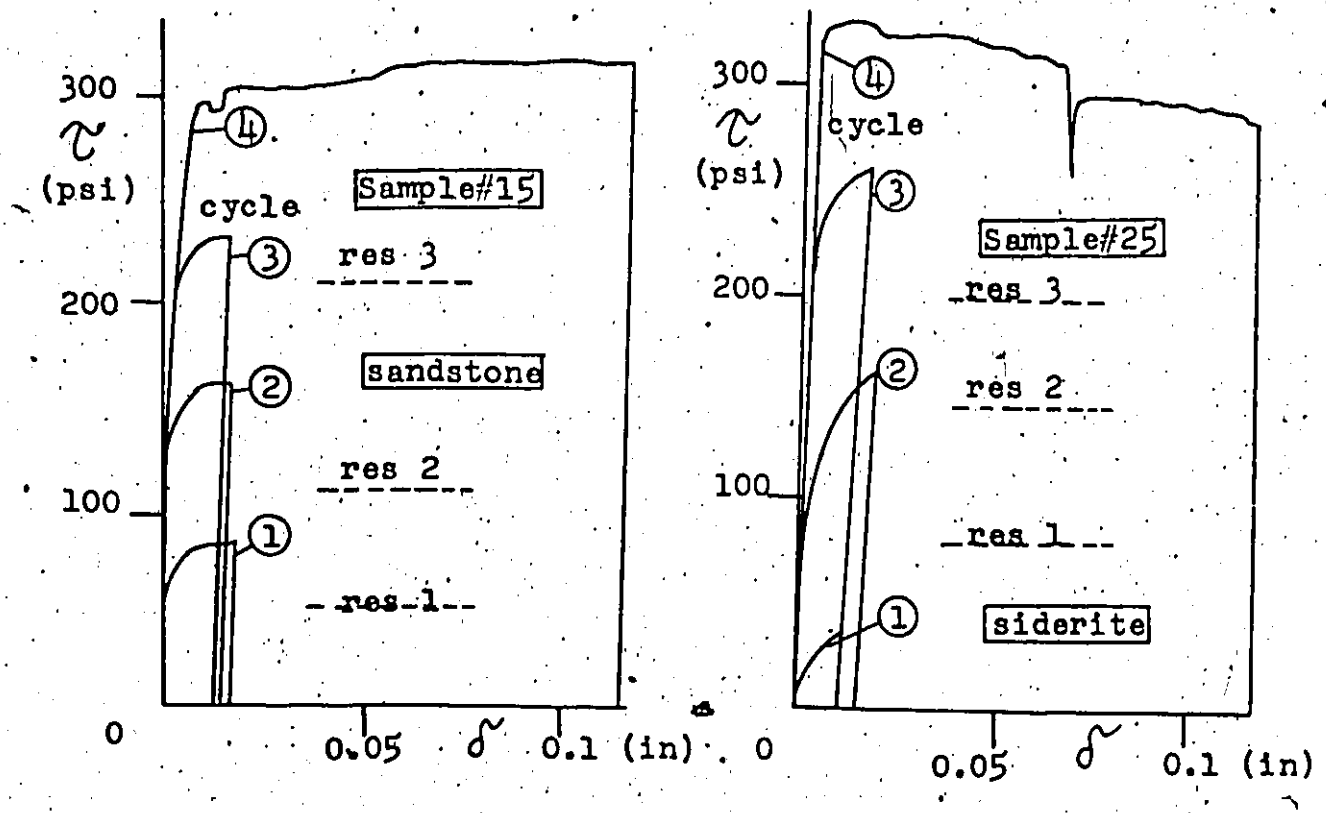

Fig. 5.6 continued

The yielding continues at an increasing rate, so that a point of maximum curvature is reached, defined as the yield point in Section 5.3. After this the curve flattens at a decreasing rate, until it becomes more or less a straight line, horizontal or rising at a flat angle. This occurs at a point defined as "peak" in Section 5.3.

All tested samples behaved elasto-plastically. This is an indication that the re-assembling procedure was successful, since in the opposite case plasto-elastic behaviour would occur as a result of the initial closure of the aperture (6).

In general, although not without exceptions, the limestone samples exhibited slow yielding with rounded curves of a similar shape for all four loading cycles (sample 1, Fig. 5.6). The sandstone samples, on the other hand, railed abruptly after reaching

a sharply defined yield point with high normal stress, whereas at low normal stress they had often gone through slow, gradual yielding (sample 14, Fig. 5.6). This different yielding behaviour suggests differences in the modes of failure between the two types of rock. Limestone apparently fails by progressive shear failure, which engages different types of asperities in turn, crushing them partially before moving to others. By such a process the effective area of shear is progressively increased. The contact area, appearing as white spots on the photographs of the sample surfaces after testing (Plates No.7 to 11) were studied under a stereo-microscope and showed very fine pulverizing and little movement of material during shear. In the case of sandstone samples, microscopic studies revealed relatively large particles being broken off the points of contact and rolled into the depressions of the joint surface. Thus sandstone apparently fails by a brittle failure of the most prominent asperities, the slow yielding at low normal stress being probably the result of rolling friction of the broken fragments.

All samples had some amount of recoverable deformation, illustrated by the slightly inclined unloading lines in Fig. 5.6. The angle of inclination of these lines was almost always equal to the initial tangent angle of the loading curves. This shows that there is, in fact, some truly elastic deformation of joints loaded in shear, although it is usually very small in magnitude. A major part of joint flexibility, especially under stresses which exceed about 50% of the peak strength, must therefore be considered irrecoverable.

Table A.2, Appendix A, summarizes the numerical data obtained from the measurements of the Unit Shear Stiffness Coefficient k_s.

Column 2 of the table represents the constant normal stress σ_n acting across the joint during each loading cycle. Columns 3, 4 and 5 contain the three characteristic shear stresses: the yield stress τ_y, peak stress τ_p, and the residual stress τ_{res} respectively, as defined in Section 5.3. Column 7 indicates the measured displacement at peak point δ_p. The displacements corresponding to the yield point and to stress at 50% of the peak are not shown in the table.

Columns 8,9 and 10 represent the values of the unit shear stiffness coefficient computed from displacements at 50% of the peak, $k_{0.5p}$, at the yield point, k_y, and the peak point, τ_p/δ_p, respectively.

As was stated in Section 5.3, only the former two values of k_s were considered representative of the true unit shear stiffness and they are presented here as practical limiting values of the parameter. Thus, for each sample we have eight different values of the parameter k_s, varying in dependence on the magnitude of the normal stress and the nonlinearity of the stress-strain curve. Given the limitations of the present computing techniques, however, the coefficient k_s is only practically usable as a single value. Therefore the measured quantities, which vary within a wide range, must be subjected to a suitable averaging procedure.

In searching for a representative average of the coefficient it is necessary to bear in mind, that each quantity in columns 8 and 9 of the table represents one point on the stress-displacement curve. Therefore, the best statistical approach to this problem appears to be a linear regressional analysis, such as the least squares method. By this method one can , at first, find a best fitting line for the two pairs of data represented by points

0.5P and Y for each loading cycle. Since the line must, of course, pass through the origin, the regression coefficient b (28) is equal to:

$$b = \frac{0.5\tau_p + \tau_y}{\delta_{0.5p} + \delta_y} \qquad \text{Eqn. 5.4}$$

Also, because the regression coefficient is by definition the slope of the regression line, we have:

$$k_{s\ \text{average}} = b$$

The average values thus obtained for each loading cycle are given in column 11 of Table A.2. They may be considered an indication of the variability of the coefficient in dependence on the normal stress.

Further treatment of the measured data consisted of obtaining the average values of $k_{s0.5p}$ and k_{sy} over the four loading cycles of each sample. The same method of analysis was used as above so that the averages were computed as follows:

$$k_{s0.5p\ \text{average}} = \frac{\sum_1^4 0.5\tau_p}{\sum_1^4 \delta_{0.5p}} \qquad \text{Eqn. 5.5}$$

and

$$k_{sy\ \text{average}} = \frac{\sum_1^4 \tau_y}{\sum_1^4 \delta_y} \qquad \text{Eqn. 5.6}$$

The resulting numbers are given as "range k_s" in column 12 of Table A.2 and they may be considered an overall measure of the variation of the secant k_s due to nonlinearity of the stress-displacement curves for each sample. Apparently, this variation

is quite substantial for some of the samples and it seems to indicate need for eventual introduction of bilinear or completely general treatment of the stress-displacement relationship in the computing technique.

Finally, column 13 of the same table represents the overall average of the coefficient, computed by fitting a straight line to all the eight representative points of each experiment by the formula:

$$k_{s\ \text{average}} = \frac{\sum_{1}^{4} 0.5\tau_p + \tau_y}{\sum_{1}^{4} \delta_{0.5p} + \delta_y} \qquad \text{Eqn. 5.7}$$

As stated above, the coefficients $k_{s0.5p}$ and k_{sy} represent the stiffness of the joint within the range of shear stress magnitudes bounded by $0.5\tau_p$ and τ_y. In order to express the later limit, τ_y, in terms of the peak strength a plot was made of τ_y / τ_p for all limestone and sandstone samples against the magnitude of the normal stress σ_n. The plot is shown in Fig. 5.7. Apparently, there is no functional relationship between the two quantities and thus the yield stress τ_y may simply be expressed as a fraction of the peak strength independent of σ_n. The magnitude of this fraction lies between 0.8 and 1.0. Thus, the above average unit shear stiffness coefficient is representative of the shear behaviour of the samples up to about 80% of the peak stress.

Among different samples, the value of k_s also varies considerably, ranging between 1.56×10^4 and 9.18×10^4 for the limestone samples, 2.45×10^4 and 18.87×10^4 for sandstone and 2.17×10^4 and 10.61×10^4 for siderite.

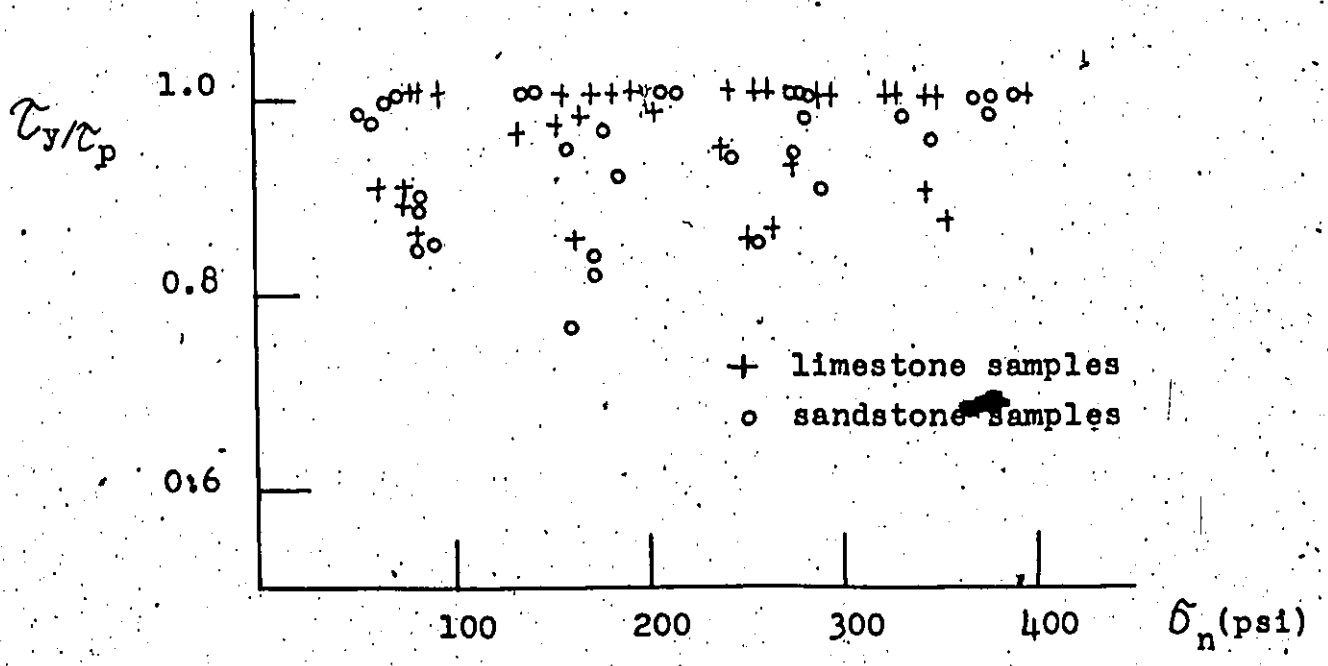

Fig. 5.7
Relationship between τ_y / τ_p and σ_n.

Table 5.8 summarizes the average values of the coefficient k_s for each type of rock, both for natural joints and saw cuts. The averages have again been obtained by the same regression formula as shown above, the characteristic points being now from all four cycles of all samples of each type of rock. All statistical treatment of the data, as well as all the other computations were carried out by a simple WATFIV computer program, the listing of which is included in Appendix A.

Table 5.8 shows the unit shear stiffness coefficient to be of the same order of magnitude, but slightly lower than the normal stiffness coefficient for the same type of rock.

The significance of the measured values of the coefficients may be depicted by using the formulas for the effective deformation parameters of a jointed rock mass, stated as Equations 7.1 and 7.5 (page 111) in Section 7.2 of the last Part of this Thesis.

Table 5.8 Overall Average Values of the stiffness coefficients

Sample type	k_n	k_s	k_{ns}
	$x10^4$psi/in		
Limestone	6.58	2.76	6.38
Limestone saw cut	-	5.80	-
Sandstone	6.85	5.25	15.57
Sandstone saw cut	-	8.59	-
Siderite	-	3.67	17.71
Siderite saw cut	-	9.10	-

Let a typical deformation modulus E be 7.0×10^6psi for limestone and 4.0×10^6psi for sandstone, and a Poisson's ratio equal to 0.2 for both types of rock. The typical horizontal joint spacing S for the locations where the samples were recovered may be taken as 12". Using the average values of k_n from Table 5.8, obtain:

$$E \text{ eff. limestone} = \left(\frac{1}{E} + \frac{1}{S_{kn}}\right)^{-1} =$$

$$= \left(\frac{1}{7.0\times10^6} + \frac{1}{12\times6.58\times10^4}\right)^{-1} = 0.71 \times 10^6 \text{psi}$$

and

$$E \text{ eff. sandstone} = \left(\frac{1}{4.0\times10^6} + \frac{1}{12\times6.85\times10^4}\right)^{-1} =$$

$$= 0.68 \times 10^6 \text{ psi}$$

Therefore the 12" spaced joints will cause the effective deformational modulus of limestone and sandstone to be roughly 0.1 and 0.2 of the respective rock substance deformation modulus.

The modulus of rigidity G of the intact rock may be computed as:

$$G = \frac{E}{2(1+\mu)} = \frac{7.0 \times 10^6}{2(1+0.2)} = 2.9 \times 10^6 \text{ psi for limestone}$$

and $$G = \frac{4.0 \times 10^6}{2(1+0.2)} = 1.5 \times 10^6 \text{ psi for sandstone}$$

Substituting the average unit shear stiffness coefficients from Table 5.8 into the formula:

$$G \text{ effective} = \left(\frac{1}{G} + \frac{1}{S_{kn}}\right)^{-1}$$

the effective modulus of rigidity is equal to 0.30×10^6 and 0.44×10^6 psi for limestone and sandstone respectively, so that the modulus of rigidity is multiplied approximately by factors or 0.1 and 0.25.

In the following, a comparison is made of some of the above data with the results of a well known plate load testing program. The generally accepted parameter describing the difference between the deformation modulus of the rock substance as determined by laboratory tests, E, and the field modulus E_f, is the modulus reduction factor (Ref. 47) given as:

$$f = E_f/E$$

Figure 5.9a, reproduced from Ref. 47, presents a correlation between the reduction factor f and the Rock Quality Designation (RQD), mentioned previously in Chapter I. The same reference also presents a correlation between RQD and fracture frequency, which

is given as the number of natural joints per foot of depth of the rock mass (Fig 5.9a). Both of these figures were developed from subsurface exploration and extensive plate load testing on nonweathered granite gneiss (Dworshak Dam site, Idaho).

The correlation in Fig. 5.9b, simplified by the diagonal line, can be used to convert the rock quality scale in Fig. 5.9a from RQD to fracture frequency. This new scale is shown below the horizontal axis of the figure and its values are, of course, inversely proportional to the average joint spacing S.

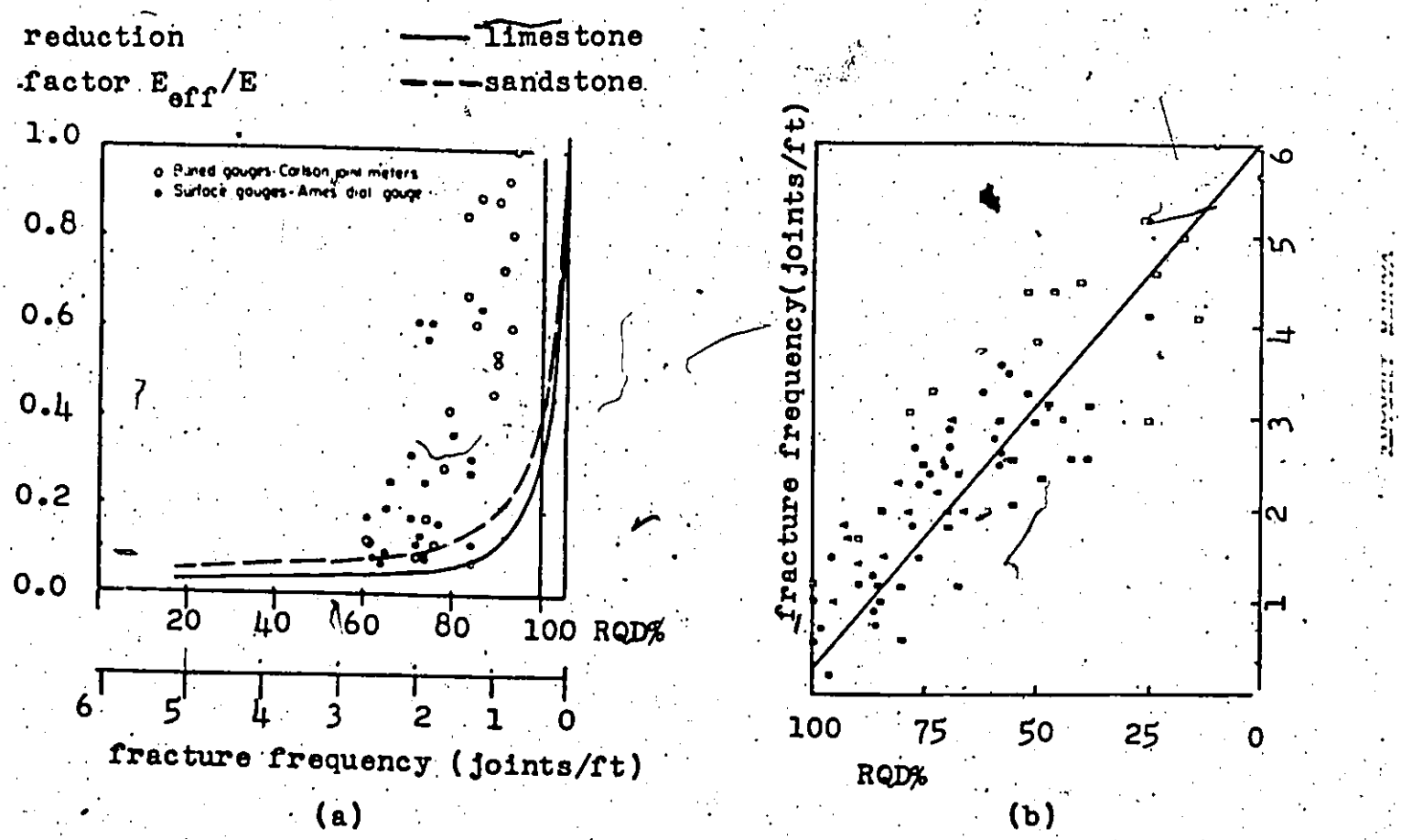

Fig. 5.9
Comparison between a plate load testing program results and the effective moduli of deformation estimated from test results(47).

For each given S, an estimate can be made of the value of the reduction factor as:

$$f = \frac{E_{eff}}{E} \qquad (7)$$

with the use of the k_n values from Table 5.8, in the same way as was done above for a spacing of 12". The values thus computed for both limestone and sandstone define the two hyperbolic curves superimposed on Fig. 5.9a. In this way, a relationship was obtained between the fracture frequency or RQD and the reduction factor f, similar to that given by Ref. 47, on the basis of joint testing only.

The fundamental assumption behind the validity of the curves in Fig. 5.7a is that the joint properties would be the same in rock zones of different fracture spacing. In future testing, this could be ascertained by a proper selection of samples.

The curves indicate a much greater influence of the joints upon the magnitude of the reduction factor than that shown by the values of reference 47. This could perhaps be expected in view of the superior hardness of the metamorphic rock tested by the latter. If substantiated by plate load testing or full scale settlement observations, the relationships represented by Fig. 5.9a could be used in practical problems for estimating the reduction factors for local rock formations. Similar relationships could, of course, be readily developed for the reduction factor of the modulus of rigidity G, with the use of the average values of k_s.

Figures 5.10a and 5.10b represent an attempt at finding a relation between the magnitude of k_{sy} (the unit shear stiffness coefficient at yield point) and the normal stress. The resulting

curves divide the tested samples roughly into two categories.

In the first category are samples whose stiffness increases more or less linearly with the normal stress. The curves representing these samples are remarkably systematic and could quite reasonably be replaced by a single line. Their tangent is slightly higher in case of the sandstone samples.

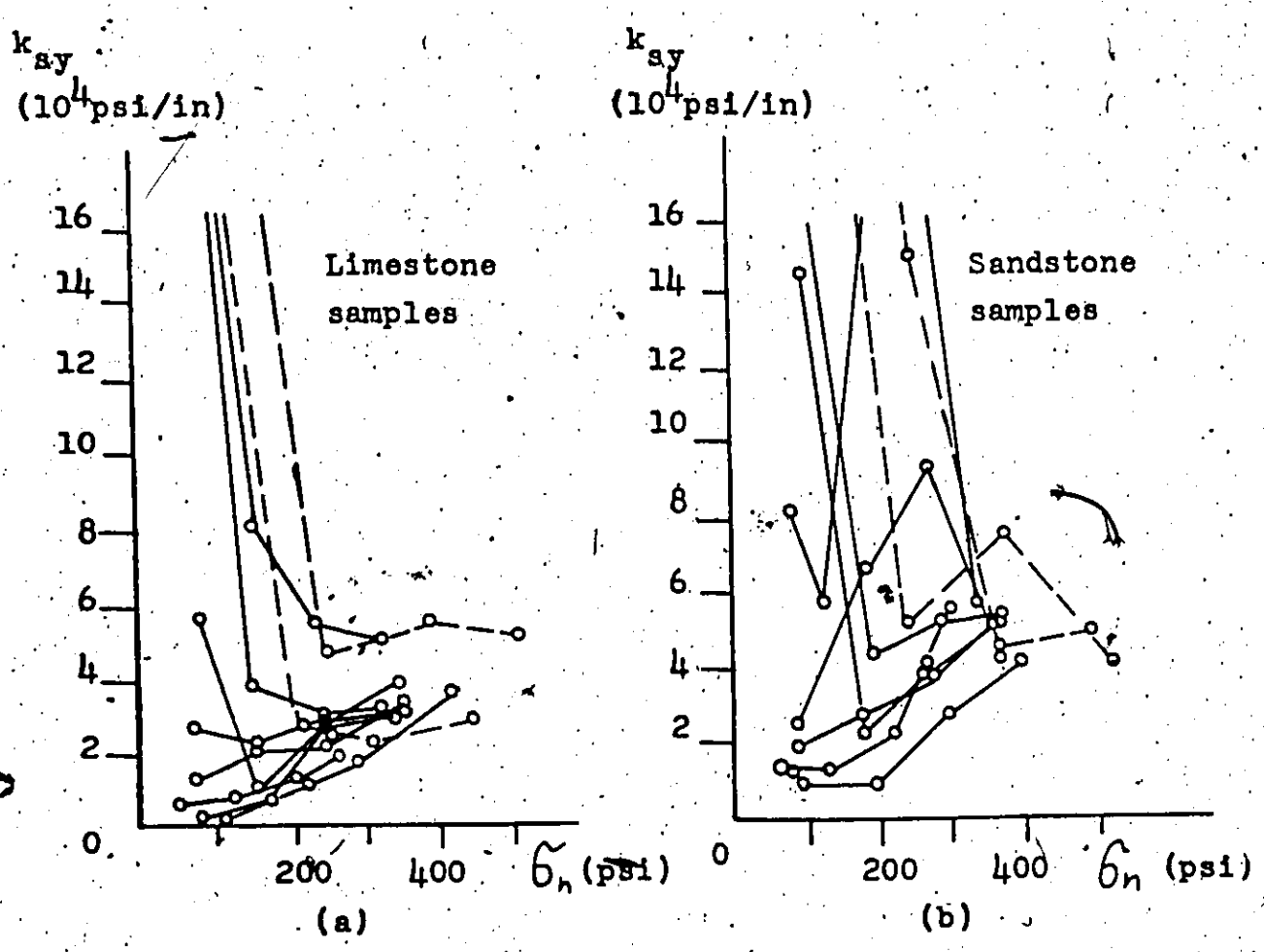

Fig. 5.10
Correlation between k_{sy} and σ_n.

In the second category are samples which at low normal stress (often only in the first loading cycle) exhibit very high stiffness. At a higher value of σ_n their stiffness rapidly decreases and the

curve becomes similar to that of the first category.

The question now arises, "how much of this behaviour is due to the experimental procedure of cycling the load and testing each sample in four stages?" It has been stated above (Section 4.2), that the testing procedure was based on the assumption, that the surface damage caused by the preceding loading cycles would have negligible effect on the behaviour of the sample in any following stage. The validity of this assumption seems to be affirmed by the plots of the strength envelopes, τ_p vs. σ_n shown in Fig. 5.11. If the shearing of the asperities in any of the loading cycles had any substantial effect on the following stages of the experiment, the strength envelopes would probably flatten down with increasing normal stress at an unusually fast rate. The curves shown in Fig.5.11 are only slightly curved and often almost straight. Strength envelopes of joints in similar rocks that can be found in literature (for example Krsmanovic, Ref.29) have similar shapes. Their curvature is explained by the changing modes of failure according to Patton's (40) or Ladanyi's (33) theory. The single exception is curve No. 25, Fig.5.11c, which shows a drop of strength in the last cycle evidently due to the surface damage suffered in the previous cycle. None of the remaining curves exhibits a similar phenomenon.

If we assume that the effect of the cycling of the load is small, the variation of the unit shear stiffness with the normal stress must be explained by the changing modes of failure of the joint asperities. From the Patton's theory it is known, that the percentage of asperities being sheared off, in contrast to those that are merely being slid over, increases with increasing normal stress.

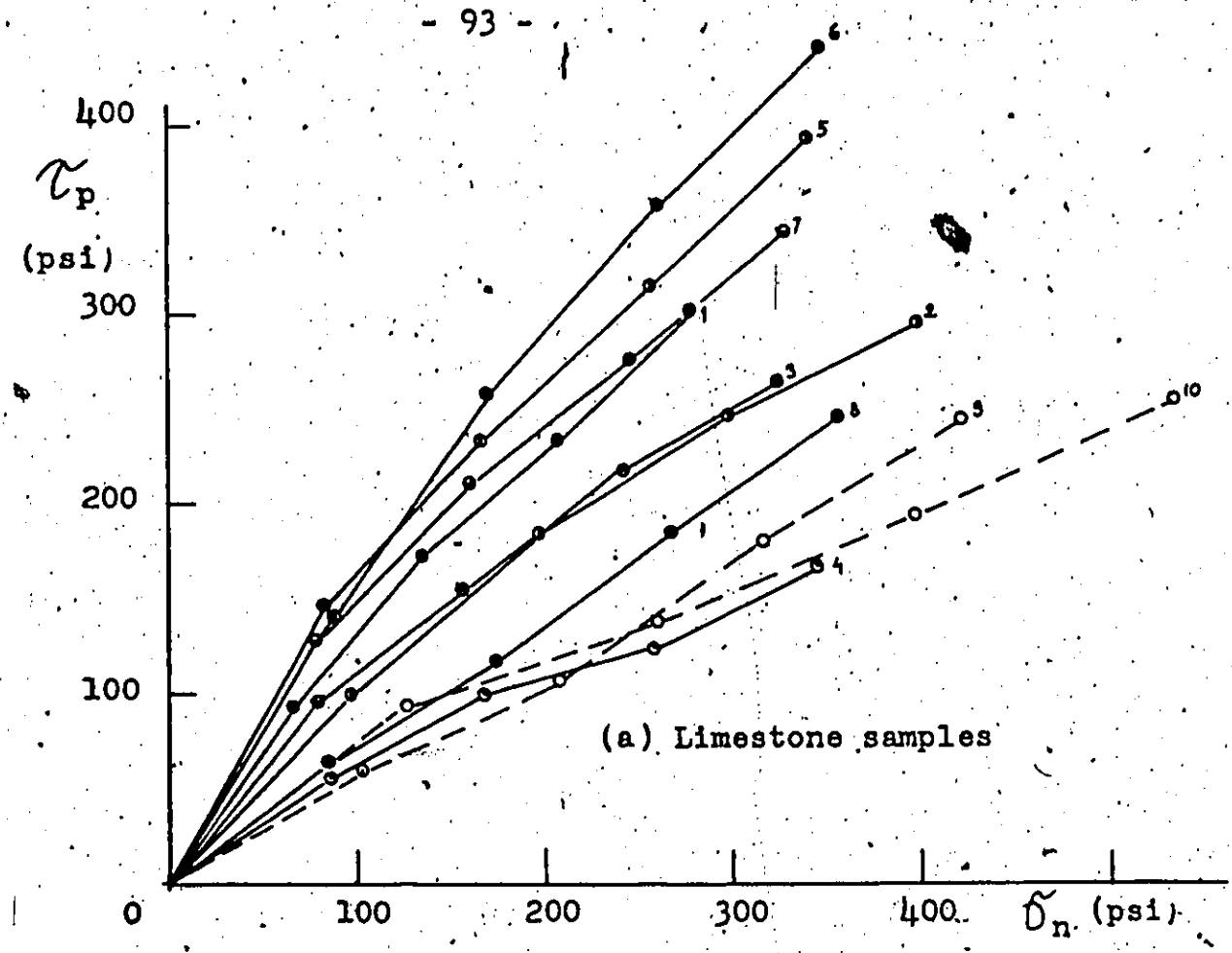

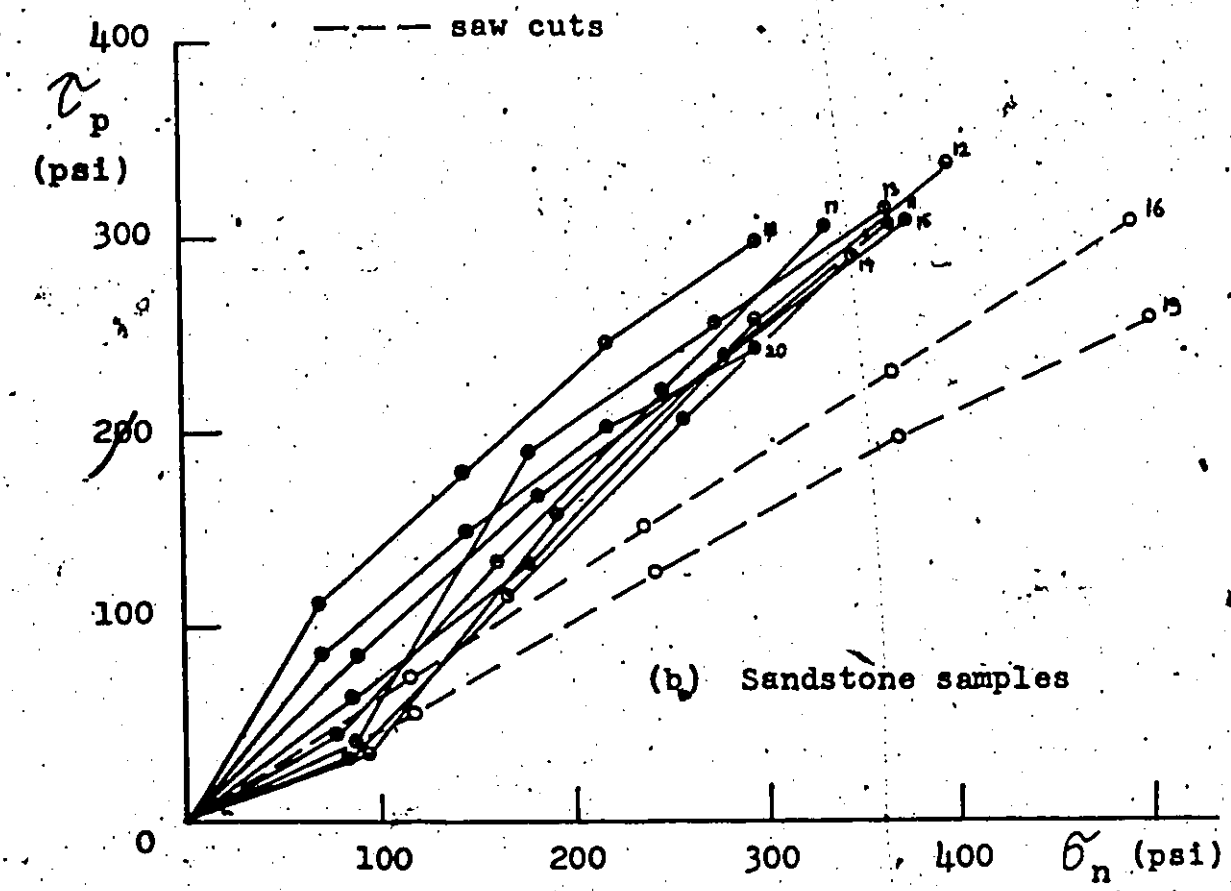

Fig. 5.11 Strength envelopes resulting from direct shear tests

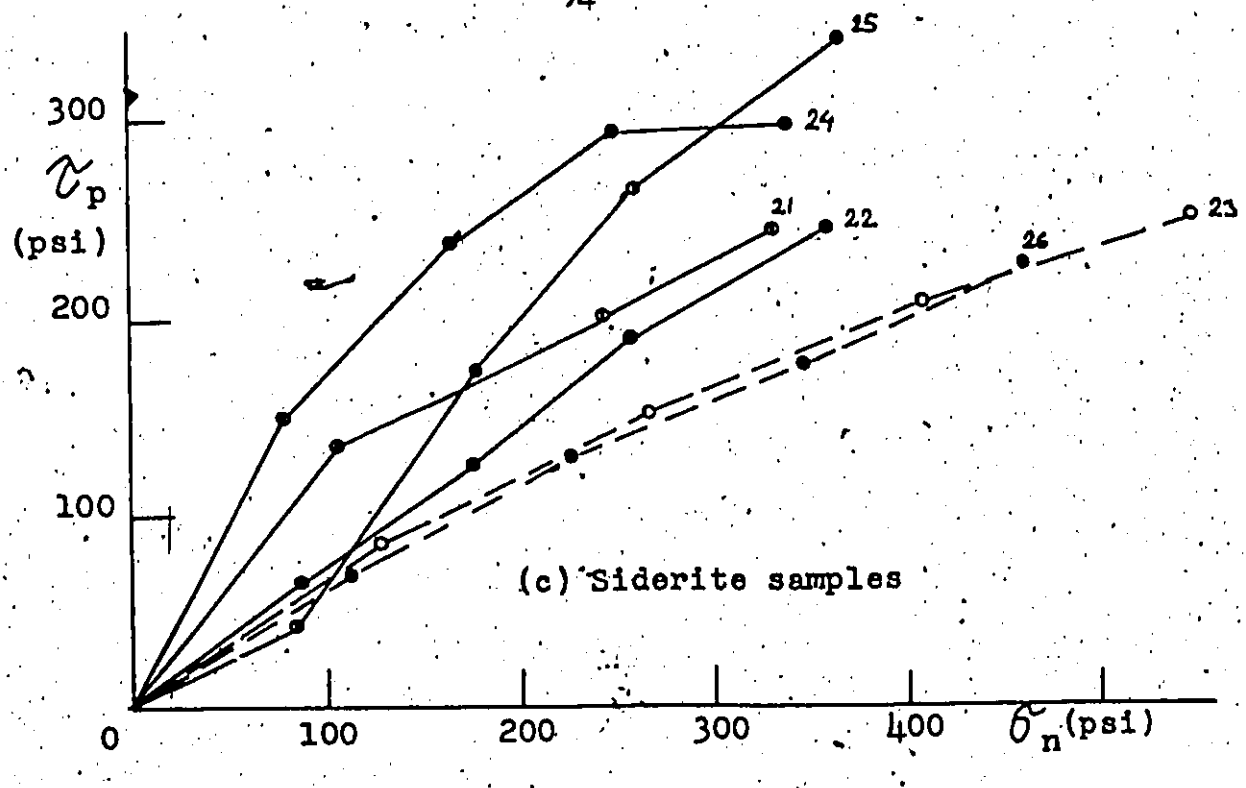

Fig. 5.11 continued

Consequently, from curves of the first category, it may be concluded that longer displacements are required to develop full resistance in sliding over asperities than in shearing them off. The high initial stiffness of the samples belonging to the second category can be explained by the action of relatively small but sharp angled asperities which are strong enough to influence the stiffness at low normal stress, but whose influence decreases as stronger asperities become engaged and sheared at higher σ_n.

The above-mentined differences in deformational behaviour connected with different modes of failure provide further argument for the need of the development of a more refined theory as mentioned in Section 4.3.

The parameter $k_{s0.5p}$ was also plotted against σ_n but these plots did not provide systematic results, probably due to the lack of precision of the experimental procedure with very small displacements.

Returning to the abovementioned strength envelopes, Fig. 5.9, it can be seen that the effective angle of inclination of the asperities i, as defined by Patton (43) varies between 0° and 30° for the limestone samples, 7° and 25° for the sandstone samples and 6° and 27° for the siderite samples. The sliding friction angle ϕ for all three types of rocks is equal approximately to 30° and is shown roughly by the lines representing the failure envelopes for sawcut samples.

Again, an attempt has been made to correlate the tangent of the strength envelopes with the field description of the samples, namely with the estimated inclination of the secondary asperities* as shown in Column 5 of Table A1, Appendix A. The result of this attempt was completely negative and it can be assumed, consequently, that the shearing behaviour of joints, at least with fast loading rates, depends mainly on the configuration of the third order asperities e.g. surface roughness. This opinion was further substantiated by the fact that the average shear stiffness coefficients for the natural joint planes are of the same order and only slightly higher than those for the saw cut surfaces (see Table 5.8, page 87).

The summary of the results of measurements of the off-diagonal stiffness coefficient k_{ns}, representing the normal movement during shear, is given in Table A3, Appendix A. All computations in this table were carried out in the same way as those described above for the values in Table A2. The overall averages of the coefficient k_{ns} are presented in Table 5.8, page 87. Their magnitude is of the same order and not much higher than that of the corresponding coefficients k_s, which seems to indicate that, at least in problems where significant confinement exists,

*For definition see page 55.

the off-diagonal stiffness coefficients should be taken into account by the computing technique.

An attempt at finding a functional relationship between k_{ns}, k_s, and σ_n was made by plotting the ratios presented in Column 9 of table A3 against the normal stress. However, this attempt was unsuccessfull.

Some of the tested joints, such as No. 3, 8 and 13 are contractant as indicated by the negative value of k_{ns}. Another interesting feature of Table A3 is the fact, that the bonded joint in sample 5 exhibits a k_{ns} value which is actually lower than the corresponding k_s. This indicates, that for some bonded discontinuities the magnitude of dilatancy may exceed the amount of tangential movement.

Section 5.5 Summary of Conclusions from the Testing of Joints.

The results of closure tests and direct shear tests on twenty-six samples of three types of rock are presented in Appendix A and discussed in the preceding sections.

The general conclusions derived from these tests may be stated as follows:

- Obtaining undisturbed samples of joints for laboratory testing is difficult. Manual sampling results in a tendency to select joints that are unweathered and unfilled. More sophisticated techniques will have to be develped for sampling other joints.
- Laboratory testing for deformability in shear imposes more rigorous requirements on the design of the testing machine than testing for strength.

- Multi-stage method of conducting the direct shear test appears to be valid with the particular type of joints tested, as long as the sample is not allowed to yield excessively in any but the last stage.
- For the particular type of joints tested, the shear stiffness varies greatly with the level of both normal stress and shear stress. Consequently, using a single value of k_s in computations may be injustified.
- The off-diagonal stiffness coefficient k_{ns} is of the same order of magnitude as the shear stiffness coefficient k_s. Therefore, it should be introduced into the computations, at least in cases where significant confinement exists.
- No satisfactory correlation between k_s or the shear strength and the field description was found, suggesting that both are dependent mainly on the surface roughness.
- The unit shear stiffness coefficient appears generally to increase with the normal stress, following a roughly linear relationship.
- The failure of limestone joints seems to occur by shearing of the asperities, whereas that of sandstone joints appears to be caused by brittle fracture of the asperities.

PART III

Application of the Finite Element Method to Certain Problems of Deformability of Rock Masses Under Surface Loading.

Objectives: As mentioned in the Preface, the objectives of the finite element work in this investigation had to be limited to only a few basic questions in order to fit the scope of the Thesis. Besides the questions posed by the use of the method in this class of problem itself, such as configuration and size of the meshes and preparation of the input data, the other particular objectives are as follows:

1. Evaluate the influence of a single joint existing in a foundation subgrade upon the distribution of stresses and displacements caused by the imposed load and compare the results with analytical solutions obtained on the basis of an assumed stress distribution (Boussinesq's theory).
2. Evaluate the influence of a single joint set on the same problem and compare the results with solutions based on an assumption of anisotropic continuity.

Under the scope of the present work it was not possible to examine any of these problems in the form of a parametric study which would require numerous computer runs and time consuming trial and error procedures. Consequently the conclusions presented below are rather qualitative than quantitative in character and their usefulness is limited to comparison and evaluation of the different approaches to the problem in question.

CHAPTER VI

Computing Techniques and Input Data.

Section 6.1 Finite Element Programs Used.

Two Finite Element programs were made available to the writer by the workers of the Mining Research Centre, Department of Energy, Mines and Resources. Both of these are modifications of programs developed originally at the Department of Civil Engineering, University of California in Berkeley.

The first of these programs incorporates a facility for iterative simulation of "no tension behaviour" (56) and it has a subroutine for forming the one-dimensional joint elements described in Section 1.4. This program was used for all problems in this work involving discontinuities. In addition to the joint elements, the program utilizes standard triangular linear displacement continuum elements in plane strain. Since the problems solved in this work are linear-elastic, only a single iterative step was used.

The second program, identified as WILAX (54) is a multipurpose program which again utilizes linear displacement elements. This program is capable of solving problems in plane strain under the conditions of transverse anisotropy and was therefore used to obtain orthotropic solutions described in Section 7.2. The other options of the WILAX, e.g. plane stress and axisymmetric geometry, bilinear yielding and internal stresses, were not utilized in this work.

Input into the above programs consisted of a complete geometry of the given mesh, zero displacement and line pressure boundary

conditions, isotropic or anisotropic material properties, joint stiffness properties and assorted control parameters. The output included displacements of each node, stresses in x and z directions, shear stresses, principal stresses and the angle of principal planes in the center of gravity of each element.

Section 6.2 Finite Element Models of Jointed Subgrades.

With the existing computational technology, it is possible to simulate jointed subgrade rock by two methods.

First, which will also be refered to as the "discontinuous" method, aknowledges the existence of joints by utilizing the joint elements mentioned in Section 1.4. In the work reported herein, the joint element meshes described in the following are, in their geometric configuration, scale models of hypothetical rock masses.

The input joint stiffness parameters are in such case equivalent to those corresponding to actual joints. In a practical situation, they would be obtained by conducting a suitably large number of tests and averaging the results. For the purpose of this work, hypothetical values of the parameters were selected.

It is possible that closely spaced joint systems might be simulated by meshes with a larger spacing than that corresponding to the scale of the model. For such approach, it would be necessary to derive "combined" stiffness parameters, incorporating the flexibility of several actual joints into a single value. To confirm the validity of this simplification, however, would require a trial study.

Second method of simulating a jointed rock mass relies on deriving "effective deformation parameters" by the formulas given

as equations 7.1 to 7.6 (Page 113). The resulting models are continuous but cross-anisotropic, with an axis of elastic symmetry which is perpendicular to the joint planes.

As stated above, one of the purposes of this part of the Thesis is to compare results obtained by the two methods.

Section 6.3 Mesh Configurations

The basic problem investigated in this work is that of a long strip foundation placed on the surface of a flat subgrade. A simple finite element mesh, numbered 1, representing this situation with the assumption of continuity and isotropy is shown in Fig. B.1, Appendix B. The problem is halved by a plane of symmetry passing through the axis of the footing. Both triangular and quadrilateral elements are used. Directly underneath the loaded area, smaller elements are utilized to account for the steepness of the stress gradient. The contact pressure from the footing is represented by a uniform line stress acting across two elements. Uniform distribution of the contact pressure was chosen in view of the assumed high rigidity of the subgrade rock and also for simplicity.

The boundary conditions include restricted horizontal displacements along the vertical boundaries of the problem and restricted vertical displacements along the lower boundary.

Choosing an adequate size of the mesh, in order to eliminate the influence of the assumed boundary conditions, required some deliberation. Figure 6.1 shows the results of three experimental runs with mesh 1 with three different magnitudes of the ratio between the total width of the mesh and the width B of the footing.

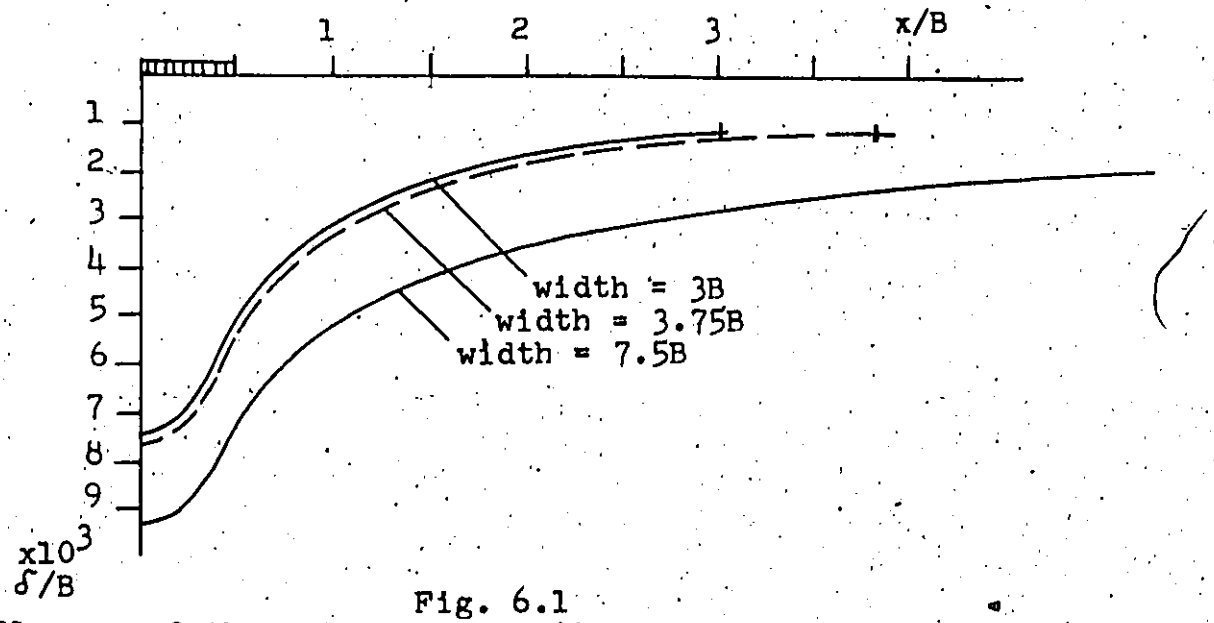

Fig. 6.1
Influence of the extent of the finite element mesh on the settlement curve.

The variations in the size of the ratio were achieved by changing the width of the extreme right column of elements and by reducing B to a half. The comparison of the resulting settlement curves shows that the width of the mesh has two effects:

1. The curve shifts laterally downwards when the mesh is widened. This fact is not detrimental to the interpretability of the results since the curves can be corrected by using a single reference datum sufficiently distant from the loaded area. It is necessary to remember that even in analytical solutions an arbitrary reference datum is required, since surface loading on a semiinfinite elastic body would theoretically yield infinite displacements.

2. The curve is flattened by the presence of the boundary. This deformation, however, affects only that part of the curve which is quite close to the boundary, say within 2B, and it is due to the lack of vertical restraint at the boundary. To eliminate this problem the common reference can be chosen to be at the distance

of 2B from the right-hand boundary of the mesh. If brought under this common reference datum, the three curves are in perfect agreement as shown in Fig. 6.2. For comparison, Fig. 6.2 also shows a settlement curve computed analytically by an integrated Boussinesq equation using the same material properties. Evidently the agreement betweeen the finite element and analytical solution is very good even for the smaller size of the mesh. For our purposes we chose the width of 7.5 B as a minimum.

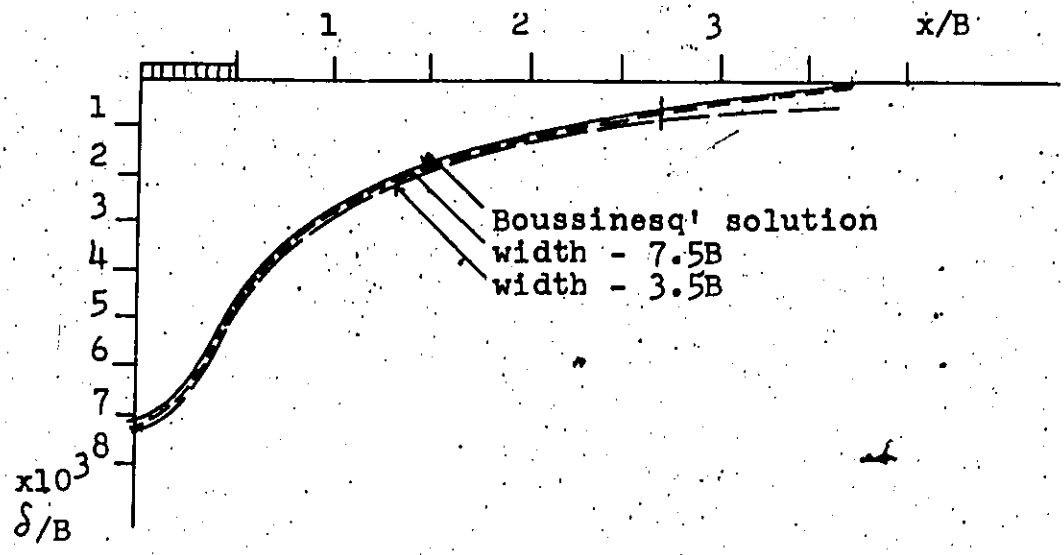

Fig. 6.2
Settlement curves brought under the common reference datum and compared with an analytical solution.

Two other meshes, including horizontal joints, were developed by slight modification of mesh 1. Mesh 2, not shown here, contains a single horizontal joint located beneath the first row of full-size elements. This mesh was used to solve several problems involving a single joint located at different depths below surface. The depth could be varied by changing the width of the loaded area which was equivalent to changing the overall scale of the problem. This is a valid procedure with nondimensional parameters. Thus for example, refering to Fig. B.1, if the half-width of the loaded area

extends over two of the small elements, as shown in the Figure, the depth of the joint is equal to B. If, on the other hand, the loaded area extends over four elements, the depth is decreased to B/2.

But since it was stipulated, as stated above, that the minimum width of the mesh should be equal to 7.5 B, it was decided not to use this method of changing the depth of the joint by modifying the overall size of the problem. Therefore another mesh was created, also similar to mesh 1, in which a single horizontal joint was located within the depth of B/2.

Mesh 3, shown in Fig.B.2, Appendix B., contains a single horizontal joint set. Spacing of the joints can again be varied by using the same procedure as described above.

Another method was used here to obtain different spacings. In this method every odd joint of the set was assigned a very high value of the stiffness parameters k_n and k_s. Thus the deformations across these joints became negligible and the mesh behaved as one with double spacing of discontinuities. The procedure was tested by "eliminating" all joints of the set, which resulted in practically equal values of stresses and displacements as those obtained from the continuous mesh No. 1. By using the same procedure, the spacing could be tripled or quadrupled as well, without changing the scale of the problem.

Mesh 4, depicted in Fig.B.3, represents a single joint set, dipping at 45°. Naturally, symmetry does not exist here and the problem must therefore be run on a full mesh. The size and boundary conditions for this mesh were the same as for mesh 1. Scaling factors were incorporated into the input mechanism of the program to enable proportional increasing of either all the vertical or

horizontal coordinates. In this way it would be possible to change the dip angle of the joint set within the range of approximately 30° to 60°. But this feature was unfortunately never used in the present work.

All of the meshes, as well as the two programs, were stored on card decks. The geometrical setup of the meshes was checked by using a plotting program.

Section 6.4 Input Parameters.

Since, as stated in the Objectives, the purpose of this investigation was neither a parametric study, nor a quantitative analysis of a specific problem, the choice of the input properties was made rather arbitrarily.

In order to keep the basic input parameters in the proper proportions, the following dimensional input values were used:

width of the footing $B = 100"$

contact stress $q = 1\ 000$ psi

Young's modulus of the intact rock $E = 3 \times 10^6$ psi

Poisson's ratio of the intact rock $\mu = 0.2$

Shear and normal stiffness coefficients of the joints $k_s = k_n = 4 \times 10^3$ psi/in

By adopting the parameters B and q as units, the following nondimensional input parameters were obtained from the above quantities:

$$\frac{E}{q} = 3 \times 10^3$$

$$\frac{k_n' B}{q} = \frac{k_s B}{q} = 400$$

$$\mu = 0.2$$

These parameters were then input as material properties into the program, with nondimensional variables being the coordinates $\frac{x}{B}$ and $\frac{z}{B}$, and joint spacing or depth $\frac{S}{B}$ or $\frac{D}{B}$. The resulting output quantities were also nondimensional, being the stresses $\frac{\sigma}{q}$ and $\frac{\tau}{q}$, and deformations $\frac{\delta x}{B}$ and $\frac{\delta y}{B}$. The advantage of this nondimensional input and output from the program was in a ready comparison of the results of different runs and the possibility of always changing only one variable at a time.

CHAPTER VII

Results and Conclusions from the Finite Element Modelling Program.

Section 7.1 Examples of the Influence of a Single Horizontal Discontinuity Upon the Stresses and Displacements Beneath a Strip Footing.

Fig. 7.1 shows the comparison of three surface settlement curves for the strip footing problem as described in the previous Chapter. The first curve is that for a continuous, homogeneous subgrade. The second and third curves represent a subgrade containing a single horizontal joint, located at a depth equal to the width of the footing B and B/2 respectively.

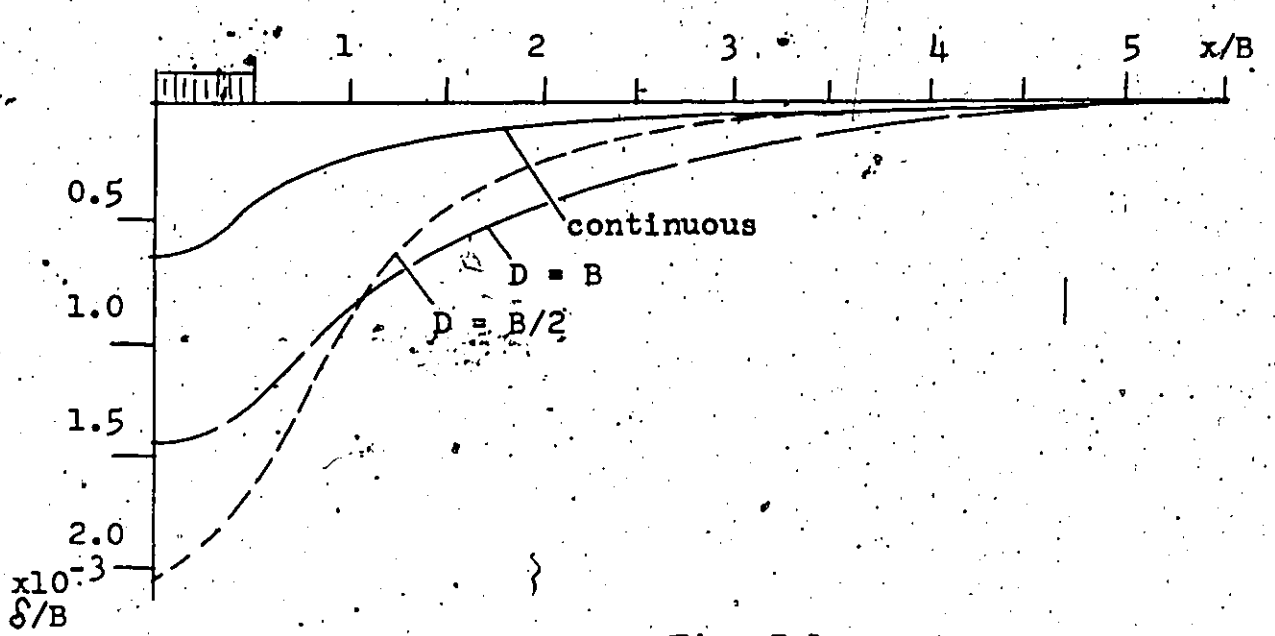

Fig. 7.1
Influence of a single horizontal joint upon the settlement curve underneath a strip footing.

The input parameters used in these three solutions were those given in Section 6.3 and the curves were brought under a common reference datum as described in Section 6.2.

Evidently, the presence of the joint in the subgrade has a

pronounced effect upon the distribution and magnitude of the settlement. We will use the above results to test two hypotheses, which might be used in practice in order to solve this particular problem without the use of a computer.

Hypothesis 1: The presence of the joint affects largely the deformations but its effect upon the stress distribution is relatively small; Therefore it would be possible to account for the additionl settlement due to the discontinuity by assuming that the Boussinesq stress distribution remains valid. The total settlement could then be computed by estimating the amount of the joint closure by dividing the vertical Boussinesq's stresses at the level of the joint by k_n, and simply adding this to the settlements obtained for the continuous case.

Table 7.2 shows the values of vertical stresses computed in nine points along the horizontal plane located at D = B/2 with the assumption of continuity. The second line of the table gives the amounts of joint closure corresponding to these stresses. In Figure 7.3, the values of joint closure are superimposed upon the settlement curve for the continuous case. In the same Figure, the settlement curve obtained from the finite element solution with the joint is also shown.

Table 7.2 Joint closures corresponding to an assumed Boussinesq's stress distribution on a joint located at D = B/2

Point No.	1	2	3	4	5	6	7	8	9
Vert. Stress (nondim.)	0.774	0.605	0.353	0.152	0.055	0.024	0.009	0.001	0.0005
Joint Closure (nondim.) $\times 10^3$ $\frac{k_n B}{q} = 400$	1.93	1.51	0.88	0.38	0.14	0.06	0.02	0.00	0.00

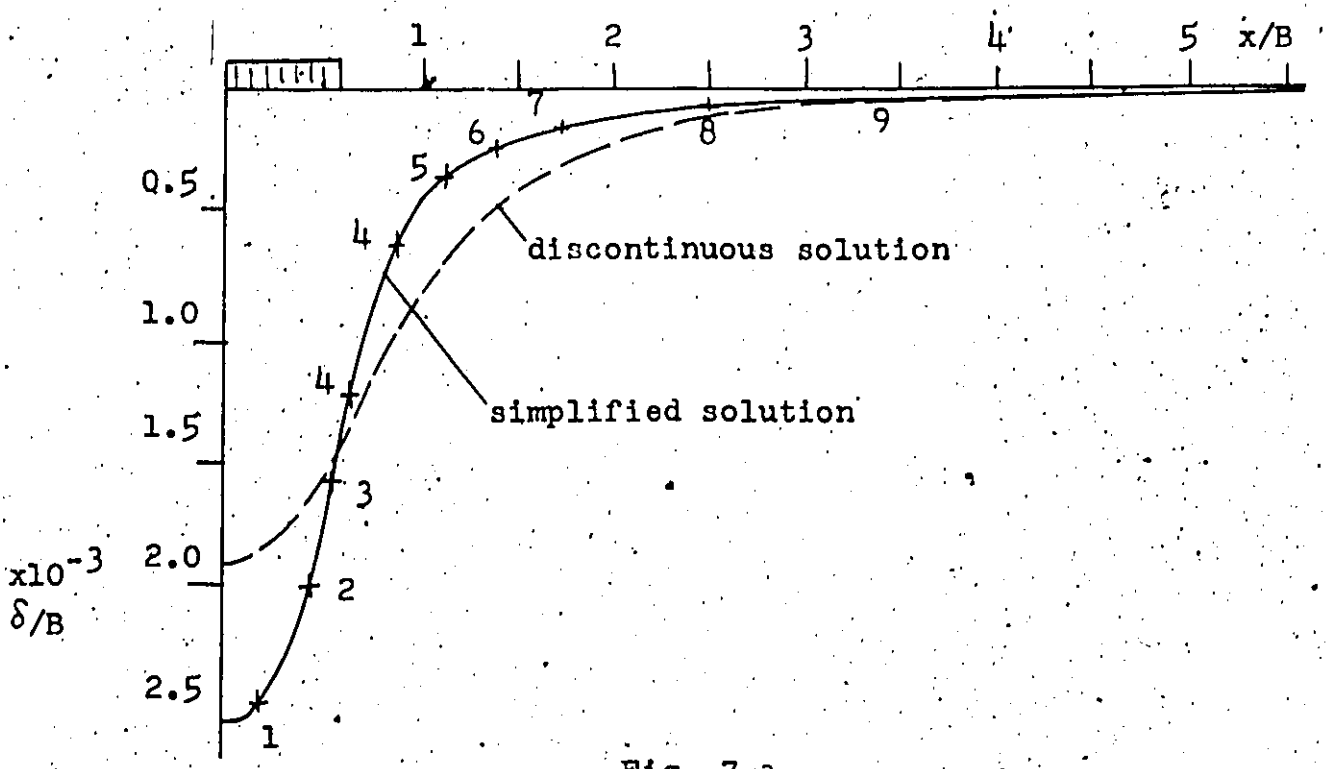

Fig. 7.3
Comparison of settlement curves computed by a finite element program and analytically.

It may be seen form this comparison, that the simplified procedure results in an overestimate of the settlements directly below the loaded area. This is caused by the fact, that the simplified approach disregards the additional bending stiffness of the layer of intact material above the joint, which acts as a beam on an elastic subgrade. But it is also true, that if there were some vertical joints in the abovementioned layer, its bending rigidity would in reality be reduced and the actual settlement curve would probably come a bit closer to the one predicted by the simplified method. In conclusion it can be stated, that the above approach would, in fact, yield a reasonably good estimate of the settlement which would in any case be on the safe side. For such approach to, be useful, however, it is necessary to know the value of the unit normal stiffness coefficient k_n.

Another practical question connected with this problem configuration has been considered by Waldorf (49) and may be stated as follows:

Hypothesis 2: A plate load test is conducted on a rock mass which contains a major horizontal discontinuity located at a certain depth.

The purpose of this test is to predict settlements of a prototype, which loads an area several times wider than the area of the plate. Obviously the effect of the discontinuity upon the settlement of the prototype will be much greater than upon that of the plate since, due to the larger width of the loaded area, the joint will be placed higher on the vertical stress diagram as shown in Fig. 7.4.

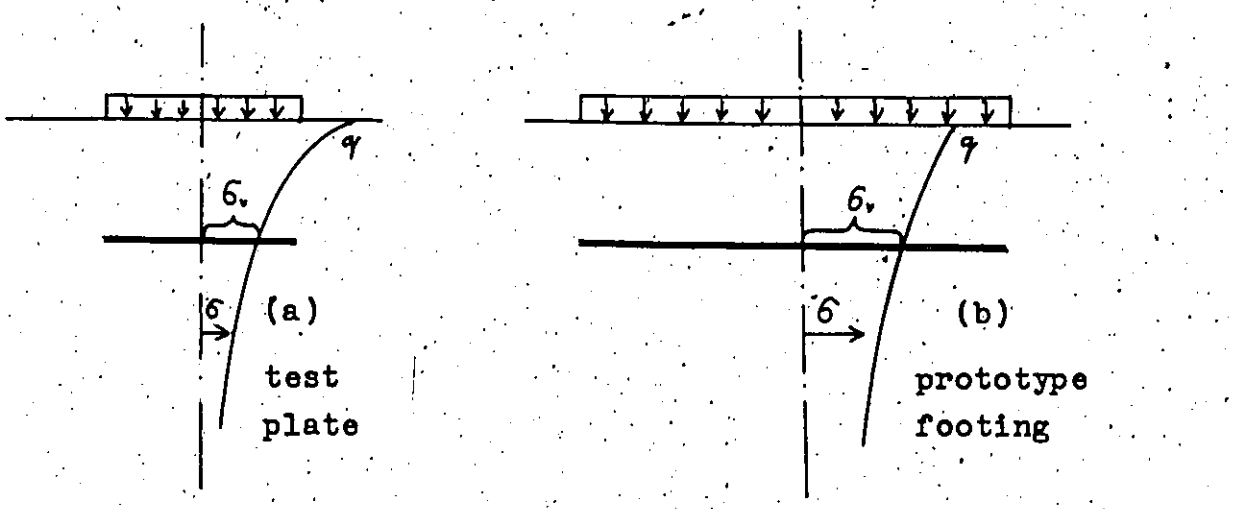

Fig. 7.4
The stress acting upon a single horizontal joint underneath a test plate and a prototype foundation.

Waldorf (49) suggested the following scaling procedure to obtain the settlement of the prototype, based upon the knowledge of the modulus of deformation of the intact rock. Firstly, the theoretical settlement of the plate is computed by the Boussinesq's theory assuming that there is no discontinuity. This value is then subtracted from the observed settlement and the resulting difference Δh is attributed to the closure of the joint. Vertical stress σ_v

acting on the joint is estimated from the elastic continuous theory and the "unit normal stiffness coefficient" can then be computed as

$$k_n = \frac{\sigma_v}{\Delta h}$$

Turning to the prototype, the inverse procedure can now bw used to obtain the predicted settlement. Again, the vertical stress at the joint is estimated, then it is divided by the above stiffness coefficient and the resulting value of the joint closure is added to the computed "continuous" settlement.

Of course, the above procedure again disregards the stress redistribution caused by the presence of the joint. With the results of the finite element analysis presented at the beginning of this Section we can again test the magnitude of the error involved in such procedure. To do this, we will attempt to predict the settlement of a strip footing with a width 2B, from that of a long "plate" which has a width B.

All necessary numerical values may be obtained by scaling from Fig. 7.1. The nondimensional settlement under the middle of the "plate" is equal to 1.41×10^{-3}. The continuous solution would give the same settlement as 0.64×10^{-3}. The "joint closure" would then be equal to $1.41 - 0.64 = 0.77 \times 10^{-3}$. At a depth equal to B, the nondimensional vertical stress is obtained from a Boussinesq's chart for a strip footing as 0.55. The nondimensional "unit normal stiffness coefficient" $\frac{kB}{q}$ is therefore equal to $0.55/0.77 \times 10^{-3} = 0.71 \times 10^{3}$. For comparison we may note, that the "real" stiffness coefficient used in the computer solution is 0.4×10^{3} as stated in Section 6.3.

In the prototype, the joint is located at the depth of B/2. The Boussinesq's chart gives a value of the vertical stress of 0.80 for this depth. The "joint closure" under the prototype would then be equal to $0.80/0.71 \times 10^{3} = 1.13 \times 10^{-3}$. The nondimensional "continuous" settlement for the prototype is again 0.64×10^{-3}. Thus the predicted nondimensional total settlement underneath the center of the prototype footing would be equal to $0.64 + 1.13 = 1.77 \times 10^{-3}$. But the same settlement, computed rigorously by the finite element program may be read from Fig.7.1 as 1.95. Thus, the above procedure yields a predicted settlement which is in error by roughly 10% on the unsafe side for a prototype to model ratio of only 2.0. The error is again due to the disregarding of the bending rigidity of the layer overlying the joint, which results in an overestimate of the joint stiffness coefficient in the first step of the procedure. It is obvious, that the magnitude of the error would increase with increasing prototype to model ratio. An extreme case of the same error is such, where the width of the loading plate is so small, that the discontinuity is hardly stressed at all.

The above conclusion seems to cast doubt on the validity of using similar procedures for interpretation of plate loading tests. It also seems to make a point for using more refined analyses based on numerical methods.

Section 7.2 Examples of a Single Joint Set.

Not unlike a layered material, jointed rock behaves anisotropically, being more rigid in the direction parallel to the discontinuities than in the perpendicular direction. Equations expressing this phenomenon in a quantitative way may be given as

follows (6):

$$E_n = \left(\frac{1}{E} - \frac{1}{Sk_n} \right)^{-1} \qquad \text{Eqn. 7.1}$$

$$E_s = E \qquad \text{Eqn. 7.2}$$

$$\mu_{ns} = \frac{\mu E_n}{E} \qquad \text{Eqn. 7.3}$$

$$\mu_{sn} = \mu \qquad \text{Eqn. 7.4}$$

$$G_{ns} = \left(\frac{1}{G} - \frac{1}{Sk_s} \right)^{-1} \qquad \text{Eqn. 7.5}$$

$$G_{sn} = G \qquad \text{Eqn. 7.6}$$

where:

E_n is the effective modulus of deformation in the direction perpendicular to the joints

E_s is the same in the direction parallel with the joints

μ_{sn} is the effective Poisson's ratio relating strains in the perpendicular direction to those in the parallel direction

μ_{ns} is the same relating strains in the parallel direction to those in the perpendicular direction

G_{ns} is the modulus of rigidity in the plane perpendicular to the joints

G_{sn} is the same in the plane parallel to the joints

E and μ are the deformation modulus and Poisson's ratio of the intact rock

$G = \frac{E}{2(1+\mu)}$ is the modulus of rigidity of the intact rock

S is the average spacing of the joints

k_n and k_s are the unit normal and shear stiffness coefficients of the rock joints.

The above equations were derived by considering the deformations of a block of jointed media under stresses acting perpendicularly and in parallel to the layers and equating the deformations with those of a block of a hypothetical anisotropic material. Upon obtaining the necessary effective deformation coefficients one can solve stress-strain problems in the jointed rock mass by utilizing the theory of elasticity of a transversally anisotropic body.

The solution of a relevant problem in transverse anisotropy, that of a line load acting on plane surface with an axis of elastic symmetry being perpendicular to the plane[2], was obtained by Michell(38) and may be stated as follows:

$$w_a = w \times K \qquad \text{Eqn. 7.7}$$

Where w_a is the vertical settlement on the transversally anisotropic ground

w is the settlement on an isotropic material with properties E and μ

and
$$K = \frac{1}{2(1-\mu)} \sqrt{\frac{A}{L}} \frac{[(AC + L)^2 - (F + L)^2]^{\frac{1}{2}}}{AC - F^2}$$

(nondimensional) Eqn. 7.8

From the form of the equation 7.7 we may see, that the effect of the transverse anisotropy is only a proportional increase in the settlements computed by the Boussinesq's theory. Therefore any solution, obtained in plane strain from an ordinary elastic theory may readily be extended for the condition of transverse anisotropy, simply by multiplying the settlements by the constant K.

---

[2] In other words the elastic properties of the material being different in vertical and horizontal directions.

The coefficients in equation 7.8 are obtained as follows:

$$A = \frac{n}{\phi}(1 - n\mu_{sn}^2)$$

$$C = \frac{1}{\phi}(1 - \mu_{sn}^2)$$

$$F = \frac{1}{\phi}\mu_{ns}(1 + \mu_{sn})$$

$$L = \frac{G}{E}$$

$$N = \frac{n}{2(1 + \mu_{sn})}$$

where $$\phi = (1 + \mu_{sn})(1 - \mu_{sn} - 2\mu_{sn}\mu_{ns})$$

$$n = \frac{E_s}{E_n}$$

and all the other constants are as defined by equations 7.1 to 7.6.

We may now use the finite element solution of the problem of a foundation on a rock mass containing a single horizontal joint set to test the validity of the approximation represented by equations 7.1 to 7.6. For this purpose, mesh No.3 is used with nondimensional input parameters as given in Section 6.3. The continuous anisotropic solution to the same problem is obtained by two means, which include computer runs by Wilax program using mesh No. 1, and analytical solutions utilizing the integrated Boussinesq's equation and the Michell's coefficient obtained from equation 7.8. Table 7.6 summarizes all the necessary data.

The solutions of two problems, with average joint spacing equal to B, and B/2, are shown in Fig. 7.5, which summarizes the results of all three methods. The settlement curves in the figure have again been brought under a common reference datum as discussed in Section 6.2.

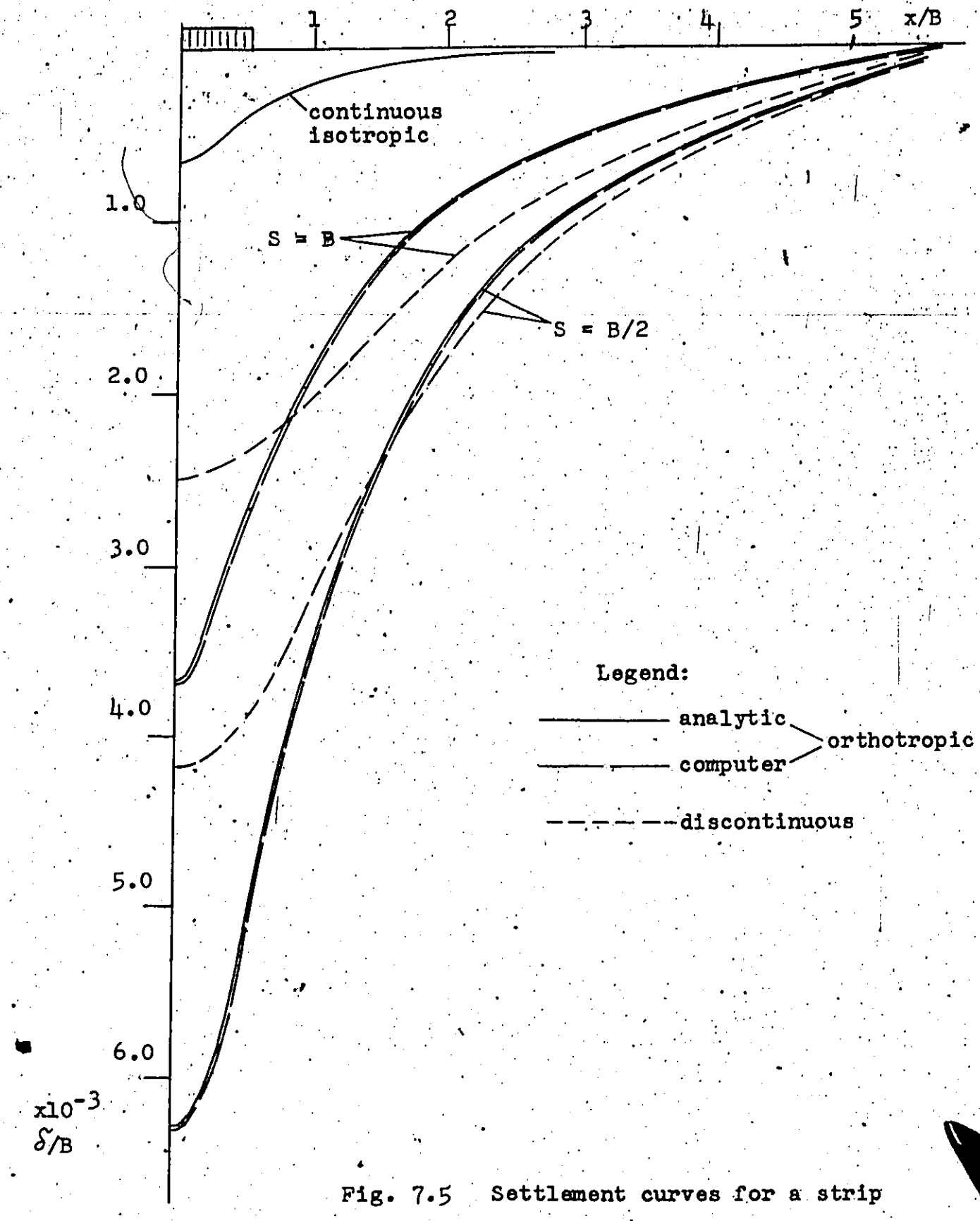

Fig. 7.5 Settlement curves for a strip footing on horizontally jointed subgrade

Table 7.6 Constants for transversal anisotropy obtained by means of equations 7.1 to 7.6 and 7.8.

Nondimensional Input Values (see Section 6.3):

$E/q = 3\,000$

$\mu = 0.2$

$\frac{k_n B}{q} = \frac{k_s B}{q} = 400$

Spacing S/B	E_n	E_s	μ_{ns}	μ_{sn}	G_{ns}	G_{sn}	K
1.0	353	3000	0.0235	0.2	303	1250	5.891
½	187	3000	0.0125	0.2	172	1250	10.351
¼	97	3000	0.065	0.2	92	1250	18.964

The analytical solutions are in perfect agreement with the anisotropic computer solutions which is a check of the correctness of the later.

The discontinuous solutions, on the other hand, differ by approximately 40% underneath the axis of the footing.

An investigation can now be made into the cause of such difference. It may be argued that the equations 7.1 to 7.6, derived on the assumption of a constant stress, are not valid under a stress gradient. We will, therefore, re-derive equation 7.1 for the case of a constant stress gradient C.

Consider a block of material consisting of n layers separated by n joints as shown in Fig. 7.7. The height of the block is h, and the spacing of the joints is S = h/n. The block is acted upon by a vertical stress σ, such as self-weight, proportional to the distance z from the top.

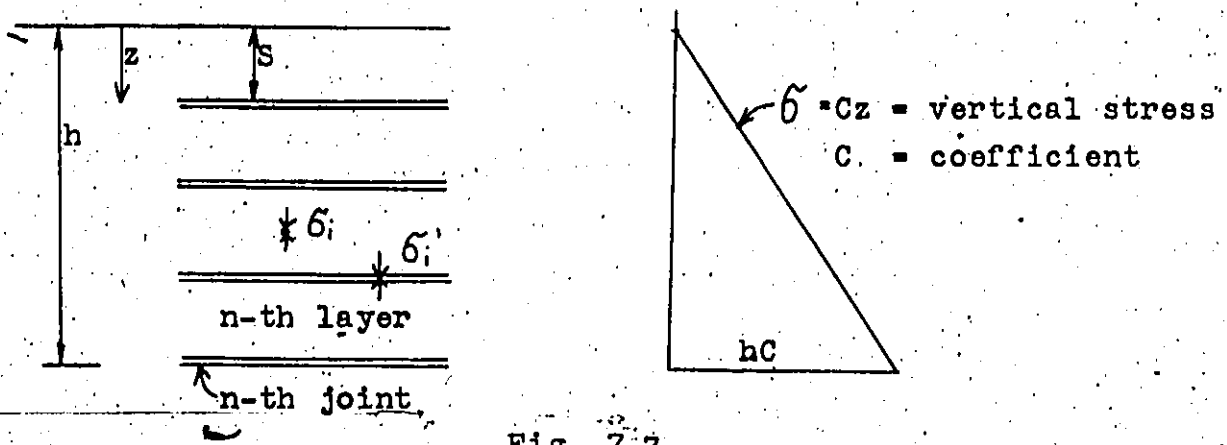

Fig. 7.7
Derivation of effective deformation modulus for the case of a constant stress gradient.

If the layers were replaced by an "equivalent" orthotropic continuum, the displacement of the top could be computed as:

$$\delta_{ortho} = C \times \frac{h}{2} \times h \times \frac{1}{E_n} = \frac{Ch^2}{2} \left(\frac{1}{E} + \frac{1}{Sk_n} \right) \qquad \text{Eqn. 7.9}$$

where of course $C \times \frac{h}{2}$ represents the average stress acting on the block.

More precisely, the displacement of the top of the jointed block may be computed as follows:

$$\delta_{jointed} = \sum_{i=1}^{n} \frac{\sigma_i S}{E} + \frac{\sigma_i'}{k_n}$$

where $\sigma_i = C\,(i - \frac{1}{2})\,S$ is the average stress in the i-th layer.
and $\sigma_i' = C \cdot i \cdot S$ is the stress in the i/th joint.

Substituting into the above, rearanging and using the relation $\sum_{i=1}^{n} i = \frac{n(n+1)}{2}$ we obtain:

$$\delta_{jointed} = \frac{Ch^2}{2} \left[\frac{1}{E} + \frac{1}{k_n S} \left(1 + \frac{1}{n}\right) \right] \qquad \text{Eqn. 7.10}$$

Comparing Equations 7.9 and 7.10 one concludes, that the absolute error involved in using the orthotropic approximation is equal to:

$$\delta_{jointed} - \delta_{ortho} = \frac{Ch^2}{2n} = \frac{Ch\,S}{2}$$

e.g. for a given h the error is directly proportional to the magnitude of the joint spacing S.

By refering to Fig. 7.5, however, it is found that the relative error of the orthotropic solution does not, in fact, decrease with smaller joint spacing as would be indicated by the above result. Therefore, one must look for another possible source of error.

Equations 7.1 to 7.6 have been derived on the assumption of unidirectional stress. The stress field underneath a foundation is, on the other hand, completely general and multidirectional. There are certain expressions (invariants) for the elastic constants of an anisotropic continuous body, which should remain constant when the reference axes are rotated. Two of such invariants are given by Lekhnitski (34) as follows:

$$I_1 = \frac{1}{E_1} - \frac{1}{E_2} - \frac{2\mu_{1,2}}{E_1} \qquad \text{Eqn. 7.11}$$

$$I_2 = \frac{1}{G_{1,2}} - \frac{4\mu_{1,2}}{E_1} \qquad \text{Eqn. 7.12}$$

where E, μ and G are elastic constants and the indices 1 and 2 represent two mutually perpendicular directions, say vertical and horizontal.

By substituting the "effective material properties" for jointed mass into equations 7.11 and 7.12 we can test their validity for problems involving general stress fields such as the problem in question. To do so, the equations 7.1 to 7.6 need to be re-derived for the case of an oblique stress which is neither parallel nor perpendicular to the jointing.

Refering to Fig. 7.8 we will compute displacements under the vertical uniform stress σ_1 and horizontal stress σ_2 acting across a single layer and a single joint inclined at the angle α to the vertical.

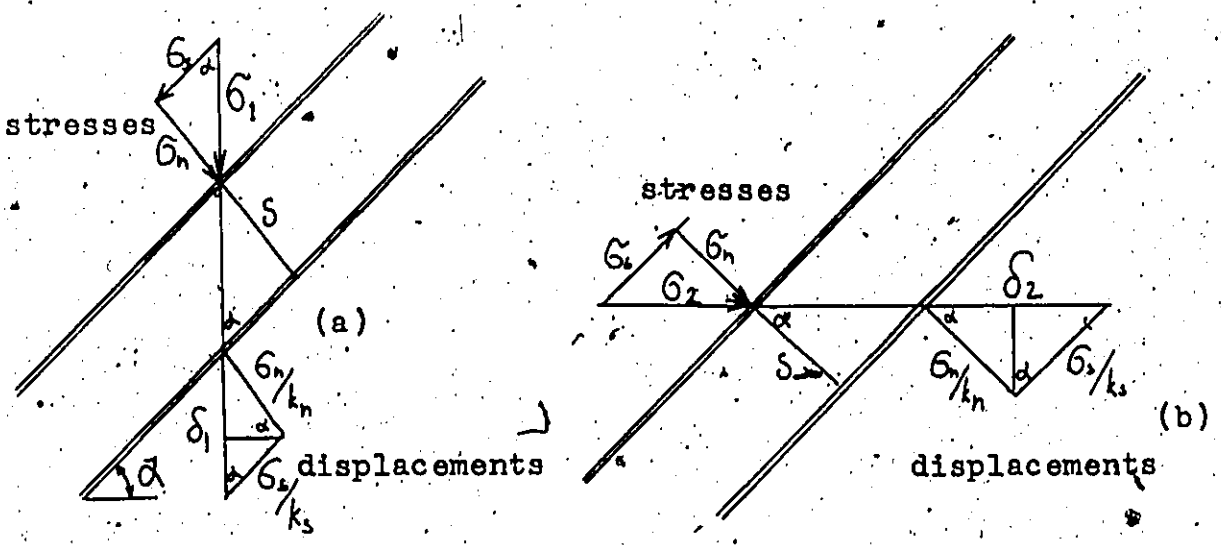

Fig. 7.8
Derivation of the effective material properties for the case of an oblique stress.

For the vertical direction (see Fig. 7.8a)

$$\delta_1 = \sigma_1 \left(\frac{S}{E \sin\alpha} + \frac{\sin^2\alpha}{k_n} + \frac{\cos^2\alpha}{k_s}\right)$$

where E, S, k_n and k_s are as defined above.

The same displacement using an "effective" modulus of deformation E, would be:

$$\delta_1 = \frac{\sigma_1 S}{E_1 \sin\alpha}$$

Combining the two equations

$$E_1 = \left[\frac{1}{E} + \sin\alpha \left(\frac{\sin^2\alpha}{S k_n} + \frac{\cos^2\alpha}{S k_s}\right)\right]^{-1} \qquad \text{Eqn. 7.13}$$

Similarly from Fig. 7.8b the following can be derived:

$$E_2 = \left[\frac{1}{E} + \cos\alpha \left(\frac{\cos^2\alpha}{S k_n} + \frac{\sin^2\alpha}{S k_s}\right)\right]^{-1} \qquad \text{Eqn. 7.14}$$

also:

$$\mu_{1,2} = \frac{-\epsilon_2}{\epsilon_1} = \frac{\mu E_1}{E} \qquad \text{Eqn. 7.15}$$

Substituting from equations 7.13, 7.14 and 7.15 into equations 7.11 and 7.12it is found that:

$$I_1 = \frac{2}{E} + (\sin^3\alpha + \cos^3\alpha)\frac{1}{S_{k_n}} + (\sin\alpha\cos^2\alpha + \cos\alpha\sin^2\alpha)\frac{1}{S_{k_s}}\frac{2\mu}{E} \qquad \text{Eqn. 7.16}$$

$$I_2 = \frac{1}{G_{1,2}} + \frac{4\mu}{E} \qquad \text{Eqn. 7.17}$$

The elastic invariants are now expressed as functions of the properties of the jointed material and the angle α between the layers and the axes of reference. Arbitrary rotation of the reference axes in now effected by changing the angle α. But the terms I_1 and I_2 represented by equations 7.16 and 7.17 are not independent of the angle α [3] and consequently are not invariants. It may further be noted, that this is so without respect to the magnitude of the spacing S. The apparent conclusion then is, that the "effective" parameters of equations 7.1 to 7.6 represent only a rough approximation of the actual elastic behaviour of the discontinuous mass, which does not improve with decreasing spacing. The error, however, again appears to be on the conservative side and therefore the above simplification will certainly still be useful in many practical problems, especially since it affords simple analytical solutions to be found with the help of equation. 7.7.

---

3 In case of Equation 7.17 this is because $G_{1,2}$ which has not been expressed in terms of α obviously is not a constant.

The last problem which has been examined with the help of the two programs is that of a foundation on a subgrade containing a single joint set dipping 45°.

Surface settlement curves resulting from two runs, with joint spacing equal to B and B/2 are shown in Fig. 7.9. Also in the same figure are superimposed settlement curves from the corresponding continuous - isotropic solution and from an orthotropic solution using the "effective" material properties for spacing S = B/2. The influence of the assumed boundary conditions on these solutions appears to be strong and is more difficult to correct. This is because the asymetry of the problem tends to produce relatively large horizontal movements. It would be necessary to try using modified boundary conditions for this problem in order to determine the exact shape of the settlement curves close to the boundary. This, however, was not done in the present work and the curves in Fig. 7.9 are presented without correction. Still, some qualitative conclusions may be drawn from the figure.

The inclined joint set has a much smaller effect on the settlement of the footing than a corresponding horizontal set (cf. Fig. 7.5). The chief difference between the discontinuous and orthotropic solution is in the fact that the orthotropic solution is symmetrical, whereas the discontinuous solution is not. In fact, the footing tilts on the layered subgrade in the sense which is opposite to the dip of the joints. The same phenomenon has actually been observed by the authors of Ref. 14 who conducted plate load tests on steeply dipping, layered shale. They observed tilting of the loading plate which, when translated to the scale of the prototype bridge, would amount to several inches of displacement at

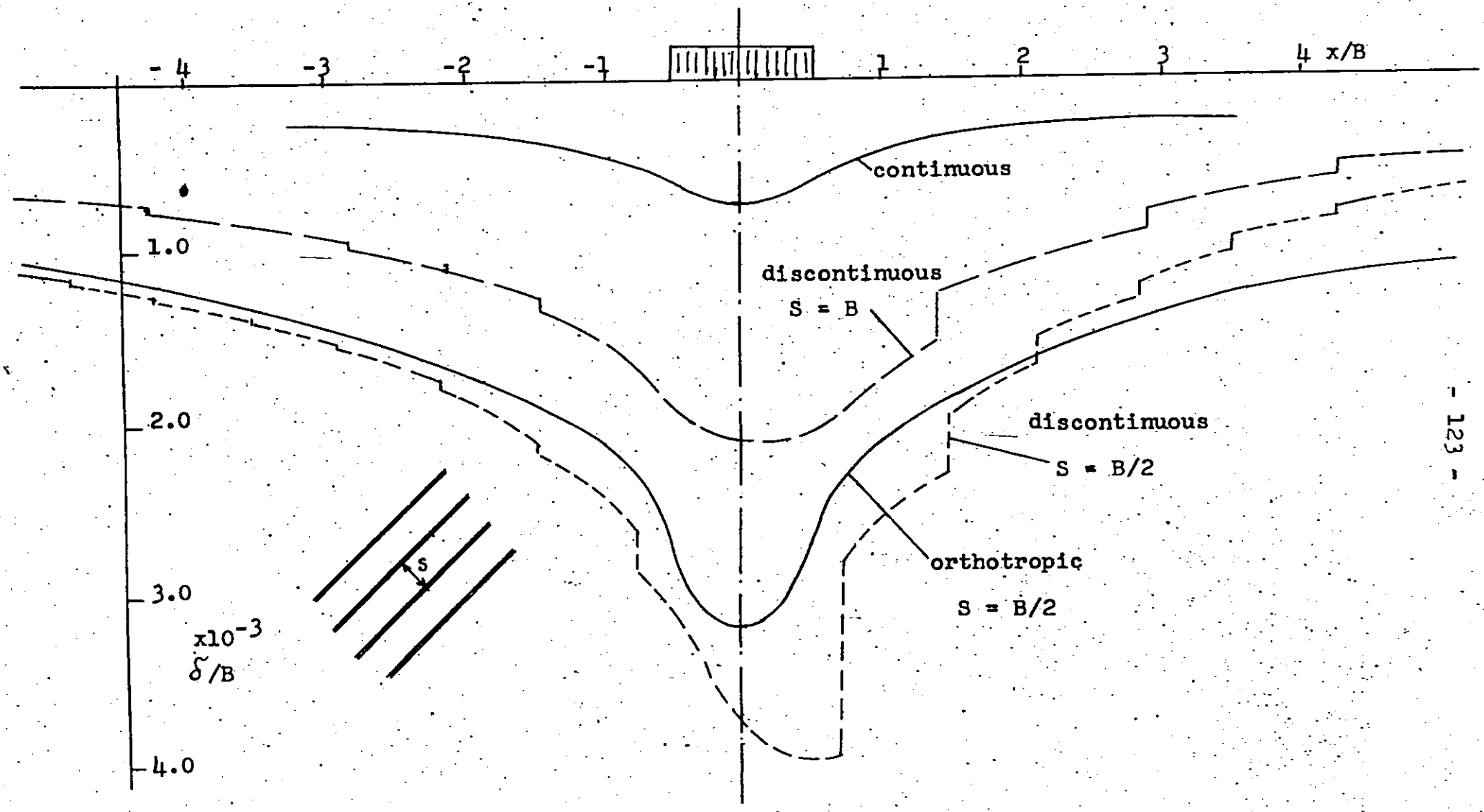

Fig. 7.9 Foundation on a subgrade containing a joint set dipping 45°

the top of the pier. The authors of the above reference also conducted inclined plate load tests to measure elastic properties of the layered mass in the directions parallel and perpendicular to the joints. Their conclusion was that the resulting deformation moduli would not give an elliptical form of the diagram of anisotropy which is a consequence of the discontinuous nature of the medium.

Section 7.3 Summary of the General Conclusions from the Finite Element Modelling Study.

The following conclusions result from the work reported in this Chapter.

- The choice of a minimum width of the finite element model creates a problem which appears more serious in jointed or anisotropic models.
- The assumption of the Boussinesq's stress distribution in jointed rock masses leads to conservative although fairly realistic estimates.
- A scaling procedure based on Boussinesq's stress distribution in jointed rock, if used to interpret a plate load test, will result in an optimistic settlement estimate.
- A jointed medium cannot be exactly represented by transverse-anisotropic continuum; the error of such representation does not decrease with closer joint spacing.
- A footing placed on a rock subgrade containing a dipping joint set will tilt in a sense opposite to the direction of the dip. This would not be predicted by a transverse anisotropic representation.

From the previous it is found that the existing analytical methods of treatment of jointed subgrades involve relatively large amounts of imprecision. However, given the difficulty of obtaining reliable data on the configuration of rock structures and on the elastic properties of the different elements, the use of the simplified methods will probably always remain justified and their imprecision will be a minor factor in the total error of the actual practical solutions. The more precise computer based methods, on the other hand, have an advantage in providing a deeper understanding of the nature of each problem in the whole and in details.

CHAPTER VIII

Suggestions for Further Research.

The approach to the problem of deformability of rock mass which was discussed in this Thesis is based on some quite recent trends both in the testing techniques and computational technology utilized by the science of Rock Mechanics. Therefore, the field in which original research could be carried out is extremely wide. The suggestions here will be limited to only two specific points, where succesfull research endeavour could produce design guidelines such as are strongly needed by the general practice of foundation engineering:

1. Joint deformability testing: If the average joint deformability parameters were reliably known for certain types of rock masses, perhaps particular formations, relationships similar to that shown in Fig. 5.7, Page 89 could possibly be used directly for estimating settlements. The parameters would have to be obtained by carefully conducted sampling and testing, judicial classification and statistical treatment of the results; the design relationships would have to be checked by large scale field load testing or performance observations. Most important in the author's opinion, is testing for stiffness under normal load, which is only marginally covered by the published literature and yet is most relevant to problems of horizontally jointed masses. The testing program should also include examinations of compressibility of infilling material of thick joints. Intact samples of such material can sometimes

quite easily be recovered from test pits or other excavations.

2. Computer parametric studies: Computer programs could be used to establish relationships between the many different variables involved in a rock mass deformation problem such as stiffness parameters, spacing, and attitude of joints. Especially important would be an investigation of the influence of vertical joints upon a horizontally bedded rock mass, which would throw more light upon the question of the representative approximate stress distribution as discussed in Chapter 7 of this Thesis.

It is understood, that computer studies by themselves, even if their results were quantitative in nature, could not provide directly design oriteria. The relations obtained from such studies, on the other hand, could help in correct interpretation of results obtained by other means, as partly illustrated by the hypothetical exmaple of a plate load test interpretation given in Section 7.1.

Several additional suggestions for future research were given in the previous chapters of this Thesis.

REFERENCES

1. Benson, R.P., D.K.Murphy and D.R.McCreath, "Modulus Testing of Rock at the Churchill Falls Underground Powerhouse, Labrador", ASTM Special Technical Publication No. 477, 1969.

2. Billings, M.P., "Structural Geology", 3rd edition, Prentice-Hall, 1972.

3. Boughton, N.O., "Correlation of Measured Foundation Modulus with the In Situ Rock Properties", Proc., International Symposium on Rock Mechanics, Madrid, 1968.

4. Bowden, F.P. and D.Tabor, "The Friction and Lubrication of Solids", London, Oxford, 1950.

5. Byerlee, J.D., "Frictional Characteristics of Granite under High Confining Pressure", Journal of Geophysical Research, Vol. 72, No. 14, July 1967.

6. Coates, D.F., "Rock Mechanics Principles", 2nd edition, Mines Branch Monograph No.874, Government of Canada, revised 1970.

7. Coates, D.F. and M.Gyenge, "Plate-load Testing of Rock for Deformation and Strenth Properties", ASTM, Special Technical Publication No. 402, 1966.

8. Coulson, J.H., "The Effects of Surface Roughness on the Shear Strength of Joints in Rock", Ph.D. Thesis, U. of Illinois, 1970.

9. Deere, D.U., "Technical Description of Rock Cores for Engineering Purposes", Rock Mechanics and Engineering Geology, Vol. 1, No. 1, 1963.

10. Deere, D.U., A.J. Hendron, F.D. Patton and E.J. Cording, "Design of Surface and Near Surface Construction in Rock", Proc., Symposium on Rock Mechanics, 8th, American Institute of Mining and Metalurgical Engineers, 1967.

REFERENCES

11. Duncan, N., and K.E.Hancock, "The Concept of Contact Stress in the Assesment of the Behaviour of Rock Masses as Structural Foundations", Proc., Congress of the Int. Soc. for Rock Mechanics, 1st. Lisbon Vol. 2, 1966.

12. Duncan, N., "Engineering Geology and Rock Mechanics", Vol.2, Int. Textbooks, 1969.

13. Dvorak, A., and P.Peter, "Field Tests on Soils and Rocks", Proc., International Conference on Soil Mechanics and Foundation Engineering, 5th, Paris, Vol. 1, 1961.

14. Dvorak, A., "Tests of Anisotropic Shales for Foundation of Large Bridges", Congress of the Int. Soc. for Rock Mechanics, 1st, Lisbon, Vol. 11, 1966.

15. Evdokimov, P.D. and D.D.Sapegin, "Stability, Shear and Sliding Resistance and Deformation of Rock Foundations", Israel Program for Scientific Translations, Jerusalem, 1967.

16. Feld, J., "Tolerance of Structures to Settlement" Design of Foundations for Control of Settlement, Proc., ASCE Vol. 80, No. SM4, 1954.

17. Fischer, K., "Zur Berechnung der Setzung Eines Starren, Mittig Belasteten Plattenstreifens auf Geschichteter Unterlage.", Beispiele zur Bodenmechanik, Wilhelm Ernst and Sohn, Berlin, 1965.

18. Goldstein, M., et al, "Investigation of Mechanical Properties of Cracked Rock", Proc., Congress of the Int. Soc. for Rock Mechanics, 1st., Lisbon, Vol. 1, 1966.

19. Goodman, R.E., R.Taylor, and T.Brekke, "A Model for the Mechanics of Jointed Rock". Proc., ASCE Vol. 94, No.SM3, 1968.

REFERENCES

20. Goodman, R.E., "The Deformability of Joints," ASTM, Special Technical Publication No. 477, 1969

21. Guerreiro, M., R.Wilson and J.L.Serafim, "Deformability Tests and some Results from Three Spanish Dam Sites", Proc., International Symposium on Rock Mechanics, Madrid, 1968.

22. Hayashi, M., "A Mechanism of Stress Distribution in the Fissured Foundation", Proc., Congress of the Int. Soc, for Rock Mechanics, 1st., Vol. III, Lisbon, 1966.

23. Heuze, F., and R.E.Goodman, "Behaviour of the Chino Limestone", Proc., Symposium on Rock Mechanics, 9th, University of Colorado, 1967.

24. Hoek, E., "Estimating the Stability of Excavated Slopes in Opencast Mines", Trans., Inst. Min. Metall., No. 79, 1970.

25. Horn, H.M., and D.U.Deere, "Frictional Characteristics of Minerals", Geotechnique, Vol. 12, 1962

26. John, K.W., "Strength and Deformability of Compression-Resisting, Regularly Jointed Discontinua", Institute of Soil and Rock Mechanics, Fredericana University, Karlsruhe, Germany, Vol. 37, 1969.

27. Kenty, J.D., "Suggested Method of Test for Direct Shear Strength Of Rock Core Specimens", ASTM, Special Technical Publication No. 479, 1970.

28. Kreyszyk, E., "Advanced Engineering Mathematics", 2nd edition, Wiley 1969.

29. Krsmanovic, D., and M.Milic, "Model Experiments on Pressure Distribution in Some Cases of Discontinuum". Rock Mechanics and Engineering Geology, Supplement 1, 1964.

REFERENCES

30. Krsmanovic, D., and Z.Langof, "Large Scale Laboratory Tests on the Shear Strength of Rocky Material", Rock Mechanics and Engineering Geology, Supplement 1, 1964.

31. Krsmanovic, D., M.Tufo and Z.Langof, "Shear Strength of Rock Masses and Possiblities of its Reproduction in Models". Proc., Congress of the Int. Soc. for Rock Mechanics, 1st., Vol. 1, Lisbon, 1966.

32. Kujundzic, B., "General Report on Behaviour of Rock Masses as Structural Foundation", Proc., Congress, of the Int. Soc. for Rock Mechanics, 1st, Vol. III, Lisbon, 1966.

33. Ladanyi, B., and G.Archambault, "Simulation of Shear Behaviour of a Jointed Rock Mass", Proc., Symposium on Rock Mechanics, 11th, Berkeley, 1969.

34. Lekhnitski, S.G., "Theory of Elasticity of an Anisotropic Elastic Body", Holden-Day, 1963

35. Locher, H.G., "Some Results of Direct Shear Tests on Rock Discontinuities", Proc., Int. Symposium on Rock Mechanics, Madrid, 1968.

36. Logan, J.M., et al., "Experimental Investigation of Sliding Friction on Multilithologic Specimens", Engineering Geology Case Histories, No. 9, 1972.

37. Mencl, V., "Dilatancy of Rocks", Rock Mechanics and Engineering Geology, Vol. 3, No. 2, 1965.

38. Michell, J.H., "The Stress Distribution in an Aelotropic Solid with an Infinite Plane Boundary", Proc., London Mathematical Society, Vol. 32, 1900.

REFERENCES

39. Patton, F.D., "Multiple Modes of Shear Failure in Rock", Ph. D. thesis, U. of Illinois, 1966.

40. Patton, F.D., "Multiple Modes of Shear Failure in Rock", Proc., Congress of the Int. Soc. for Rock Mechanics, 1st, Vol. 1, Lisbon 1966.

41. Price, N.J., "Fault and Joint Development in Brittle and Semi-Brittle Rock", Pergamon Press, 1966.

42. Rengers. N., "Influence of Surface Roughness on the Friction Properties of Rock Planes", Proc., Congress of the Int. Soc. for Rock Mechanics, 2nd, Vol. 1, Belgrad, 1968.

43. Rengers, N., "Unebenheit und Reibungswiederstand von Gestainstrennflachen", Veröffentlichungen der Universitat Fredericana in Karlsruhe, Heft 47, 1971.

44. Rocha, M., "Statement of the Physical Problem of the Arch Dam", Theory of Arch Dams, J.R. Rydzewski, Ed., Pergamon Press, Oxford 1964.

45. Skempton, A.W., and D.H.MacDonald, "The Allowable Settlement of Buildings", Proc., Institution of Civil Engineers, Structural and Building Division Meeting, May 1956.

46. Skempton, A.W., and D.H. MacDonald, "The Allowable Settlement of Buildings", discussion, Proc., Institution of Civil Engineers, Structural and Building Division Meeting, May 1956.

47. Stagg, K.G., "In situ tests on the rock mass", Chapter 5 in Rock Mechanics in Engineering Practice, K.G.Stagg and O.C.Zienkiewicz, Ed., Wiley, 1968.

REFERENCES

48. Trollope, D.H., "The Mechanics of Discontinua or Clastic Mechanics in Rock Problems," Chapter 9 of Rock Mechanics in Engineering Practice, K.G.Stagg and O.C. Zienkiewicz, Ed., Wiley, 1968.

49. Waldorf, W.A., J.F.Veltrop and J.J.Curtis, "Foundation Modulus Tests for Karadj Arch Dam", Proc., ASCE, Vol.89, No. SM4, 1963.

50. Wallace, G.B., F.J.Slebir and F.A.Anderson, "In situ Methods for Deformation Modulus Used by the Bureau of Reclamation", ASTM, Special Technical Publication No. 477, 1969.

51. Ward, W.H. and J.B.Burland, "Assesment of the Deformation Properties of Jointed Rock in the Mass", Proc., International Symposium on Rock Mechanics, Madrid, 1968.

52. Wilson, A.E., "Geology of the Ottawa-St.Lawrence Lowland", Geological Survey of Canada Memoir 241, 1946.

53. Withers, J.H., "Sliding Resistance along discontinuities in Rock Masses". Ph. D. thesis, University of Illinois, 1964.

54. Yu, J.S. and G.Attar-Hassan, "User's Manual for the Wilax Finite Element Program", Dept. of Energy, Mines and Resources, Mines Branch, Internal Report 1972/87, Government of Canada, 1972

55. Zienkiewicz, O.C. and K.G.Stagg, "The Cable Method of In Situ Testing", Proc., Congress of the Int. Society for Rock Mechanics, 1st, Vol. 1, Lisbon, 1966.

REFERENCES

56. Zienkiewicz, O.C. and Y.K.Chenng, "The Finite Element Method in Structural and Continuum Mechanics", McGraw-Hill, London, 1967.

57. Zienkiewicz, O.C., S.Valliapan, and I.P.King, "Stress Analysis of Rock as a No Tension Material", Geotechnique, Vol. 18, 1968.

58. Zienkiewicz, O.C. et al, "Analysis of Non-Linear Problems in Rock with Particular Reference to Jointed Rock Systems", Proc., Congress of the Int. Society for Rock Mechanics, 2nd, Vol. 3, Belgrad, 1971.

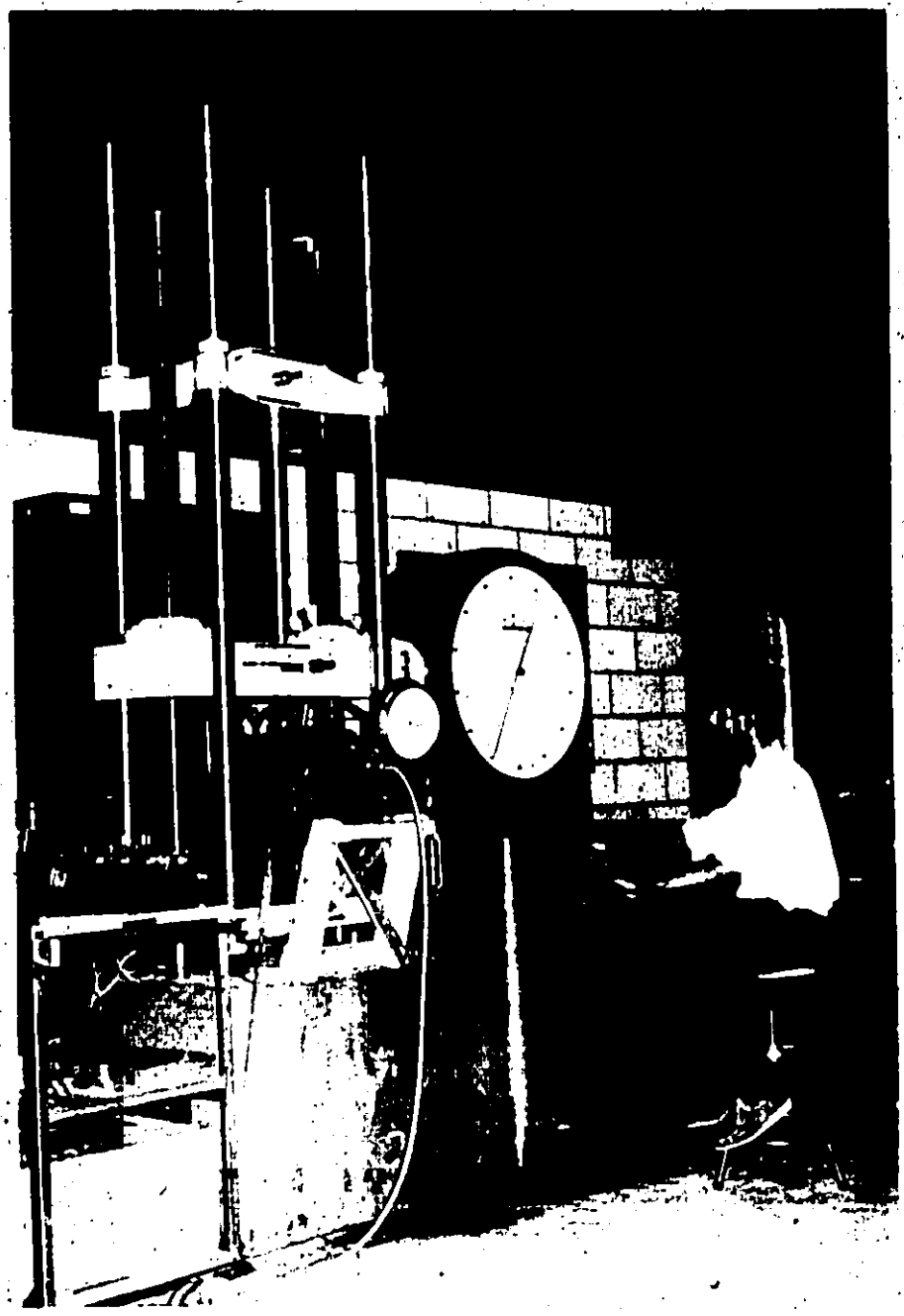

Plate 1.

Operation of the direct shear testing machine.

Plate 2.

Side view of the assembled direct shear testing machine.

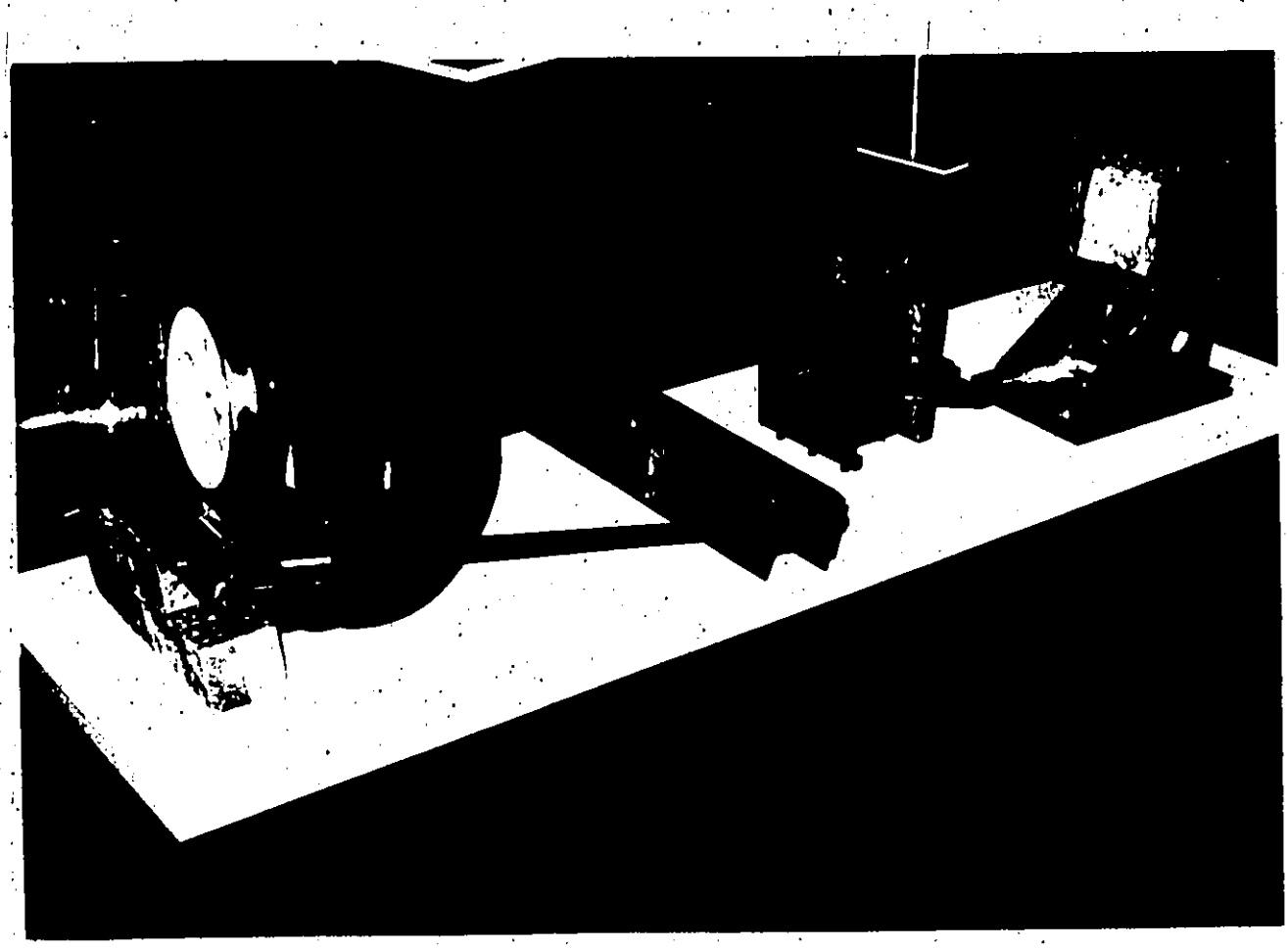

Plate 3.

The disassembled testing machine, showing the loading frame and the bellows, lower and upper box and shoe.

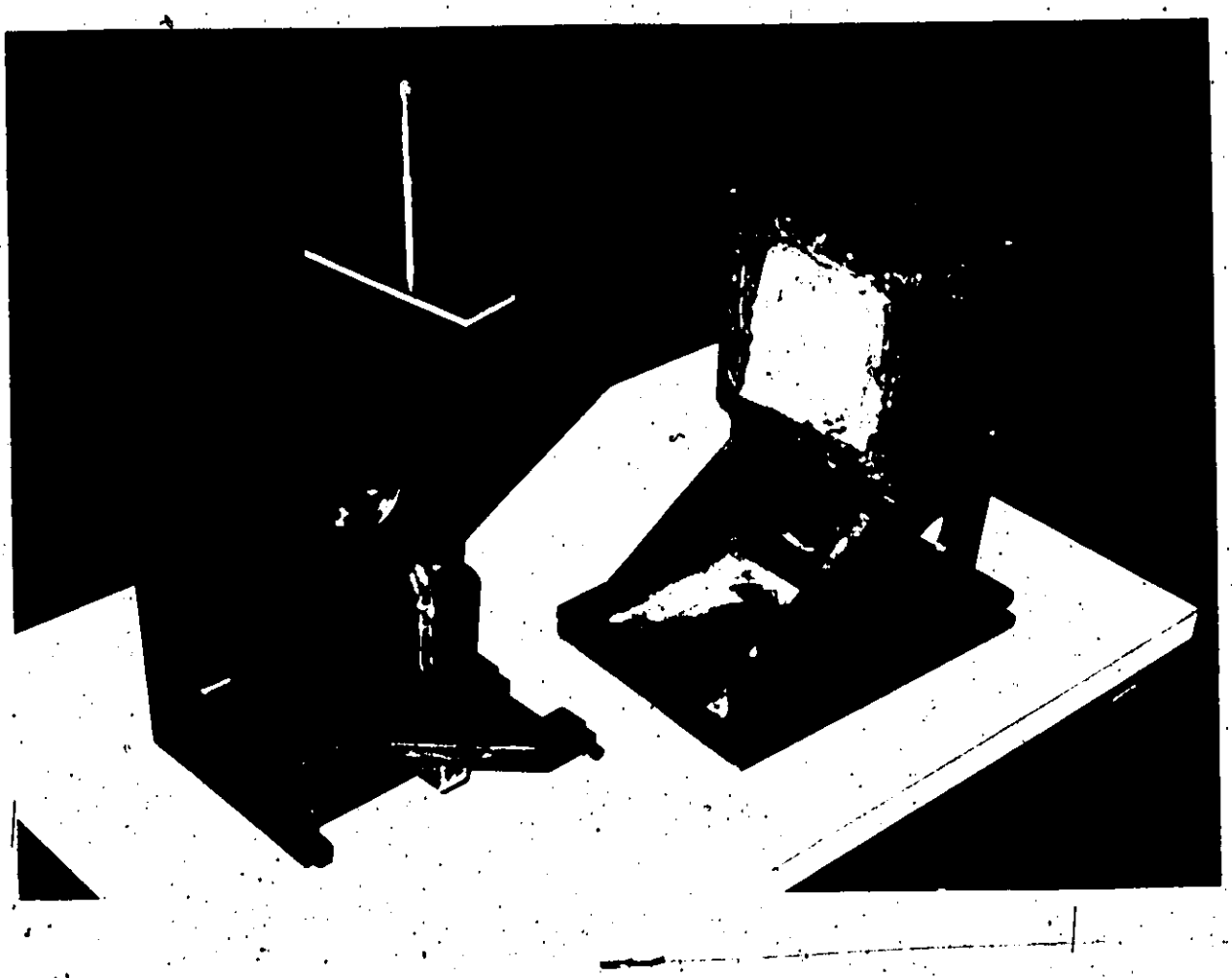

Plate 4.

Close up of the boxes, showing the lateral restraint brackets.

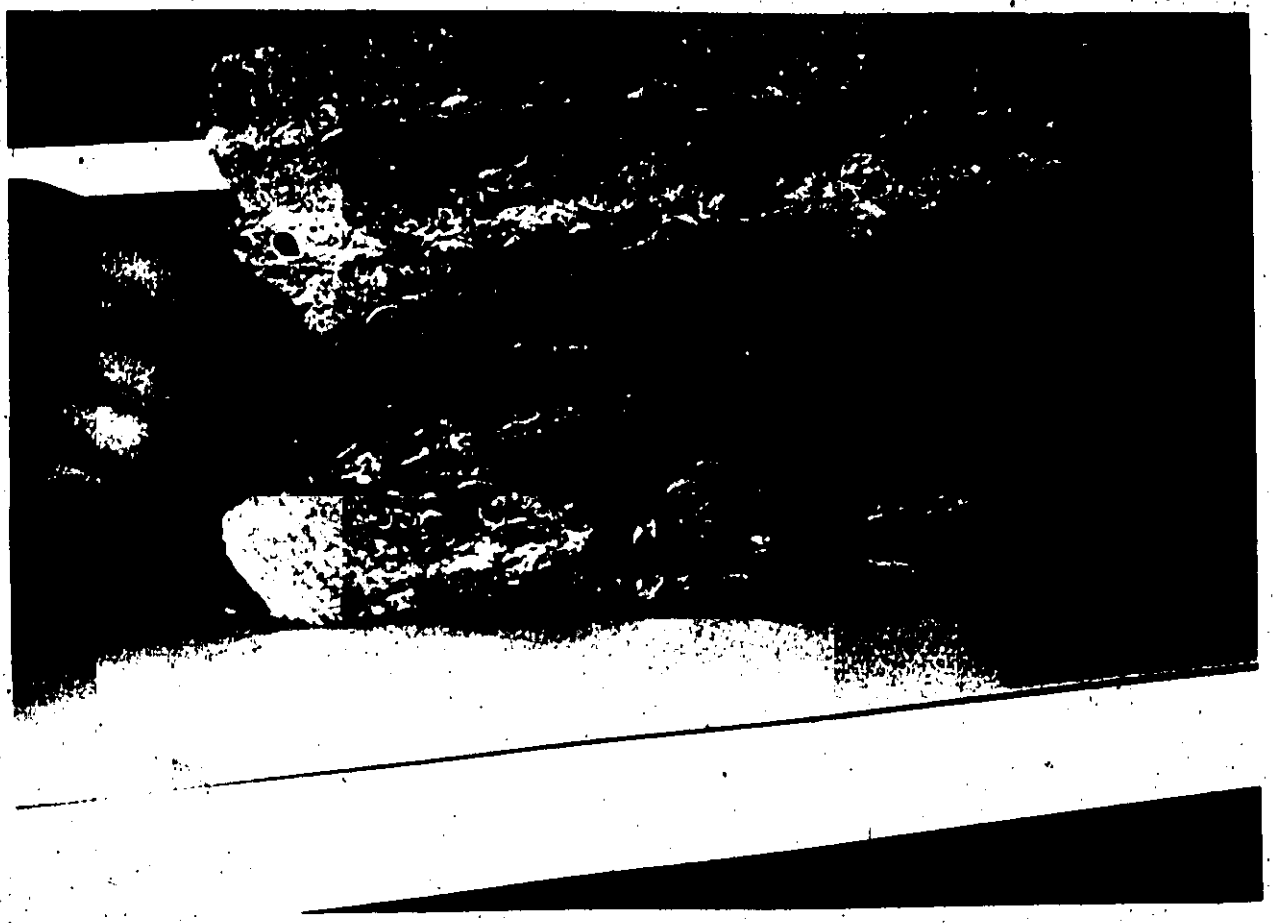

Plate 5.

Typical profile of a limestone bedding plane (Sample 1).

Plate 6.

Casting mould, sample cast in concrete, sample after cutting, the empty shear boxes.

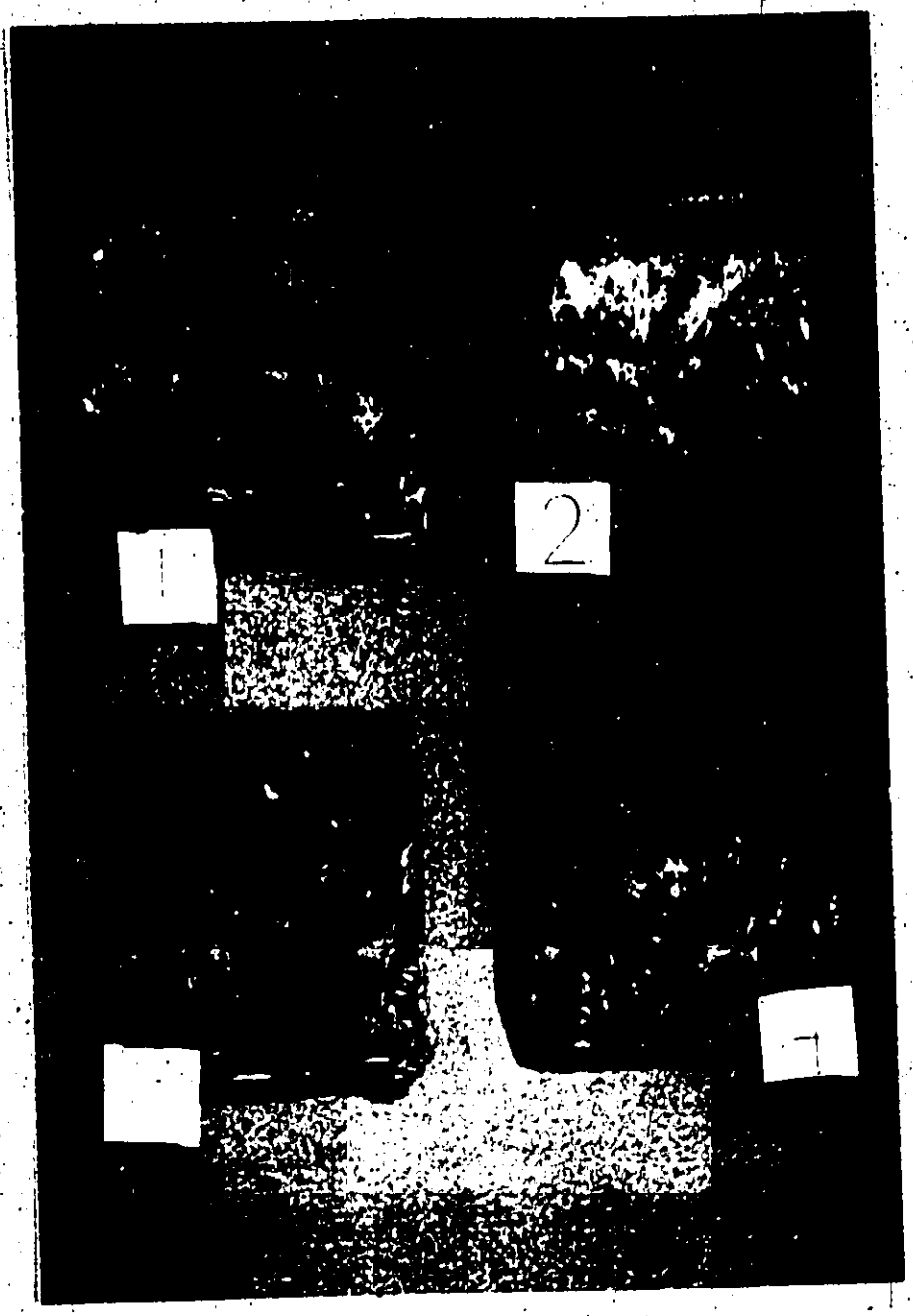

Plate 7.

Sample 1, 2, 3 and 4 after testing.

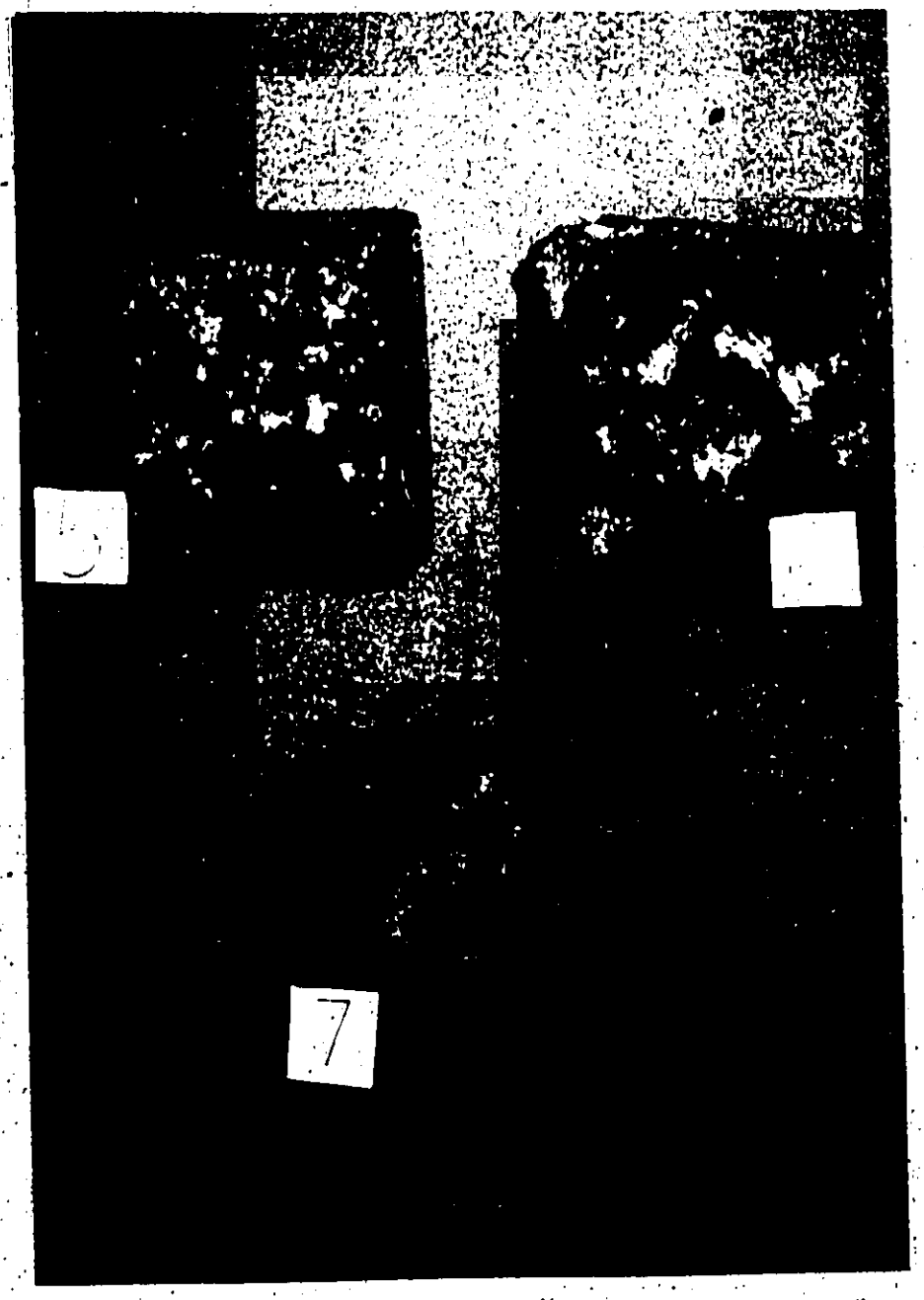

Plate 8.

Samples 5, 6, and 7 after testing.

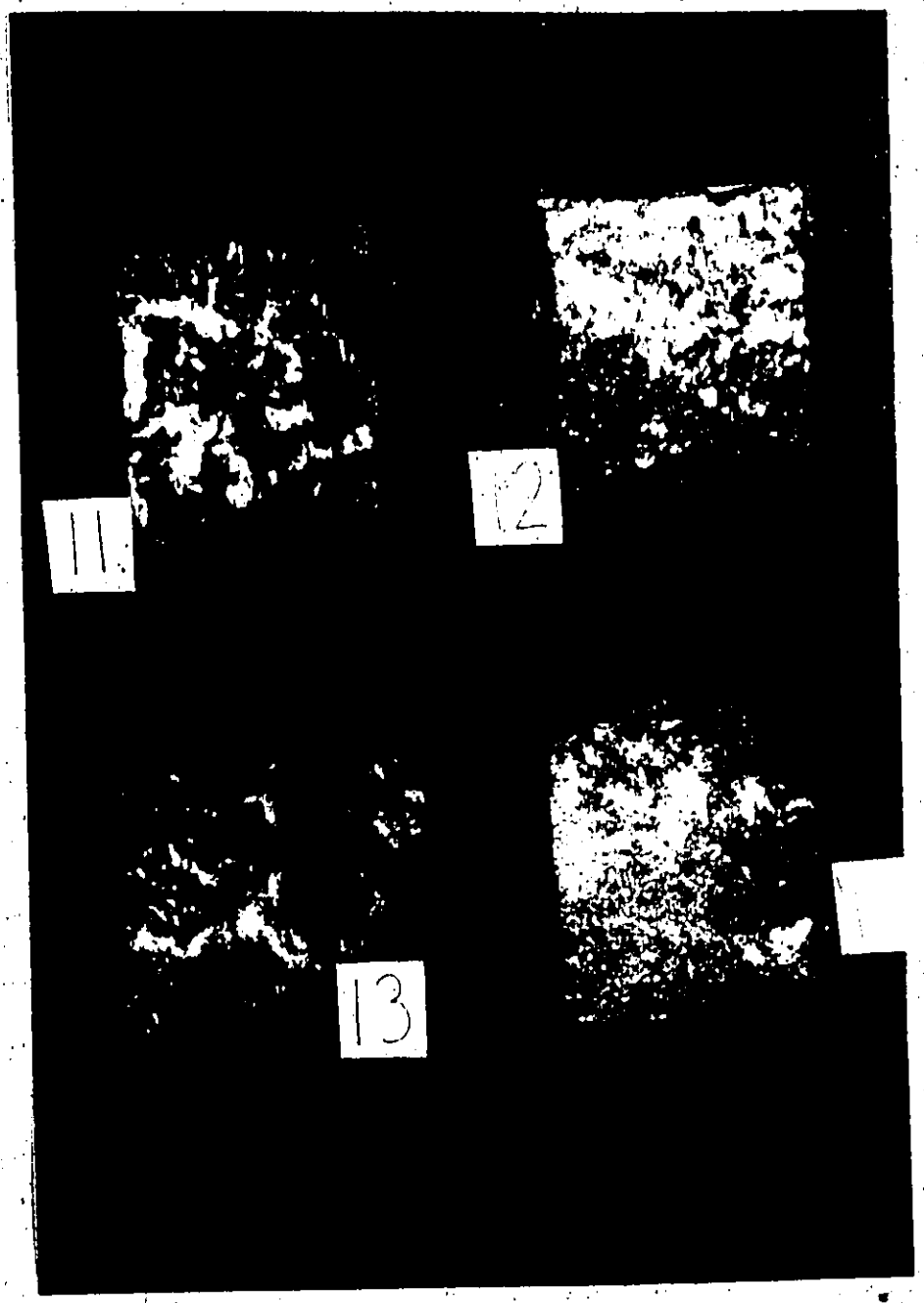

Plate 9.

Samples 11, 12, 13 and 14 after testing.

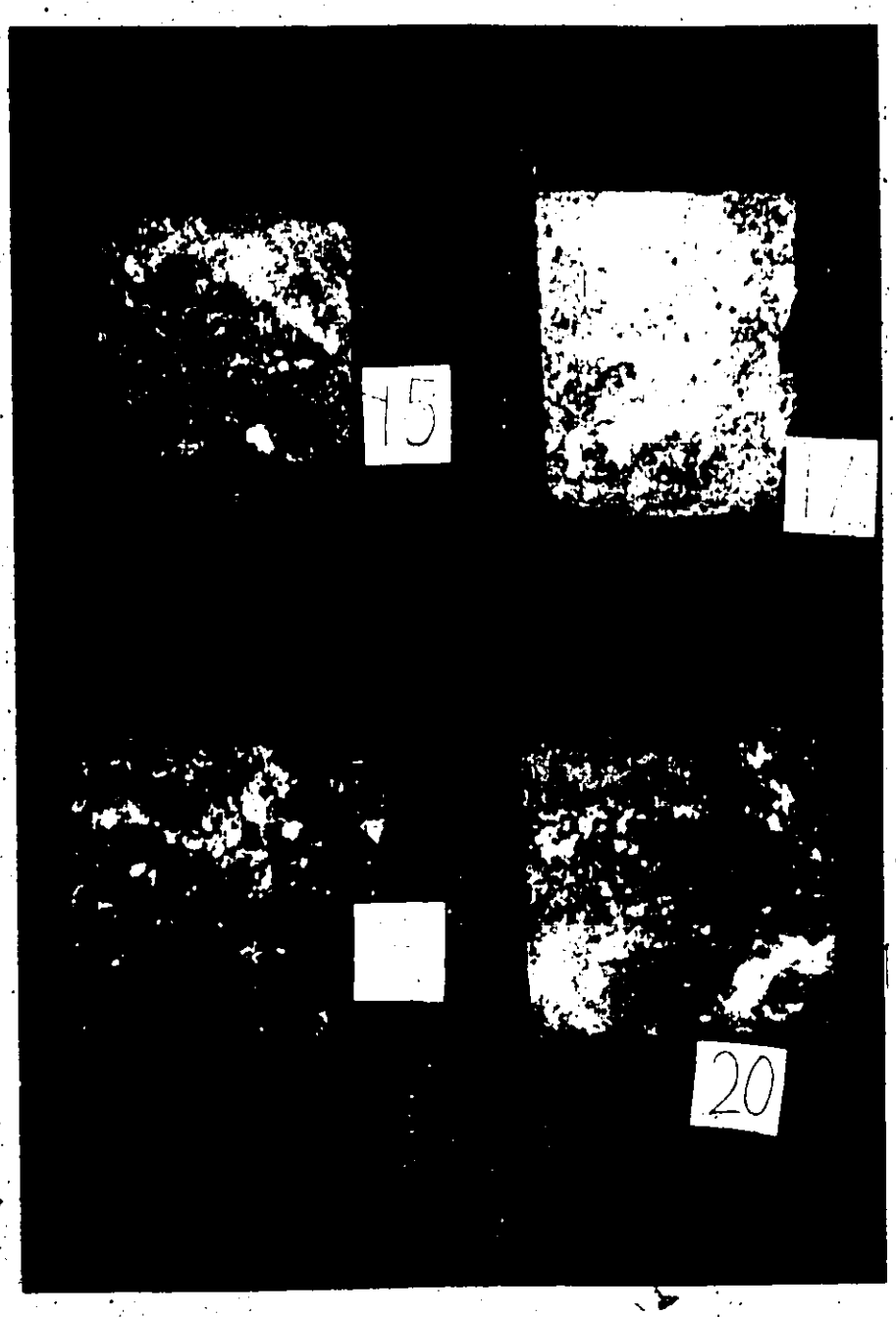

Plate 10.

Samples 15, 17, 18 and 20 after testing.

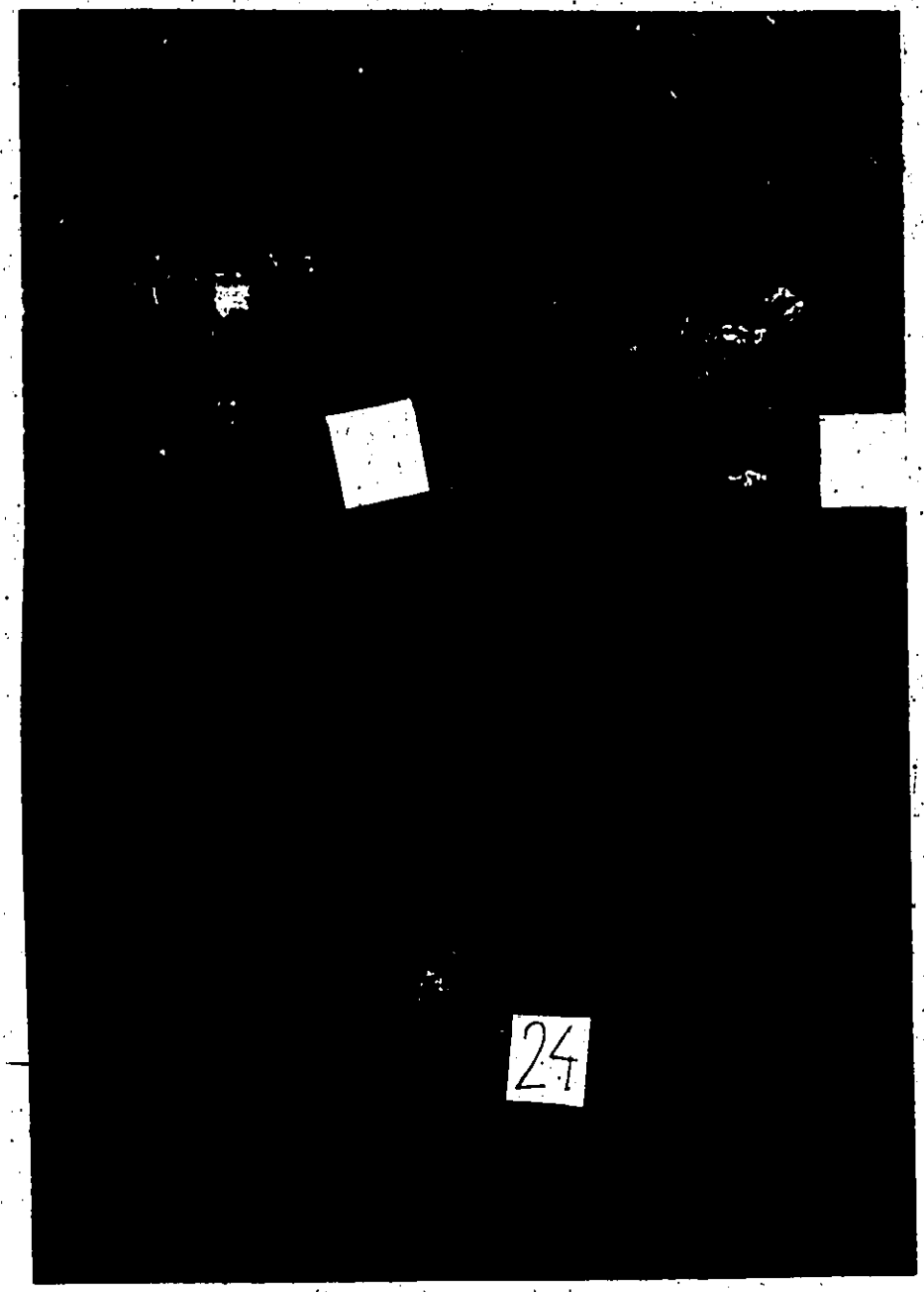

Plate 11.

Samples 21, 22 and 24 after testing.

APPENDIX A

Testing data

Contents:

- Table A.1, Visual description of the samples.
- Table A.2, Results of the measurements of k_s.
- Table A.3, Results of the measurements of k_{ns}.
- Figure A.4, Copies of the shear load-displacement plots obtained by an automatic x - y recorder during the direct shear tests.
- Figure A.5, Graphical summary of the joint closure tests.
- WATFIV computer program for handling the direct shear test results.

Table A-1 Visual Description of the Samples.*

Sample No.	Rock	Area (in^2)	Tightness	← Surface Features → Primary	Secondary	Roughness	Alteration	Contact
1	Limestone	30.3	closed	planar	0.3-0.4/2"	rough, angular	discoloured	well distributed
2		21.2	tight	planar	0.2"/2"	rough, angular	fresh	concentrated
3		26.0	closed	planar	0.2"/1"	smooth	fresh	isolated
4		24.6	closed	planar	0.1"/1"	rough, rounded	fresh	isolated
5		24.7	bonded	planar	0.15"/1"	rough, angular	fresh	well distributed
6		24.3	closed	planar	0.5"/2"	rough, rounded	discoloured	well distributed
7		25.5	closed	planar	0.2"/1.5"	rough, rounded	fresh	well distributed
8		23.7	Not recorded					
9		20.0	Saw cut	-	-	-	-	concentrated
10		15.8	Saw cut	-	-	-	-	concentrated
11	Sandstone	23.1	closed	planar	0.1"/1"	rough, angular	sl.discoloured	well distributed
12		21.4	closed	planar	0.1"/1"	rough, angular	sl.discoloured	well distributed
13		23.1	closed	sl.curved	steps 0.02" high	rough, angular	sl.discoloured	isolated
14		24.5	closed	planar	steps 0.05" high	rough, angular	fresh	isolated
15		22.6	closed	planar	steps 0.05"	rough, angular	fresh	isolated
16		17.3	Saw cut	-	-	-	-	concentrated
17		25.4	closed	planar	0.05"/1"	rough, angular	fresh	well distributed
18		28.7	closed	sl.curved	0.2"/1.5"	rough, angular	fresh	concentrated
19		17.0	Saw cut	-	-	-	-	well distributed
20		28.7	closed	planar	steps 0.05" high	rough, angular	fresh	concentrated
21	Siderite	19.1	fight	sl.curved	steps 0.05" high	smooth	fresh	isolated

*For definitions see page 56

Cont.next page

Table A-1 Continuation

Sample No.	Rock	Area (in^2)	Tightness	←Surface Features→ Primary	Secondary	Roughness	Alteration	Contact
22	↑	23.8	tight	sl.curved	steps 0.05" high	smooth	fresh	isolated
23	Siderite	15.5	Saw cut	-	-	-	-	isolated
24	Siderite	25.3	tight	sl.curved	steps 0.05" high	smooth	fresh	isolated
25	Siderite	23.5	tight	sl.curved	steps 0.05" high	smooth	fresh	isolated
26	↓	18.4	Saw cut	-	-	-	-	concentrated

Table A-2 Results of the Measurements of k_s.*

1	2	3	4	5	6	7	8	9	10	11	12	13
sample no and area	σ_n	τ_y	τ_p	τ_{res}	τ_{res}/τ_p	δ_p	$k_{s0.5p}$	k_{sy}	τ_p/δ_p	k_s av	range k_s	k_s
sq.in	psi				---	in	10^4 psi/i					
1 30.3	65	84	92	86	0.93	0.023	2.3	0.71	0.40	0.04	1.16 to 4.45	1.56
	136	165	172	-	-	0.027	5.0	0.91	0.64	1.26		
	207	228	231	-	-	0.024	4.6	1.2	0.96	1.60		
	278	280	305	305	0.1	0.037	5.4	1.7	0.83	2.28		
2 21.2	92	99	99	93	0.94	0.027	0.83	0.37	0.37	0.45	1.26 to 4.05	1.64
	194	183	183	178	0.97	0.015	3.0	1.2	1.2	1.52		
	296	248	248	259	1.05	0.015	12.0	1.6	1.6	2.33		
	398	289	289	295	1.02	0.008	144.0	3.6	3.6	5.35		
3 26.0	75	86	92	83	0.90	0.005	46.0	86.0	1.8	66.1	3.79 to 90.87	5.68
	158	149	154	146	0.95	0.009	77.0	3.7	1.7	5.51		
	241	206	217	206	0.95	0.017	108.0	3.2	1.3	4.76		
	325	263	263	263	1.00	0.008	132.0	3.3	3.3	4.88		
4 24.6	80	51	59	25	0.43	0.008	29.0	2.8	0.74	4.23	2.30 to 10.65	3.21
	167	85	100	86	0.87	0.029	25.0	1.3	0.34	1.96		
	255	104	122	166	1.36	0.032	6.1	3.0	0.38	3.66		
	343	150	167	252	1.51	0.032	10.0	3.0	0.52	4.03		
5 24.7	79	146	146	156	1.07	0.004	73.0	3.6	3.6	5.33	2.59 to 135.9	3.85
	167	231	231	243	1.05	0.010	115.0	2.3	2.3	3.43		
	254	316	316	291	0.92	0.013	158.0	2.4	2.4	3.62		
	342	395	395	328	0.83	0.015	197.0	2.6	2.6	3.92		
6 24.3	81	58	144	128	0.89	0.001	1.0	5.8	14.0	1.62	2.25 to 8.19	3.02
	169	252	258	224	0.87	0.021	129.0	1.2	1.2	1.81		
	258	355	355	333	0.94	0.013	177.0	2.7	2.7	4.06		
	347	438	438	411	0.94	0.014	219.0	3.1	3.1	4.66		

*For explanation of the terms see pages 83 to 86.

Cont.next page

Table A-2 Continuation

1	2	3	4	5	6	7	8	9	10	11	12	13
Sample No and area	σ_n	τ_y	τ_p	τ_{res}	τ_{res}/τ_p	δ_p	$k_{sq.5p}$	k_{sy}	τ_p/δ_p	k_s av	range k_s	k_s
sq.in	psi				---	in	10^4 psi/in.					
	77	117	129	73	0.57	0.010	65.0	116.0	1.3	90.7	6.25	
7	162	212	212	163	0.77	0.002	106.0	8.5	8.5	12.2	to	9.18
25.5	246	274	274	231	0.84	0.005	137.0	5.5	5.5	8.07	119.6	
	331	341	341	341	1.00	0.007	170.0	4.5	4.5	6.73		
	83	63	63	72	1.13	0.020	1.4	0.32	0.32	0.43	1.25	
8	174	118	118	137	1.16	0.013	5.9	0.91	0.91	1.27	to	1.71
23.7	265	158	171	194	1.14	0.012	10.0	2.6	1.4	3.58	6.08	
	356	213	219	234	1.07	0.010	15.0	4.0	2.0	5.38		
	98	60	60	60	1.00	0.001	30.0	60.0	60.0	45.0	2.92	
9	206	105	109	109	1.00	0.005	54.0	2.6	2.2	3.89	to	
20.0	314	175	180	180	1.00	0.004	90.0	2.2	1.3	3.27	74.5	4.32
saw cut	422	247	247	247	1.00	0.008	124.0	3.1	3.1	4.58		
	124	95	95	95	1.00	0.001	47.0	19.0	19.0	23.7	5.68	
10	261	139	139	139	1.00	0.003	70.0	4.6	4.6	6.74	to	
15.8	397	195	195	195	1.00	0.004	97.0	5.6	5.6	8.11	85.2	8.25
saw cut	534	253	253	253	1.00	0.005	127.0	5.1	5.1	7.45		
	85	53	61	65	1.07	0.011	30.0	2.6	0.55	3.97	4.01	
11	178	106	140	140	1.00	0.032	70.0	2.6	0.44	4.29	to	5.78
23.1	272	216	233	199	0.86	0.029	23.0	3.9	0.80	5.55	30.8	
	365	306	306	303	0.99	0.055	31.0	5.6	5.6	7.66		
	92	28	33	82	2.50	0.004	3.3	1.1	0.82	1.48	1.92	
12	192	145	156	179	1.14	0.032	1.7	0.72	0.49	0.90	to	2.45
21.4	293	234	255	280	1.10	0.037	13.0	3.1	0.69	4.25	5.11	
	394	313	313	333	1.06	0.007	13.0	4.2	4.2	5.40		

Cont.nex page

Table A-2 Continuation

1	2	3	4	5	6	7	8	9	10	11	12	13
Sample no and area	σ_n	τ_y	τ_p	τ_{res}	τ_{res}/τ_p	δ_p	$k_{s0.5p}$	k_{sy}	τ_p/δ_p	k_s av	range k_s	k_s
sq.in	psi				---	in	10^4 psi/in					
	85	35	39	36	0.92	0.040	19.0	34.0	0.10	27.0	3.73	
13	178	156	188	173	0.92	0.028	9.4	2.2	0.67	3.09	to	4.54
23.1	272	253	253	226	0.89	0.006	6.3	4.2	4.2	4.75	7.75	
	365	309	309	290	0.94	0.007	7.7	4.4	4.4	5.16		
	80	31	31	51	1.67	0.003	15.0	1.2	1.2	1.77	5.09	
14	168	86	114	180	1.57	0.016	57.0	6.6	0.74	10.2	to	7.63
24.5	256	173	204	228	1.12	0.023	102.0	9.6	0.89	14.5	78.1	
	344	275	275	290	1.05	0.006	137.0	5.0	5.0	7.38		
	87	73	86	33	0.38	0.018	43.0	15.0	0.48	19.4	5.50	
15	182	159	165	100	0.60	0.017	82.0	4.5	0.97	6.71	to	8.10
22.6	278	232	237	199	0.84	0.016	118.0	5.2	1.5	7.62	99.1	
	373	305	305	323	1.06	0.006	153.0	5.5	5.5	8.18		
	113	72	72	72	1.00	0.000	36.0	72.0	72.0	54.1	6.28	
16	238	150	150	150	1.00	0.001	75.0	15.0	15.0	20.5	to	
17.3	363	228	228	228	1.00	0.005	114.0	4.6	4.6	6.72	94.6	9.09
saw cut	488	306	306	306	1.00	0.006	153.0	5.1	5.1	7.53		
	77	44	44	31	0.71	0.000	22.0	44.0	44.0	33.2	10.81	
17	162	126	132	91	0.69	0.006	66.0	126.0	2.2	96.0	to	15.44
25.4	247	205	218	177	0.81	0.008	109.0	20.0	2.7	28.5	87.2	
	332	295	303	276	0.91	0.012	151.0	5.9	2.5	8.76		
	68	110	110	91	0.83	0.008	55.0	1.5	1.5	2.17	2.22	
18	143	178	178	178	1.00	0.014	89.0	1.3	1.3	1.89	to	3.29
20.7	219	246	246	240	0.98	0.011	123.0	2.3	2.3	3.48	104.0	
	294	290	298	275	0.92	0.006	149.0	5.4	5.4	7.98		

Cont. next page

Table A-2 Continuation

1	2	3	4	5	6	7	8	9	10	11	12	13
Sample No and area	σ_n	τ_y	τ_p	τ_{res}	τ_{res}/τ_p	δ_p	$k_{s0.5p}$	k_{sy}	τ_p/δ_p	$k_{s\ av}$	range k_s	k_s
sq.in	psi				---	in	10^4 psi/in					
	115	54	54	47	0.86	0.000	27.0	54.0	54.0	40.8	5.98	
19	242	126	126	129	1.02	0.003	63.0	5.1	5.1	7.30	to	8.06
17.0	369	194	194	235	1.21	0.003	19.0	7.8	7.8	9.71	26.4	
saw cut	496	259	259	303	1.17	0.006	26.0	4.7	4.7	6.47		
	68	87	87	91	1.04	0.001	44.0	8.7	8.7	11.9	13.6	
20	144	148	148	160	1.08	0.003	74.0	5.9	5.9	8.54	to	18.87
28.7	219	200	200	226	1.13	0.001	100.0	20.0	20.0	27.3	84.9	
	294	244	244	279	1.14	0.001	122.0	49.0	49.0	70.4		
	103	105	131	105	0.80	0.023	65.0	2.1	0.57	3.34	7.04	
21	216	178	183	199	1.09	0.016	92.0	4.0	1.1	5.86	to	10.61
19.1	329	225	243	298	1.23	0.007	122.0	19.0	3.5	26.7	110.6	
	442	280	327	335	1.02	0.014	164.0	56.0	2.4	73.9		
	82	34	63	70	1.12	0.013	31.0	34.0	0.48	32.6	3.08	
22	173	109	126	126	1.00	0.012	63.0	7.3	1.1	10.8	to	4.67
23.8	264	183	189	205	1.08	0.008	94.0	4.1	2.4	6.03	78.3	
	355	248	248	235	0.95	0.013	124.0	2.0	2.0	2.95		
	126	84	84	93	1.12	0.002	42.0	4.2	4.2	5.99	6.59	
23	266	150	150	161	1.08	0.003	75.0	6.0	6.0	8.65	to	9.52
15.5	405	206	206	216	1.05	0.004	103.0	5.2	5.2	7.55	86.5	
saw cut	544	252	252	271	1.08	0.002	126.0	13.0	13.0	18.0		
	77	150	150	51	0.34	0.038	1.2	0.40	0.40	0.51	1.63	
24	163	237	237	162	0.68	0.008	12.0	3.0	3.0	3.95	to	2.17
25.3	248	294	294	231	0.79	0.009	147.0	3.3	3.3	4.85	6.35	
	334	296	296	296	1.00	0.005	148.0	5.9	5.9	8.72		

Cont.next page

Table A-2 Continuation

1	2	3	4	5	6	7	8	9	10	11	12	13
Sample No and area	σ_n	τ_y	τ_p	τ_{res}	τ_{res}/τ_p	δ_p	$k_{s0.5p}$	k_{sy}	τ_p/δ_p	k_s av	range k_s	k_s
sq.in	psi				---	.in	10^4 psi/in					
	83	43	43	85	2.00	0.011	0.97	0.39	0.39	0.48	2.82	
25	175	170	170	149	0.87	0.015	6.60	1.2	1.2	1.62	to	3.76
23.5	267	257	266	200	0.75	0.013	133.0	8.6	2.1	12.59	11.01	
	359	336	336	281	0.84	0.000	168.0	336.0	336.0	252.1		
	106	71	71	98	1.38	0.003	35.0	2.8	2.8	4.08	6.01	
26	224	128	128	160	1.26	0.003	64.0	4.3	4.3	6.18	to	8.66
18.4	341	174	174	217	1.25	0.003	87.0	7.0	7.0	10.0	75.07	
saw cut	459	228	228	272	1.19	0.002	114.0	11.0	11.0	16.3		

Table A.3 - Results of the Measurements of k_{ns}.*

1	2	3	4	5	6	7	8	9
Sample No. & Area	σ_n	$k_{ns0.5p}$	$k_{ns\ y}$	$\tau_p/\Delta h$	$k_{ns\ av.}$	Range k_{ns}	k_{ns}	k_{ns}/k_s
sq. in.	psi	10^4 psi/in						-
	65	3.1	1.0	-	1.4	2.16		
1	136	86.0	1.4	-	2.1	to	3.11	1.99
30.1	207	23.0	2.5	2.3	3.6	18.19		
	278	153.0	4.7	2.3	7.1			
	92	49.0	1.1	1.1	1.6	2.75		
2	194	9.1	2.5	2.5	3.3	to	3.80	2.33
21.2	296	18.0	2.8	2.8	4.0	16.4		
	398	21.0	6.0	6.0	7.9			
	75	46.0	86.0	92.0	66.0	-20.7		
3	158	-7.7	- 15.0	-15.0	- 11.0	to	-17.2	-3.06
26.0	241	-5.4	- 10.0	-14.0	- 7.9	-13.0		
	325	132.0	- 53.0	-53.0	- 99.0			
	80	29.0	51.0	59.0	40.0	43.4		
4	167	50.0	- 17.0	-20.0	- 34.0	to	87.7	27.29
24.6	255	61.0	20.0	24.0	27.0	-111.0		
	343	-17.0	19.0	-	78.0			
	79	3.6	0.77	0.77	1.0	1.42		
5	167	3.3	1.2	1.2	1.5	to	1.85	0.48
24.7	254	5.3	1.7	1.7	2.1	4.73		
	432	6.6	2.0	2.0	2.6			
	81	-3.8	- 2.9	- 7.2	- 3.3	10.3		
6	169	129.0	8.4	-	12.0	to	29.3	9.71
24.3	258	-11.0	7.1	7.1	16.0	-12.2		
	347	-15.0	9.3	9.3	20.0			
	77	65.0	117.0	-	90.0	6.7		
7	162	106.0	5.3	5.3	7.7	to	9.81	1.07
25.5	246	137.0	6.9	6.9	10.0	120.0		
	331	171.0	5.7	5.7	8.4			
	83	- 1.3	- 1.8	- 1.8	- 1.6	-4.28		
8	174	- 2.4	- 2.6	- 2.6	- 2.5	to	-4.03	-2.36
23.7	265	- 2.8	- 3.2	- 3.8	- 3.0	-3.62		
	356	110.0	213.0	219.0	161.0			
	85	- 6.0	-	-	-	32.5		
11	178	70.0	106.0	-	88.0	to	45.71	7.91
23.1	272	23.0	22.0	23.0	22.0	185.0		
	365	153.0	31.0	31.0	42.0			
	92	16.0	-	-	-	41.1		
12	192	- 7.8	- 29.0	-	- 15.0	to	28.90	11.82
21.4	293	-25.0	12.0	-	24.0	-29.1		
	394	156.0	8.7	8.7	13.0			

*See page 96.

Table A.3 - continuation

1	2	3	4	5	6	7	8	9
Sample No. & Area	σ_n	$k_{ns0.5p}$	$k_{ns\ y}$	$\tau_{p/h}$	$k_{ns\ av.}$	Range k_{ns}	k_{ns}	k_{ns}/k_s
sq. in.	psi	10^4 psi/in						-
	85	-	-	-	-	-53.8		
13	178	44.0	-31.0	23.0	-62.0	to	-23.92	-5.27
23.1	272	- 6.3	-17.0	- 17.0	-11.0	-11.6		
	365	-10.0	52.0	52.0	-52.0			
	80	-	-	-	-	9.12		
14	168	57.0	8.6	5.7	13.0	to	12.02	1.58
24.5	256	20.0	10.0	8.2	12.0	28.4		
	344	27.0	7.9	7.9	10.0			
	87	2.9	2.1	-	2.3	5.24		
15	182	21.0	5.9	-	7.8	to	6.59	0.81
22.6	278	39.0	7.7	-	11.0	13.22		
	373	19.0	5.5	5.5	7.3			
	77	-	-	-	-	23.11		
17	162	66.0	18.0	-	24.0	to	31.85	2.06
25.4	247	109.0	29.0	-	39.0	116.0		
	332	151.0	20.0	20.0	28.0			
	68	5.0	1.7	1.7	2.1	4.24		
18	144	13.0	2.5	1.0	3.5	to	5.56	1.69
28.7	219	61.0	-	-	184.0	14.8		
	294	19.0	5.0	5.0	6.6			
	68	8.7	17.0	17.0	13.0	25.2		
20	144	74.0	30.0	30.0	37.0	to	29.12	1.54
28.7	219	100.0	29.0	29.0	38.0	42.5		
	294	122.0	24.0	24.0	33.0			
	103	-	-	-	-	13.4		
21	216	18.0	5.1	5.2	6.7	to	18.64	1.76
19.1	329	122.0	20.0	12.0	29.0	63.2		
	442	164.0	21.0	11.0	32.0			
22	82	2.1	2.2	3.1	2.2	38.2		
23.8	173	63.0	-11.0	- 8.4	- 19.0	to	26.87	4.67
	264	94.0	36.0	-38.0	46.0	17.4		
	355	124.0	50.0	50.0	62.0			
	77	-7.5	30.0	30.0	-45.0	15.1		
24	163	12.0	4.0	3.9	5.1	to	24.06	11.10
25.3	248	-29.0	-	-	-88.0	- 122.0		
	336	148.0	-	-	445.0			
	83	-	-	-	-	9.49		
25	175	85.0	11.0	11.0	16.0	to	10.94	2.91
23.5	267	6.6	8.6	-	7.8	15.7		
	359	34.0	8.4	8.4	11.2			

Figure A.4, Copies of the shear load-displacement plots obtained by an automatic x - y recorder during the direct shear tests. The normal force, applied and held constant during each loading cycle, was equal to the following:

cycle 1 - 2 000 lbs
cycle 2 - 4 070 lbs
cycle 3 - 6 300 lbs
cycle 4 - 8 400 lbs

For details of the testing procedure see pp 68 and 69.

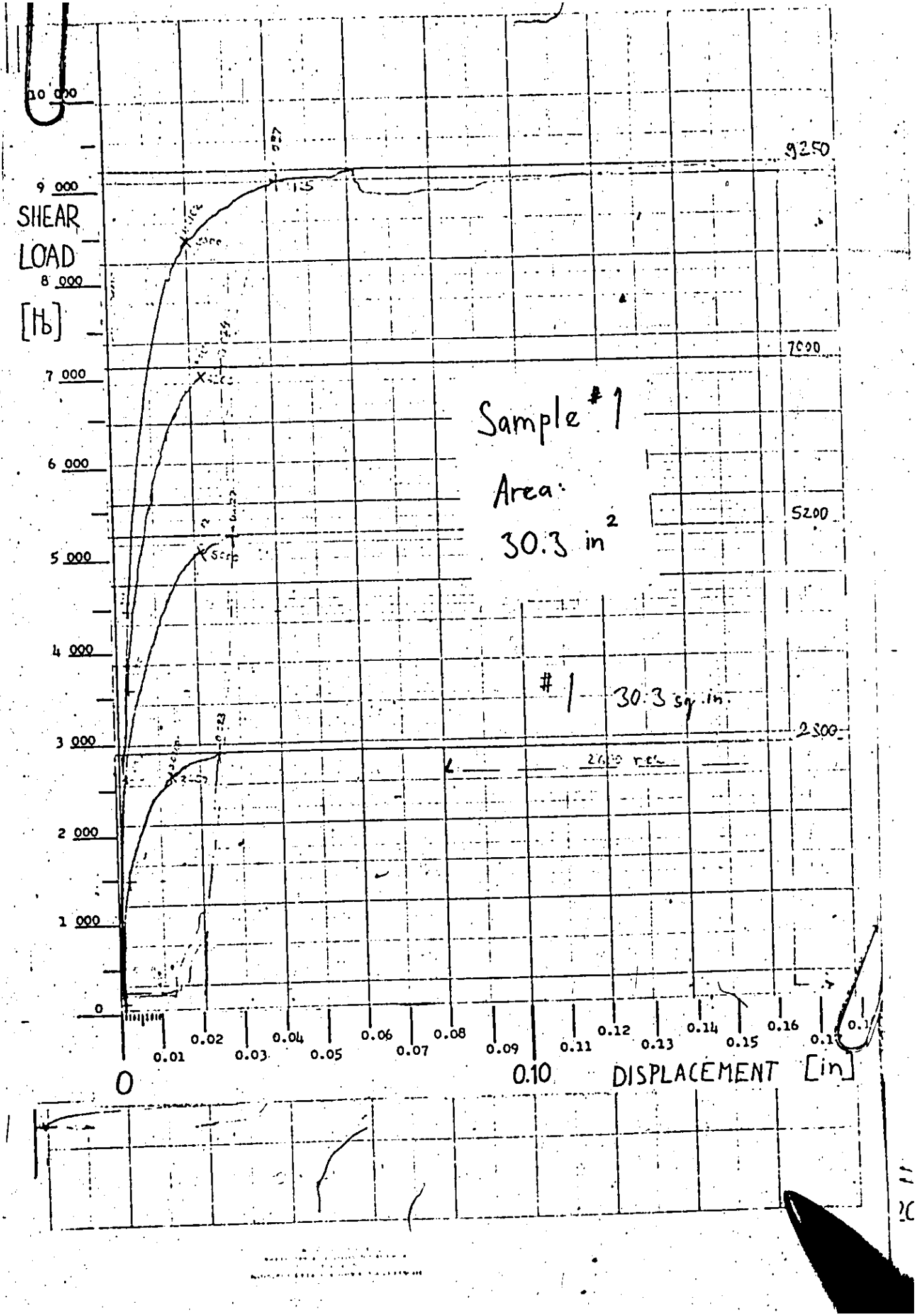
SHEAR LOAD [lb]
10 000
9 000
8 000
7 000
6 000
5 000
4 000
3 000
2 000
1 000
0
9250
7090
5200
2300
Sample #1
Area:
30.3 in²
#1 30.3 sq. in.
0.01
0.02
0.03
0.04
0.05
0.06
0.07
0.08
0.09
0.10
0.11
0.12
0.13
0.14
0.15
0.16
0
DISPLACEMENT [in]

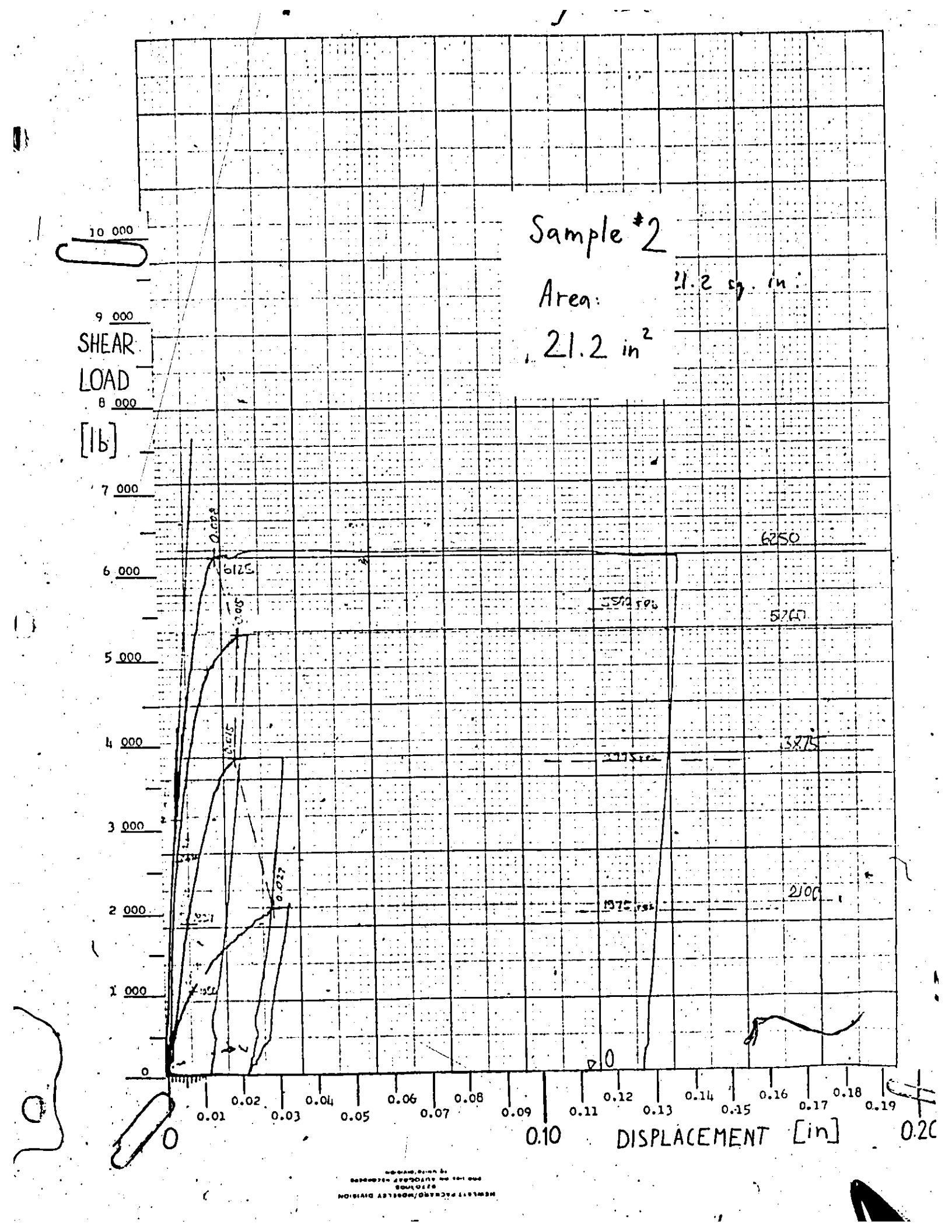
Sample #2
Area:
21.2 in²
21.2 sq. in.
SHEAR LOAD [lb]
10 000
9 000
8 000
7 000
6 000
5 000
4 000
3 000
2 000
1 000
0
6250
5210
3875
2100
0.005
0.010
0.020
0.01
0.02
0.03
0.04
0.05
0.06
0.07
0.08
0.09
0.10
0.11
0.12
0.13
0.14
0.15
0.16
0.17
0.18
0.19
0.20
DISPLACEMENT [in]

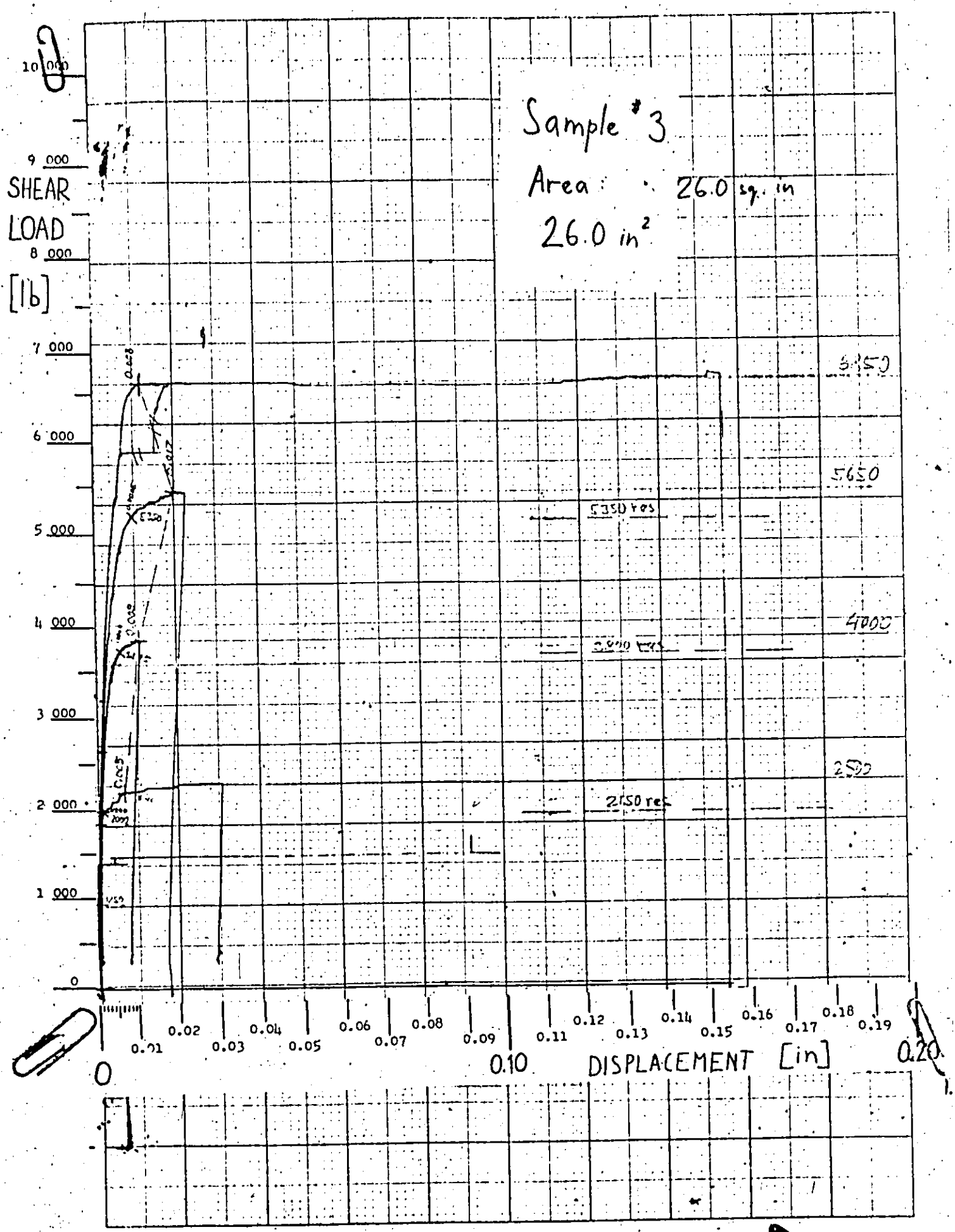
Sample #3
Area : 26.0 sq. in
26.0 in²
SHEAR LOAD [lb]
10 000
9 000
8 000
7 000
6 000
5 000
4 000
3 000
2 000
1 000
0
5350
5650
4000
2500
2150 rec
0.01
0.02
0.03
0.04
0.05
0.06
0.07
0.08
0.09
0.10
0.11
0.12
0.13
0.14
0.15
0.16
0.17
0.18
0.19
0.20
DISPLACEMENT [in]

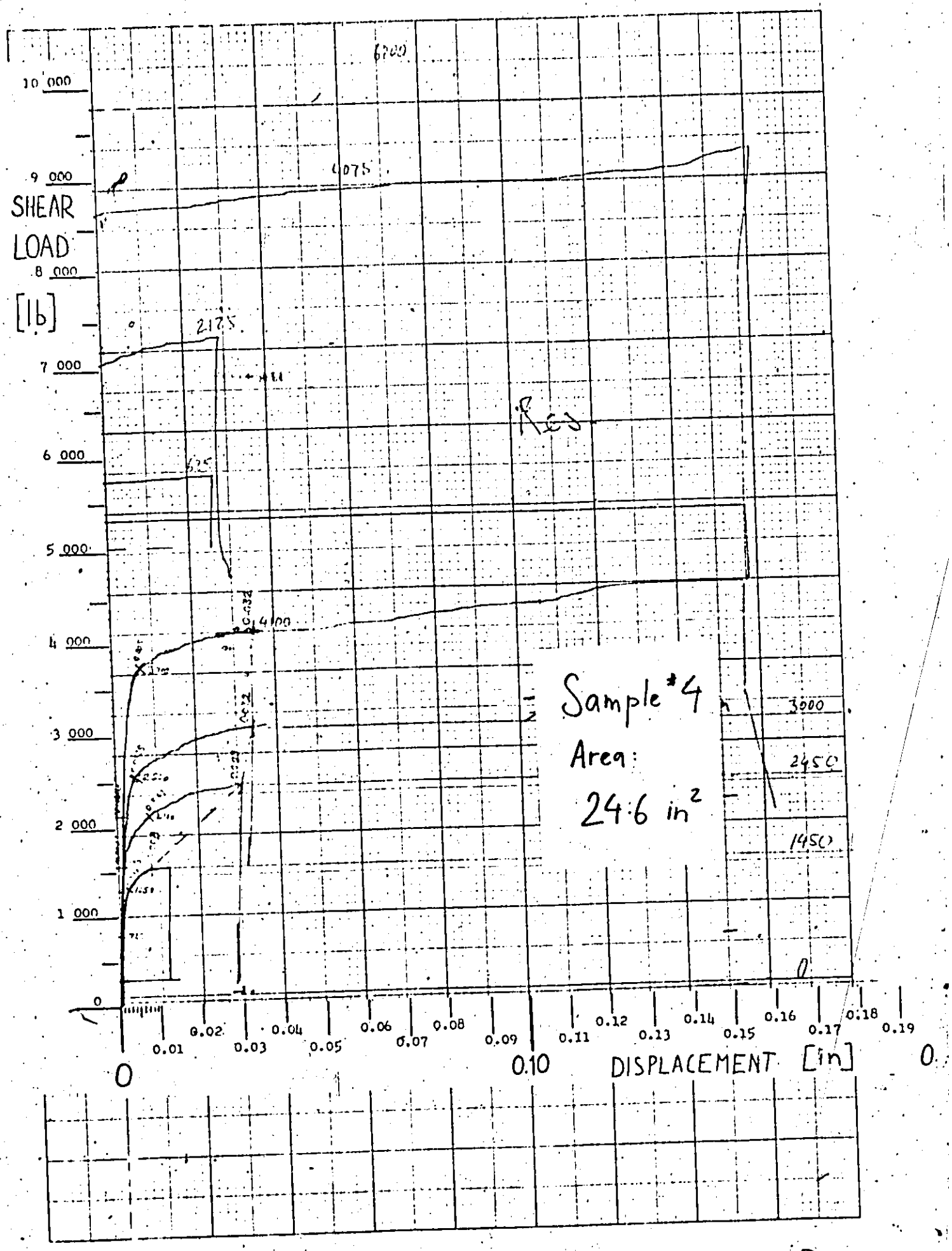
SHEAR LOAD [lb]
10 000
9 000
8 000
7 000
6 000
5 000
4 000
3 000
2 000
1 000
0
6700
6075
2175
625
4100
3000
2450
1450
0
Sample #4
Area:
24.6 in²
0.01
0.02
0.03
0.04
0.05
0.06
0.07
0.08
0.09
0.10
0.11
0.12
0.13
0.14
0.15
0.16
0.17
0.18
0.19
DISPLACEMENT [in]

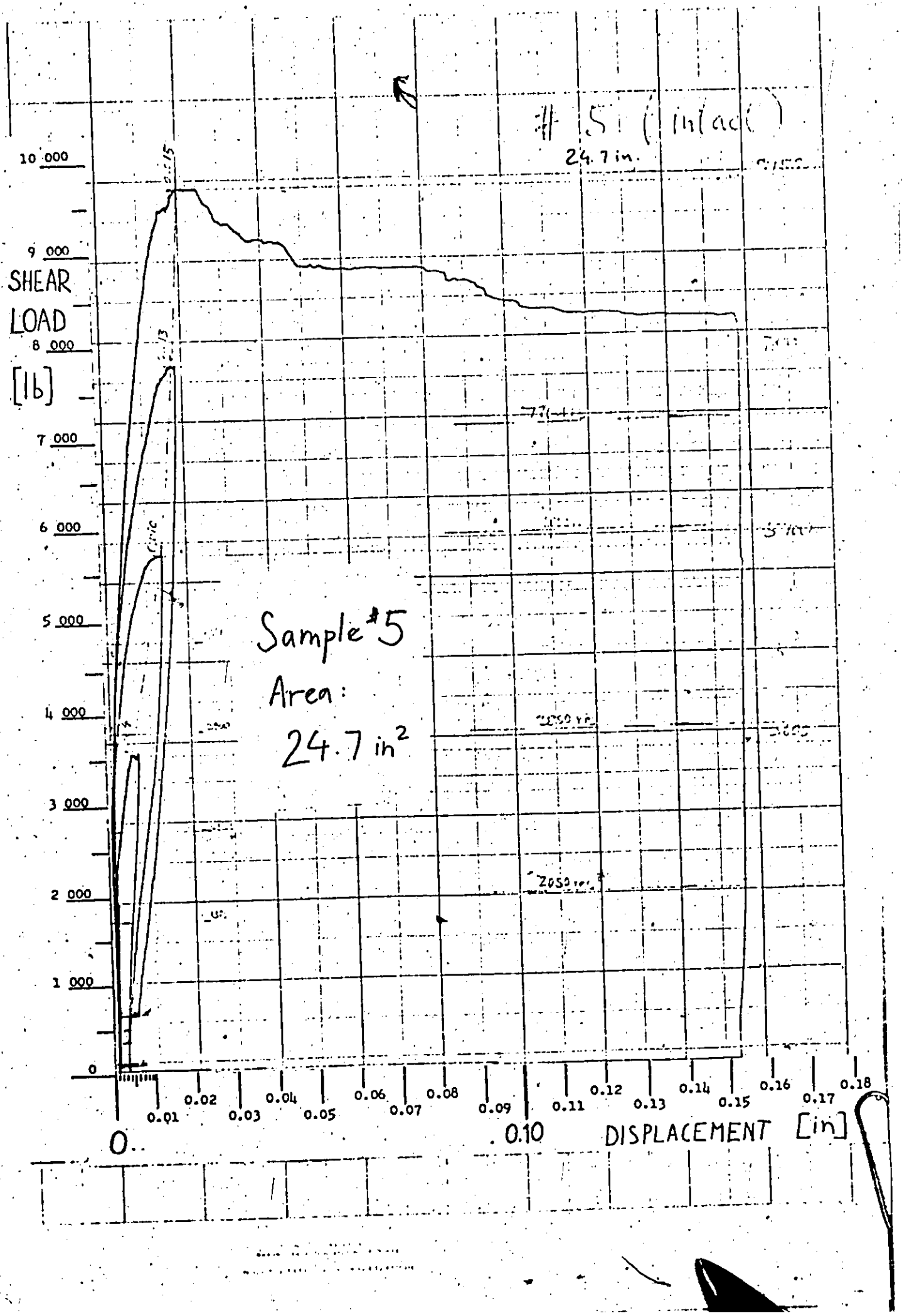
#5 (intact)
24.7 in.
SHEAR LOAD [lb]
10 000
9 000
8 000
7 000
6 000
5 000
4 000
3 000
2 000
1 000
0
Sample #5
Area:
24.7 in²
0.01
0.02
0.03
0.04
0.05
0.06
0.07
0.08
0.09
0.10
0.11
0.12
0.13
0.14
0.15
0.16
0.17
0.18
DISPLACEMENT [in]

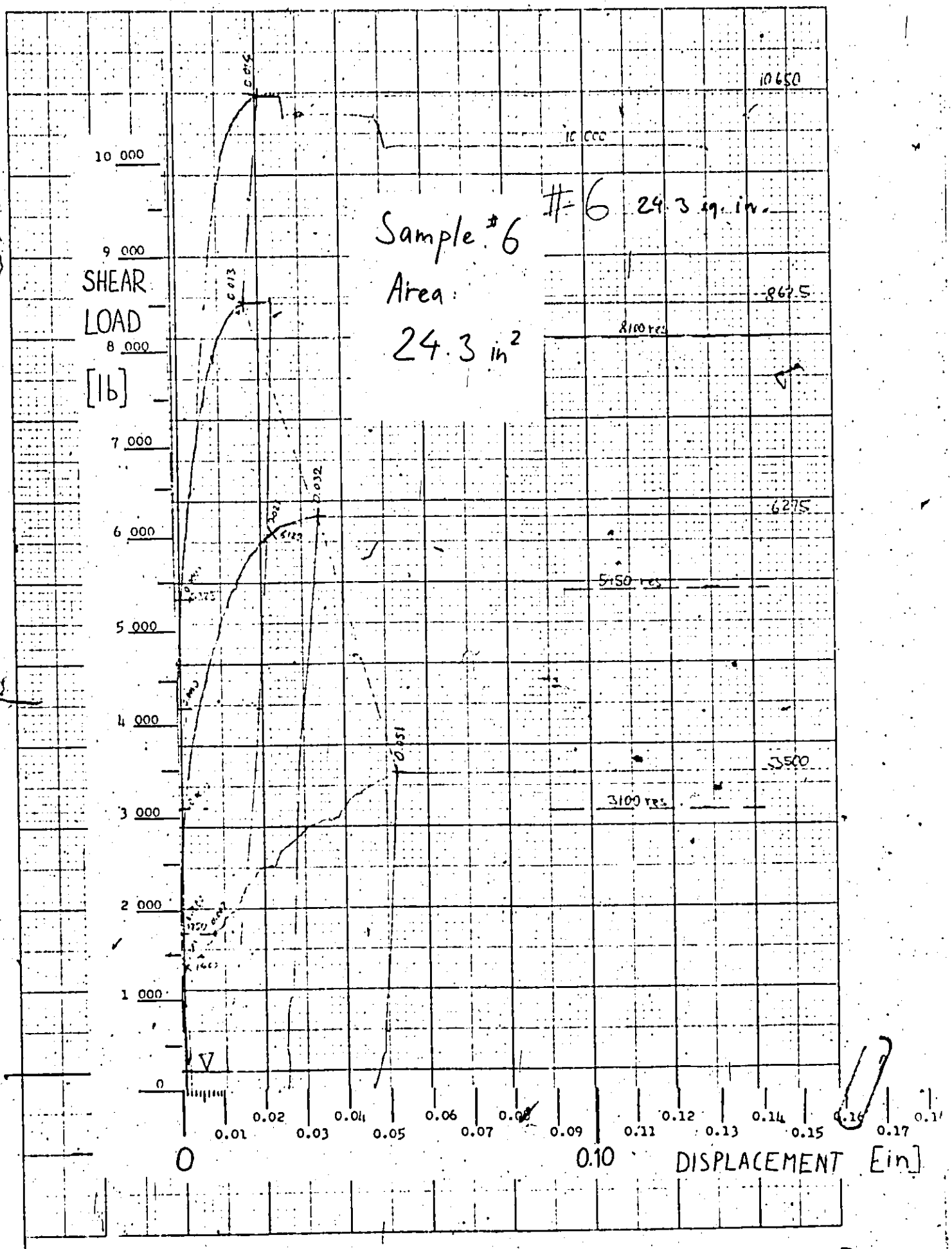
Sample #6
Area:
24.3 in²
#6 24.3 sq. in.
SHEAR LOAD [lb]
10 000
9 000
8 000
7 000
6 000
5 000
4 000
3 000
2 000
1 000
0
10650
10 000
8625
8100 PSI
6275
5150 PSI
3500
3100 PSI
0.013
0.032
0.051
0.01
0.02
0.03
0.04
0.05
0.06
0.07
0.08
0.09
0.10
0.11
0.12
0.13
0.14
0.15
0.16
0.17
0
DISPLACEMENT [in]

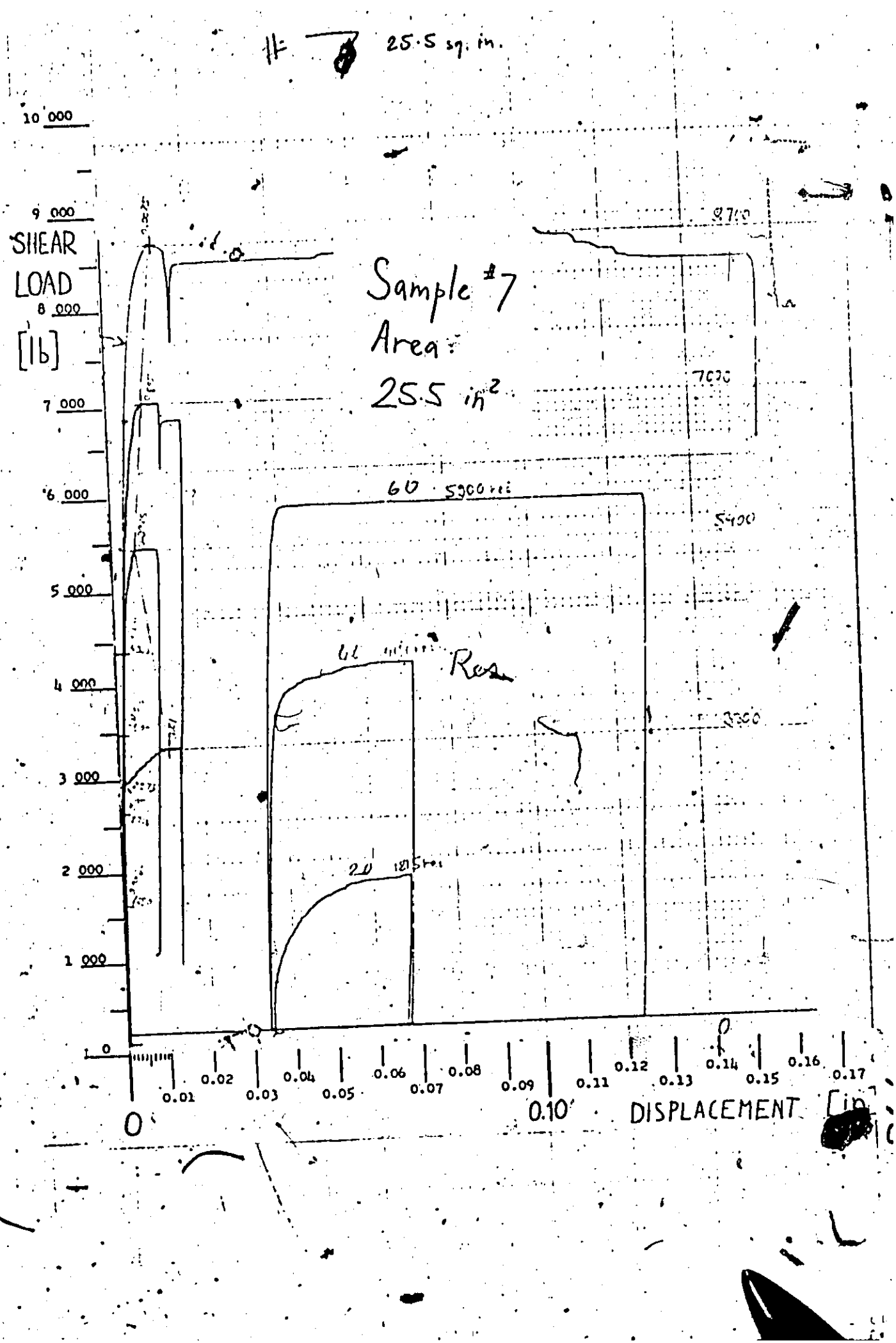
25.5 sq. in.
10 000
9 000
SHEAR
LOAD
8 000
[lb]
7 000
6 000
5 000
4 000
3 000
2 000
1 000
0
Sample #7
Area:
25.5 in²
9700
7000
5400
3300
0
0.01
0.02
0.03
0.04
0.05
0.06
0.07
0.08
0.09
0.10
0.11
0.12
0.13
0.14
0.15
0.16
0.17
DISPLACEMENT [in.]

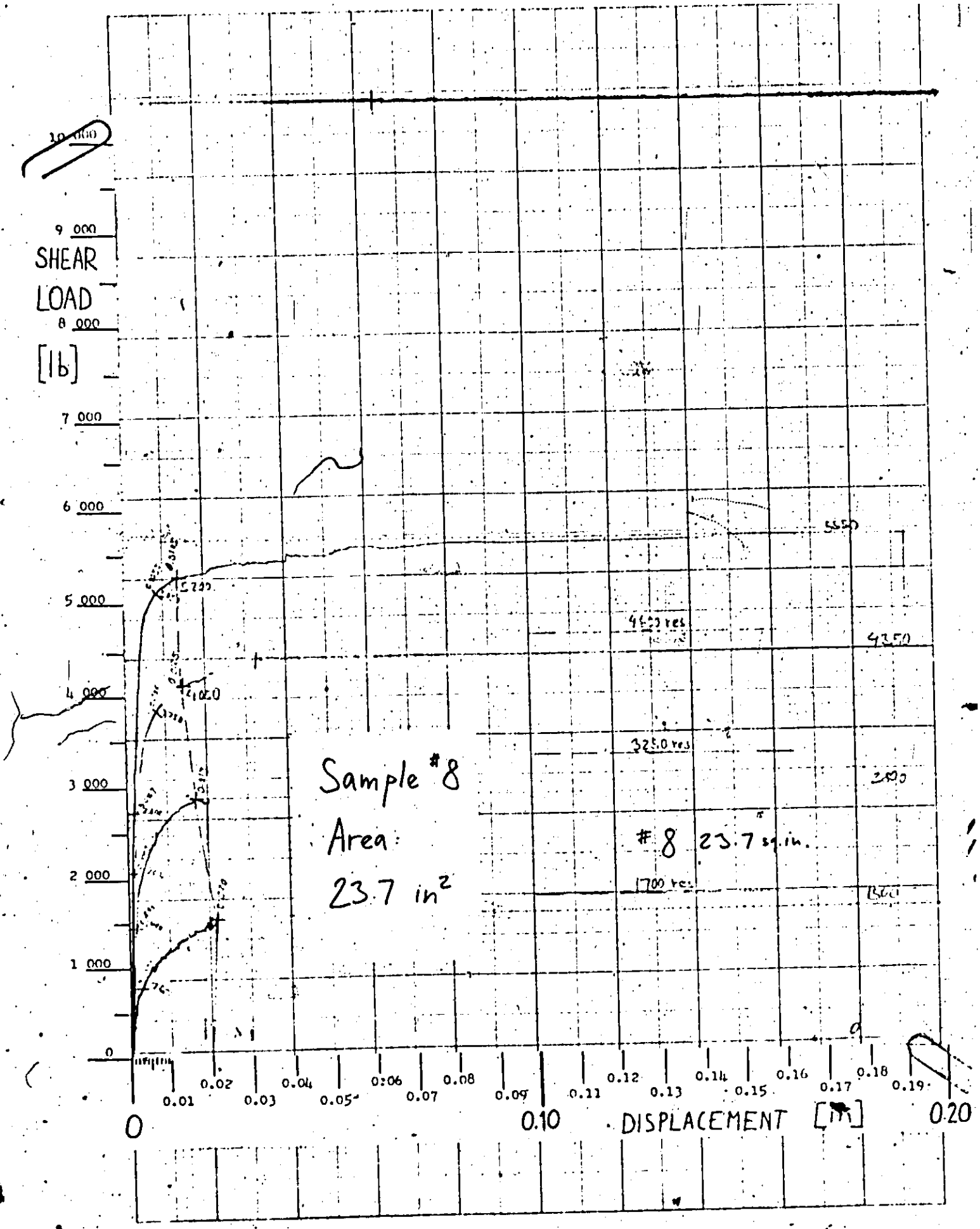
SHEAR LOAD [lb]
10 000
9 000
8 000
7 000
6 000
5 000
4 000
3 000
2 000
1 000
0
0.01
0.02
0.03
0.04
0.05
0.06
0.07
0.08
0.09
0.10
0.11
0.12
0.13
0.14
0.15
0.16
0.17
0.18
0.19
0.20
DISPLACEMENT [in]
Sample #8
Area:
23.7 in²
#8 23.7 sq.in.
5550
4250
3250
2000
1700 res
1500

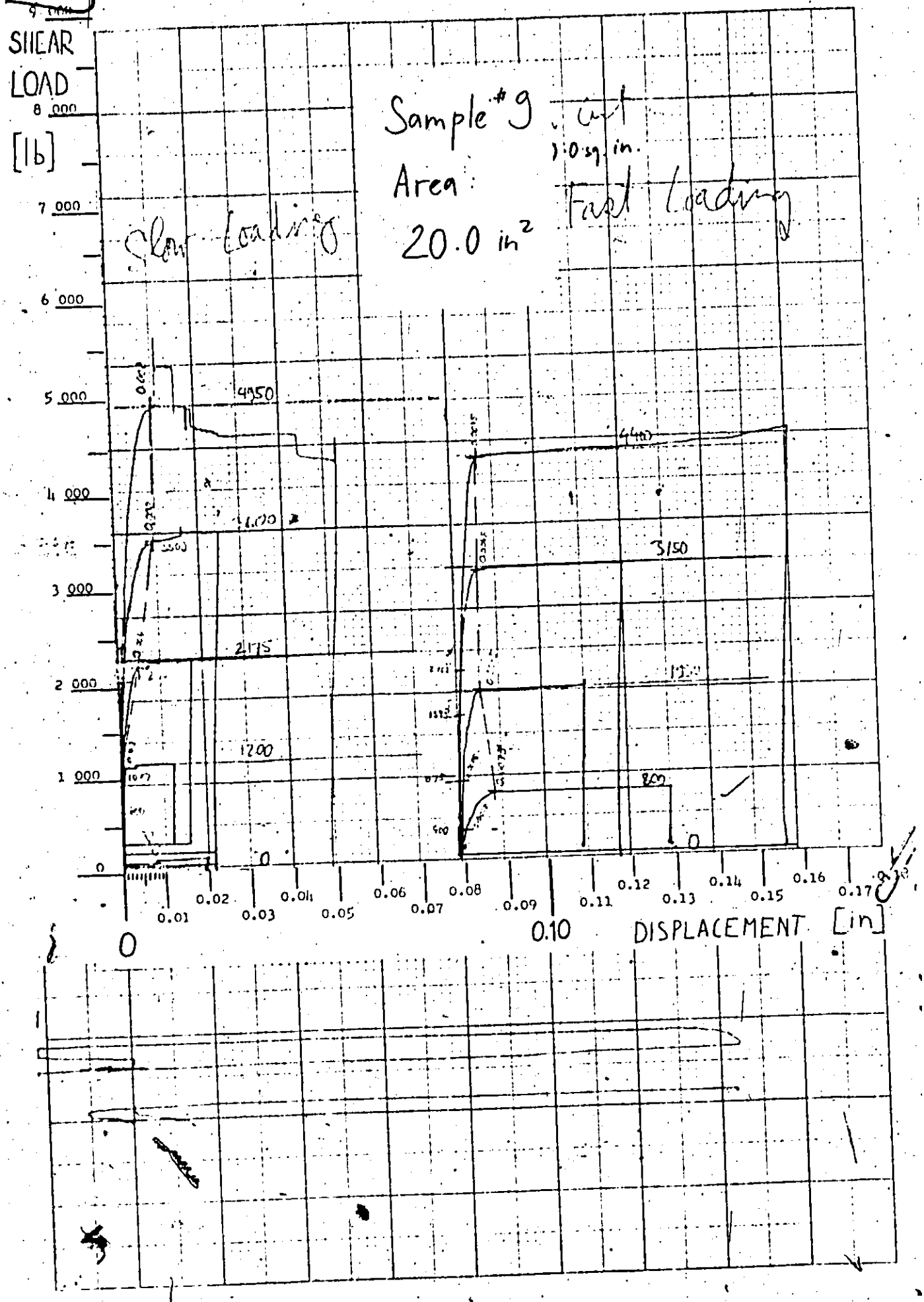
SHEAR LOAD [lb]
8 000
7 000
6 000
5 000
4 000
3 000
2 000
1 000
0
Sample #9 cut
Area: 20.0 in²
Slow Loading
Fast Loading
4950
4400
3150
2175
1200
800
0
0.01
0.02
0.03
0.04
0.05
0.06
0.07
0.08
0.09
0.10
0.11
0.12
0.13
0.14
0.15
0.16
0.17
DISPLACEMENT [in]

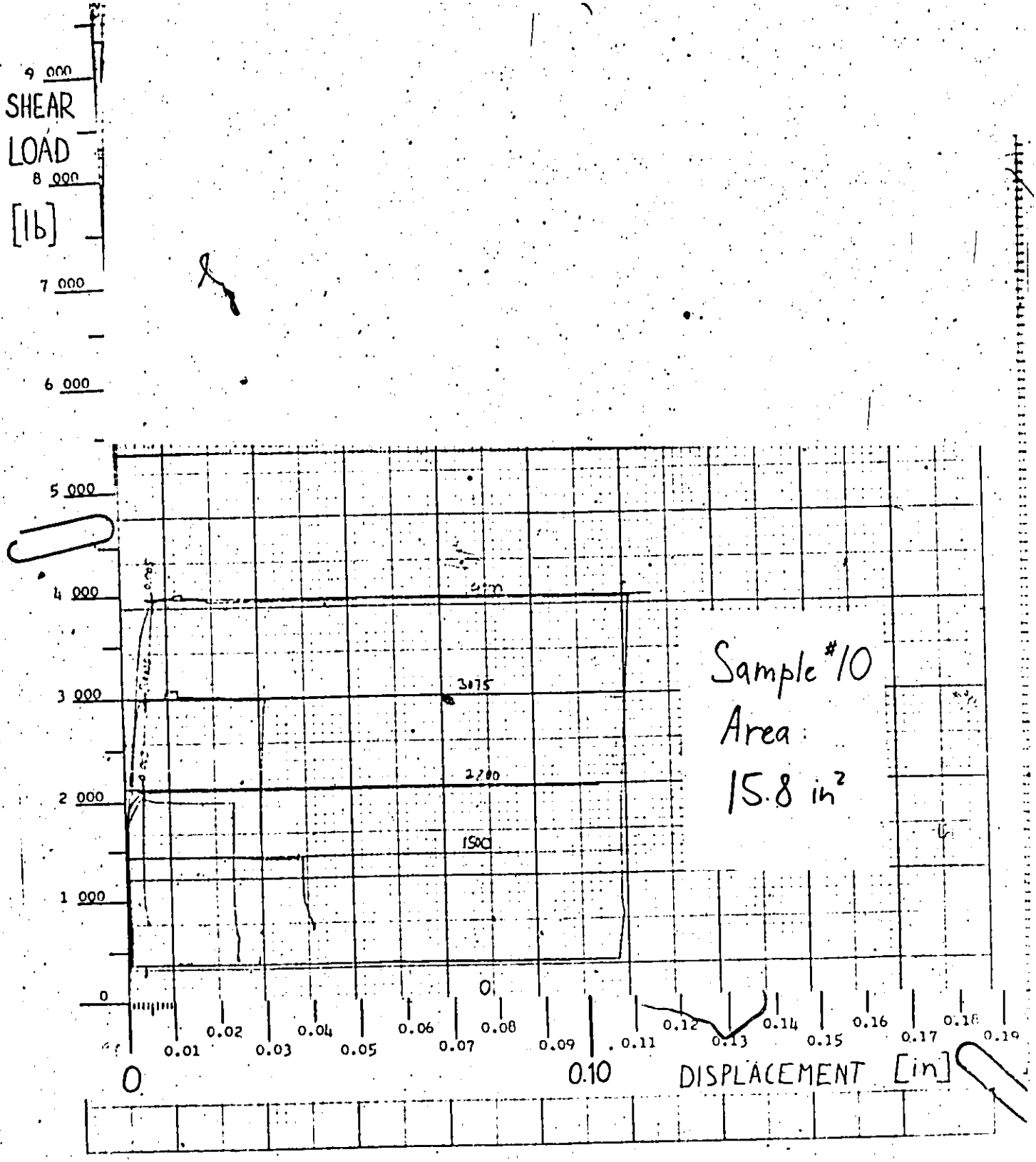
SHEAR
LOAD
[lb]
9 000
8 000
7 000
6 000
5 000
4 000
3 000
2 000
1 000
0
3075
2700
1500
Sample #10
Area:
15.8 in²
0.01
0.02
0.03
0.04
0.05
0.06
0.07
0.08
0.09
0.10
0.11
0.12
0.13
0.14
0.15
0.16
0.17
0.18
0.19
0
DISPLACEMENT [in]

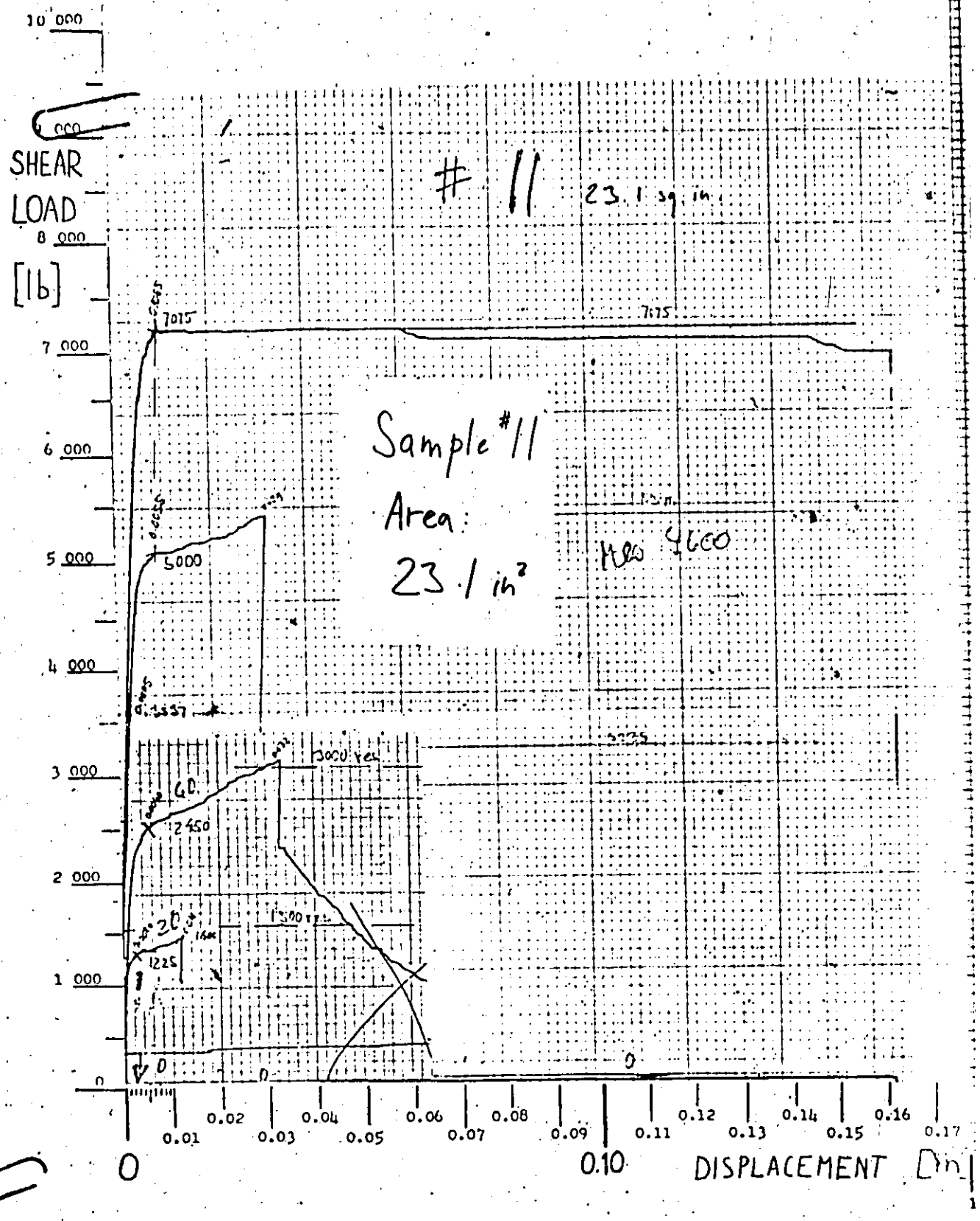
#11 23.1 sq in.
SHEAR LOAD [lb]
10 000
9 000
8 000
7 000
6 000
5 000
4 000
3 000
2 000
1 000
0
7015
7175
5000
2450
1225
Sample #11
Area:
23.1 in²
Hw 4600
0.01
0.02
0.03
0.04
0.05
0.06
0.07
0.08
0.09
0.10
0.11
0.12
0.13
0.14
0.15
0.16
0.17
DISPLACEMENT

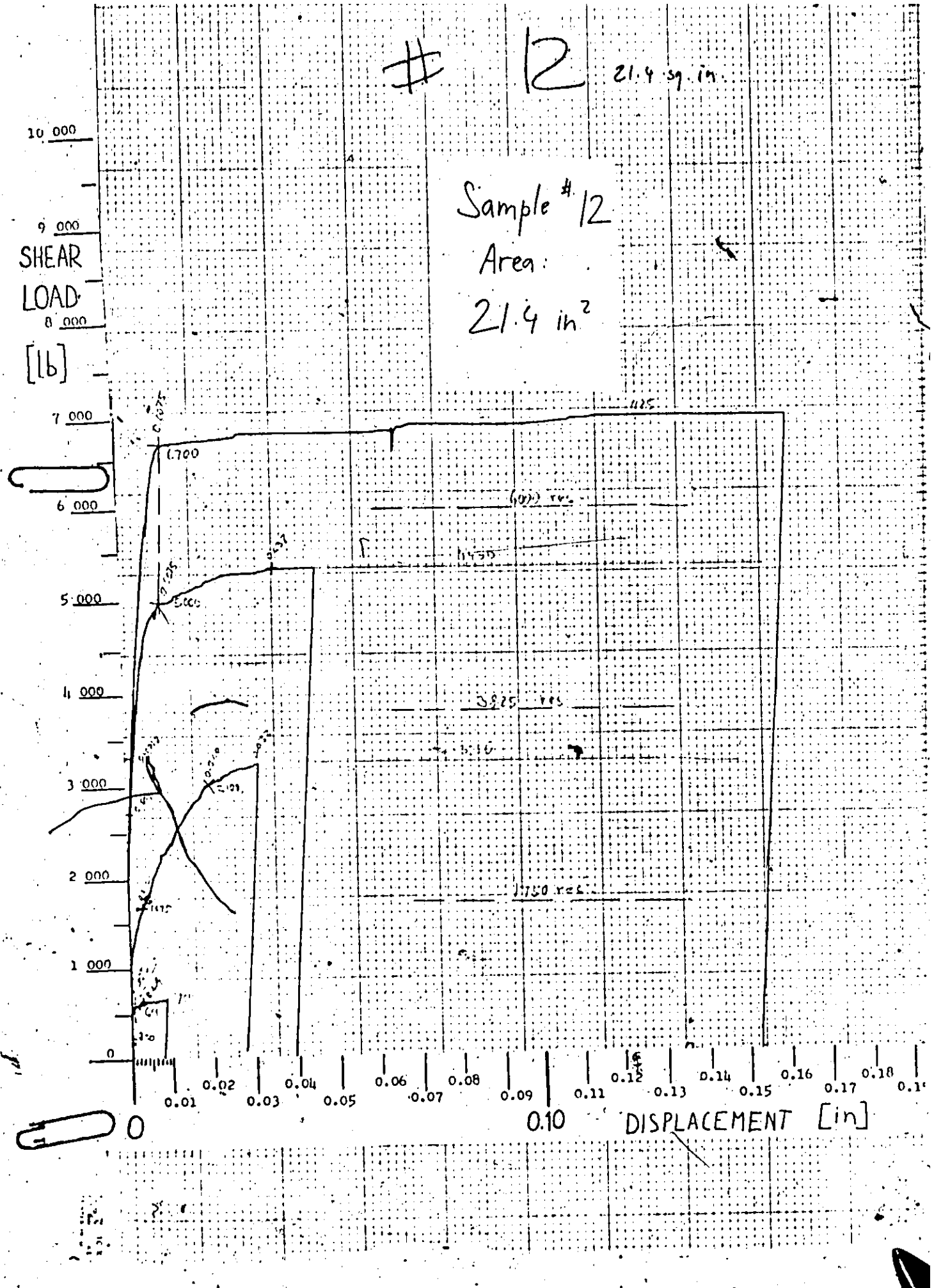
#12 21.4 sq. in.
Sample #12
Area:
21.4 in²
SHEAR LOAD [lb]
10 000
9 000
8 000
7 000
6 000
5 000
4 000
3 000
2 000
1 000
0
0.01
0.02
0.03
0.04
0.05
0.06
0.07
0.08
0.09
0.10
0.11
0.12
0.13
0.14
0.15
0.16
0.17
0.18
DISPLACEMENT [in]

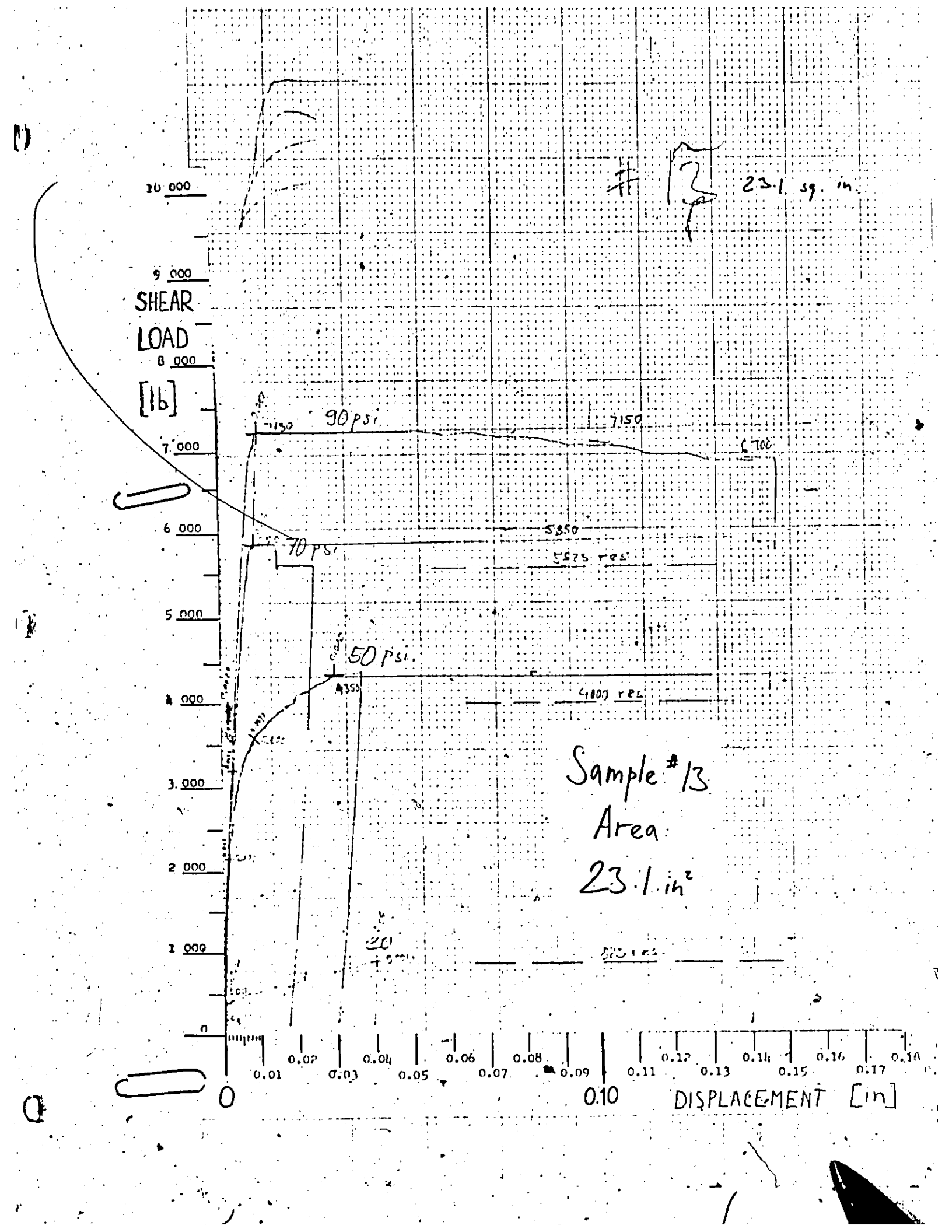
23.1 sq. in.
SHEAR LOAD [lb]
10 000
9 000
8 000
7 000
6 000
5 000
4 000
3 000
2 000
1 000
0
90 psi.
7150
7150
6700
70 psi.
5850
5575 res.
50 psi.
4800 res.
Sample #13
Area
23.1 in²
0
0.01
0.02
0.03
0.04
0.05
0.06
0.07
0.08
0.09
0.10
0.11
0.12
0.13
0.14
0.15
0.16
0.17
0.18
DISPLACEMENT [in]

#14 24.5 sq. in.

Sample #14

Area:

24.5 in²

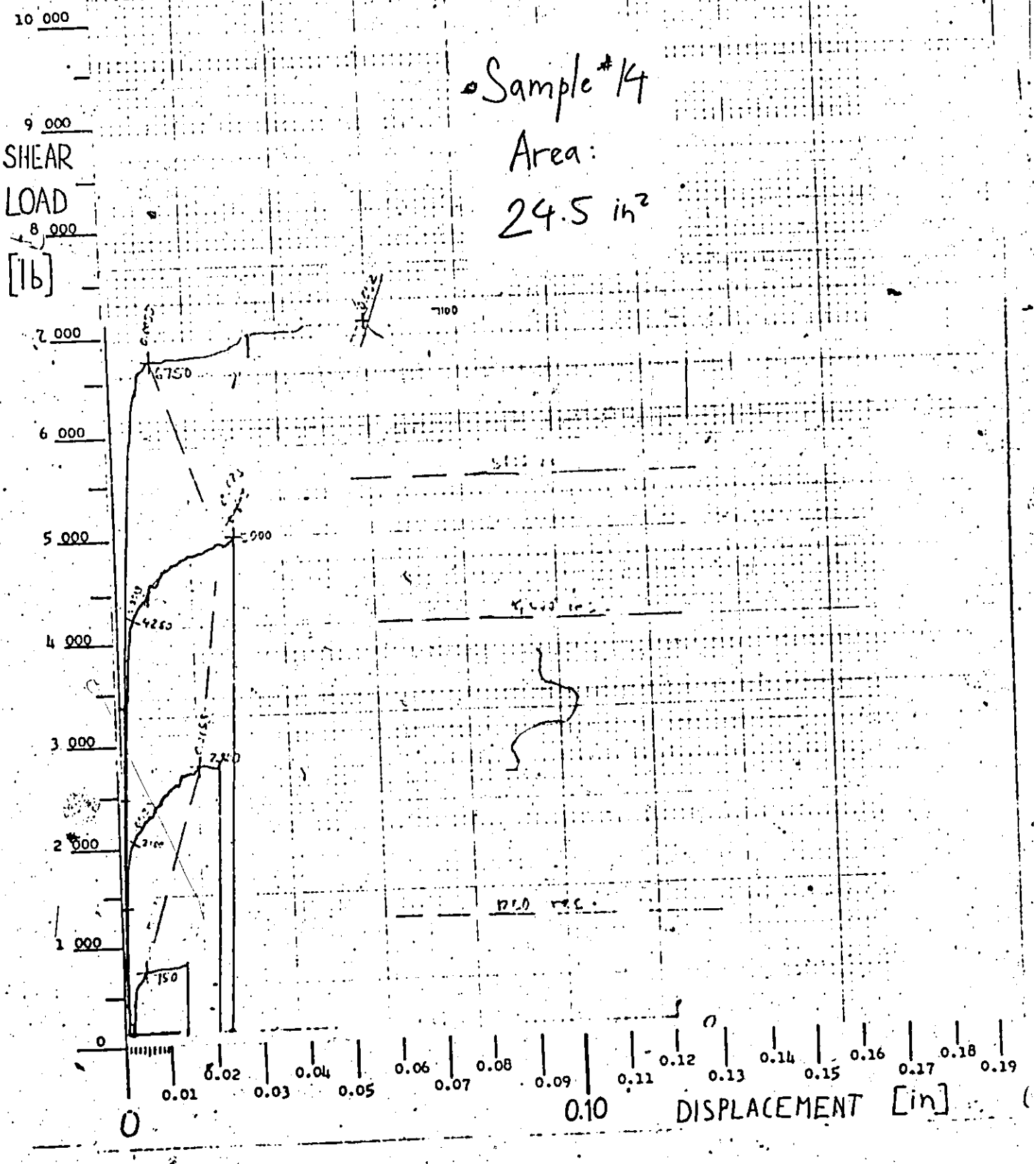

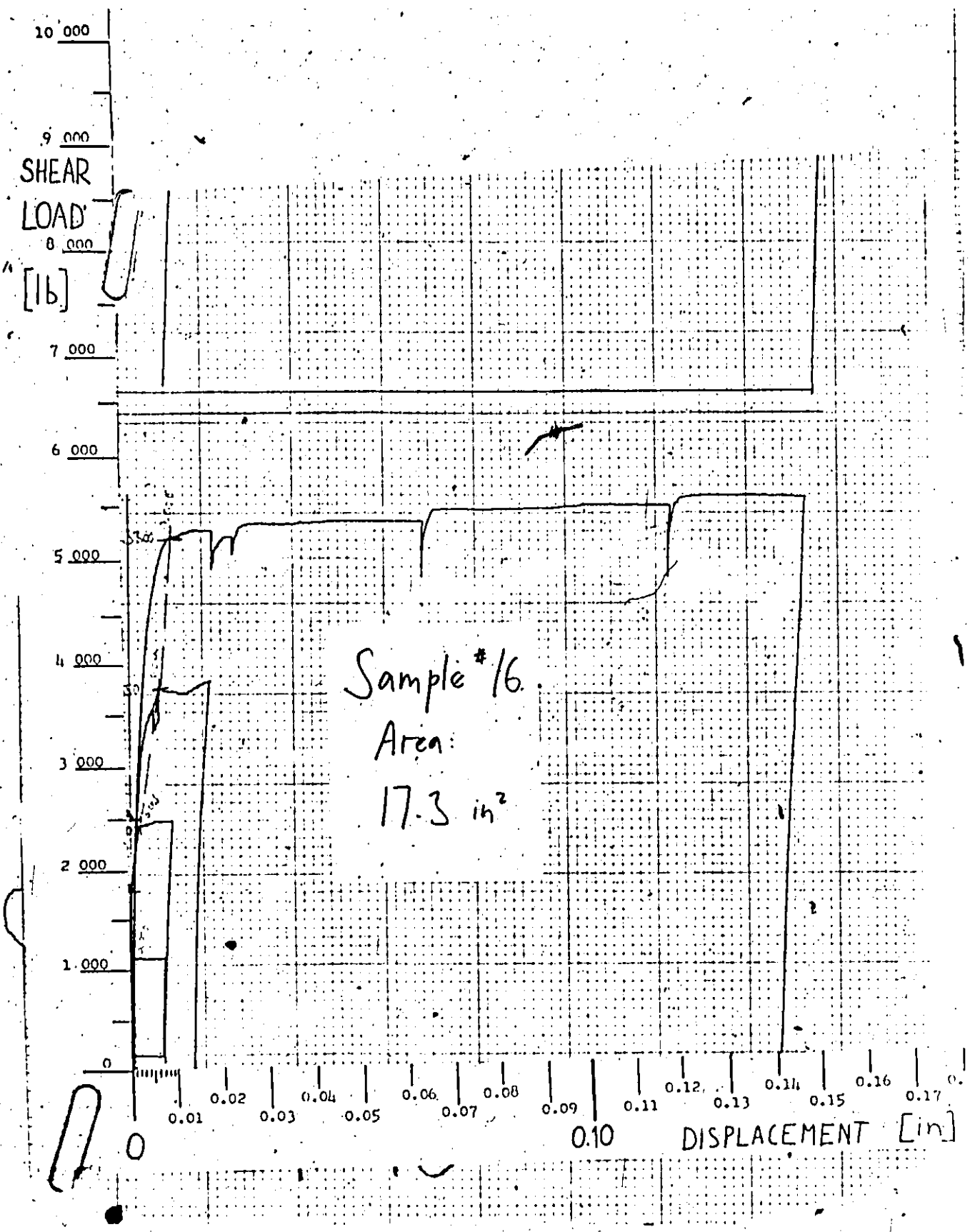
10 000
9 000
SHEAR
LOAD
8 000
[lb]
7 000
6 000
5 000
4 000
3 000
2 000
1 000
0
Sample #16.
Area:
17.3 in²
0.01
0.02
0.03
0.04
0.05
0.06
0.07
0.08
0.09
0.10
0.11
0.12
0.13
0.14
0.15
0.16
0.17
0
DISPLACEMENT [in]

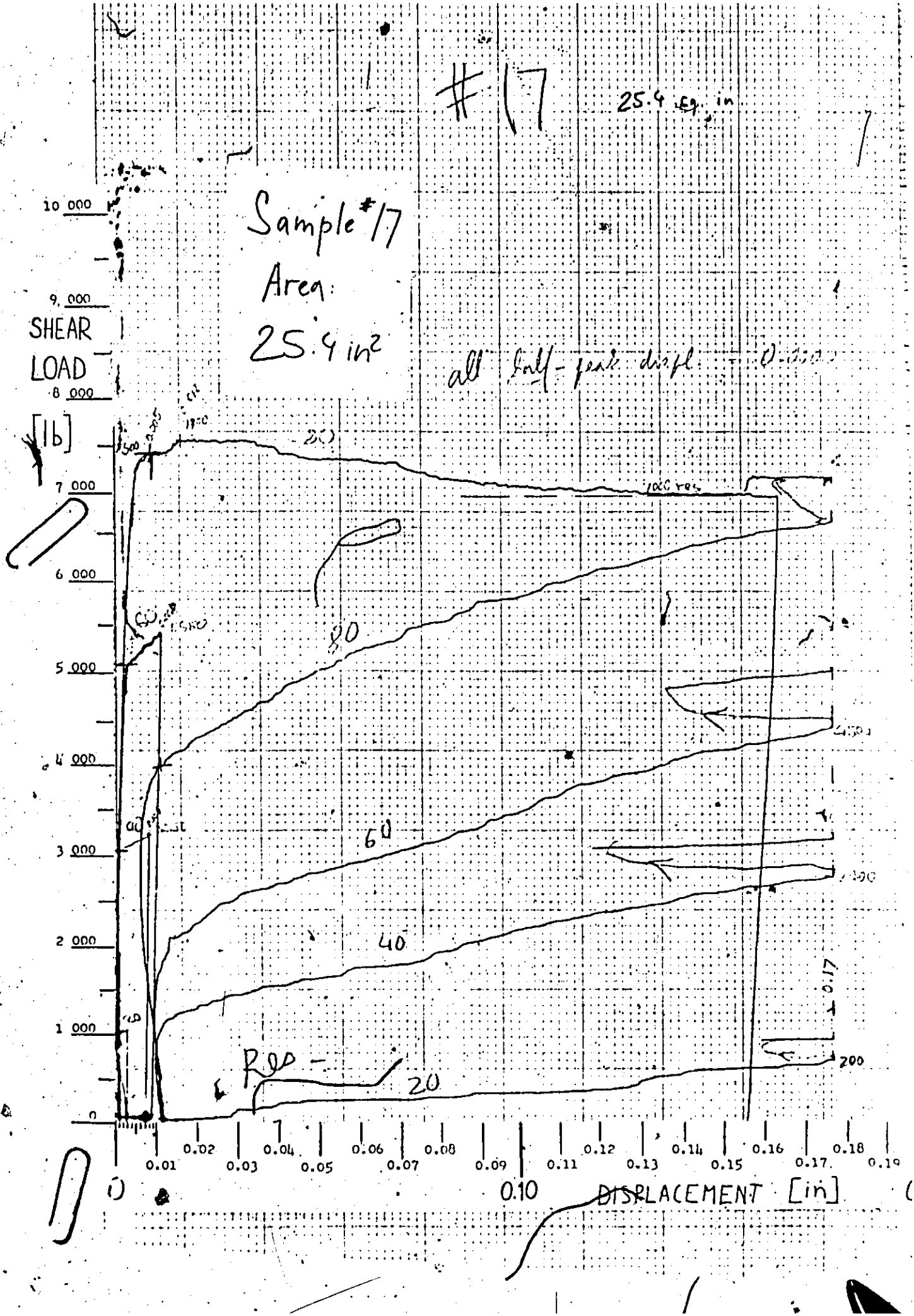
#17
25.4 sq. in
Sample #17
Area:
25.4 in²
all half-peak displ.
SHEAR LOAD [lb]
10 000
9 000
8 000
7 000
6 000
5 000
4 000
3 000
2 000
1 000
0
80
60
40
20
0.01
0.02
0.03
0.04
0.05
0.06
0.07
0.08
0.09
0.10
0.11
0.12
0.13
0.14
0.15
0.16
0.17
0.18
0.19
DISPLACEMENT [in]

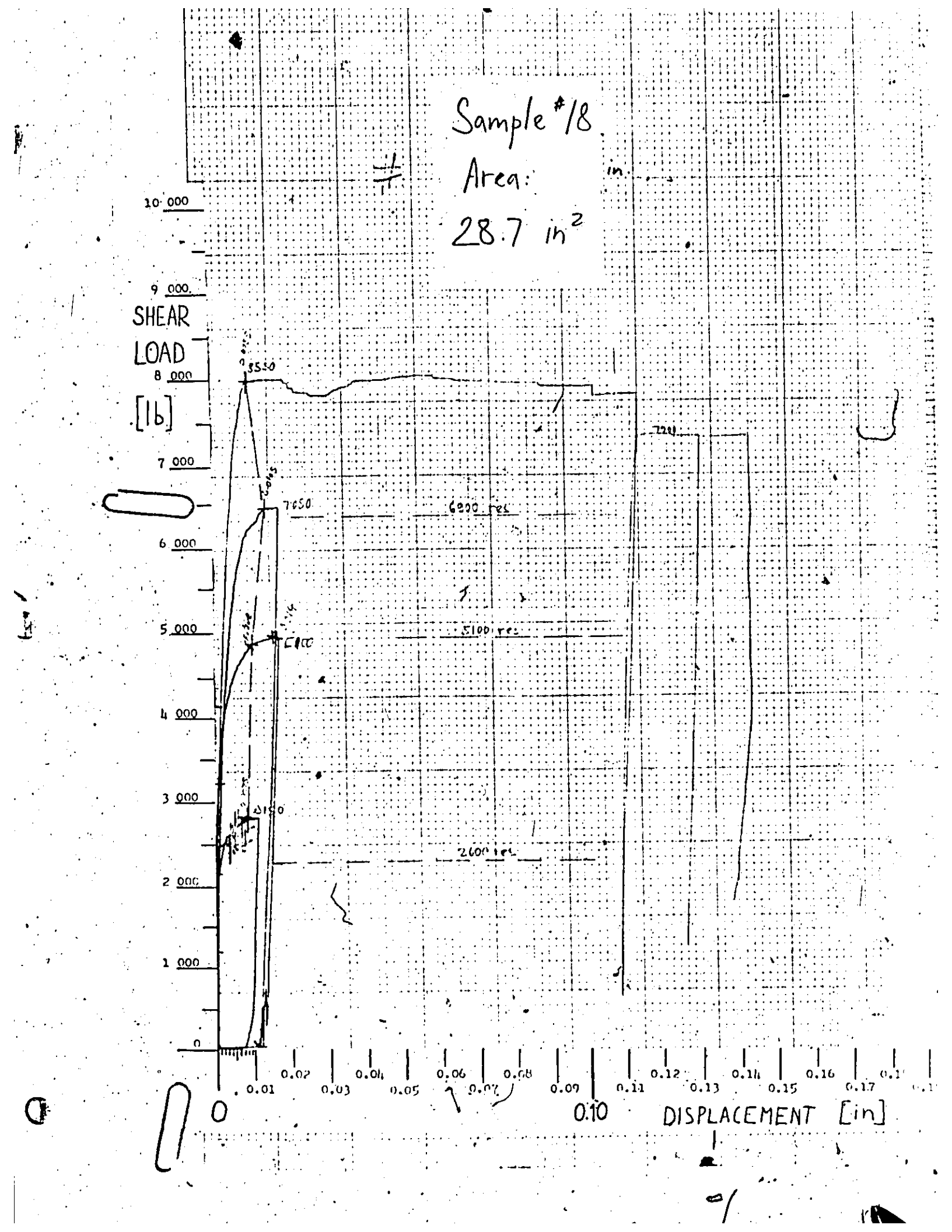
Sample #18
Area:
28.7 in²
SHEAR LOAD [lb]
10 000
9 000
8 000
7 000
6 000
5 000
4 000
3 000
2 000
1 000
0
8550
7650
6000 res
5100 res
2600 res
0.01
0.02
0.03
0.04
0.05
0.06
0.07
0.08
0.09
0.10
0.11
0.12
0.13
0.14
0.15
0.16
0.17
DISPLACEMENT [in]

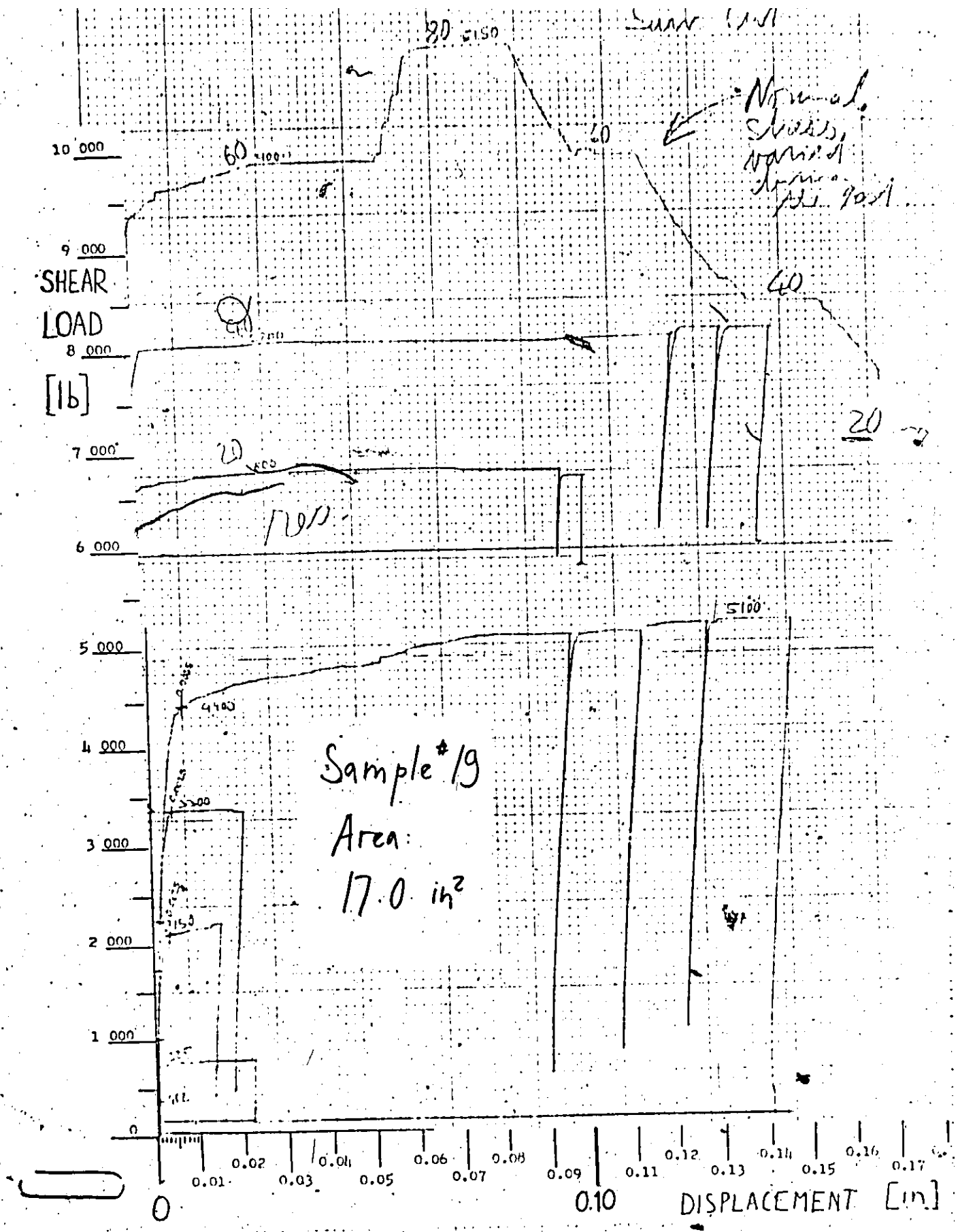
SHEAR LOAD [lb]
10 000
9 000
8 000
7 000
6 000
5 000
4 000
3 000
2 000
1 000
0
0.01
0.02
0.03
0.04
0.05
0.06
0.07
0.08
0.09
0.10
0.11
0.12
0.13
0.14
0.15
0.16
0.17
DISPLACEMENT [in.]
Sample #19
Area:
17.0 in²
Normal Stress, Varied

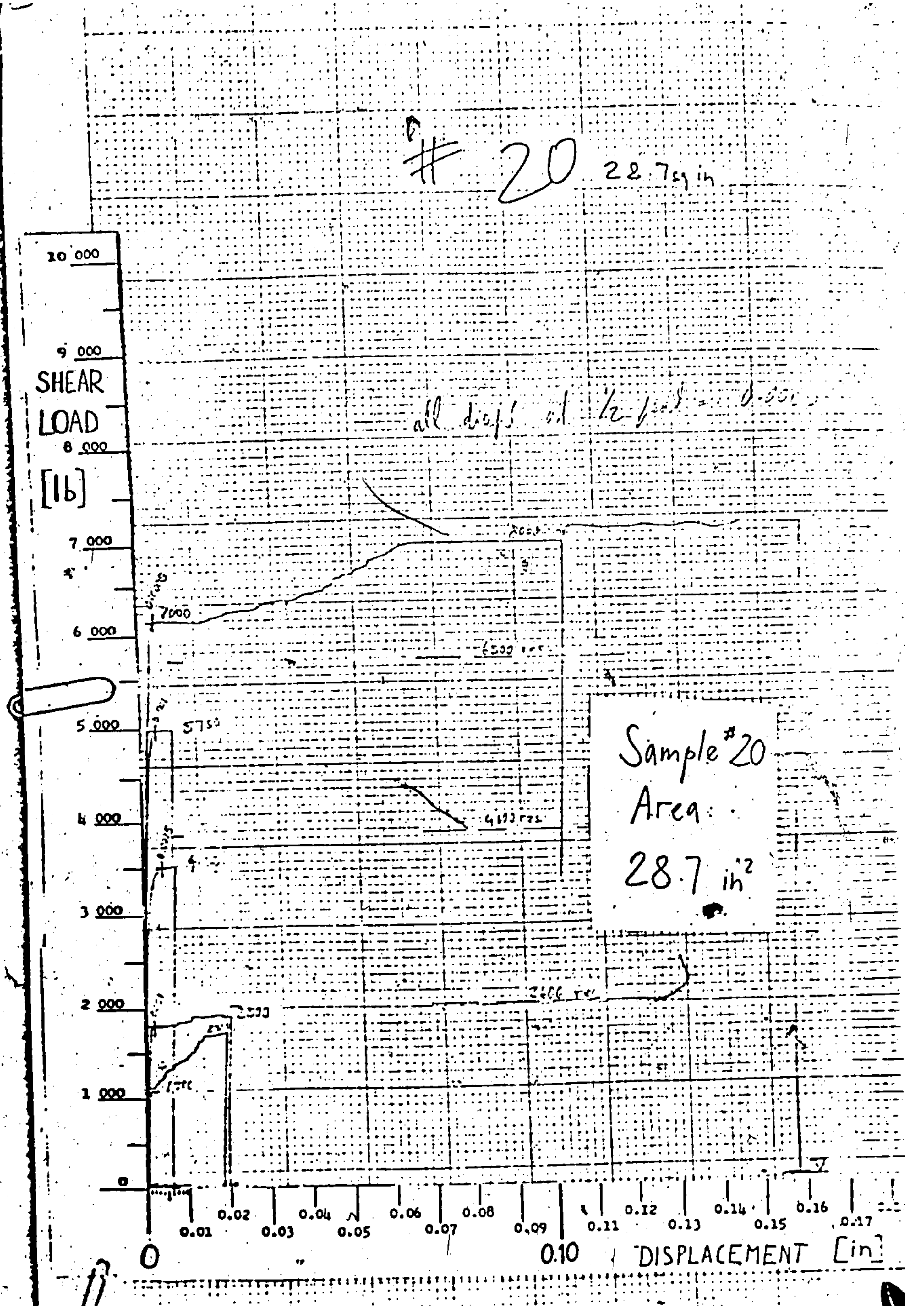
#20 28.7 sq in
SHEAR LOAD [lb]
10 000
9 000
8 000
7 000
6 000
5 000
4 000
3 000
2 000
1 000
0
7000
5750
2000
Sample #20
Area:
28.7 in²
0
0.01
0.02
0.03
0.04
0.05
0.06
0.07
0.08
0.09
0.10
0.11
0.12
0.13
0.14
0.15
0.16
0.17
DISPLACEMENT [in]

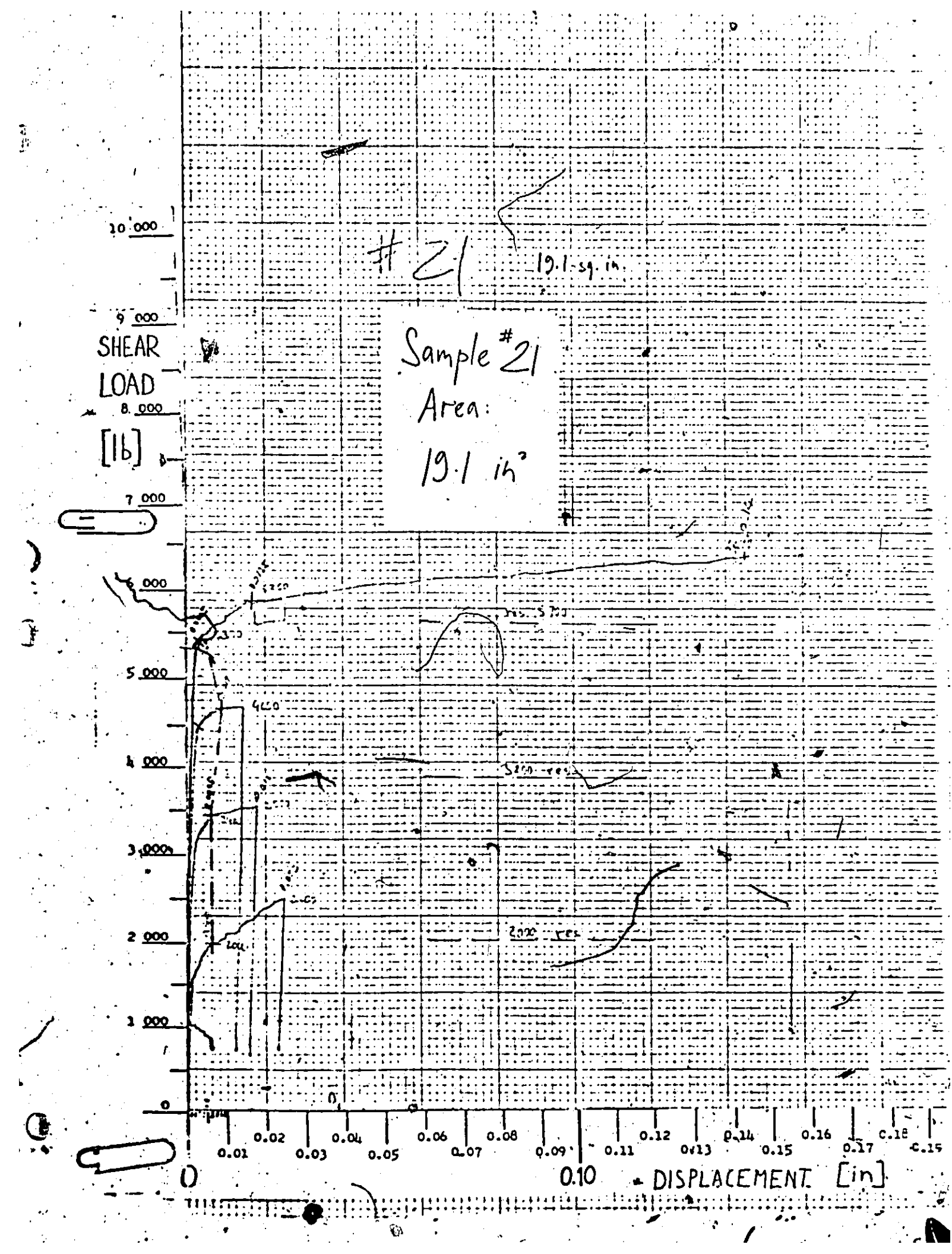
#21 19.1 sq. in.
Sample #21
Area:
19.1 in²
SHEAR LOAD [lb]
10 000
9 000
8 000
7 000
6 000
5 000
4 000
3 000
2 000
1 000
0
0.01
0.02
0.03
0.04
0.05
0.06
0.07
0.08
0.09
0.10
0.11
0.12
0.13
0.14
0.15
0.16
0.17
0.18
0.19
DISPLACEMENT [in]

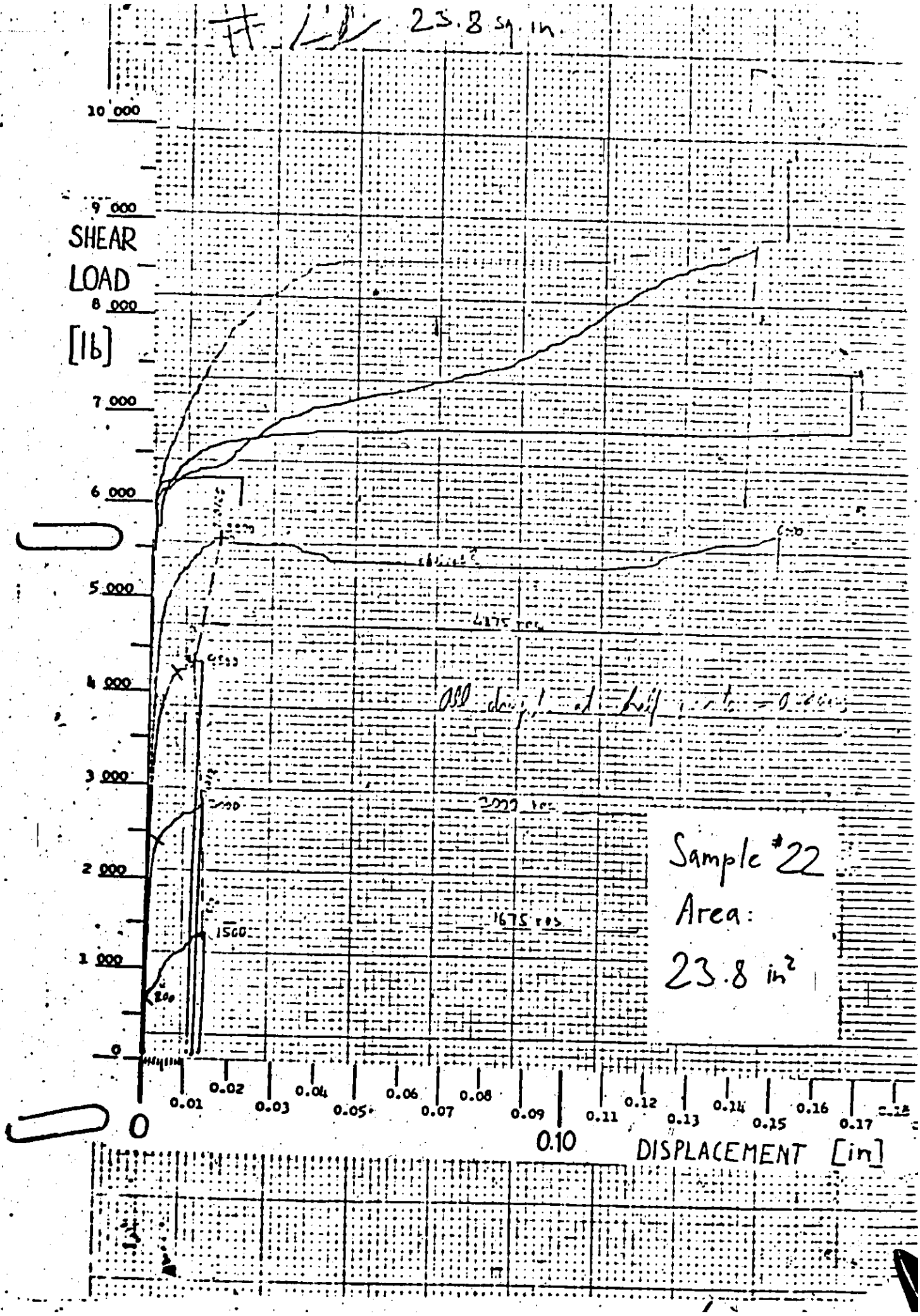
23.8 sq. in.
SHEAR LOAD [lb]
10 000
9 000
8 000
7 000
6 000
5 000
4 000
3 000
2 000
1 000
0
0.01
0.02
0.03
0.04
0.05
0.06
0.07
0.08
0.09
0.10
0.11
0.12
0.13
0.14
0.15
0.16
0.17
DISPLACEMENT [in]
Sample #22
Area:
23.8 in²

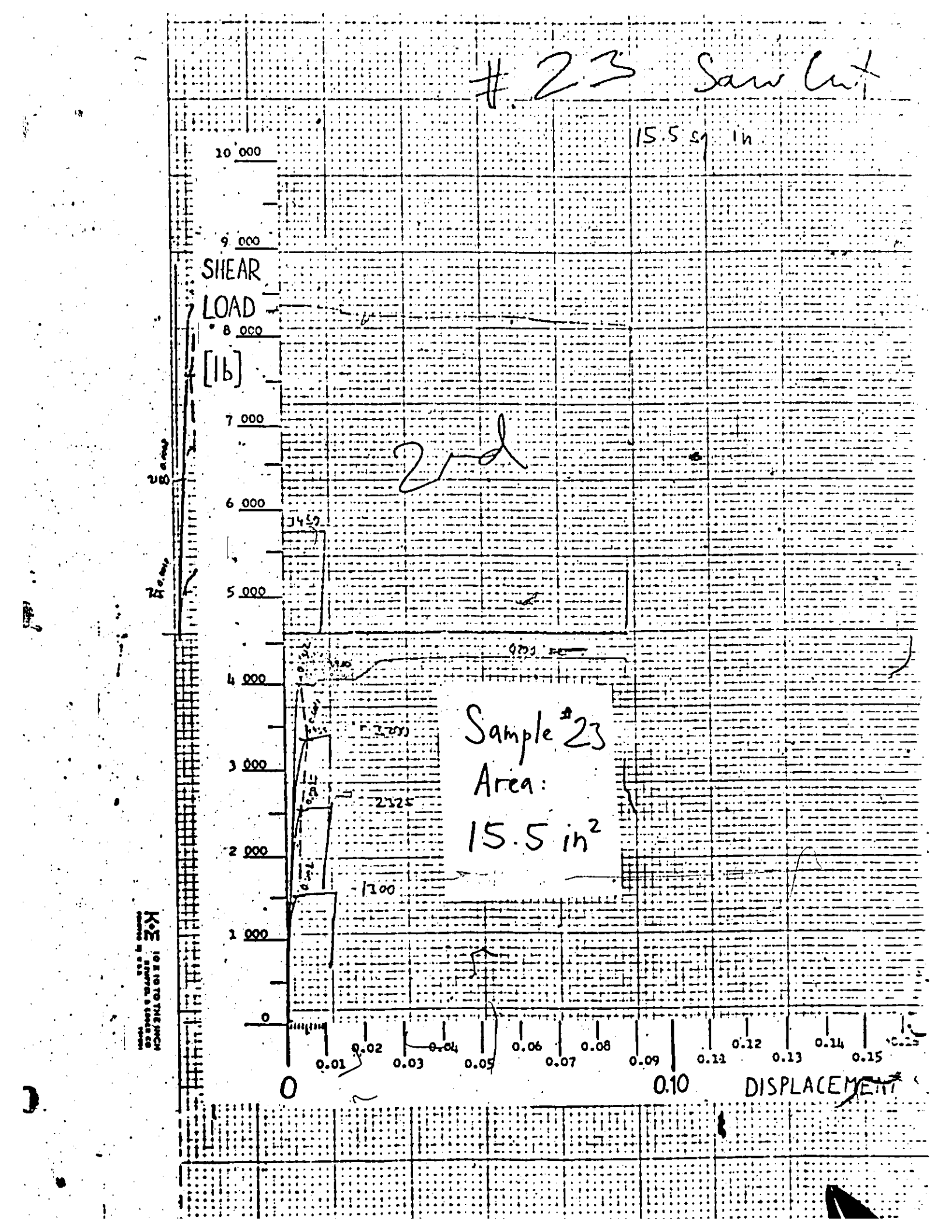
#23 Saw Cut
15.5 sq in
SHEAR LOAD [lb]
10 000
9 000
8 000
7 000
6 000
5 000
4 000
3 000
2 000
1 000
0
2nd
Sample #23
Area:
15.5 in²
0.01
0.02
0.03
0.04
0.05
0.06
0.07
0.08
0.09
0.10
0.11
0.12
0.13
0.14
0.15
0
DISPLACEMENT

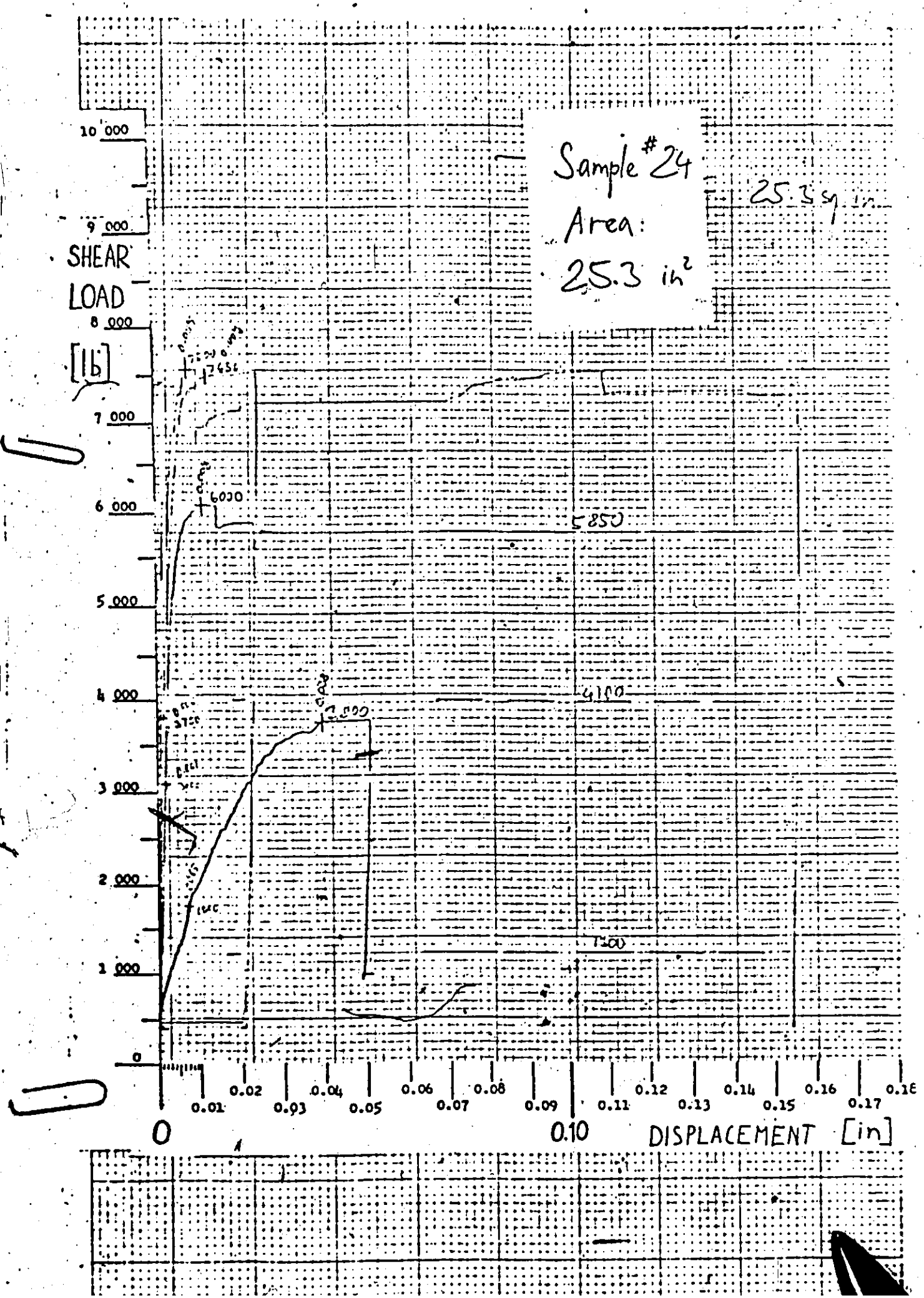
Sample #24
Area:
25.3 in²
25.3 sq in
SHEAR LOAD [lb]
10 000
9 000
8 000
7 000
6 000
5 000
4 000
3 000
2 000
1 000
0
6030
5850
4100
4200
1200
0.01
0.02
0.03
0.04
0.05
0.06
0.07
0.08
0.09
0.10
0.11
0.12
0.13
0.14
0.15
0.16
0.17
0
0.10
DISPLACEMENT [in]

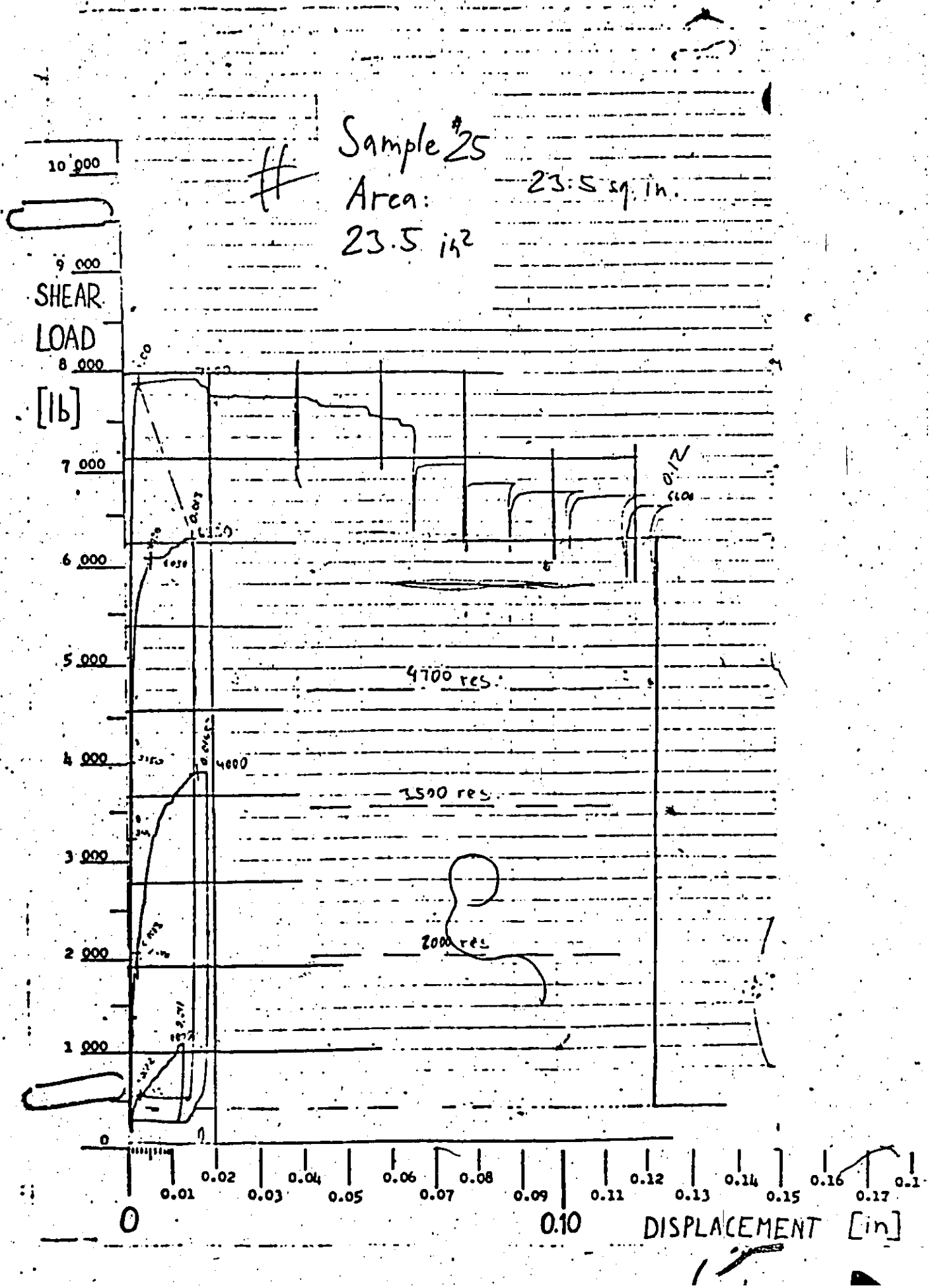
Sample #25
Area:
23.5 in²
23.5 sq. in.
SHEAR LOAD [lb]
10 000
9 000
8 000
7 000
6 000
5 000
4 000
3 000
2 000
1 000
0
4700 res.
3500 res.
2000 res.
0.01
0.02
0.03
0.04
0.05
0.06
0.07
0.08
0.09
0.10
0.11
0.12
0.13
0.14
0.15
0.16
0.17
0
DISPLACEMENT [in]

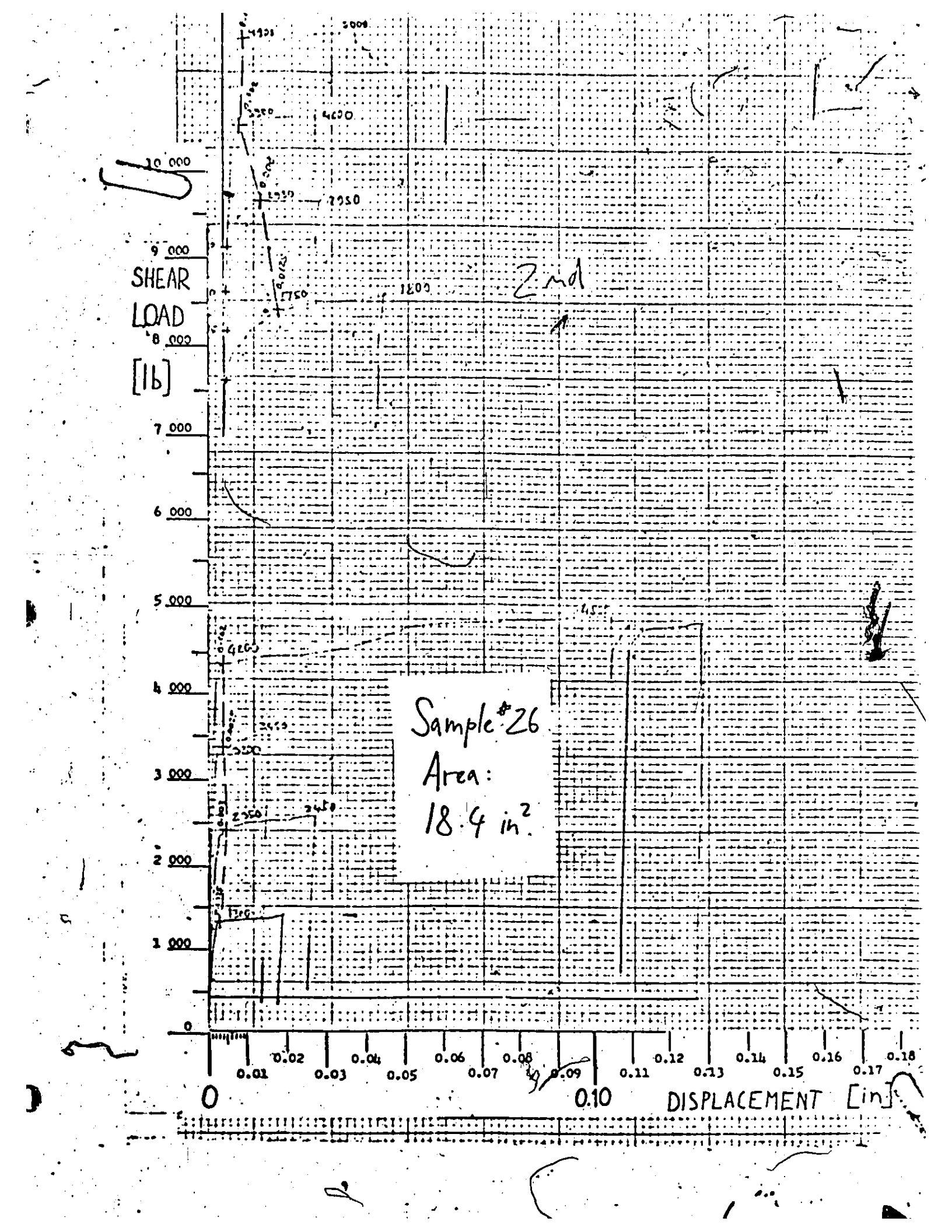
SHEAR LOAD [lb]
10 000
9 000
8 000
7 000
6 000
5 000
4 000
3 000
2 000
1 000
0
2nd
Sample #26
Area:
18.4 in²
0.01
0.02
0.03
0.04
0.05
0.06
0.07
0.08
0.09
0.10
0.11
0.12
0.13
0.14
0.15
0.16
0.17
0.18
0
DISPLACEMENT [in]

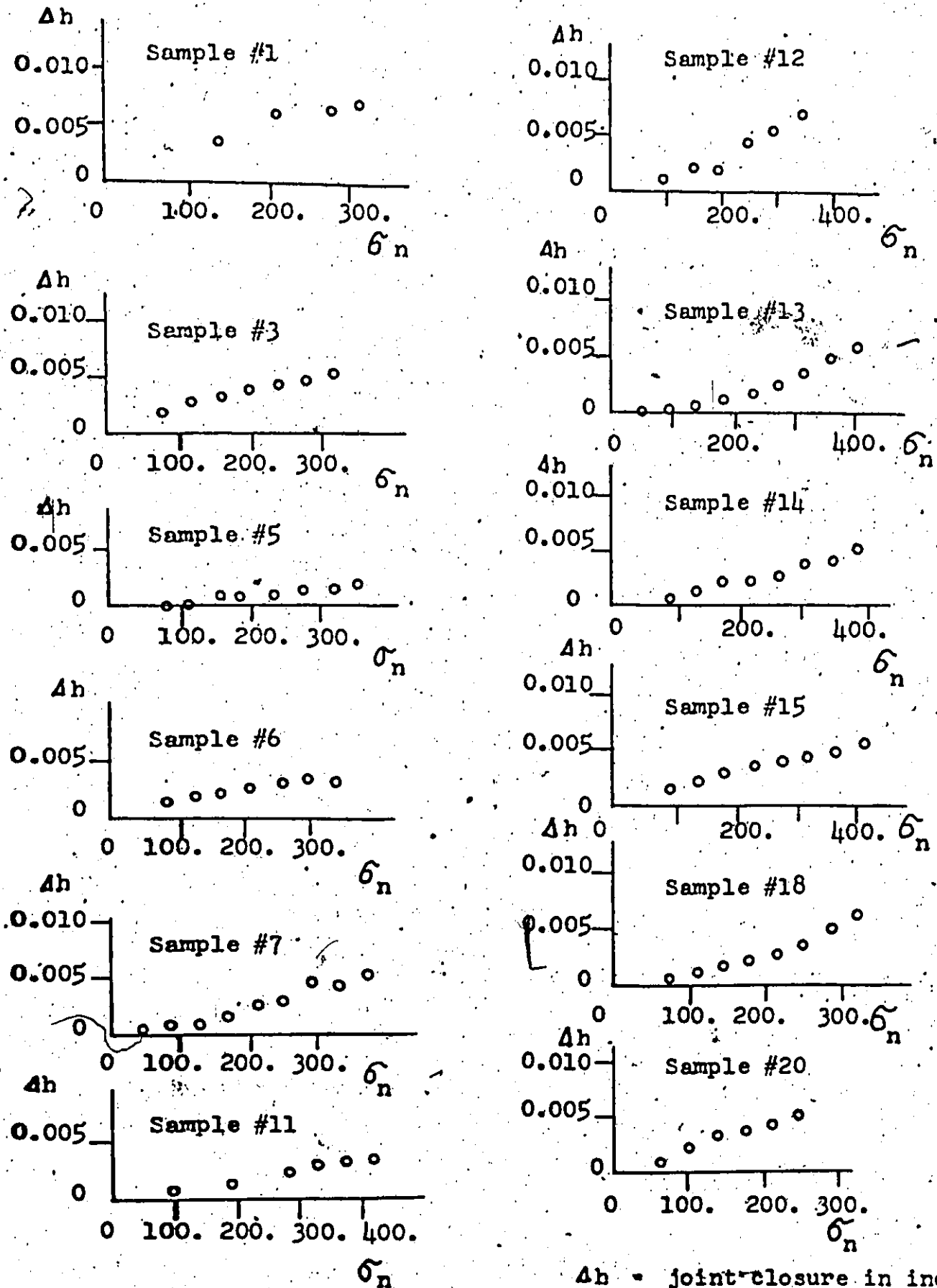

Δh = joint closure in inches

σ_n = applied normal stress in psi

Figure A.5, Graphical summary of the joint closure tests.

(For definitions see pp. 74 and 75.)

WATFIV JOB,CARD

```
      $JOB      WOOLLEDGE ... [illegible]
C               DIRECT SHEAR TEST DATA
C
            REAL KM,KY,KNM,KNY,KP,KNP
            REAL PNN(4),PN
            REAL KAV,KNAV
            SAVU=0.
            SAVL=0.
            SNAVL=0.
            DO 1 I=1,26
            SMU=0.
            SML=0.
            SYU=0.
            SYL=0.
             SNML=0.
            SNYL=0.
            DO 4 J=1,4
      4     PNN(J)=20.*FLOAT(J)*108.-200.
            READ,AREA,IND
            PRINT 5,I,AREA
      5     FORMAT('0','SAMPLE NO',I5,'                        AREA =',F6.1)
            PRINT 8
      8     FORMAT('0',2X,'SIGMA N   TAU Y    TAU P    DFL P    KN0.5P  KNY
          2TAU/DFL KN AV    KSN.5P   KSN Y    TAUP/H   KSN AV   TAU RE   TRES/TP').
            DO 2 J=1,4
            READ 3,TY,TP,DM,DY,DP,HM,HY,HP,TR
      3     FORMAT(2F5.0,6F3.0,F5.0)
            IF(TP.EQ.0.0)TP=TY
            IF(DM.EQ.0.)DM=1.
            IF(DY.EQ.0.)DY=1.
            IF(DP.EQ.0.)DP=DY
            IF(HM.EQ.0.)HM=1.
            IF(HM.EQ.500.)HM=1.0E-10
            IF(HY.EQ.500.)HY=1.0E-10
            IF(HY.EQ.0.)HY=1.
            IF(HP.EQ.500.)HP=1.0E-10
            IF(HP.EQ.0.)HP=HY
            TY=TY/AREA
            TP=TP/AREA
            PN=PNN(J)/AREA
            TR=TR/AREA
            RAT=TR/TP
            KM=TP/(2.*DM)
            KY=TY/DY
            KP=TP/DP
            KNM=TP/(2.*HM)
            KNY=TY/HY
            KNP=TP/HP
            SMU=SMU+TP/2.
            SML=SML+DM
            SYU=SYU+TY
            SYL=SYL+DY
            SNML=SNML+HM
            SNYL=SNYL+HY
            KAV=(TP/2.+TY)/(DM+DY)
            KNAV=(TP/2.+TY)/(HM+HY)
            DP=DP/10000.
            PRINT 6,PN,TY,TP,DP,KM,KY,KP,KAV,KNM,KNY,KNP,KNAV,TR,RAT
      6     FORMAT(' ',3F8.1,F8.4,8F8.2,F8.1,F8.2)
      2     SMAX=SMU/SML
```

```
57                SMIN=SYU/SYL
58                SNMAX=SMU/SNML
59                SNMIN=SYU/SNYL
60                TOT=(SMU+SYU)/(SML+SYL)
61                TOTN=(SMU+SYU)/(SNML+SNYL)
62                SRMAX=SNMAX/SMAX
63                SRMIN=SNMIN/SMIN
64                STOT=TOTN/TOT
65                PRINT 7,SMAX,SMIN,TOT
66          7     FORMAT('0','KN 0.5 =',F8.2,15X,'KN Y =',F8.2,15X,'KN =',F8.2)
67                PRINT 10,SNMAX,SNMIN,TOTN
68          10    FORMAT('0','KSN 0.5 =',F8.2,15X,'KSN Y =',F8.2,15X,'KSN=',F8.2)
69                PRINT 9,SRMAX,SRMIN,STOT
70          9     FORMAT('0','RATIOS BETWEEN KSN & KN ARE',F8.2,'FOR 0.5P',F8.2,'F
          2OR TY',F8.2,' OVERALL')
71                SAVU=SAVU+SMU+SYU
72                SAVL=SAVL+SML+SYL
73                SNAVL=SNAVL+SNML+SNYL
74                IF(IND.GT.9)GO TO 15
75                GO TO 1
76          15    RTOT=SAVU/SAVL
77                RNTOT=SAVU/SNAVL
78                SAVU=0.
79                SAVL=0.
80                SNAVL=0.
81                PRINT 17,RTOT,RNTOT
82          17    FORMAT('0','THE OVERALL REGRESSION VALUES ARE  ','KS=',F8.2,'KSN
          2=',F8.2)
83          1     CONTINUE
84                STOP
85                END
```

SENTRY

MPLE NO 1 AREA = 30.3

SIGMA N	TAU Y	TAU P	DEL P	KN0.5P	KNY	TAU/DEL	KN AV	KSN.5P	KSN Y	TAUP/H	KSN AV	TAU PE
64.7	84.2	92.4**	0.0230	2.31	0.71	0.40	0.94	3.08	1.05********		1.37	85.8
136.0	165.0	171.6	0.0270	5.05	0.91	0.64	1.26	85.81	1.38********		2.07	0.0
207.3	227.7	231.0	0.0240	4.62	1.20	0.96	1.60	23.10	2.53	2.31	3.61	0.0
278.5	290.5	305.3	0.0370	5.45	1.73	0.83	2.28	152.64	4.68	2.35	7.10	305.3

0.5) = 4.45 KN Y = 1.16 KN = 1.56

N 0.5 = 18.19 KSN Y = 2.16 KSN= 3.11

TIOS BETWEEN KSN & KN ARE 4.09FOR 0.5P 1.86FOR TY 1.99 OVERALL

MPLE NO 2 AREA = 21.2

SIGMA N	TAU Y	TAU P	DEL P	KN0.5P	KNY	TAU/DEL	KN AV	KSN.5P	KSN Y	TAUP/H	KSN AV	TAU RE
92.5	99.1	99.1	0.0270	0.93	0.37	0.37	0.45	49.53	1.10	1.10	1.63	93.2
194.7	182.8	182.8	0.0150	3.05	1.22	1.22	1.52	9.14	2.50	2.50	3.30	178.1
296.2	248.1	248.1	0.0150	12.41	1.65	1.65	2.33	17.72	2.85	2.85	3.96	259.4
398.1	298.9	288.9	0.0080	144.46	3.61	3.61	5.35	20.64	6.02	6.02	7.88	294.8

0.5 = 4.05 KN Y = 1.26 KN = 1.64

N 0.5 = 16.38 KSN Y = 2.75 KSN= 3.80

APPENDIX B

Finite element meshes.

Fig. B.1 Finite element mesh No. 1.

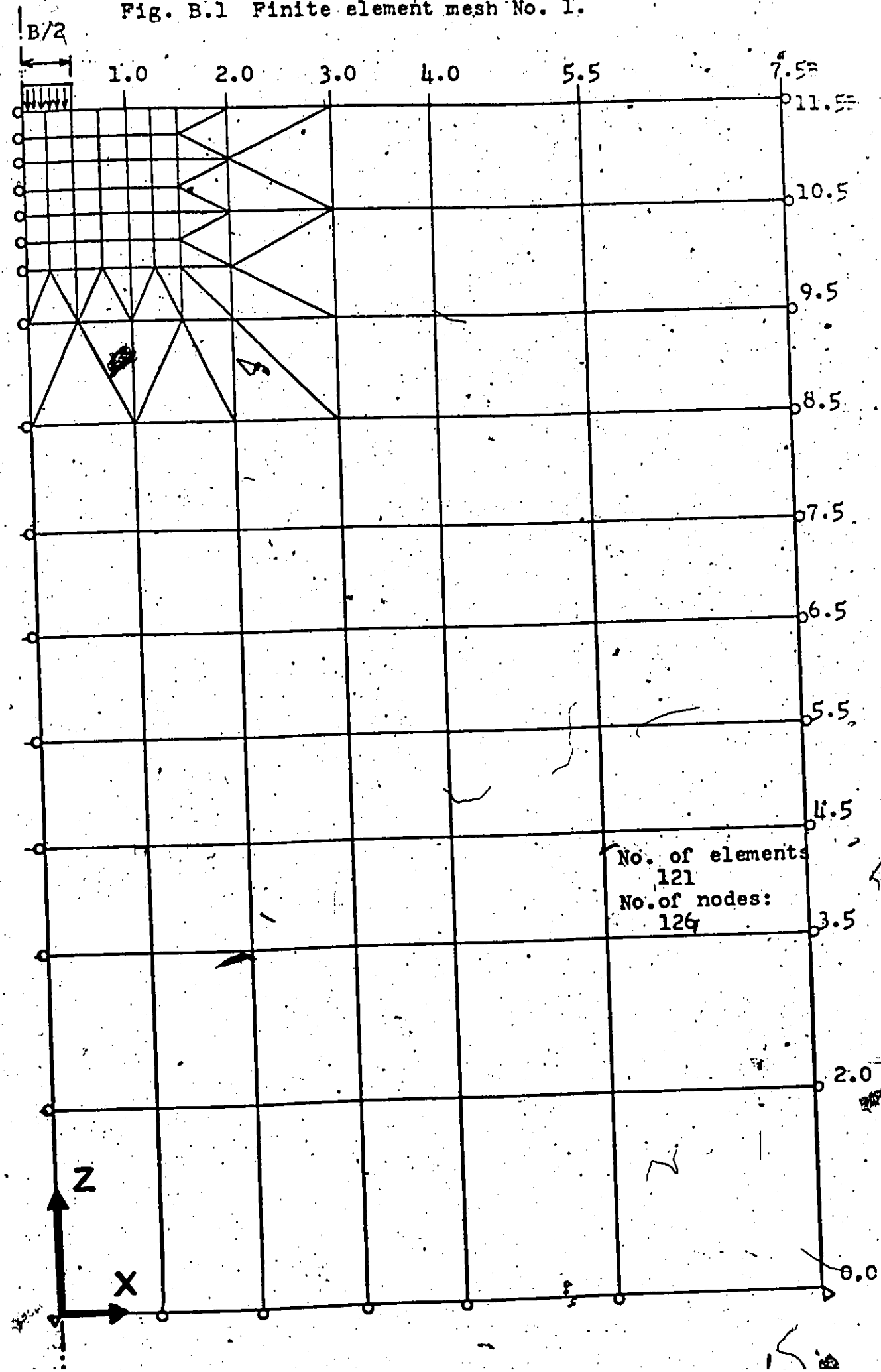

Fig. B.2 Finite element mesh No.3.

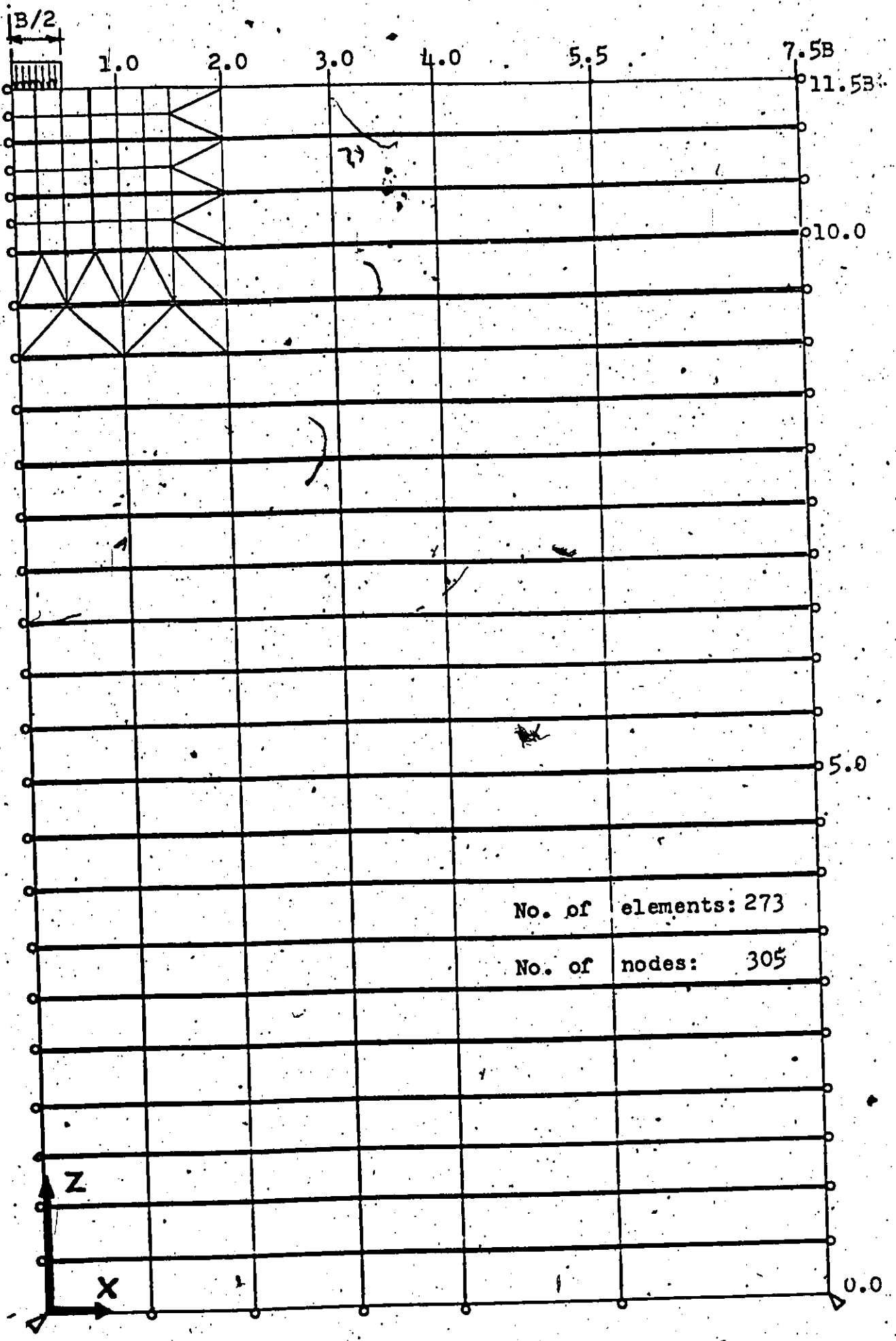

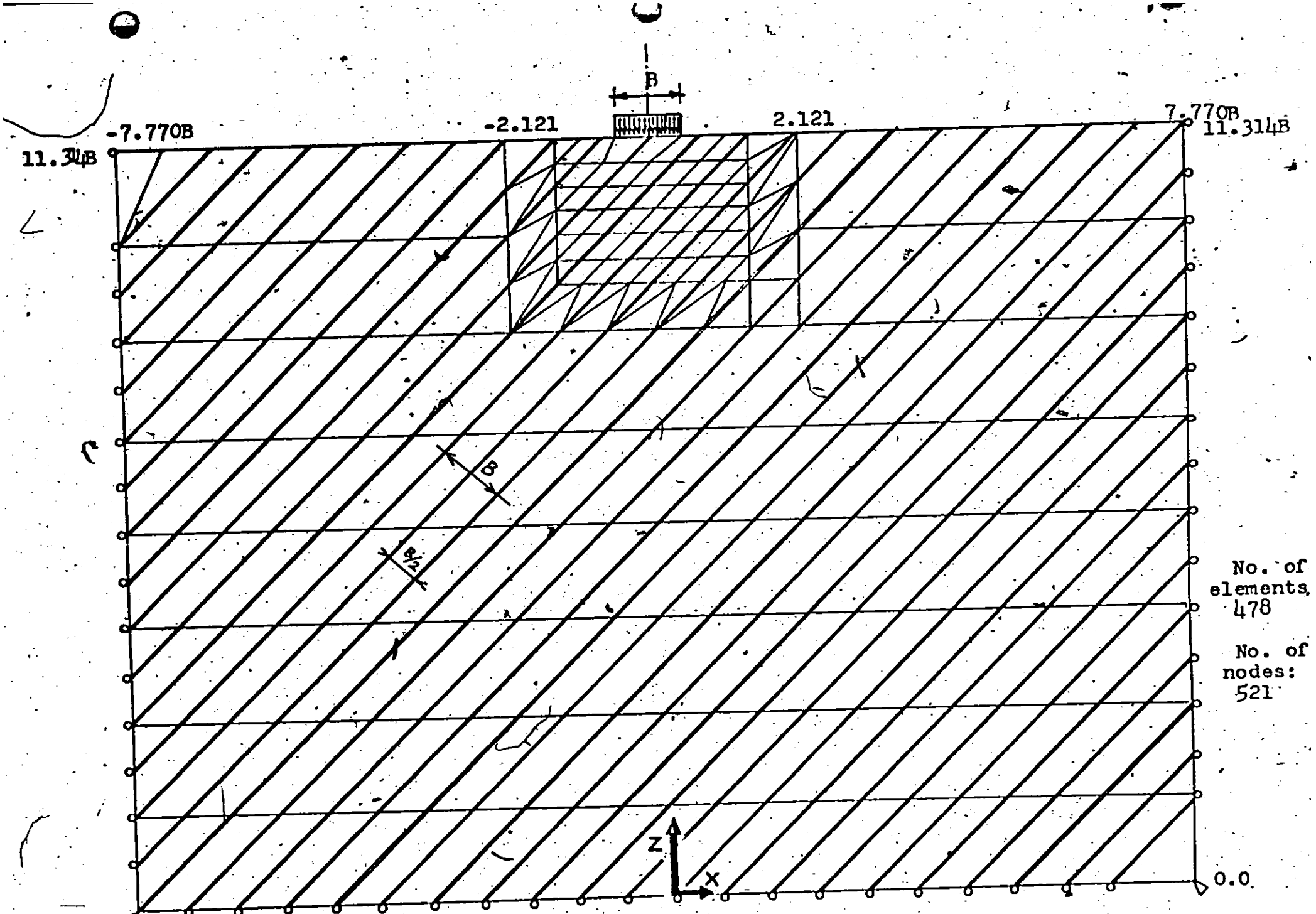

Fig. B.3 Finite element mesh No. 4.

APPENDIX C

Some Additional Notes on the Design of the Direct Shear Testing Machine.

Figures C.I and C.II represent the shop drawings of the shear boxes, loading shoes and lateral restraint brackets.

In Figure C.I the slip bearing plates are shown to be inclined at 2°. The purpose of this was to even furter reduce the friction along the bearing during a normal movement of the box. The design was, however, later revised to exclude this feature since, for contractant joints, the inclination of the bearing would add to the angle of friction and thereby increase the error, rather than decrease it.

The structural design of the welds and bolts in the shoe included consideration of a moment, caused by the maximum design shear force (10 ton) acting through an arm of about 2½ inches (estimated) and tending to rotate the box out of its grip with the shoe.

The purpose of the circular hole in the side of the shoe is mainly to relieve some weight and facilitate the handling of the piece. It is also considered beneficial in decreasing the stiffness of the part of the shoe which is in direct contact with the box and so aiding in shifting the transferred load closer towards the gap between the boxes.

A single type of bolt, high tension 5/16 in. diameter, was used throughout the design. All of the parts, with the exception of the boxes and the loading frame, were manufactured from the same size of flat stock. Thus, the variety of material ordered was reduced to a minimum.

The lateral restraint pins were fabricated from a 3/8 in. diameter carbon drill rod and hardened by heat treatment. A spare set of these was made and tested to failure in a compression testing machine. The resulting yield loads were recorded as 8 625 lbs and 9 000 lbs.

The loading frame of the machine was designed to withstand maximum normal force of 10 tons. The reason for this was to enable possible future replacement of the bellows for one of higher capacity than that presently used.

During the operation of the machine the end of the loading frame on the bellows side needs to be safely supported against lateral instability. This was achieved by placing the frame on timber props (see Plates 1 and 2) and tying it down securely with a yoke, consisting of a strong wire tightened by turnbuckles. A note of caution is attached to the frame, since the failure of the operator to tighten the yoke properly before applying the air pressure in the bellows might result in a damage to the apparatus.

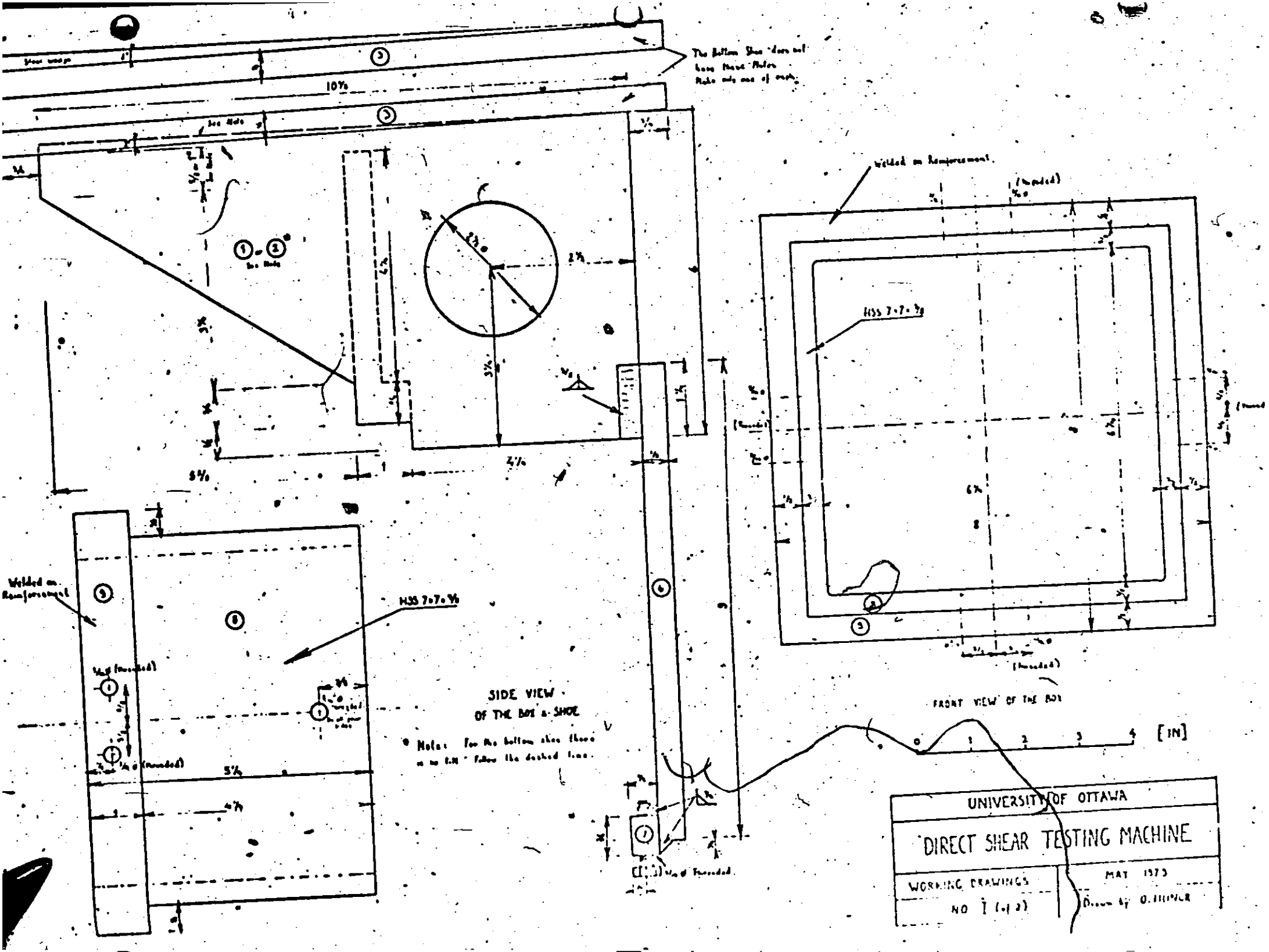
Welded on Reinforcement
HSS 7×7×½
SIDE VIEW OF THE BOX & SHOE
FRONT VIEW OF THE BOX
[IN]
UNIVERSITY OF OTTAWA
DIRECT SHEAR TESTING MACHINE
WORKING DRAWINGS
NO 1 (of 2)
MAY 1973

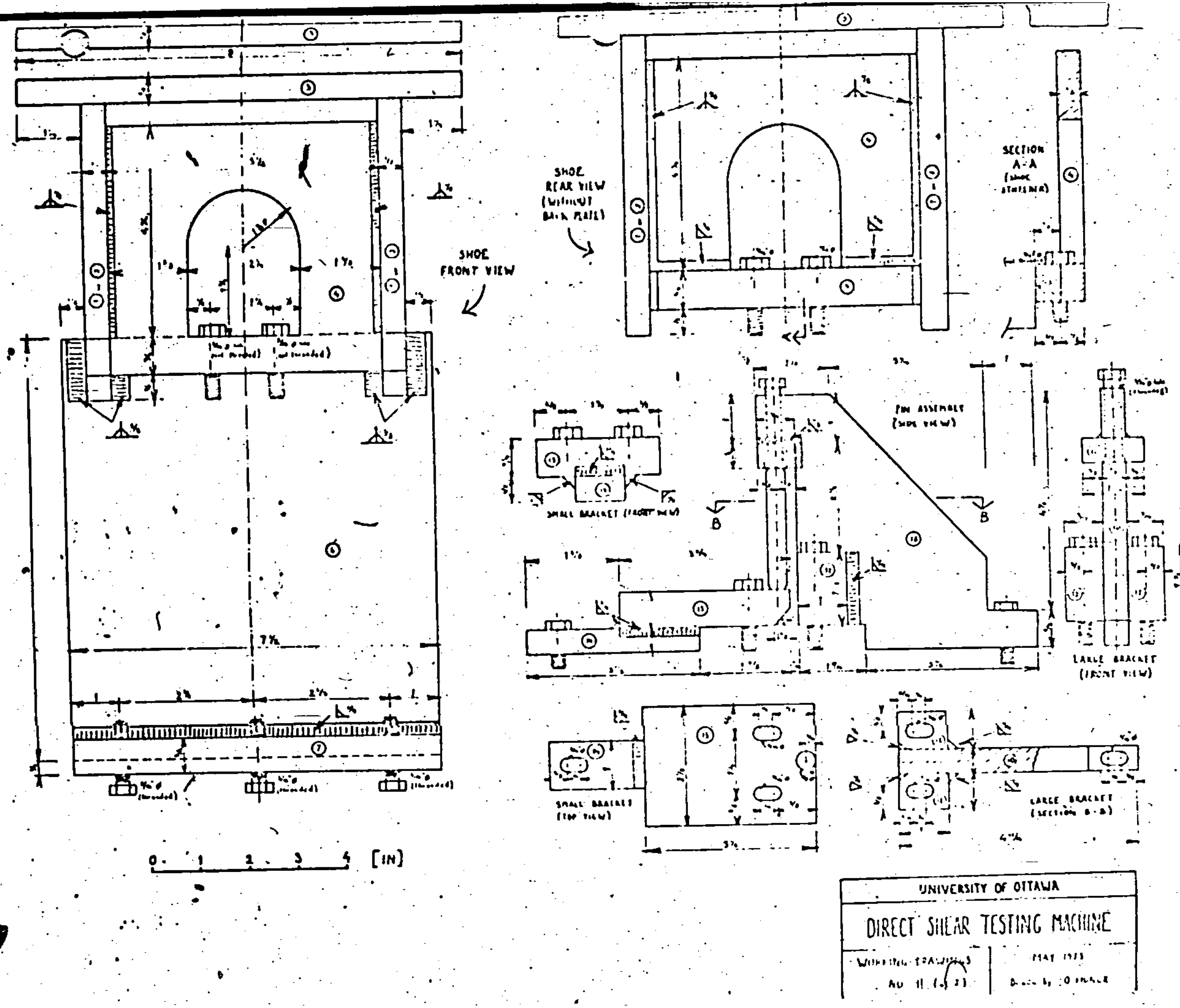
SHOE FRONT VIEW
SHOE REAR VIEW (WITHOUT BACK PLATE)
SECTION A-A (SHOE STIFFENER)
PIN ASSEMBLY (SIDE VIEW)
SMALL BRACKET (FRONT VIEW)
LARGE BRACKET (FRONT VIEW)
SMALL BRACKET (TOP VIEW)
LARGE BRACKET (SECTION B-B)
0 1 2 3 4 [IN]
UNIVERSITY OF OTTAWA
DIRECT SHEAR TESTING MACHINE
WORKING DRAWINGS
MAY 1973